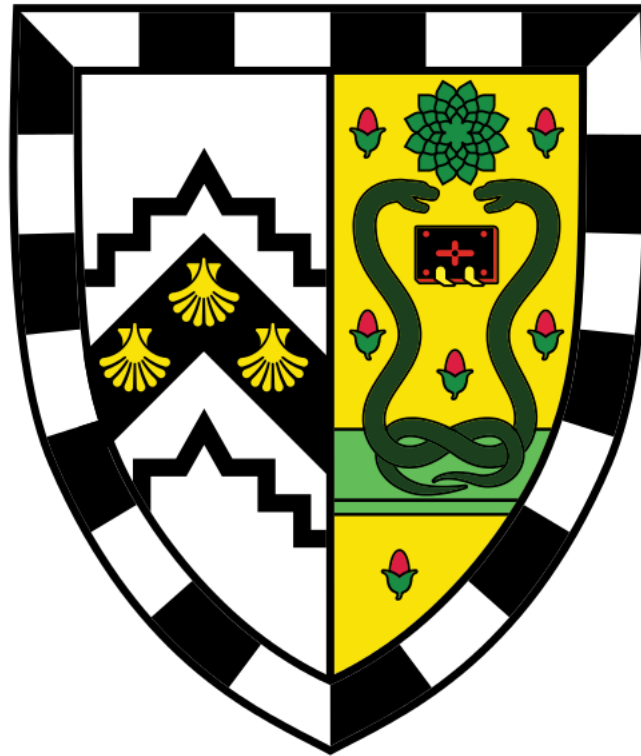


# The role of *Arid1a* and *Tet1* in ductal cell-driven liver regeneration



**UNIVERSITY OF  
CAMBRIDGE**

**Mikel Alexander McKie**  
**College:** Gonville and Caius College  
**Supervisor:** Dr Meritxell Huch  
**Date of submission:** September 2019

This thesis is submitted for the degree of Doctor of Philosophy

## Declaration

This dissertation is the result of my own work and includes nothing which is the outcome of collaboration except as declared in the Preface (see external contributions) and specified in the text.

It is not substantially the same as any that I have submitted, or, is being concurrently submitted for a degree or diploma or other qualification at the University of Cambridge or any other university or similar institution except as declared in the Preface and specified in the text. I further state that no substantial part of my dissertation has already been submitted, or, is being concurrently submitted for any such degree, diploma or other qualification at the University of Cambridge or any other University or similar institution except as declared in the Preface and specified in the text.

It does not exceed the prescribed word limit for the relevant Degree Committee.

## Abstract

**Title: The role of *Arid1a* and *Tet1* in ductal cell-driven regeneration**

**Author: Mikel Alexander Mckie**

The liver has several robust and potent mechanisms of repair after damage despite slow homeostatic turnover. In cases of extreme toxic damage, where the hepatocyte compartment is severely compromised and unable to proliferate, a bi-potent ductal population arises that is able to expand and differentiate into both hepatocytes and ductal cells. The regulation of the activation of this ductal progenitor population is poorly understood. We have taken advantage of 3D organoid cultures that model the activation of bi-potent ductal progenitors to identify potential candidates involved in organoid establishment and maintenance. Using knock down experiments, we identified the epigenetic modifiers *Arid1a* and *Tet1* as important candidates for ductal progenitor maintenance and establishment, respectively, *in vitro*. Further *in vitro* analysis of several genetic models of *Arid1a* showed that reduction but not ablation of *Arid1a* results in enhanced proliferation and survival of organoid culture. In addition, *Arid1a* defective organoids lacked the ability to differentiate into functional hepatocytes *in vitro*. Therefore, *Arid1a* is important for regulating the differentiation and proliferative nature of ductal progenitors *in vitro*. On the other hand, we found that reduction or loss of *Tet1* resulted in abolished establishment and maintenance of organoid culture, suggesting an important role of *Tet1* in the activation of the progenitor state from a mature ductal cell. In line with this, we found that a hypomorphic mouse model of *Tet1* showed a significantly reduced ductal regenerative response when challenged with acute liver damage. Furthermore, chronically damaged hypomorphic mice maintained significant fibrosis over *WT* mice. Finally, ductal specific genetic ablation of *Tet1* coupled with lineage tracing showed that *Tet1* mutant ductal cells formed significantly smaller regenerative hepatocyte clusters. As a result, *Tet1* is crucial for the activation and function of ductal bi-potent progenitors both *in vivo* and *in vitro*. Taken together, the role of *Arid1a* and *Tet1* in organoid culture and liver regeneration suggests that regulation of the epigenetic landscape is crucial to determine cell fate decisions during the damage-regeneration response.

# Table of Contents

<i>Declaration</i>	2
<i>Abstract</i>	3
<i>Table of Contents</i>	4
<i>External Contributions</i>	7
<i>Abbreviations</i>	8
<b>1. Introduction</b>	<b>10</b>
<b>1.1 Liver Anatomy and function</b>	<b>10</b>
<b>1.2 Liver homeostasis and regeneration</b>	<b>13</b>
<b>1.3 Modelling adult stem cell function</b>	<b>19</b>
<b>1.4 Epigenetic regulation of chromatin accessibility and cell fate</b>	<b>24</b>
<b>1.5 The physiological role of <i>Tet1</i> and 5-methylcytosine oxidation</b>	<b>33</b>
<b>1.6 The role of <i>Arid1a</i> and the BAF complex in development and epithelial regeneration.</b>	<b>38</b>
<b>1.7 Project Aims</b>	<b>42</b>
<b>2. Materials and Methods</b>	<b>43</b>
<b>2.1 Organoid studies</b>	<b>43</b>
2.1.1 Organoid derivation and maintenance	43
2.1.2 siRNA Transfection	44
2.1.3 Organoid differentiation	46
2.1.4 Terminal hepatocyte differentiation assays	47
2.1.5 RNA extraction and RT-qPCR	47
2.1.6 Fluorescence activated cell sorting (FACS)	48
2.1.7 Western Blot	49
2.1.8 Chromatin immunoprecipitation (ChIP)	49
2.1.9 RNA sequencing and analysis	50
<b>2.2 Animal studies</b>	<b>51</b>
2.2.1 Animal breeding and maintenance	51
2.2.2 Genotyping	51
2.2.3 Tamoxifen injection	52
2.2.4 CCl <sub>4</sub> treatment	52
2.2.5 DDC treatment	52

2.2.6 AAV8-p21 delivery	53
2.2.7 Serum preparation and analysis	53
<b>2.3 Histology, immunohistochemistry and immunofluorescence</b>	<b>54</b>
2.3.1 Tissue preparation and embedding	54
2.3.2 Immunohistochemistry	54
2.3.3 Haematoxylin and eosin stain	55
2.3.4 Picrosirius Red stain	56
2.3.5 Thick OCT section immunofluorescence	56
2.3.6 Thin OCT section immunofluorescence	57
2.3.7 Organoid immunofluorescence	57
<b>2.4 Liver wholemount staining protocols</b>	<b>59</b>
2.4.1 Tissue preparation	59
2.4.2 Vibratome sectioning	59
2.4.3 See Deep brain optical tissue clearing	59
2.4.4 CUBIC optical tissue clearing	60
<b>2.5 Statistical analysis</b>	<b>60</b>
<b>3. Results</b>	<b>61</b>
<b>3.1 Identification of <i>Arid1a</i> and <i>Tet1</i> as candidates involved in ductal progenitor dynamics</b>	<b>61</b>
<b>3.2 The role of <i>Arid1a</i> in ductal progenitor maintenance and differentiation.</b>	<b>68</b>
3.2.1 Dosage of <i>Arid1a</i> modulates the proliferative and differentiation capacity of ductal progenitors <i>in vitro</i> .	68
3.2.2 Modulation of <i>Arid1a</i> specifically in ductal progenitors <i>in vivo</i> .	85
<b>3.3 The role of <i>Tet1</i> in ductal driven liver regeneration.</b>	<b>88</b>
3.3.1 Generation of animal models to study the role of <i>Tet1</i> in the liver.	88
3.3.2 Reduction of <i>Tet1</i> expression results in less ductal proliferation <i>in vitro</i> and <i>in vivo</i> .	91
3.3.3 Reduced <i>Tet1</i> expression leads to impaired liver regeneration after chronic liver damage.	99
3.3.4 Ductal specific genetic ablation of <i>Tet1</i> causes diminished function of <i>bona fide</i> bi-potent ductal progenitors <i>in vitro</i> and <i>in vivo</i> .	103
3.3.5 Ductal cells undergo significant global changes in levels of 5mC and 5hmC DNA modification upon liver damage.	114
<b>3.4 Optical tissue clearing can provide insights into the proliferative heterogeneity of the ductal compartment.</b>	<b>118</b>
<b>4. Discussion</b>	<b>123</b>
<b>4.1 Organoids as a model of ductal cell-driven liver regeneration</b>	<b>123</b>

<b>4.2 The role of <i>Arid1a</i> in bi-potent ductal progenitor maintenance and differentiation.</b>	<b>126</b>
4.2.1 <i>Arid1a</i> gene dosage regulates bi-potent ductal progenitor proliferation.	126
4.2.2 <i>Arid1a</i> regulates could cell fate transitions through modulating hallmarks of ductal progenitor state	128
4.2.3 A model for the role of <i>Arid1a</i> in bi-potent ductal progenitor maintenance and differentiation	129
<b>4.3 The role of <i>Tet1</i> in ductal cell-driven liver regeneration.</b>	<b>131</b>
4.3.1 Global reduction of <i>Tet1</i> levels results in impaired activation of ductal cell-driven regeneration following acute damage	131
4.3.2 <i>Tet1</i> is crucial for the resolution of fibrosis following chronic liver damage	132
4.3.3 Epithelial cell-specific genetic ablation of Tet1 inhibits normal ductal cell-derived hepatocyte generation.	133
4.3.4 Is <i>Tet1</i> a regulator of proliferation or of progenitor activation?	135
4.3.5 A model for the role of <i>Tet1</i> in ductal cell-driven liver regeneration	137
<b>4.3 Ductal proliferation dynamics suggest the existence of a heterogenous population with differing proliferative capacities.</b>	<b>139</b>
<b>4.4 Conclusion</b>	<b>140</b>
<i>Acknowledgements</i>	142
<i>Table of Figures</i>	144
<i>List of Tables</i>	146
<i>Bibliography</i>	147

## External Contributions

I would like to thank the following individuals for their contribution to this work; Dr Meritxell Huch for carrying out the microarray analysed in Figure 3.1, Dr Luigi Aloia for carrying out the siRNA knock-down, gene expression, ChIP analysis and organoid formation studies used in Figures 3.2, 3.3, 3.4, 3.7, 3.15, 3.20, 3.28, 3.37 and 3.38, Dr Gianmarco Mastrogiovanni for initially generating the *Arid1a* CRISPR mutant described in Figure 3.5, Lucia Cordero-Espinosa for the 5mC/5hmC staining analysed in Figure 3.37, Richard Butler for generating a tool for quantifying 5mC/5hmC staining intensity analysed in Figure 3.37, Robert Arnes for histological support and haematoxylin and eosin staining used in Figure 3.25, Dr Olivia Harris for providing protocols used in section 3.4 and finally Drs Meritxell Huch, Ayla Newton and Christopher Hindley for critical proofreading.

## Abbreviations

3,5-diethoxycarbonyl-1,4-dihydrocollidine – DDC

5-carboxylcytosine – 5caC

5-formylcytosine – 5fC

5-hydroxymethylcytosine – 5hmC

5-methylcytosine – 5mC

A/T rich interacting domain – ARID

Adenine – A

Alanine transaminase – ALT

Animal Welfare and Ethical Review Body – AWERB

Arginine methyltransferases – PRMTs

Base excision repair – BER

Bovine serum albumin – BSA

*Brm/Brg1* Associated Factor – BAF

Carbon tetrachloride – CCl<sub>4</sub>

Chromatin immunoprecipitation – ChIP

Cystic Fibrosis Transmembrane Regulator – CFTR

Cytosine – C

DNA methyltransferases – DNMTs

epidermal growth factor – EGF

Epithelial Cell Adhesion Marker – EpCAM

Extracellular matrix – ECM

Fluorescence activated cell sorting – FACS

Foetal bovine serum – FBS

fumarylacetoacetate hydrolase – Fah

Glutamate dehydrogenase – GLDH

Guanine – G

hepatocyte growth factor – HGF

Heterochromatin protein 1 – HP1

Histone acetyltransferases – HATs

Histone deacetylases – HDACs

Histone methyltransferases – HMTs

Horseshoe peroxidase – HRP

Imitation switch – ISWI  
Immunoprecipitation – IP  
Intestinal stem cell – ISC  
Low density lipoprotein – LDL  
Lysine demethylases – KDMs  
Methyl- binding protein – MBP  
Neutral buffered formalin – NBF  
Nucleosome depleted region – NDR  
Optimal cutting temperature – OCT  
Osteopontin – OPN  
Partial hepatectomy – PHx  
Phosphate-buffered saline – PBS  
Polybromo BAF – pBAF  
Primordial germ cell – PGC  
Rho kinase inhibitor – Ri  
See deep brain – SeeDB  
Small intestine – SI  
Superfamily 2 – SNF2  
Switch/Sucrose non-fermentable – SWI/SNF  
Telomerase reverse transcriptase – TERT  
Ten-eleven translocation – TET  
Three Dimensional – 3D  
Thymine – T  
Thymine DNA glycosylase – TDG  
Thyroxine binding globin – TBG  
Transcription factors – TF  
Transcriptional start site – TSS  
Transit Amplifying – TA  
Trimmed Means of M-values – TMM  
Tris-buffered saline – TBS  
Uracil – U

# 1. Introduction

## 1.1 Liver Anatomy and function

The liver is the largest internal organ in the body and is instrumental in maintaining chemical homeostasis. The organ itself has a lobular structure, in humans it is made up of four main lobes, and relies on a complex cellular organisation to carry out its plethora of functions (Abdel-Misih and Bloomston, 2010). The main resident cell types that make up the cellular menagerie present in the liver are the epithelial hepatocytes and cholangiocytes (which shall be referred to as ductal cells for the rest of this work), as well as stellate cells, Kupffer cells and endothelial cells (Thurman, Kauffman and Jungermann, 1986).

The functional units of the liver are called hepatic lobules. These are polygonal structures defined by a central vein through which blood exits the liver and joins the hepatic vein. Blood enters the liver through the portal vein and hepatic artery, and these together with the biliary duct which is made up of ductal cells, form the portal triad located on the periphery of each hepatic lobule. Blood moves from the portal region to the central vein via a specialised fenestrated network of vasculature known as the sinusoids, made up of endothelial cells (Wisse *et al.*, 1985). Fenestration throughout the sinusoid facilitates fast and efficient transport of metabolites to and from hepatocytes and the blood stream. Stellate cells are located in an interstitial space between the sinusoidal endothelium and the hepatocytes called the space of Disse. Kupffer cells are located in the sinusoidal endothelial wall allowing direct access to the blood stream (Figure 1.1).

To overcome the relative simplicity of the histological features of the liver the organ takes advantage of several unique cell types that together carry out the large number of biological features. Hepatocytes are the most populous cell type in the liver making up roughly 80% of the human liver parenchyma (Blouin, Bolender and Weibel, 1977). Hepatocytes carry out the majority of the metabolic functions of the liver such as storage and regulation of glucose (via glycogen), detoxification of endogenous and exogenous chemicals, lipid and cholesterol metabolism, synthesis of clotting agents and bile production. Hepatocyte functions are regulated through a system of metabolic zonation (Gebhardt, 1992). The metabolic zones are structured along the hepatic lobule and are classically numbered 1 – 3 moving from the portal triad to the central vein.

Several converse pathways are restricted to opposing ends of the zonation to avoid intracellular futile cycles. The concept is nicely demonstrated with the regulation of glucose metabolism. Gluconeogenesis is carried out largely in the periportal zones (Zone 1) whereas much of the glycolysis is restricted to perivenous zones (Zone 3) (Kietzmann, 2017). Separating gluconeogenesis and glycolysis into distinct metabolic zones means overall glucose flux can be controlled by regulating the two pathways in independent cells rather than having to reverse flux single in a metabolically homogenous model (Gebhardt, 1992). Therefore, metabolic zonation is exquisitely suited to ensure systemic glucose homeostasis throughout cycles of feeding and starvation during which the liver will store glucose as glycogen or release glucose respectively.

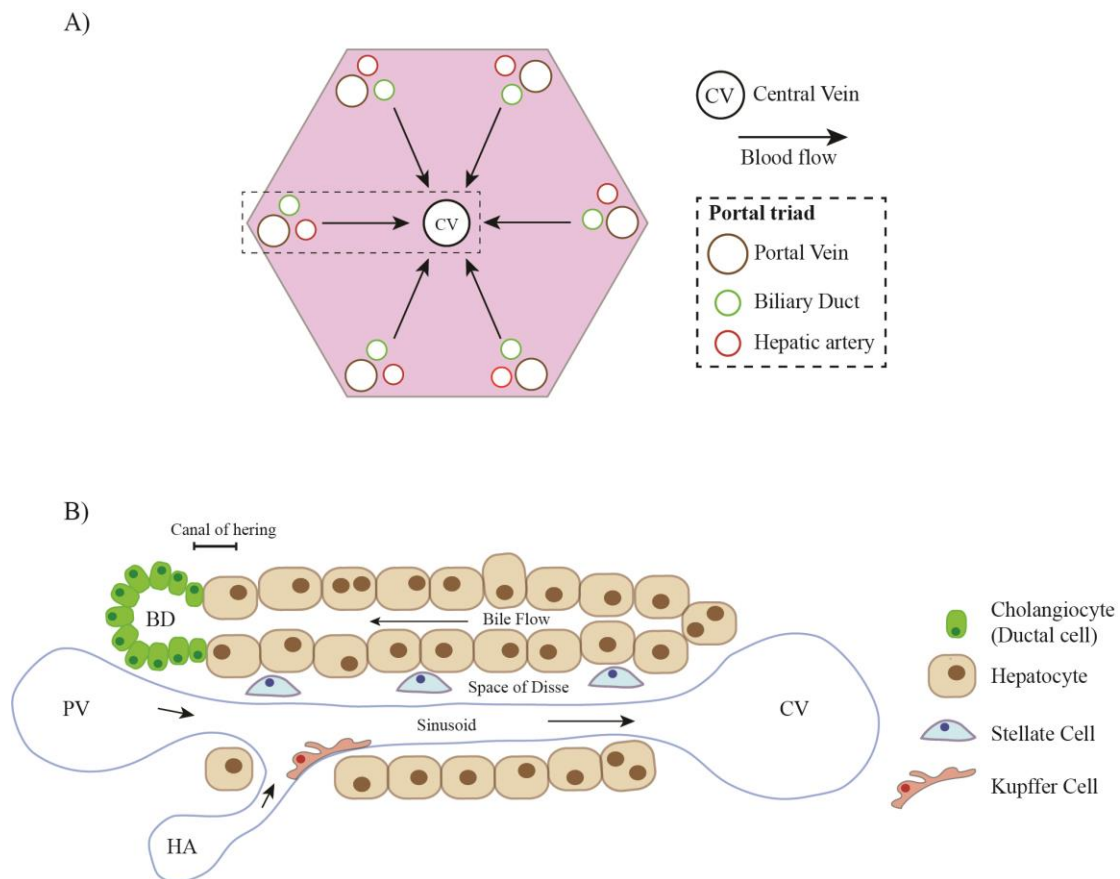


**Figure 1.1 – The structure of the hepatic lobule.** A) A schematic of the polygonal nature of the hepatic lobule. B) A schematic of the cross-section (indicated in dashed box in (A)) of the hepatic lobule showing the localisation of the resident cell types of the liver.

Ductal cells are ciliated cuboidal epithelial cells that form the bile ducts making up 3-5% of the liver and although significantly less metabolically active than

hepatocytes are essential for bile secretion (Kanno *et al.*, 2000). The hepatocyte compartment carries out production of bile itself and transports it through a specialised lumen in their apical membrane known as the bile canaliculus. Bile then moves to the bile ductules through the canal of Hering, before being transported to the gall bladder and ultimately reaching the small intestine via the common bile duct. However, the role of the bile duct is not limited to transport and ductal cells carry out several important modifications to the bile composition before secretion. For instance, ductal cells express the cystic fibrosis transmembrane regulator (CTFR) that facilitates the efflux of Cl<sup>-</sup> into the duct lumen (Cohn *et al.*, 1993). This in turn powers the HCO<sub>3</sub><sup>-</sup>/Cl<sup>-</sup> exchanger AE2, resulting in bicarbonate transport into the lumen. The overall effect on the bile is an increase in pH, which is crucial to neutralise acidic gastric fluid in the gut (Alpini *et al.*, 1996). The secretion of bile itself into the gut is crucial for the uptake of fat and fat-soluble metabolites, as well as providing a route to expel waste products such as excess bilirubin. More detailed metabolic roles of ductal cells and bile are reviewed in detail elsewhere (Boyer, 2013).

Kupffer cells are specialised macrophages that stand as guardians to protect against infection from bacteria rich blood originating from the gut. They make up 80-90% of the total macrophages in the body and thus underlines the liver's importance in the systemic innate immune system (Bilzer, Roggel and Gerbes, 2006). Furthermore, Kupffer cells are crucial for haemoglobin turnover as they are able to target defective blood cells or haemoglobin rich vesicles that fragment from the erythrocytes over time, facilitating recovery of haem and regulating the level of systemic haemoglobin, which has been shown to be a source of oxidative stress (Terpstra and van Berkel, 2000; Willekens *et al.*, 2005). Stellate cells are involved in storage of several metabolites such as vitamin A and lipids, as well as controlling the composition of the extracellular matrix (ECM) in the space of Disse (Wake, 1971). Interestingly, upon damage, stellate cells activate to a myofibroblast like state and are responsible for the production of fibrotic collagen (Mederacke *et al.*, 2013; Iwaisako *et al.*, 2014; Tsuchida and Friedman, 2017). Harmony between all cell types within the hepatic lobule described above is required for efficient liver function with each performing specialised roles.

In order to work efficiently, the liver takes advantage of significant intercellular and intracellular heterogeneity and therefore, tight homeostatic and regenerative pathways are required to maintain the complex tissue organisation in the face of damage or cellular stress.

## 1.2 Liver homeostasis and regeneration

Throughout life a delicate balance needs to be struck between proliferation and cell death. The proliferative burden of an organ is largely dependent on the cellular turnover. Hepatic cellular turnover in rats was elegantly measured by following the incorporation of  $H^3$  into hepatic nuclei after a pulse of tritiated-thymidine showing a cellular lifespan of between 200 and 400 days (MacDonald, 1961). Considering a lifespan of a rat is three years the liver may only self-renew ~3 times throughout the duration of the animal's life. More recent studies, taking advantage of lineage tracing strategies to follow either *Sox9*<sup>+</sup> ductal cells or *Axin2*<sup>+</sup> central vein hepatocytes without damage have shown that each cell type is restricted to their respective compartments (B D Tarlow, Finegold and Grompe, 2014; Wang *et al.*, 2015). Taken together, in the absence of damage, the liver epithelium is supported by slow self-renewal within each epithelial compartment.

However, the relative quiescence of the liver hides a raft of regenerative potential in response to damage powered by extensive plasticity within the epithelial compartment (Aloia, Mckie and Huch, 2016). Although the unique regenerative capacity of the liver was first immortalised in the eternal torture of Prometheus from Greek mythology, it was validated and came to prominence in modern science through the seminal work of Higgins and Anderson (1931) (Higgins, Anderson, 1931). They were instrumental in characterising partial hepatectomy (PHx) procedures where up to 60% of the liver is removed. Remarkably, after such a surgery the liver is able to regenerate lost tissue volume and rescue liver function within days. This rapid regeneration is facilitated by an elegantly orchestrated pattern of compensatory proliferation in all resident cell types of the liver (Michalopoulos and DeFrances, 1997). Early studies followed proliferation by autoradiography and found that hepatocytes were the first to proliferate after PHx with a peak of proliferation after 24 hours, followed by the other cell types such as the ductal cells and sinusoidal cells (Grisham, 1962; Rabes *et al.*, 1976). It is important to note that during this potent regenerative response that occurs in recovery from PHx the liver does not regrow the removed lobes, but rather the remaining healthy lobes increase their size and capacity to compensate the lost function of the resected lobes (Taub, 2004). Therefore, regeneration after PHx is largely response from healthy tissue to a gross change in organ size. Indeed, this effect can be both positive and negative, as studies have shown that while transplants

from smaller animals to larger animals result in the donor organ growing in size transplants from larger animals to smaller animals results in a decrease in donor liver size after xenograft (Francavilla *et al.*, 1988; Starzl *et al.*, 1993). This remarkable ‘hepatostat’ function that maintains liver size as a proportion of body size may provide interesting insights for surgical applications but does not reflect the regenerative response characteristic of acute or chronic liver pathologies (Miyajima, Tanaka and Itoh, 2014; Cordero-Espinoza and Huch, 2018).

The liver has a prominent role in the detoxification of toxins produced within the body as well as exogenous factors. This coupled with the high metabolic load of hepatocytes leads to high cellular stress. Elevated levels of such damage lead to pathologies such as non-alcoholic fatty liver disease and liver cirrhosis which together form a significant clinical burden (Lim and Kim, 2008; Asrani *et al.*, 2013). In cases of toxic damage, the liver can regenerate through an emergent stem/progenitor cell with atypical ductal morphology, classically referred to as the oval cell, able to proliferate and differentiate into both hepatocytes and ductal cells (Evarts *et al.*, 1987, 1989). The oval cell was first identified and characterised after hepatotoxic oncogenic treatments in rats that severely compromised the hepatocyte compartment (Farber, 1956; Solt, Medline and Farber, 1977; Shinozuka *et al.*, 1978).

The existence and cellular source of the bi-potent progenitor pool has been a controversial issue over the past three decades. The extensive proliferative potential of hepatocytes evident after PHx suggests that hepatocytes may harbour stem cell capacity that could be the foundation of such an adult stem cell population. In line with this, early studies showed that hepatocytes had massive clonogenic potential. Taking advantage of a mouse model of hereditary tyrosinemia type I, leading to liver disease as a result of fumarylacetoacetate hydrolase deficiency (*Fah*<sup>-/-</sup>), Overturf and colleagues were able to show that only 1000 normal hepatocytes were required to repopulate a diseased liver and restore normal liver function in mice (Overturf *et al.*, 1996). A subsequent study by the same group then pushed this substantial ability by serially transplanting normal hepatocytes into 6 sequential *Fah*<sup>-/-</sup> hosts ultimately showing that hepatocytes could undergo 69 cell divisions, similar to that of a haematopoietic stem cell (Overturf *et al.*, 1997).

With the advent of lineage tracing technology more recent studies attempted to identify and characterise the molecular and differentiation potential of any facultative hepatocyte stem cell. Interestingly, in a similar manner to their metabolic potential,

hepatocytes are heterogeneous in their stem cell function. One study labelled the hepatocyte compartment by repopulating a diseased liver (*Fah*<sup>-/-</sup>) with fluorescently labelled but otherwise normal hepatocytes and after chemical damage found labelled ductal cells suggesting that hepatocytes harbour a capacity of regeneration through a bi-potent progenitor mechanism (Tarlow *et al.*, 2014). Furthermore, a periportal hepatocyte population expressing some ductal markers such as *Sox9* was identified and these were termed hybrid hepatocytes. Lineage tracing from these hybrid hepatocytes after damage showed that they were bi-potent and could repopulate both the ductal and hepatocyte compartment (Font-Burgada *et al.*, 2015). A larger but likely overlapping periportal *Mfsdf2*<sup>+</sup> hepatocyte population was also identified that shared similar characteristics to the earlier characterised hybrid hepatocytes (Pu *et al.*, 2016). A further unipotent hepatocyte stem cell population was identified surrounding the central vein, the hepatocytes were found to be responsive to Wnt and expressed *Axin2*. The *Axin2*<sup>+</sup> population was shown to be integral in the slow homeostasis of the hepatocyte compartment only (Wang *et al.*, 2015). Furthermore, a recent subsequent study has shown that after central vein specific liver damage an emergent mid-lobular *Axin2*<sup>+</sup> population drives hepatocyte regeneration (Zhao *et al.*, 2019). Finally, a population of hepatocytes that are distributed across all lobular regions that express high levels of telomerase reverse transcriptase (TERT) have been shown to support hepatocyte homeostasis and regeneration in response to damage (Lin *et al.*, 2018).

In summary, there is a growing body of evidence that the hepatocyte compartment has the capacity not only to maintain its own homeostasis but upon damage to facilitate the regeneration of both hepatocytes and ductal cells. They are therefore good candidates to be the foundation of a bi-potent progenitor regenerative response.

However, this proved to be only half the story as early experiments by Farber treating rats with carcinogens that drastically impaired hepatocyte function, either in isolation or in conjunction with PHx identified an emergent population of cells with atypical ductal morphology that were described as “small oval cells” (Farber, 1956; Evarts *et al.*, 1989; Fausto and Campbell, 2003). The cell population from then on coined as oval cells, was found to arise near the ducts of the liver, specifically the canals of Hering, and could be a potential alternative cellular source for liver regeneration. However, despite the early identification of oval cells and their potential regenerative capacity their biology and significance in liver regeneration has only started to become

clear over the last twenty years with the advent of *in vitro* cell culture techniques as well *in vivo* cell tracing by lineage tracing.

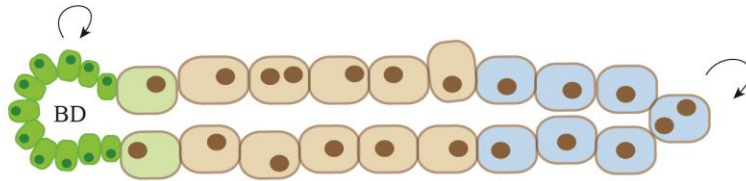
Several groups demonstrated the regenerative capacity of oval cells by identifying and isolating of the ductal progenitors using *in vitro*. Two studies identified that Epithelial Cell Adhesion Marker (EpCAM) and CD133 (*Prom1*) marked a ductal population that act as bi-potent oval cells when transplanted in the injured liver (Rountree *et al.*, 2007; Yovchev *et al.*, 2007; Suzuki *et al.*, 2008) Furthermore, *Lgr5* was found to be expressed upon liver damage and upon isolation cells were grown as 3D organoids maintaining their bi-potential capacity *in vitro* and *in vivo* (Huch, Dorrell, *et al.*, 2013). Despite identification and isolation of ductal bi-potent cells *in vitro*, their lineage potential *in vivo* during liver damage was not answered by these studies and has remained in question. Further doubt was cast on the significance of oval cells through several studies that followed the fate of ductal cells after damage by labelling all ductal cells or conversely, marked the whole hepatocyte compartment to identify emergent unmarked cells which originate from non-parenchymal cells found that there was no contribution to the hepatocyte pool from the ductal compartment. Together suggesting the *in vitro* progenitor capacity of oval cells described by the studies above could be an artefact of *in vitro* culture and do not represent a bona fide progenitor population *in vivo* (B. D. Tarlow, Finegold and Grompe, 2014; Schaub *et al.*, 2014; Yanger *et al.*, 2014).

However, most recently these conflicting studies have been reconciled by three seminal studies which found that the cellular context during liver damage was crucial for oval cell function. By taking advantage of novel genetic models and modes of liver damage the studies were able to severely compromise the hepatocyte compartment which led to drastic inhibition hepatocyte proliferation. This ultimately proved key to unlocking the oval cell's regenerative capacity *in vivo*. Hepatocyte impairment was carried out by either hepatocyte specific genetic ablation of *Mdm2* or  $\beta$ 1-Integrin, hepatocyte specific overexpression of *p21*, or by severe chronic damage by 3,5-diethoxycarbonyl-1,4-dihydrocollidine (DDC) treatment. *Mdm2* is an E3 ubiquitin ligase responsible for the degradation of TP53 and in its absence there was shown to be wide spread apoptosis and senescence in the hepatocyte compartment resulting in the rapid activation of ductal derived progenitors that repopulate the hepatocyte pool (Lu *et al.*, 2015). In a similar manner liver damage combined with hepatocyte specific deletion of  $\beta$ 1-Integrin, which results in impaired signalling through the epidermal growth factor (EGF) and hepatocyte growth factor (HGF) pathways (Speicher *et al.*,

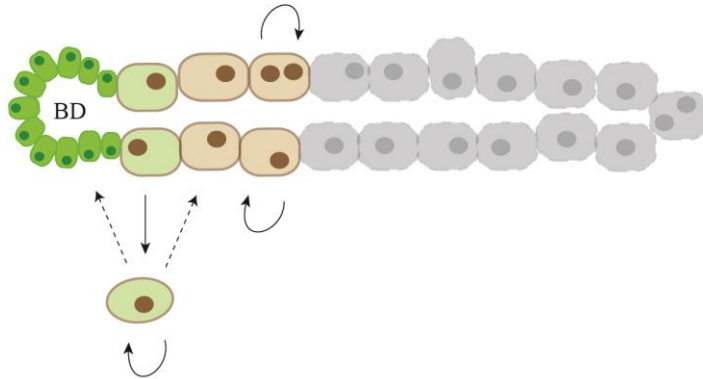
2014), resulted in significant ductal contribution to the hepatocyte compartment. Interestingly, liver damage combined with hepatocyte specific over expression of *p21* which is a hallmark of non-alcoholic steatosis and chronic hepatitis C infection (Marshall *et al.*, 2005; Richardson *et al.*, 2007), resulted in a similar significant ductal contribution to hepatocyte regeneration. Finally, it was shown that massive chronic DDC induced liver damage without any genetic alteration resulted in the activation of ductal derived bi-potent progenitors (Deng *et al.*, 2018). Shorter DDC damage experiments did not result in the same ductal progenitor activation suggesting that hepatocyte impairment must be severe for the ductal bi-potent cell response.

Since the first description of liver regeneration it has become clear that the epithelial compartment is highly plastic, and that the regenerative response is determined by the mode, severity and cellular context of the liver damage (summarised in Figure 1.2). It is only in the most severe cases of liver damage (where the hepatocyte compartment is impaired from division or its proliferative capacity is exhausted) that a ductal bi-potent progenitor becomes activated to facilitate repair. Considering that such an extensive failure of the hepatocyte compartment is a common feature of chronic liver diseases in the clinical setting, understanding how the activation of ductal progenitors is regulated might provide insights into new treatment strategies for liver disease.

A) Homeostatic liver



B) Acute chemical/physical damage - Hepatocyte compartment viable



C) Chronic chemical damage - Hepatocyte compartment compromised

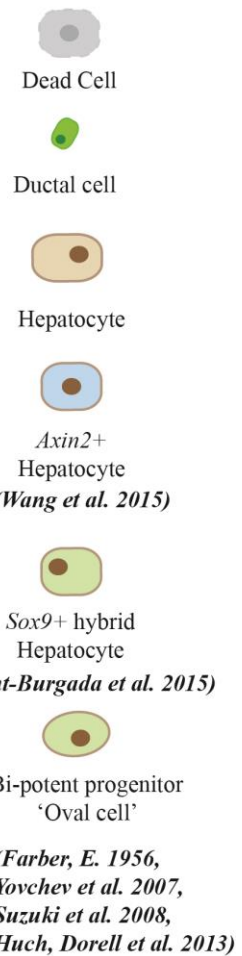
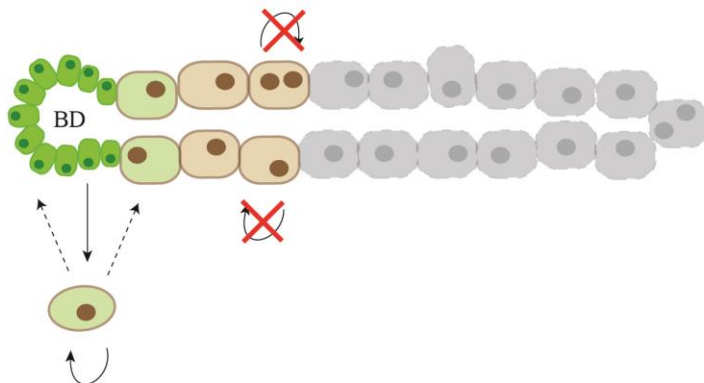


**Figure 1.2 – The liver demonstrates several modes of regeneration in a damage and cellular context dependent manner.** A) During homeostasis the liver is maintained by slow division of mature cell types. B) In response to acute chemical or physical damage liver regeneration is facilitated by increased proliferation in mature cell compartments or in some cases by specialised hepatocyte populations such as the *Sox9*<sup>+</sup> hybrid hepatocyte. C) After chronic damage where hepatocytes are unable to proliferate a ductal progenitor emerges which can repopulation the hepatocyte and ductal compartments.

### 1.3 Modelling adult stem cell function

Since the first descriptions of liver adult stem/progenitor cells there has been extensive study in the field leading to the characterisation of many animal models of liver damage enabling investigation of several aspects of their involvement in the liver's regenerative response (described in section 1.2). However, studies into the regulation of ductal regeneration have been hampered by the lack of faithful *in vitro* models. A solution has arisen over the past decade with the introduction of three-dimensional (3D) culture systems that have revolutionised the study of adult stem cell dynamics and function. Such culture systems allow the growth of both adult pluripotent (embryonic or otherwise induced) and neonatal stem cells into an organoid culture. Organoids are defined as a 3D cell structure that intrinsically assemble into defined organised patterns that resemble or at least recapitulate some of the features of the organ of origin (Huch and Koo, 2015).

Liver organoids can be derived from both adult and embryonic stem cells that ultimately affect the system's role and function. Accordingly, hepatoblasts have long been the subject of intense study as the embryonic bi-potent cell population responsible for the generation of both hepatocytes and ductal cells making them excellent targets for study (Miyajima, Tanaka and Itoh, 2014; Gordillo, Evans and Gouon-Evans, 2015). Hepatoblasts arise from the ventral foregut at the same time as the emergent pancreas at E8.5 of mouse development (Rodríguez-Seguel *et al.*, 2013). The developing liver is segregated from nascent pancreatic precursors via a tightly regulated concentration gradient of FGF and BMP laid down by the mesoderm (Gualdi *et al.*, 1996; Rossi *et al.*, 2001). The higher concentrations of FGF and BMP define hepatic specification, whereas precursors in lower concentrations are destined for a pancreatic fate (Deutsch *et al.*, 2001; Serls *et al.*, 2005). After specification the nascent hepatoblasts follow a precise set of cues in order to mature and form the foetal liver. At E9.5 there is a migration of hepatoblasts into the septum transversum mesenchyme that requires signalling from developing endothelial cells (Matsumoto *et al.*, 2001). This migration leads to the formation of the liver bud from which the foetal liver forms. As the liver parenchyme develops it receives mitogenic signals in the form of HGF, MidKine and Pleiotropin that facilitate growth of the hepatoblast compartment (Onitsuka, Tanaka and Miyajima, 2010). CD49f/Thy1<sup>+</sup> mesenchymal cells then directly contact the hepatoblasts to drive further maturation (Hoppo *et al.*, 2004). There is also evidence

that blood cells present in the liver as a result of its role in haematopoiesis during development provide signals via oncostatin M that promote hepatocyte fate (Kamiya *et al.*, 1999; Matsui *et al.*, 2002).

By mimicking the cell signals that drive hepatoblast development it has been possible to direct induced pluripotent stem cells to hepatic fate and then derive both ductal cells and hepatocytes in 3D culture systems (Snykers *et al.*, 2009; Sampaziotis *et al.*, 2015). It has also been shown that rather than mimicking chemical signals it is possible to drive liver development of induced pluripotent stem cells in a dish via co-culture with mesenchymal and endothelial cells. This remarkable organoid culture system rapidly self-organises into a liver bud like structure with evidence of hepatic function once ectopically transplanted into animal hosts (Takebe *et al.*, 2013). Despite the remarkable capacity of these models to generate tissue for future cell therapy strategies, they do not model the bi-potent liver stem cell directly. Instead these models only transiently exhibit a hepatoblast fate before differentiating into mature cell types. It may be possible to adjust these models to provide the correct signalling to capture a hepatoblast population and indeed several groups have described conditions in which hepatoblast like cells can be cultured (Tanimizu *et al.*, 2003, 2004; Takayama *et al.*, 2013). Although these studies may provide useful models of hepatoblast function, they are unlikely to persist postnatally and are not the bi-potent population emergent after liver damage (Hindley, Cordero-Espinoza and Huch, 2016). Therefore, understanding their regulation may have limited application beyond the embryo.

Capturing the adult liver progenitor state was first described through the isolation of the emergent *Lgr5*<sup>+</sup> population upon toxic liver damage (Huch, Dorrell, *et al.*, 2013). These progenitors were grown in a 3D Matrigel matrix in media supplemented with EGF, HGF, FGF and Rspodin1. Rspodin1 is the *Lgr5* ligand and results in increased sensitivity to the Wnt pathway. The *Lgr5*<sup>+</sup> cells once isolated and grown in the 3D conditions organise into cystic organoid structures with a single cell layer epithelium. They were found to express markers of progenitor (*Lgr5*, *Trop2*, *Tbx3*), ductal (*Krt19*, *Epcam*) and hepatocyte (*Ttr*, *Hnf4a*) fates. Remarkably induction of liver damage was not required for organoid derivation, and the study also showed that placing an isolated ductal tree fragment into culture resulted in molecularly indistinguishable organoids. This crucial experiment showed that ductal cells have the capacity to form *Lgr5*<sup>+</sup> progenitors and that the culture conditions are enough to model the signalling in the activation of the progenitor state after liver damage *in vitro*. A

subsequent study then showed that with little modification the isolation of single EpCAM<sup>+</sup> ductal cells from healthy human liver biopsies were able to grow into organoids that were phenotypically similar to the mouse equivalents (Huch *et al.*, 2015). This highlights the innate ductal capacity to acquire a progenitor fate.

In order to truly model adult stem cell behaviour the liver organoid cultures described by Huch *et al.* needed to satisfy two criteria to fulfil the role of a stem cell: (1) the ability to self-renew; and (2) the ability to differentiate into the function cells of the tissue of origin (Lajtha, 1979). In the original studies organoid cultures were grown in culture for up to 1 year whilst maintaining genetic stability, thus fulfilling the self-renewal criteria (Huch, Dorrell, *et al.*, 2013; Huch *et al.*, 2015). Once switched to defined culture conditions, which involved the inhibition of the notch and TGF- $\beta$  pathways and the addition of BMP-7 for human cultures, the liver organoids could differentiate towards the hepatocyte fate. These differentiated organoids could also be transplanted into *Fah*<sup>-/-</sup> mice and fully mature to functional hepatocytes *in vivo*. This shows that ductal derived organoids are able to differentiate into both mature epithelial cell types of the liver fulfilling the second criteria for *bona fide* adult stem cells.

An important feature of adult ductal derived liver organoids is stability of the progenitor state *in vitro*. The organoids remain bi-potent and proliferative and don't freely differentiate until induced. Taken together with the fact that we can activate the progenitor state from otherwise healthy ductal tissue means we can elegantly dissect the mechanisms of ductal progenitor activation and differentiation by manipulating culture conditions. These features highlight the power of liver organoids as a model of ductal progenitors and a tool to study their dynamics.

Recently two groups described the derivation of 3D liver organoids from primary mouse and human hepatocytes (Hu *et al.*, 2018; Peng *et al.*, 2018). Remarkably, the hepatocyte organoids were able to be expanded long term as well as differentiate into both hepatocytes and ductal like cells. Hence hepatocyte organoids exhibit similar stem cell capacity as ductal organoids. It is perhaps not surprising that organoid systems have been derived from both hepatocytes and ductal cells due the heterogeneous and plastic nature of liver regeneration (described in section 1.2), where there is extensive evidence of both ductal and hepatocyte compartments having progenitor capacity (Choi *et al.*, 2014; Tarlow *et al.*, 2014; Yanger *et al.*, 2014; Font-Burgada *et al.*, 2015; Lu *et al.*, 2015; Raven *et al.*, 2017). In line with this, the hepatocyte organoid gene expression profile has been shown to closely resemble that

of proliferating hepatocytes after PHx. Furthermore, the culture conditions of the hepatocyte organoids are remarkably similar to their ductal derived counterparts. Hepatocyte organoids and ductal organoids are grown with EGF, FGF, HGF and Rspodin1 with hepatocyte organoids needing further activation of the WNT and TNF- $\alpha$  pathways. This significant overlap suggests that the hepatocyte or ductal derived progenitor population rely on very similar signalling to support their expansion.

In any case with the advent of 3D organoid culture techniques there are now excellent models of both hepatocyte and ductal liver progenitors that will allow investigation of their dynamics. During our studies we have focussed on ductal organoids as a model of ductal driven liver regeneration specifically and further mention of liver organoid culture within this document will refer to the ductal derived organoids characterised by Huch and colleagues.

As with any model system liver organoids are simplified representations of aspects of liver regeneration that help us to answer more complicated biological questions (Mead and Karp, 2019). Therefore, it is important to discuss the limitations of organoids as a model in order to properly design experiments and understand their results (Huch *et al.*, 2017). For instance, liver function and regeneration (see chapters 1.1 and 1.2) are dependent on several different cell types. However, organoids only represent the ductal component in isolation, therefore, can only be used to study ductal cell biology. It could be argued as you are able to differentiate the ductal organoids to a hepatocyte-like fate you are also able to model hepatocyte function. While this differentiation capacity was shown by Huch and colleagues, the emergent hepatocyte-like population are unlikely to represent truly mature hepatocytes as are found *in vivo* (Huch, Dorrell, *et al.*, 2013). Following, it was shown ductal organoid derived hepatocytes are unable to fully repopulate *Fah*<sup>-/-</sup> mouse livers, a process that was shown to be highly efficient when using fully mature hepatocytes. It may be possible to refine the differentiation protocol to fully recapitulate hepatocyte differentiation but even in this case the organoids would not be able to model the other niche or stromal components of the liver. Taken together, in their current state organoids are suited to be used as a hypothesis generating tool for studying cell intrinsic functions of ductal cells.

Another important factor to discuss is how comparable the culture conditions are compared to what ductal cells may encounter physiologically. Liver organoids are grown in media rich in growth factors such as EGF and FGF as well as high levels of

WNT agonists. In addition to these soluble factors the organoids themselves are grown in an extracellular matrix generated from mouse sarcoma cells called “Matrigel”, the components of which are poorly defined. These conditions are vastly pro-proliferative so we must be wary that liver organoids could be an artificial cell population that superficially resembles *in vivo* ductal progenitors born out these highly specific culture conditions (Reya and Clevers, 2005; Scaltriti and Baselga, 2006; Ornitz and Itoh, 2015). On the other hand, it is important to note that the culture conditions were not chosen for their proliferative properties but rather due to the involvement of the invoked signalling pathways in liver development and regeneration. For instance, recently it was shown that in response to liver damage that central vein endothelial cells become a potent source of WNT ligand, which helps to drive proper regeneration (Wang *et al.*, 2015). Therefore, the growth conditions of organoids attempt to mimic the extracellular cues that are active during liver regeneration and that drive ductal progenitor activity essentially replacing the niche cell signalling.

Liver organoid culture is a developing technology which can provide great insights into liver biology. However, as explained above there are limitations and as a model it is a vast simplification of the properties of *bona fide* ductal progenitors. Although, this does not mean they are not useful, only that those limitations need to be accounted for. In this work, we make use of the vast advantage of liver organoids being an *in vitro* system amenable to high throughput analysis to screen for potential regulators and pathways involved in ductal driven regeneration. Crucially, we then attempt to validate those candidates in animal models of regeneration in order to validate and learn the physiological role of the candidate in question. Therefore, we can avoid spurious conclusions generated as a result of some aspect of the model whilst maintaining the massive benefit of the *in vitro* organoid system.

## 1.4 Epigenetic regulation of chromatin accessibility and cell fate

Throughout this work we have focussed on understanding the epigenetic regulators involved in the activation of ductal progenitors in response to liver damage. To set the scene I will give a brief description of the field of epigenetics before discussing the motivation and reasoning for focussing on epigenetic mechanism. The seminal work by Watson, Crick and Franklin characterised the double helix structure of DNA and its capacity to store information, thus giving birth to the 'central dogma' of modern biology (Watson and Crick, 1953). The theory states that information stored in DNA is transcribed into transient RNA molecules which are further translated to functional proteins (Crick, 1970). The regulation and machinery behind these processes has been the subject of intense study since the central dogma was first postulated. However, it rapidly became clear that the linear flow of information could not wholly explain gene regulation and that there were significant interactions between proteins/RNA and the genome that were required to facilitate gene expression changes, going against the flow of information originally postulated in the central dogma (Chen *et al.*, 2017). As a result, scientists began to study how modification of DNA and its associated proteins affect gene expression, developing the field of epigenetics.

DNA is made up of three main structural features: (1) the negatively charged phosphate backbone; (2) a deoxyribose; (3) and a base. Together these form the functional unit of DNA - the nucleotide (Levene, 1919). There are four different bases found in DNA: Guanine (G); Adenine (A); Thymine (T); and Cytosine (C). There is also a fifth base exclusively found in RNA - Uracil (U). The human genome is a linear string DNA sequence formed through phosphodiester linkages between the phosphate backbone of one nucleotide to the deoxyribose of the preceding nucleotide (Travers and Muskhelishvili, 2015). The double helical nature of the DNA is facilitated by Watson-Crick base pairing between bases G-C and A-T that bring two complimentary DNA strands together (Chargaff *et al.*, 1951; Watson and Crick, 1953).

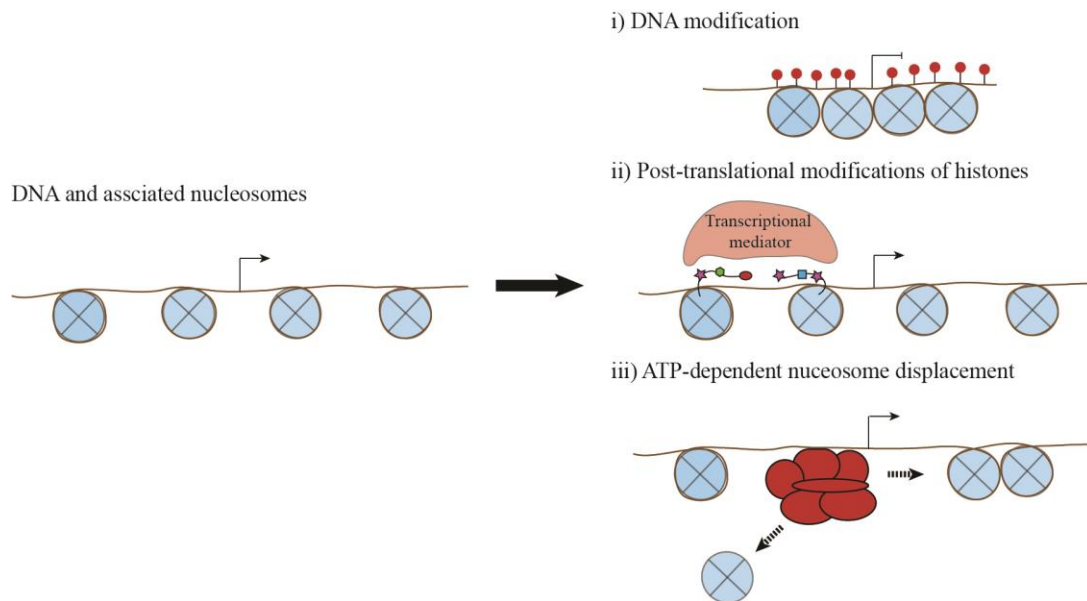


**Figure 1.3 – Epigenetic methods of gene regulation.** A schematic demonstrating the three main methods of epigenetic regulation: (1) DNA modification; (2) post-translational modification of histones; and (3) ATP-dependent histone reshuffling.

An average eukaryotic cell contains roughly 2m of DNA, to store such a large linear molecule inside a nucleus the DNA must undergo a high level of packing and compaction. At the lowest level of organisation 147 bp of DNA is wrapped around an octamer of histone proteins which together form nucleosomes (Kornberg, 1974; Richmond and Davey, 2003). Each histone octamer is made up of two of each of the four histone monomers H2A, H2B, H3 and H4. Histone proteins have a unique structure with a positively charged N terminal tail domain which is enriched in arginine and lysine residues (Phillips and Johns, 1965). The positive charge of histones is crucial to bind with the negatively charged DNA backbone. The further linker histone H1 can bind the DNA in between nucleosomal units and helps form higher order nucleosome arrangements such as chromatin fragments and ultimately the 3D organisation of chromosomes (Kornberg and Lorch, 1999). The level of packing at specific genomic loci will affect the accessibility of those regions and thus will have a drastic effect on gene expression. For instance, having a tightly packed enhancer region or transcriptional start site (TSS) will stop the efficient binding of transcription factors (TFs) or the transcriptional machinery to the respective gene and reduce its expression (Knezetic and Luse, 1986; Lorch, LaPointe and Kornberg, 1987; Kireeva *et al.*, 2005; Bondarenko *et al.*, 2006).

Epigenetics is the study of the modifications that alter the chromatin accessibility at specific genomic loci and modulate gene expression. These epigenetic modifications can either be directly on the DNA or affect the associated chromatin proteins, but crucially they do not alter the DNA sequence. There are broadly three categories of modification: (1) deposition of chemical DNA modifications; (2) post-translational modification of histones; (3) and nucleosome rearrangements and depletion. Each type of modification will have dedicated proteins or protein complexes that write, read and erase the specific modification in response to external stimuli, facilitating a dynamic system of gene regulation.

The most abundant chemical modification of DNA in humans is methylation. This involves the covalent addition of a methyl group to the cytosine ring most commonly generating 5-methylcytosine (5mC). Modified cytosines are largely found in the context of CG dinucleotides called CpG sites, 80% of CpG sites are methylated in the human genome (Ehrlich *et al.*, 1982). Methylation of CpG sites and promoter regions enriched in CpG sites (referred to as CpG islands) is heavily associated with gene silencing (Bird, 2002). The mechanism by which this happens is context dependent and as such is not fully understood (Miranda and Jones, 2007). For instance, in some cases where TFs bind CpG islands, methylation can reduce their binding efficiency. This was shown to be the case for *c-myc*, a TF associated with proliferation and a prominent oncogene, where DNA methylation inhibits *c-myc* binding and action (Prendergast, Lawe and Ziff, 1991). Perhaps the most prominent mechanism of methylation mediated gene repression is through modulation of the adjacent histone modifications. Promoters permissive for transcription are usually associated with nucleosomes with lysine 4 of histone H3 (H3K4) methylated. Methylation of CpG islands has been shown to inhibit the binding of H3K4 methyltransferases and therefore stop the generation of the permissive modification (Birke *et al.*, 2002; Ayton, Chen and Cleary, 2004; Lee and Skalnik, 2005). Furthermore, a family of methyl-binding proteins (MBP) exists which include MeCP2, MBD1, MBD2 and MBD3 that can bind methylated CpG sites (Hendrich and Bird, 1998; Hendrich *et al.*, 1999). Their mode of action is not wholly understood, however several MBPs have been shown to mediate repression by recruiting histone deacetylases and other co-repressors to methylated regions (Jones *et al.*, 1998; Nan *et al.*, 1998; Zhang *et al.*, 1999; Kondo *et al.*, 2005). Finally, DNA methylation can affect nucleosome positioning and depletion. Promoter regions of actively expressed genes are often depleted of nucleosomes facilitating

efficient binding of the transcriptional machinery. Studies have shown that DNA methylation results in increased histone occupancy in such nucleosome depleted regions (NDRs) resulting in reduced gene expression (Davey, Pennings and Allan, 1997; Patel, Graunke and Pieper, 1997). The underlying mechanism is a subject of study, but it has been shown that MeCP2 can bind chromatin remodelling proteins such as *Brahma*, the catalytic subunit of the SWI/SNF remodelling complex (Harikrishnan *et al.*, 2005). As a result, MeCP2 may target methylated regions for remodelling by recruiting remodelling complexes.

In mammals, DNA methylation is carried out by a family of DNA methyltransferases (DNMTs) which take advantage of *S*-adenosyl-methionine to provide methyl- groups. DNMT1 is largely concerned with the maintenance of DNA methylation by preferentially binding hemi-methylated DNA generated through cell division (Bestor, 1992; Pradhan *et al.*, 1999). On the other hand, *de novo* methylation is carried out by DNMT3a and DNMT3b (Okano, Xie and Li, 1998; Hsieh, 1999; Okano *et al.*, 1999). A catalytically inactive family member also exists (DNMTL) which is not directly involved in methylation but may provide a mechanism of targeting regions to be methylated. DNMTL can bind both DNMT3a and unmethylated H3K4 (a mark of inactive genes) suggesting that it can target Dnmt3a induced methylation to inactive genes (Jia *et al.*, 2007; Ooi *et al.*, 2007).

DNA can become unmethylated either passively or actively. Passive demethylation is reliant on the fact that the genome wide methylation pattern is not maintained during DNA replication with the new strand of DNA being bereft of any methylation. As mentioned above DNMT1 with its binding partner UHRF1 replaces the lost methylation (Bostick *et al.*, 2007; Sharif *et al.*, 2007). Active demethylation has recently become a prominent new mechanism with the characterisation of the ten-eleven translocation (Tet) family of genes. The family is made up of three members (*Tet1*, 2 and 3) which all can oxidise 5mC primarily to 5 hydroxymethylcytosine (5hmC) and further oxidative products in a stepwise fashion (Tahiliani *et al.*, 2009). The oxidative products of 5mC can then be removed through cell division or a base excision repair (BER) dependent mechanism (Rasmussen and Helin, 2016). The function and physiological role of the Tet family will be discussed in detail in section 1.5.

DNA methylation has a wide range of physiological roles, from inactivation of x-linked genes to stable silencing of genomic mobile elements such as transposons and

viral elements (Mohandas, Sparkes and Shapiro, 1981; Woodcock *et al.*, 1997; Walsh, Chaillet and Bestor, 1998; Bourc'his and Bestor, 2004; Hellman and Chess, 2007). Perhaps the most prominently studied role of DNA methylation is the massively dynamic CpG methylation that occurs during mammalian development (Hemberger, Dean and Reik, 2009). There are two major phases of global demethylation: right after fertilization as the emergent zygote goes through early pre-implantation development to the morula stage; and a second wave between E10.5 and E13.5 during primordial germ cell specification (Rougier *et al.*, 1998; Lee *et al.*, 2002; Santos *et al.*, 2002; Hajkova *et al.*, 2008). In both cases the global demethylation is crucial to facilitate totipotent and pluripotent states in the developing embryo (Surani, Hayashi and Hajkova, 2007). In line with this it has been shown that DNA methylation is crucial in reprogramming fully differentiated cells into induced pluripotent stem cells (Simonsson and Gurdon, 2004; Mikkelsen *et al.*, 2008). DNA methylation is essential for lineage restrictions during development and to reverse or change cell fate the methylome must be erased or modulated via demethylation.

As explained above, histone octamers are the foundation for the fundamental units of DNA organisation, therefore, it is not surprising that post translational modification of the histone monomers can drastically alter the chromatin organisation and modulate gene transcription. Histones can be methylated, phosphorylated, acetylated, sumoylated, ubiquitinated, ADP ribosylated and deiminated at a wide array of positions in each of the four monomers (Li, Carey and Workman, 2007). The combination of modifications within one histone or nucleosome forms a histone code that will recruit activators or repressors of transcription as well as chromatin remodellers to modulate gene transcription. The effect of specific histone modifications can be highly contextual based on the composition of the overall histone code. However, there are some well described modifications of gene activation and repression. Active genes are usually associated with mono- or tri-methylation of histone H3 lysine-4 (H3K4me1 or H3K4me3) and acetylation of lysine-27 (H3K27ac). Whereas silenced genes are associated with trimethylation of histone H3 lysine-27 and -9 (H3K27me3 and H3K9me3) (Bannister and Kouzarides, 2011).

The mode of action by which histone modifications can affect chromatin accessibility can be either: the chemical modification alters the interaction dynamics between the DNA and nucleosome; or the histone code will recruit certain modulators of gene transcription. For example, acetylation of a histone lysine will remove the

positive charge of the residue and thereby heavy acetylation may increase DNA accessibility by reducing the electrostatic attraction between the nucleosome and DNA (Reinke and Hörz, 2003). A case of this can be found in the promoter region of  $\beta$ -globin that has been shown to be associated with histones that are heavily acetylated resulting in an increased sensitivity to DNase activity. This suggests that a reduction in the positive nature of histones may cause DNA to dissociate from nucleosomes more easily and facilitate more transcription (Kiefer *et al.*, 2008). On the other hand, modulators of gene transcription can ‘read’ and bind to the histone code directly via a variety of specialised protein domains such as the Royal family, which include: chromodomains; tudor domains; and MBT domains. These domains are all specialised to bind methylated lysine residues (Maurer-Stroh *et al.*, 2003; Kim *et al.*, 2006). An example of a histone reader is heterochromatin protein 1 (HP1). It is recruited to H3K9me3 via its N-terminal chromodomain and once bound HP1 can then dimerise and facilitate higher order chromatin structure and repress gene expression (Bannister *et al.*, 2001; Lachner *et al.*, 2001).

Regardless of the mode of modulation the histone modifications themselves are deposited by a series of histone acetyltransferases (HATs), histone methyltransferases (HMTs), protein arginine methyltransferases (PRMTs), or removed by histone deacetylases (HDACs) and lysine demethylases (KDMs) (Bannister and Kouzarides, 2011). The activity of these ‘writers’ and ‘erasers’ are tightly controlled by external stimuli and facilitate the dynamic nature of histone modifications and resultant chromatin accessibility. These enzymes are often found as subunits of larger chromatin remodelling complexes such as the NuRD and Polycomb complexes (Zhang *et al.*, 1999; Basta and Rauchman, 2015; Chittock *et al.*, 2017).

The final level of epigenetic regulation is the gross movement of nucleosomes to increase or decrease chromatin accessibility (Saha, Wittmeyer and Cairns, 2006). Two major complexes involved in this task are the Switch/Sucrose non-fermentable (SWI/SNF) complex (also known as the BAF complex and discussed in more detail in section 1.6) and the Imitation switch (ISWI) complex. Both complexes work in a similar manner with a central ATP dependent subunit and several associated subunits that will direct the activity of the catalytic component (Vignali *et al.*, 2000). Both chromatin remodelling complexes have remarkably varied physiological functions, from development to splicing, and this is likely due to their diverse complex compositions which can specify different functions. For instance, *Snf2*, the catalytic

subunit of the ISWI complex, is essential for early embryonic development where genetic ablation results in failure to develop beyond E7.5 (Stopka and Skoultschi, 2003). Whilst *Brm*, one catalytic subunit of the BAF complex, has been shown to promote inclusion of variant exons of the *Cd44* gene by facilitating pausing of transcription elongation (Batsché, Yaniv and Muchardt, 2006).

Chromatin remodellers largely work either by replacing core histones with specific histone variants that alter the nucleosome dynamics or by increasing or decreasing nucleosome occupancy at specific genomic loci by nucleosome sliding or ejection. As an example, the SWR1 family of chromatin remodellers have been shown to be required for the exchange of histone H2 with the variant H2A.Z which creates a less stable nucleosome and can facilitate increased transcription of associated genes (Mizuguchi *et al.*, 2004).

It is important to note that each of these levels of epigenetic regulation do not work in isolation and there is significant cross talk, where gene modulation is usually facilitated by coordinated alterations of all modes of chromatin regulation discussed here. Therefore, for a cell to change fate either naturally through development or artificially through reprogramming, it requires the action of several regulators of chromatin accessibility (Hemberger, Dean and Reik, 2009).

As a result, the basic modes of epigenetic regulation as explained above provide powerful tools to facilitate significant changes in cell fate. Such examples of epigenetic regulation of cell fate and development are ample during embryogenesis an early development (Boland, Nazor and Loring, 2014). For instance, it was shown that histone modifications play a crucial role in the expression of key cardiomyocyte specific lineage markers in a time dependent manner. More specifically, cardiac lineage specific genes begin with high levels of the repressive H3K27me3 during pluripotency. However, as cardiac development progresses there is a gradual loss of H3K27me3 mediated repression leading to expression marked by concomitant increase in H3K4me3 (Paige *et al.*, 2012). This elegantly ensures the correct and one-way development and differentiation of cardiomyocyte tissue over time. However, despite several examples of epigenetic mediated cell fate changes in development the role of epigenetic players in the regulation of adult stem cell fate has remained poorly understood. This is likely down to two major factors, the lack of *in vitro* models of adult stem cell function and second being the lack of evidence that epigenetic state could be

transient and whether there were the pathways that could modulate chromatin in the adult in response to environmental cues.

In the first instance, the isolation and culture of murine embryonic stem cells in 1981 was a seminal moment for the study of development, as from a single cell population there was the potential to study the development of tissues of any of the three germ layers (Martin, 1981). Therefore, embryonic stem cells provided a model system allowing for the detailed dissection of the changes in chromatin state through development and the epigenetic players that control them. However, it has only been with the advent of organoid technology over the past decade that we have become able to model adult stem biology in the same way (Clevers, 2016). However, advance research has been further slowed by the fact that each adult stem cell population of interest requires their own specific organoid (or other *in vitro*) model system whereas much of development could be modelled starting from embryonic stem cells by altering the growth conditions (Murry and Keller, 2008). Furthermore, whilst there has been rapid development in this field and several different models of different adult stem cell populations there is no guarantee that all different regenerative tissues could be modelled in such an *in vitro* system (Clevers, 2016). In any case, the development of organoids to model adult stem cells has allowed us to probe their biology and begin to investigate how epigenetic regulators, which have such prominent roles during development, can also be involved in adult systems of regeneration.

The second barrier to the study of epigenetics has been somewhat down to the lack of knowledge surrounding the mechanisms that allow chromatin state to change dynamically in response to signalling in the adult. Classically epigenetic regulation has been seen as a mechanism of stable lineage commitment during development. For example, the dosage of genes on the x chromosome needs to be tightly controlled, those with the XX genotype must express half the amount of X-linked genes as compared to those with a single X chromosome in order to develop correctly. This is achieved through an epigenetic mechanism where long non-coding RNA *XIST* interacts with a single X chromosome of an XX pair in a random manner. *XIST* can then recruit the Polycomb repression complex 2 (PRC2) to mediate genetic repression (Boland, Nazor and Loring, 2014). This repressive epigenetic state is stable and is inherited throughout development. However, it is now clear that the chromatin state as a static arrangement is wrong, and the chromatin landscape is extremely dynamic and there are epigenetic pathways that allow tight regulation throughout development and into the adult. For

instance, dynamic histone modification has been shown to be crucial for the correct cyclical nature of mammalian hair follicle stem cell growth. *Ezh2*, a component of PRC2 and H3K27me3 methyltransferase is essential for proper hair follicle stem cell proliferation. Loss of *Ezh2* leads to increased expression of cell cycle inhibitors and concomitant decreased stem cell proliferation (Tarayrah and Chen, 2013). Moreover, beyond the better functional understanding of dynamic epigenetics there have also been significant developments in the knowledge surrounding the epigenetic regulators themselves. For instance, the Tet family of genes was only first discovered in 2009 before which it was thought that the only method of DNA demethylation was passively by DNA replication (Tahiliani *et al.*, 2009). However, the discovery of the Tet proteins show that DNA methylation can be removed in an active and gene specific fashion underlining a powerful new method to dynamically regulate the methylome. Therefore, it is clear that recent work has expanded the number of epigenetic regulators and their functions which underline the dynamic and plastic nature of chromatin state.

The activation of mature ductal cells to a bi-potent liver progenitor in response to liver damage is one such example of cell fate changes where epigenetics may play a significant role. Furthermore it has even been postulated in that the change in cell fate resembles a reversion to an embryonic hepatoblast-like state (Miyajima, Tanaka and Itoh, 2014). It is therefore likely that epigenetic remodelling will need to take place to facilitate the change in cell fate. Taking advantage of liver organoids as a model for ductal progenitors and the increased understanding of the dynamic nature of chromatin state and the epigenetic regulators that control them, we are for the first time, able to break through the classical barriers to study explained above and assess the epigenetic mechanisms surrounding ductal cell activation in response to liver damage.

Throughout the course of this work we focus on the epigenetic regulators *Tet1* and *Arid1a*, therefore, I will now discuss the background and function of these genes.

## 1.5 The physiological role of *Tet1* and 5-methylcytosine oxidation

The hunt for the mammalian DNA demethylase has been long and full of controversies (Ooi, Bestor and Pfeifer, 2008). The first evidence of such an enzyme was described by Gjerset and Martin in 1982 where they described a protease sensitive DNA methylation activity was found in the nuclear extracts of mouse erythroleukemic cells (Gjerset and Martin, 1982). However, the protein responsible for this activity could not be isolated and characterised. More than a decade later another group described an RNAase sensitive fraction with demethylation activity suggesting that the native demethylase is actually a ribozyme or RNA dependent complex (Weiss *et al.*, 1996). However, there was evidence against such a model and again no further characterisation was possible (Swisher *et al.*, 1998). Later studies then implicated a Thymine DNA glycosylase, the BER pathway and the methyl binding protein MBP2 in active demethylation (Bhattacharya *et al.*, 1999; Barreto *et al.*, 2007; Cortázar *et al.*, 2007). In all cases there were conflicting reports and questions as to the involvement of these candidates in rapid DNA demethylation (Hendrich *et al.*, 2001; Jin, Guo and Pfeifer, 2008). The enigma was finally cracked by Tahilani and colleagues who characterised the founding member of the Tet family, *Tet1* (Tahiliani *et al.*, 2009).

*Tet1* is part of a family of three proteins with the ability to oxidise 5mC to 5hmC and the further cytosine oxidative derivatives 5-formylcytosine (5fC) and 5-carboxylcytosine (5caC) in a step wise manner (Ito *et al.*, 2011; Rasmussen and Helin, 2016)(Figure 1.4). They are large proteins with several conserved structural domains between them. Each TET protein consists of a double stranded  $\beta$ -helix domain, binding sites for its cofactors  $\text{Fe}^{2+}$  and 2-oxoglutarate and a cysteine enriched domain (Hu *et al.*, 2013; Hashimoto *et al.*, 2014). The conserved domains make up the catalytic dioxygenase activity of the TETs. Structural studies have shown that the catalytic domain has significant substrate specificity for methylated CpG sites (Hu *et al.*, 2015). TET1 and 3 also have a classical CXXC zinc finger domain that can facilitate DNA binding (Zhang *et al.*, 2010; Xu *et al.*, 2012).

*Tet1* dependent oxidation of 5mC does not ultimately result in an unmodified base in isolation but demethylation is facilitated by a passive or active mechanism. The passive mechanism is dependent on the cell cycle. The maintenance of 5mC throughout the cell cycle is facilitated by Dnmt1, which can bind hemi-methylated DNA (explained in section 1.4). However, when Dnmt1 is bound to hemi-methylated DNA containing

5hmC its activity is significantly reduced, therefore, DNA may not re-methylated through cell division resulting in unmodified cytosine on both strands of DNA in two rounds of DNA replication (Valinluck and Sowers, 2007; Hashimoto *et al.*, 2012). However, recent evidence has shown that Dnmt1 partners Uhrf1/2 can bind 5hmC DNA *in vivo* and could drive the maintenance of 5mC through cell divisions by diluting the 5hmC modification (Frauer *et al.*, 2011; Zhou *et al.*, 2014). Furthermore, Dnmt3a/b have also been shown to have no significant bias against CpG sites containing 5hmC and could facilitate the maintenance of the 5mC after oxidation (Hashimoto *et al.*, 2012; Ji *et al.*, 2014). Taken together further investigation of this passive mechanism is needed to understand whether it plays a significant role in TET dependent DNA methylation *in vivo*.

Active demethylation removes modified cytosines independently from the cell cycle. This is achieved through thymine DNA glycosylase (TDG) mediated base excision and repair through the BER pathway. TDG was originally described to remove mismatched pyrimidines, however, since the characterisation of the oxidative products 5fC and 5caC it was shown that TDG can excise the modified cytosine leaving an abasic site in the DNA (Krokan, Standal and Slupphaug, 1997; He *et al.*, 2011; Maiti and Drohat, 2011). The removal of the modified cytosine then triggers the BER pathway to repair the site creating an unmodified cytosine (Parikh, Mol and Tainer, 1997). It is important to note that 5hmC is not removed by the same mechanism as it is not a substrate for TDG (Maiti and Drohat, 2011). Therefore, it is either removed by a passive mechanism or by further oxidation by the TETs.

Interestingly, the TETs do not have equal preference for each oxidation step from the conversion of 5mC to 5caC. Structural studies of human TET2 have shown that the hydroxyl- and carbonyl- groups of 5fC and 5caC respectively generate increased bonding within the catalytic active site resulting in a less reactive complex. 5fC and 5caC substrates are held further away from the critical Fe<sup>2+</sup> cofactor (Hu *et al.*, 2013, 2015). As a result, it is not surprising that the rate of reaction of the conversion of 5mC to 5hmC has been shown to be significantly faster than subsequent oxidation steps (Ito *et al.*, 2011)(Figure 1.4). In line with the kinetics of TET activity it has been found that there is a stable pool of 5hmC, and to a lesser extent 5fC, likely due to processivity of the TETs (Bachman *et al.*, 2014, 2015). 5hmC forms the largest population of the 5mC oxidative products but interestingly it cannot be removed by the TDG/BER active demethylation and can only result in demethylation by cell cycle

dependent passive demethylation or by further action of the TETs, which is likely to increase the stability.

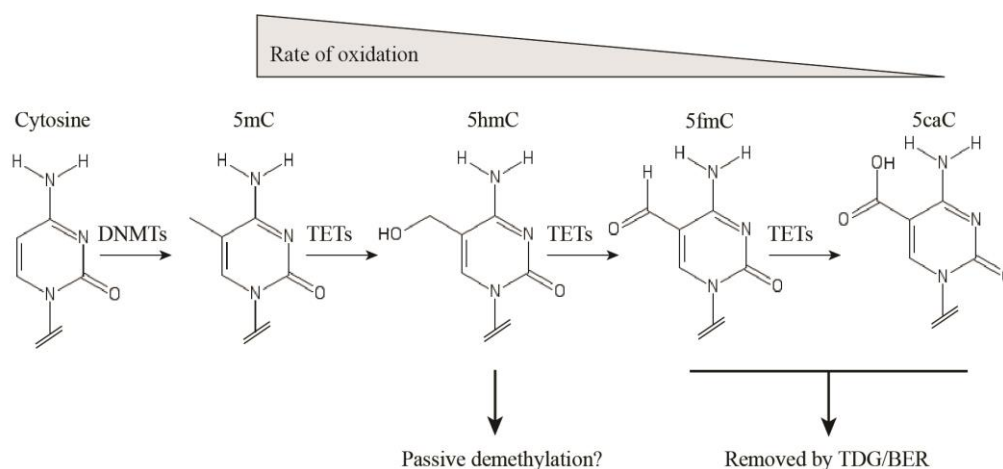


**Figure 1.4 – The TET family oxidises 5mC in a step-wise manner facilitating the active removal of methylated cytosine.** A schematic showing the chemical structure of the oxidative derivatives of 5mC, these include, 5hmC, 5fC, and 5caC, and their subsequent mode of removal. Gradient indicates reflects rate of reaction. Adapted from Rasmussen and Helin (2016).

Following the discovery that the 5hmC and 5fC modifications are stable (explained above), it is interesting to speculate that they themselves are epigenetic modifiers and can modulate chromatin accessibility in a similar manner to the varied mechanisms of regulation that are mediated by 5mC (see section 1.4). To facilitate such a function the epigenetic modification would need ‘readers’ that can bind the modification and either directly mediate chromatin regulation or recruit further proteins to facilitate a function. Specific binding partners of 5hmC have not yet been well characterised but several proteins have been found to bind 5fC with high affinity (Iurlaro *et al.*, 2013; Spruijt *et al.*, 2013). These include transcription factors in the forkhead box family, several components of the chromatin remodelling NuRD complex as well as proteins involved in the DNA damage response (Iurlaro *et al.*, 2013). The latter is likely due to the components required for the TDG/BER dependent demethylation. In any case, it suggests that 5fC may act as an independent chromatin modifier that can alter chromatin accessibility.

As the hunt for specific effectors of the 5hmC modifier continues it is important to note that it has been shown that several mediators of 5mC do not bind 5hmC. Therefore, despite the current lack of specific activity 5hmC can remove the repressive nature of 5mC by displacing the negative mediators of transcription that were initially recruited. For instance, methyl-binding proteins MBD1, MBD2 and MBD4 bind 5hmC

with significantly lower affinity when compared to 5mC (Jin, Kadam and Pfeifer, 2010; Hashimoto *et al.*, 2012). Therefore, we may consider 5hmC as a permissive modification for transcription. Interestingly, it also means that full demethylation is not required to remove the repressive effects of 5mC and through oxidation 5mC mediated repression can be reversed.

The TETs and TET dependent 5mC oxidation have varied physiological roles from development to adulthood, but commonly they are involved in cell fate transitions. Throughout development there are two phases of global demethylation (see section 1.4): first during early preimplantation development; and second during primordial germ cell (PGC) specification. It has been shown that both TET1 and TET2 are crucial for DNA demethylation and epigenetic reprogramming to PCG fate (Hackett *et al.*, 2013). Using null mutant mice it was shown that TET1/2 are dispensable for postnatal development but similar genetic ablation of TET3 (or all three members) results in early termination of preimplantation development (Dawlaty *et al.*, 2011, 2013, 2014; Gu *et al.*, 2011; Quivoron *et al.*, 2011; Kang *et al.*, 2015). This suggests that the role of each individual TET is not overlapping and they have non-redundant functions at different stages of development. Beyond embryonic development the TETs have been implicated in somatic reprogramming to iPSCs where their ablation dramatically reduces reprogramming efficiency, suggesting that TET dependent 5mC oxidation is crucial for the acquisition of iPSC fate (Doege *et al.*, 2012; Costa *et al.*, 2013). The TETs have also been shown to be crucial in both the maintenance of self-renewal in the intestinal stem cell (ISC) and the activation of axonal growth in mature neurons (Kim *et al.*, 2016; Weng *et al.*, 2017). In the first instance, it was shown that 5hmC was enriched in the ISC compartment and was quickly lost during intestinal differentiation and cell migration along the villus. In line with this, the authors demonstrated that when *Tet1* null mutants were backcrossed to generate a pure background significant postnatal lethality was apparent due to collapse of the intestine of mutant mice. Further analysis showed that *Tet1* was crucial for maintained expression of *lgr5* and other Wnt targets such as *Axin2* resulting in loss of stem cell capacity in the ISC compartment (Kim *et al.*, 2016). In neurons, *Tet1* was recently shown to be crucial for the activation of regeneration upon injury where *Tet1* knockdown resulted in reduced regeneration of retinal ganglion neurons after axonal damage (Weng *et al.*, 2017).

These studies demonstrate the remarkably dynamic role of *Tet1* (and the family as a whole) in cell fate changes and plasticity during embryogenesis as well as in adult

systems of tissue homeostasis and regeneration. The ductal response to liver damage relies on activation of mature ductal cells to acquire a bi-potential *Lgr5*<sup>+</sup> progenitor state (Huch, Dorrell, *et al.*, 2013)(See section 1.2). *Tet1* was shown to be involved in remarkably similar processes in the adult by the two studies by Weng *et al* and Kim *et al*, heavily implicating *Tet1* as a candidate to modulation the acquisition of the progenitor state after liver damage (Kim *et al.*, 2016; Weng *et al.*, 2017). However, the role of *Tet1* in regeneration of the liver epithelium is yet to be characterised.

## 1.6 The role of *Arid1a* and the BAF complex in development and epithelial regeneration.

The Switch/Sucrose non-fermentable (SWI/SNF) complex is a large multi-subunit chromatin remodelling complex originally discovered in yeast (Neugeborn and Carlson, 1984; Stern, Jensen and Herskowitz, 1984). The exact number of subunits is dependent on species, the mammalian SWI/SNF complexes are made up of ~12 subunits including one of two subunits with ATPase activity (*Brg1* or *Brm*) and several associated factors together known as the *Brm/Brg1* Associated Factor (BAF) complex (Tang, Nogales and Ciferri, 2010). The BAF complex works by using energy derived from ATP hydrolysis to shuffle nucleosomes, allowing the complex to change the chromatin landscape at a particular locus (Havas *et al.*, 2000).

The first insight into the mechanism of nucleosome movement was the discovery that the ATPases are part of the superfamily 2 (SNF2) group of DNA and RNA translocases and helicases (Eisen, Sweder and Hanawalt, 1995; Singleton and Wigley, 2002). In line with this, it was shown that several chromatin remodellers were able to translocate across linear DNA in a 3'→5' direction (Whitehouse *et al.*, 2003; Saha, Wittmeyer and Cairns, 2005, 2006). Structural studies of the BAF complex ATPase and related SNF2 family members found that the enzymes are made up of two subdomains: a torsion domain that can translocate DNA; and a tracking domain that ensures directionality of movement (Kim *et al.*, 1998; Velankar *et al.*, 1999; Dürr *et al.*, 2005). The subunits bind two internal sites of the nucleosome before the torsion domain changes conformation and pulls DNA from the proximal linker region creating a 'wave' within a cleft between the two domains of the ATPase (Saha, Wittmeyer and Cairns, 2005). The increased torsion of the under twisted wave of DNA is then resolved towards the distal linker region of DNA guided by the tracker domain acting as a 'ratchet' (Havas *et al.*, 2000; Gavin, Horn and Peterson, 2001). Therefore, the action of ATP hydrolysis is nucleosome movement along DNA by a 'wave/ratchet' mechanism (Saha, Wittmeyer and Cairns, 2006).

As explained in section 1.4 nucleosomes form a substantial barrier to transcription, therefore targeted nucleosome repositioning activity of the BAF complex can dramatically alter gene expression (Kireeva *et al.*, 2005; Bondarenko *et al.*, 2006). However, the complex has also been shown to bind other regulators of chromatin accessibility and transcription. For instance, the BAF complex is essential for the

repression of neural genes through the REST transcription factor (Battaglioli *et al.*, 2002). Moreover, the complex has been shown to recruit HDACs to regulate G1/S transition of the cell cycle (Zhang *et al.*, 2000). Taken together, there is growing evidence that the BAF complex can modulate gene expression in several ways beyond its native nucleosome shuffling activity. As a result of the pleiotropic modes of action it is not surprising that the BAF complex is a prolific transcriptional regulator activating and repressing a plethora of genes (Ho *et al.*, 2009a; Euskirchen *et al.*, 2011). The ATPase associated factors can be split into core factors which are invariable, and the other factors which have distinct structural or functional homologues that are able to switch forming complexes with different compositions (Wang, Côté, *et al.*, 1996; Wang, Xue, *et al.*, 1996; Kadoch and Crabtree, 2015).

The regulation of neural development is an excellent example of BAF specialisation and composition dependent function and involves three distinct BAF complexes: esBAF; npBAF; and nBAF (Ho and Crabtree, 2010). Early development has been shown to be dependent on a specific set of BAF components together known as the esBAF. The components include *Brg1* (not *Brm*) and a *Baf155* homodimer as well as a full complement of core invariable components (Ho *et al.*, 2009a). Accordingly mouse knock out models demonstrate *Brg1* is essential for zygotic genome activation and proliferation of the inner cell mass, whereas mutation of *Brm* results in viable mice (Reyes *et al.*, 1998; Bultman *et al.*, 2000, 2006). Furthermore, genetic ablation of *Baf155* results in preimplantation lethality in mammalian development (Kim *et al.*, 2001). The npBAF complex is then crucial for the differentiation of neural progenitors from embryonic stem cells. The npBAF can include: either *Brm* or *Brg1*; a *Baf155/Baf170* heterodimer; *Baf60c*; and *Baf45a*. In line with this, both *Brg1* and *Baf45a* are crucial for proper NOTCH and sonic hedgehog signalling, as well as proliferation of neural progenitors (Lessard *et al.*, 2007). Finally, as neural progenitors mature they replace *Baf45a* and *Baf53a* with *Baf45b* and *Baf53b* forming the nBAF complex. These changes are crucial for the BAF complex to interact with CREST that regulates dendritic outgrowth (Lessard *et al.*, 2007; Wu *et al.*, 2007). The involvement of unique BAF complexes is best described in neural development but has also been implicated in cardiac development and may be a common mechanism for directing tissue specific differentiation (Lickert *et al.*, 2004; Z. Wang *et al.*, 2004; Huang *et al.*, 2008; Lange *et al.*, 2008; Ho and Crabtree, 2010).

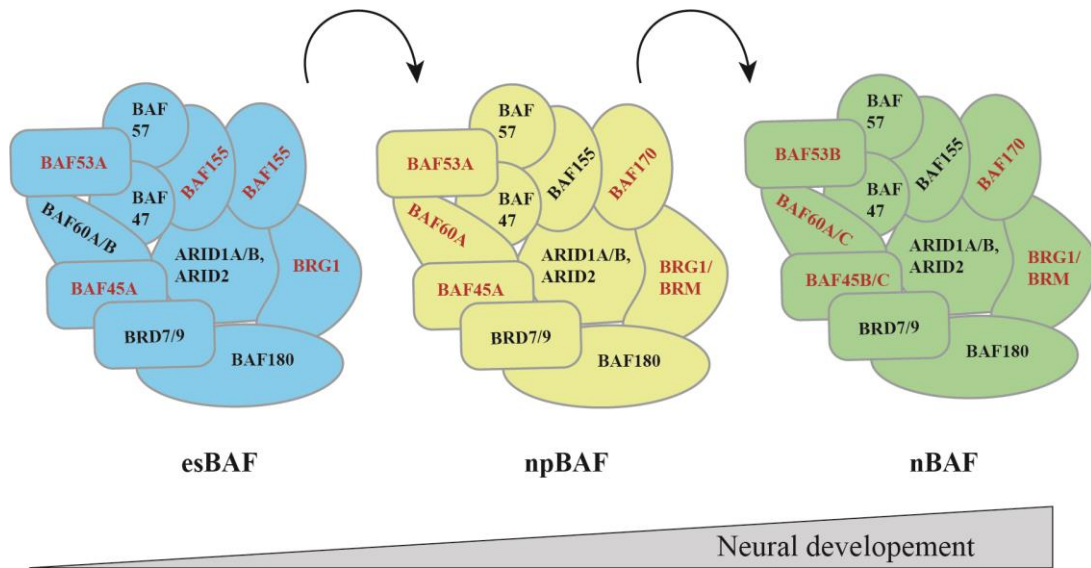


**Figure 1.5 – Specialisation of the BAF complex modulates specific gene networks driving neural development.** A schematic showing the composition of the BAF complex during neural development, crucial components of the embryonic BAF (esBAF), neural progenitor BAF (npBAF) or neural BAF (nBAF) are indicated in red. Adapted from Ho and Crabtree (2010).

A/T rich interacting domain (Arid) 1a (also known as BAF250a) is one component of the complex characterised by its DNA binding ARID domain (Tang, Nogales and Ciferri, 2010). *Arid1a* has two functional homologues *Arid1b* and *Arid2*, all three are mutually exclusive forming a core component of the BAF complex (Kortschak, Tucker and Saint, 2000; X. Wang *et al.*, 2004; Wilsker *et al.*, 2005; Xu, Flowers and Moran, 2012). *Arid1a* and *Arid1b* have both been implicated in maintaining the self-renewal of embryonic stem cells suggesting that they are functionally overlapping (Gao *et al.*, 2008; Yan *et al.*, 2008). In accordance with this it has been shown that there is significant synthetic lethality between *Arid1a* and *Arid1b* (Kelso *et al.*, 2017). Furthermore, genome wide analysis of targets of each of three Arid family members found that *Arid1a* and *Arid1b* have overlapping targets (Raab, Resnick and Magnuson, 2015). On the other hand, *Arid2* plays a more independent role as it forms a unique variation of the BAF complex together with *Baf180* known as the polybromo BAF (pBAF complex). The pBAF complex has been implicated in cardiac and osteoblast development as well as being frequently mutated in cases of renal cancer (Z. Wang *et al.*, 2004; Huang *et al.*, 2008; Xu, Flowers and Moran, 2012; Porter and Dykhuizen, 2017).

Mathur and colleagues showed that genetic ablation of *Arid1a* leads to loss of binding of the BAF complex at 79% of canonical BAF binding sites and a concomitant with a loss of H3K27ac in enhancer regions (Mathur *et al.*, 2017). Therefore, *Arid1a* is crucial for the recruitment and function of the BAF complex. Reflecting the central role of *Arid1a* it is not surprising that it has been found to be one of the most commonly mutated components in cancer with mutations being seen in liver cancer (both hepatocellular and cholangiocarcinoma), colon, gastric and pancreatic cancer, suggesting that *Arid1a* is a prolific tumour suppressor (Wang *et al.*, 2011, 2014; Biankin *et al.*, 2012; Muzny *et al.*, 2012; Chan-on *et al.*, 2013).

Recently *Arid1a* has also been implicated in liver damage and epithelial regeneration. Hepatocyte specific genetic ablation of *Arid1a* resulted in spontaneous and progressive phenotypes reminiscent of steatohepatitis as well as increased appearance of liver cancer in response to oncogenic treatment (Fang *et al.*, 2015). Moreover, another study showed that ubiquitous mutation of *Arid1a* enhances regeneration in the liver and skin epithelium in response to damage (Sun *et al.*, 2016). The enhanced regeneration was a result of boosted proliferation through inactivation of *E2f4*, a repressor of cell cycle progression. Taken together *Arid1a* may guard against unregulated cell proliferation by cooperation with *E2f4* and this may form the basis of the tumour suppressor activity.

However, these studies do not interrogate the role of *Arid1a* in ductal progenitor regeneration specifically and as it is mutated heavily in cholangiocarcinoma, which is a largely ductal cancer, it would be interesting to study the effect of *Arid1a* in a ductal population. As explained above tissue specific gene expression can be facilitated by unique compositions of BAF components, thus by manipulating *Arid1a* in a ductal specific manner we would be able to understand whether an *Arid1a* containing complex is required for the plasticity required in ductal driven liver regeneration.

## 1.7 Project Aims

1. To use liver organoids as a model of ductal cell-driven regeneration to find candidate epigenetic regulators in their activation by taking advantage of gene expression analysis and siRNA knockdown.
2. To assess the role of *Arid1a* in ductal progenitor maintenance and differentiation by manipulating liver organoid culture conditions to induce hepatocyte-like differentiation.
3. To take advantage of several animal models of liver damage and *Tet1* deletion to understand its role in ductal cell driven regeneration.
4. To apply optical clearing tools to whole liver tissue to facilitate the visualisation and study of ductal proliferation dynamics during damage and regeneration.

## 2. Materials and Methods

### 2.1 Organoid studies

#### 2.1.1 Organoid derivation and maintenance

Organoids were isolated and maintained according to conditions optimised by Huch et al. 2013. In brief, livers were dissected from adult mice and dissociated using an enzymatic mix of collagenase (Sigma, C9407) and dispase (Gibco, 17105041) at 37°C (Collagenase 0.0125%, Dispase 0.0125%, 1% FBS dissolved in DMEM/F12). After 3 hours of digestion biliary ducts were manually picked and placed in 3D culture using matrigel (Corning, 356231) to form a matrix. Biliary ducts at this stage were cultured with organoid isolation medium (Table 2.1). After 4-7 days of these initial culture conditions media was changed to normal organoid expansion medium (Table 2.1). Organoids were also derived from single cells by taking advantage of a fluorescence activated cell sorting strategy. Livers were digested as describe above to generate a biliary duct enriched solution, the solution was then further dissociated to single cells by incubation with Tryple 5x solution (Life technologies, A12177-01) for 10 minutes at 37°C. The resulting solution was filtered twice through a 40um cell strainer to remove large clumps of cells and counted with a haemocytometer. Single cells were transferred to polypropylene FACS tubes and blocked in 2% FBS in DMEM/F12 (Life technologies, 31966021) for 10 minutes at 4°C. Cells were then labelled with fluorophore conjugated antibodies described in Table 2.7, for 30 minutes at 4°C at a concentration of 1 µl of antibody/1x10<sup>6</sup> cells in 1% FBS in DMEM/F12. Cells were then washed twice in 1% FBS in DMEM/F12, sorted using a MoFlo cell sorter and collected in advanced DMEM (Life technologies, 12634028) supplemented with Rho kinase inhibitor (Ri) at a concentration of 10 µM. The organoid forming fraction was defined as EpCAM+Cd45-Cd11b-Cd31- and were seeded at experimental dependent densities in matrigel with organoid isolation medium (Table 2.1). Again, after 4-7 days of these initial culture conditions media was changed to normal organoid expansion medium (Table 2.1). All medium compositions are made in Advanced DMEM/F12 supplemented with a cocktail growth factors, see Table 2.1 for concentrations and manufacturer's details. After organoids were established in culture they were passaged once per week by removing the matrigel and mechanically dissociating the organoid

structures before reseeding in matrigel at a ratio of 1:4 to 1:6. All cell culture was maintained at 37°C and 5% CO<sub>2</sub> unless otherwise stated.

*Table 2.1 – 3D organoid growth media recipes*

Component	Manufacturer (Cat #)	Culture conditions		
		Isolation	Expansion	Differentiation
EGF	Peprotech (AF-100-15)	50 ng/ml	50 ng/ml	-
HGF	Peprotech (100-39)	50 ng/ml	50 ng/ml	25 ng/ml
FGF10	Peprotech (100-26)	100 ng/ml	100 ng/ml	100 ng/ml
Gastrin	Sigma (G9145)	10 nM	10 nM	10 nM
Nicotinamide	Sigma (N0636)	10 mM	10 mM	-
R-spondin1 (Conditioned media)	In house	10%	10%	-
Wnt3a (Conditioned media)	In house	30%	-	-
Noggin	Peprotech (120-10C)	100 ng/ml	-	-
Rho kinase inhibitor	Sigma (Y0503)	10 µM	-	-
DAPT	Sigma (D5942)	-	-	10 µM
A8301	Tocris bioscience (2939/10)	-	-	500 nM
Dexamethosone	Sigma (D4902)	-	-	3 µM
N-acetylcystine	Sigma (A9165)	4 mM	4 mM	4 mM
N2 (100x)	Life technologies (17502048)	1x	1x	1x
B27 (50x)	Life technologies (12587010)	1x	1x	1x
Glutamax (100x)	Invitrogen (35050-068)	1x	1x	1x
HEPES	Invitrogen (15630-56)	10 mM	10 mM	10 mM
Penicillin/Streptomycin (100x)	Invitrogen (15140-122)	1x	1x	1x
All media made in advance DMEM				

### 2.1.2 siRNA Transfection

To perform siRNA knockdown  $1 \times 10^4$  cells either EpCAM<sup>+</sup> cells freshly isolated from healthy liver or established organoids were transfected with a pool of 4 ON-Targetplus siRNA (Dharmacon, custom plate) for each candidate gene or with the 4 independent Tet1 siRNA using Lipofectamine RNAimax (Life Technologies, 13778075) according to manufacturer's instruction. After that, cells and Lipofectamine-RNA mix were spun at 600g at 32°C for 45 minutes and then incubated for 4 hours at 37°C. Cell suspension was then collected, spun for 5 minutes at 300g and seeded in matrigel in Isolation medium in order to allow organoid formation. Organoid formation efficiency was assessed 6 days later. siRNA sequences used are listed in Table 2.2.

Table 2.2 – siRNA sequence library

Pool Catalog #	Duplex Catalog #	Gene	Gene Accession	Sequence
L-040694-01	J-040694-09	<i>Arid1a</i>	XM_992304	AGAUGUGGGUGGACCGGUA
L-040694-01	J-040694-10	<i>Arid1a</i>	XM_992304	AAGCAUUGCCCAAGAU CGA
L-040694-01	J-040694-11	<i>Arid1a</i>	XM_992304	GGACAGGGGAUCAUAUGUA
L-040694-01	J-040694-12	<i>Arid1a</i>	XM_992304	CCUUGGGGAUGUUAAGUUA
L-053908-01	J-053908-09	<i>Arid1b</i>	XM_898196	CGAUGGACCCAAUGGUGAU
L-053908-01	J-053908-10	<i>Arid1b</i>	XM_898196	CAAGAAAGGCUAUGGAACUA
L-053908-01	J-053908-11	<i>Arid1b</i>	XM_898196	CAGUUGUAUGGGAUGGGUA
L-053908-01	J-053908-12	<i>Arid1b</i>	XM_898196	CCAUGAAGACUUGAAUUUA
L-054678-01	J-054678-09	<i>Arid5b</i>	NM_023598	GGUCCAUGCUUAAACGGAU
L-054678-01	J-054678-10	<i>Arid5b</i>	NM_023598	CGGAGAAAGUCCACGUCAA
L-054678-01	J-054678-11	<i>Arid5b</i>	NM_023598	GUGAUGAGUUCGCGCCAAA
L-054678-01	J-054678-12	<i>Arid5b</i>	NM_023598	ACAAUAACUGUGACGGUAA
L-044249-00	J-044249-05	<i>Smarcc1</i>	NM_009211	CCGAAUGGAUCGUAAACGUU
L-044249-00	J-044249-06	<i>Smarcc1</i>	NM_009211	CAUCCUGGUUGAUAUAUA
L-044249-00	J-044249-07	<i>Smarcc1</i>	NM_009211	GAAUUGGGCUAACAAGUUG
L-044249-00	J-044249-08	<i>Smarcc1</i>	NM_009211	GAACAAUCUGUCAGCUAGA
L-065628-01	J-065628-09	<i>Cbx6</i>	NM_028763	ACGUAUUAACGCAGCGAUU
L-065628-01	J-065628-10	<i>Cbx6</i>	NM_028763	AGUCAGAGGUGCUCGUAUCU
L-065628-01	J-065628-11	<i>Cbx6</i>	NM_028763	GAAAGCGGCUGACGGGUAA
L-065628-01	J-065628-12	<i>Cbx6</i>	NM_028763	GUJAAUGGCAAGGAACCUAA
L-043098-01	J-043098-09	<i>Cdh4</i>	NM_009867	CGGUGGAUAUGAACGGUAA
L-043098-01	J-043098-10	<i>Cdh4</i>	NM_009867	GGAAAGCGCGUCUACCGAAU
L-043098-01	J-043098-11	<i>Cdh4</i>	NM_009867	CCGCCAUUCUGGACCGAGA
L-043098-01	J-043098-12	<i>Cdh4</i>	NM_009867	CGACAACCGUCCGAGUUC
L-045497-00	J-045497-05	<i>Dnajc2</i>	NM_009583	GAUCAAGGAGCUCAUAAA
L-045497-00	J-045497-06	<i>Dnajc2</i>	NM_009583	CUUCGGAAUCUGUGCAAGA
L-045497-00	J-045497-07	<i>Dnajc2</i>	NM_009583	GAAUGGGGAGUGGCAUAAA
L-045497-00	J-045497-08	<i>Dnajc2</i>	NM_009583	GGAAUCACUUCUCGGAACA
L-053728-01	J-053728-09	<i>Ehm12</i>	NM_147151	UAAACAAGGAGGCGAGGUU
L-053728-01	J-053728-10	<i>Ehm12</i>	NM_147151	CCAUGAACAUUCGACCGCAA
L-053728-01	J-053728-11	<i>Ehm12</i>	NM_147151	CAGGACAGGUGGACGUCAA
L-053728-01	J-053728-12	<i>Ehm12</i>	NM_147151	CCAAAGAAAGAAUGCGGAA
L-041870-01	J-041870-09	<i>Foxj2</i>	NM_021899	CUAACAAUCUACUGUGUA
L-041870-01	J-041870-10	<i>Foxj2</i>	NM_021899	GCAAAGUUCGUCGAGGAU
L-041870-01	J-041870-11	<i>Foxj2</i>	NM_021899	AGAGGGAAUCGGCGGAGAU
L-041870-01	J-041870-12	<i>Foxj2</i>	NM_021899	GUAAAGGGGAGUAGAAUUA
L-059718-01	J-059718-09	<i>Foxj3</i>	NM_172699	GAAGGAAAGCUGUCGAAUU
L-059718-01	J-059718-10	<i>Foxj3</i>	NM_172699	GUACAACCUCCAGAACGA
L-059718-01	J-059718-11	<i>Foxj3</i>	NM_172699	UCAUGAAUCCACCGAGUAA
L-059718-01	J-059718-12	<i>Foxj3</i>	NM_172699	GGUCAUUAAGAUAGGUUCA
L-044314-01	J-044314-09	<i>Foxn3</i>	NM_183186	GGAUGCGGACUGAGAGCGA
L-044314-01	J-044314-10	<i>Foxn3</i>	NM_183186	GGGAAAACAAGGUAUCGUCA
L-044314-01	J-044314-11	<i>Foxn3</i>	NM_183186	CCACAAAUGCCAUCGGCCU
L-044314-01	J-044314-12	<i>Foxn3</i>	NM_183186	CUAUGAUUUGUGGCAUA
L-040287-02	J-040287-22	<i>Hdac1</i>	NM_008228	GGGAGAAAGGUGGUCGCAAG
L-040287-02	J-040287-23	<i>Hdac1</i>	NM_008228	ACUAUGGUCUACCCGAAA
L-040287-02	J-040287-24	<i>Hdac1</i>	NM_008228	UGAACUACCCACUGCGAGA
L-040287-02	J-040287-25	<i>Hdac1</i>	NM_008228	CCAGAACAUACGAGUAC
L-046158-00	J-046158-05	<i>Hdac2</i>	NM_008229	CCAAUGAGUUGCCAUUAUA
L-046158-00	J-046158-06	<i>Hdac2</i>	NM_008229	CAAUUGGGCUGGAGGUA
L-046158-00	J-046158-07	<i>Hdac2</i>	NM_008229	ACAGGAGACUUGAGGGAUA
L-046158-00	J-046158-08	<i>Hdac2</i>	NM_008229	CAAAAGUGAUGGAGAUUA
L-040701-01	J-040701-13	<i>Id1</i>	NM_010495	GGCCUUAUGUUGCGUGA
L-040701-01	J-040701-14	<i>Id1</i>	NM_010495	GGGAAAGACACUACCGCAG
L-040701-01	J-040701-15	<i>Id1</i>	NM_010495	GGUUUGAUCAACAGAGCCU
L-040701-01	J-040701-16	<i>Id1</i>	NM_010495	CGGAGCAAAGCGUGGCCAU
L-060495-00	J-060495-05	<i>Id2</i>	NM_010496	CUUCUGAGCUUAUGUCGAA
L-060495-00	J-060495-06	<i>Id2</i>	NM_010496	GCAAAUUAUCUGUGGCUA
L-060495-00	J-060495-07	<i>Id2</i>	NM_010496	GGUGAGGUCGUUAAGAAA
L-060495-00	J-060495-08	<i>Id2</i>	NM_010496	CCAAAUAUAUCCAGUUA
L-046974-01	J-046974-09	<i>Klf2</i>	NM_008452	CCUUGCACAUAGAAGCGACA
L-046974-01	J-046974-10	<i>Klf2</i>	NM_008452	CCAUGGGAUUGGACGGUCU
L-046974-01	J-046974-11	<i>Klf2</i>	NM_008452	CGGCA CGGAUGAGGACCUA
L-046974-01	J-046974-12	<i>Klf2</i>	NM_008452	GGUGAGAAGCCUUAUCAUU
L-040001-01	J-040001-13	<i>Klf4</i>	NM_010637	CGACUAACCGUUGGCGUGA
L-040001-01	J-040001-14	<i>Klf4</i>	NM_010637	CCGAGGAGUUAACGACCU
L-040001-01	J-040001-15	<i>Klf4</i>	NM_010637	CCAUAUAUUGGUCGAGGA
L-040001-01	J-040001-16	<i>Klf4</i>	NM_010637	AGAUUAAGCAAGAGGCGGU
L-062477-01	J-062477-09	<i>Klf5</i>	NM_009769	GCAUCAACAUAGAACGUCUU
L-062477-01	J-062477-10	<i>Klf5</i>	NM_009769	CUUCCAAAUCGGCGAUUCA
L-062477-01	J-062477-11	<i>Klf5</i>	NM_009769	UCCACAGACCAUGCGUAA
L-062477-01	J-062477-12	<i>Klf5</i>	NM_009769	GAUCUGGAGAGCGACGUA

Table 2.2 – siRNA sequence library (cont.)

Pool Catalog #	Duplex Catalog #	Gene	Gene Accession	Sequence
L-047291-00	J-047291-05	<i>Lgr4</i>	XM_899191	GCAGUCACCCUCCGACAGUU
L-047291-00	J-047291-06	<i>Lgr4</i>	XM_899191	GCACGUUGCUUGGCCUCAUC
L-047291-00	J-047291-07	<i>Lgr4</i>	XM_899191	GCCAUUAUCUACACUAAAC
L-047291-00	J-047291-08	<i>Lgr4</i>	XM_899191	GAAACACGGAUCA GUCUCA
L-045520-00	J-045520-05	<i>Lgr5</i>	NM_010195	GCAUUUGCCUGAACUUAAGA
L-045520-00	J-045520-06	<i>Lgr5</i>	NM_010195	GUAGCUGGCUGAUCCGAAU
L-045520-00	J-045520-07	<i>Lgr5</i>	NM_010195	GUACAUCUCUCCAUAAAG
L-045520-00	J-045520-08	<i>Lgr5</i>	NM_010195	GGAAUCGGCUGCCAAAUCG
L-065198-01	J-065198-09	<i>Kdm1a</i>	NM_133872	GUUGAGUGGGCUUCGAGAA
L-065198-01	J-065198-10	<i>Kdm1a</i>	NM_133872	GAGAACACACA AUCGGGAA
L-065198-01	J-065198-11	<i>Kdm1a</i>	NM_133872	CAUAAAGA CUGCUCGAGAA
L-065198-01	J-065198-12	<i>Kdm1a</i>	NM_133872	GAAACAAGAAUUUAACCGGU
L-047318-00	J-047318-05	<i>Mbd3</i>	NM_013595	GAAUAAAGUCGCCAGCGU
L-047318-00	J-047318-06	<i>Mbd3</i>	NM_013595	GCAACAAGGUGCAAGAGCGA
L-047318-00	J-047318-07	<i>Mbd3</i>	NM_013595	GAA GCUAAGUGGAUUGAGU
L-047318-00	J-047318-08	<i>Mbd3</i>	NM_013595	UGGAGGAGCUUGCCCGAGA
L-040631-01	J-040631-09	<i>Kmt2a</i>	XM_994852	CGGCAAAUGGA GCGAGUUU
L-040631-01	J-040631-10	<i>Kmt2a</i>	XM_994852	GCACAGUGGGUCACGAAUU
L-040631-01	J-040631-11	<i>Kmt2a</i>	XM_994852	CUGUUGAAUUCUCGGACUA
L-040631-01	J-040631-12	<i>Kmt2a</i>	XM_994852	UUAUAGAUGCAUCGUGUAA
L-051444-00	J-051444-05	<i>Kmt2c</i>	XM_920472	GGACACAAGA UUAUCAUCA
L-051444-00	J-051444-06	<i>Kmt2c</i>	XM_920472	GCGGUGAA CUGCCGGAAAGU
L-051444-00	J-051444-07	<i>Kmt2c</i>	XM_920472	GCAACAACCAAAGGGAAUC
L-051444-00	J-051444-08	<i>Kmt2c</i>	XM_920472	GCAUUCACUCUCGAAAAG
L-042769-01	J-042769-09	<i>Rybp</i>	NM_019743	GCUUGUAUGUUA CGGAAAA
L-042769-01	J-042769-10	<i>Rybp</i>	NM_019743	GGAGAUGAAUGAAUGUA
L-042769-01	J-042769-11	<i>Rybp</i>	NM_019743	CAUUAAGCAUGUGUGUUA
L-042769-01	J-042769-12	<i>Rybp</i>	NM_019743	GCGAUUGCUUGUUAAGUAU
L-056591-00	J-056591-05	<i>Smarca2</i>	NM_026003	AGACUUAACGAAUACUAU
L-056591-00	J-056591-06	<i>Smarca2</i>	NM_026003	UAAAAGGAGCGAAUCCGUAA
L-056591-00	J-056591-07	<i>Smarca2</i>	NM_026003	GGAGAAA GACGUCUAGCUU
L-056591-00	J-056591-08	<i>Smarca2</i>	NM_026003	CGAAAUCUGUGAA GGUGAA
L-041135-00	J-041135-05	<i>Smarca4</i>	NM_011417	GACGGAAUGCGGAGGCUUA
L-041135-00	J-041135-06	<i>Smarca4</i>	NM_011417	CAAA CUGGGCGUAUGAAUU
L-041135-00	J-041135-07	<i>Smarca4</i>	NM_011417	GAGACUAUCCUCAUUAUUC
L-041135-00	J-041135-08	<i>Smarca4</i>	NM_011417	GAUCCUCACUGGCACAGA U
L-059106-01	J-059106-09	<i>Sox17</i>	NM_011441	GAGGUGGACC GCA CGGAAU
L-059106-01	J-059106-10	<i>Sox17</i>	NM_011441	AAGACGAA CGCAAGCGGUU
L-059106-01	J-059106-11	<i>Sox17</i>	NM_011441	GCGUUGACC UUGGCAGAGA
L-059106-01	J-059106-12	<i>Sox17</i>	NM_011441	GCGUCAAGCUGUUUUGUUU
L-059108-01	J-059108-09	<i>Sox9</i>	NM_011448	CGCAAUACGACUACGCUGA
L-059108-01	J-059108-10	<i>Sox9</i>	NM_011448	GUAAAAGGAAGGUAA CGAUU
L-059108-01	J-059108-11	<i>Sox9</i>	NM_011448	GAAUAAAA CCUUAAGCGU
L-059108-01	J-059108-12	<i>Sox9</i>	NM_011448	CGACGUGGACAUCGGUGAA
L-062861-01	J-062861-09	<i>Tet1</i>	XM_920196	AGGAAGA GGCACUACGUU
L-062861-01	J-062861-10	<i>Tet1</i>	XM_920196	GGUUGGAA GCUGUUCGCUA
L-062861-01	J-062861-11	<i>Tet1</i>	XM_920196	AUUUCAACUCCGACGUAAA
L-062861-01	J-062861-12	<i>Tet1</i>	XM_920196	CCA CAUCAACACACGGAGU
L-058965-00	J-058965-05	<i>Tet2</i>	XM_895573	ACUCAUGGGUCAAUUCUUA
L-058965-00	J-058965-06	<i>Tet2</i>	XM_895573	GUACUUAAGUUAUGGAAAC
L-058965-00	J-058965-07	<i>Tet2</i>	XM_895573	GGAAAGUGCGGAAA GAAU
L-058965-00	J-058965-08	<i>Tet2</i>	XM_895573	GAAAGCAGCUCGAAA GCGU
L-054156-01	J-054156-09	<i>Tet3</i>	XM_977752	CCA CAUAA GCUACGCAAAA
L-054156-01	J-054156-10	<i>Tet3</i>	XM_977752	AGGCCAAGCUCUACGGGAA
L-054156-01	J-054156-11	<i>Tet3</i>	XM_977752	GGUGAGUACUGGGCCGAAA
L-054156-01	J-054156-12	<i>Tet3</i>	XM_977752	GUGCAA GGGUCA GGCUUU

### 2.1.3 Organoid differentiation

Organoids were differentiated towards a hepatocyte fate by switching medium to a defined differentiation medium (Table 2.1) 2 days after seeding in expansion medium. The differentiation medium is refreshed every two days. At day 10 after onset of differentiation the media is further supplemented with Dexamethasone (3  $\mu$ M). Organoids were then analysed 4 days after the addition of dexamethasone.

#### **2.1.4 Terminal hepatocyte differentiation assays**

Albumin secretion was determined by ELISA (Universal biologicals, EMA3201-1). Differentiation media was refreshed 24 hours prior to the experimental endpoint and then removed. The media was centrifuged at 20,000g for 15 minutes at 4°C and the supernatant removed discarding any cellular debris. We then determined albumin concentration in the supernatant by ELISA, following the manufacturer's protocol. Cellular cytochrome p450 activity was determined by incubation with a fluorescent substrate (Promega, V8901). Organoids were removed from their matrigel by washing thoroughly with cold phosphate-buffered saline (PBS) twice and incubation in cell recovery solution (Corning, 354253) for 20 minutes at 4°C. The isolated organoids were then washed once in hepatocyte medium (Thermo Fisher, 17705021) medium supplemented with 10% FBS and finally incubated for 8 hours at 37°C (5% CO<sub>2</sub>) in hepatocyte medium supplemented with EGF, gastrin, HGF and PFBE substrate. After incubation, the cells and media were collected and spun down at 600g. The supernatant was removed and incubated in a 1:1 mix with the luciferin detection reagent for 20 minutes at room temperature, protected from light. After which luminescence was detected using a benchtop luminometer (Glomax, 1901-002) with 0.25 seconds of signal integration. Finally, the cell pellet was dissociated into single cells by incubation 1x Triple (Life technologies, 12605010) for 5 minutes at 37°C before being counted with a haemocytometer. Enzyme activity was expressed as Relative luminescence units (RLU) per 1x10<sup>6</sup> cells. Low Density Lipoprotein (LDL) uptake was determined by incubation with a fluorescent analogue of LDL, 1,1'-dioctadecyl-3,3,3',3'-tetramethyl-indocarbocyanine perchlorate LDL (Di-Ac-LDL)(Bioquote, BT-902). Organoid growth media (either differentiation or expansion) was supplemented with Di-Ac-LDL at a concentration of 10 µg/mg and incubated overnight at 37°C (5% CO<sub>2</sub>). Organoid nuclei were then stained using DRAQ5 (Thermo scientific, 62251) diluted 1/500 in PBS and imaged using confocal microscopy (Leica SP5).

#### **2.1.5 RNA extraction and RT-qPCR**

RNA was extracted from the tissue, organoids or freshly sorted EpCAM+Cd45-Cd11b-Cd31- cells by the RNeasy mini or micro kit (Quiagen, 74004) following the

manufactures protocol. cDNA was generated in a two-step reaction with 50-250 ng of RNA using M-MLV Reverse transcriptase, RNase H minus, point mutant (Promega, M3682) following manufacturers protocol. Finally, qPCR was carried out with primers to detect specific gene expression (Table 2.3) using the iTaq universal SYBR green supermix (Bio-Rad, 172-5124) using the manufacturers protocol.

Table 2.3 – qPCR/ChIP detection primer sequences

Gene	Marker	Detection	Forward primer (5'-3')	Reverse primer (5'-3')
<i>Arid1a</i>	BAF complex	qPCR	CATGGGCAGCCTCTTATG	GGATGAGGACTTTGCTGGTT
<i>Arid1b</i>	BAF complex	qPCR	ATGGGTACTCACCCCACTC	GGCAGTAGCCACTCACAGC
<i>Baf155</i>	BAF complex	qPCR	TGGCTGAGACCAGTGATGAG	ATGAACCTTCCAGGGCTTTT
<i>Brg1</i>	BAF complex	qPCR	TCCAACGTCAGCTGAGACAG	GGCCACAGACCAGGTGATAT
<i>Brm</i>	BAF complex	qPCR	CGTGAGCGATTTTGACAGTG	GTCCAGGATGGTCACTCGTT
<i>Arid5b</i>	Arid family	qPCR	AAGAATTTTGTCCTTGGCGA	GTACCCACTTGACCAGGCTT
<i>Tet1</i>	Tet family	qPCR	ATTGAGGTGGAGAAGTGGG	GGAGAAGGGTTGGTTTGC
<i>Tet2</i>	Tet family	qPCR	ATCCAAACCGAAGCTGAATG	CTTGCCCTACCACCGTTTTA
<i>Tet3</i>	Tet family	qPCR	AGATGTGGCCTCAATGATGA	CATATTTGACCCGTTGAAG
<i>Hdac2</i>	NurD cpmlex	qPCR	CATGGCGTACAGTCAAGGAG	TCATCCGGATTCATGAGGC
<i>Hdac1</i>	NurD cpmlex	qPCR	GGGCACCAAGAGGAAAGTCT	AGCAAATTTGAGTCATGCG
<i>Mbd3</i>	NurD cpmlex	qPCR	CCCCAGCGGGAAGAAGTTC	CGGAAGTCGAAGGTGCTGAG
<i>Rybp</i>	Polycomb complex	qPCR	AGACCAGCGAAACAAACCAC	AGGAGGAGCGAGTCTTTTCC
<i>Cbx6</i>	Polycomb complex	qPCR	GGAACCGGTCATTGGGAAG	TAGAGCGCAAATGTGCCAAAC
<i>Dnaje2</i>	Polycomb complex	qPCR	CCCCTTGGACAACAGAAGAA	AGCTTCTTGGCTTTCACCA
<i>Lgr5</i>	Progenitor	qPCR	GGAAATGCTTTGACACACATT	GGAAATTCATCAAGGTTAATATA
<i>Sox9</i>	Progenitor	qPCR	CTCCTAATGCTATCTTCAAG	GCTTCAGATCAACTTTGC
<i>Axin2</i>	Progenitor	qPCR	TGTCAGCAAAAACCTTTC	CTTCTCTTGAAGGACCTGA
<i>Tr</i>	Hepatoblast/Early differentiation	qPCR	TGGACACCAAAATCGTACTGG	CAGAGTCGTTGGCTGTGAAA
<i>Alb</i>	Hepatoblast/Early differentiation	qPCR	GTCCGTAGCATGCGGGAGG	GCGCAGATGACAGGGCGGAA
<i>Glul</i>	Terminal hepatocyte differentiation	qPCR	GCTGCAAGACCCGTACCCT	TTCCACTCAGGTAACCTTCCACA
<i>Cyp3a11</i>	Terminal hepatocyte differentiation	qPCR	CCTTCCAGCCTTGTAAAGGAA	CCGTGGCACAACCTTTAGAA
<i>Lgr5_TSS</i>	Progenitor	ChIP	GCTTCTGCAGCTCACCAGAC	CTGCTGCACACAGTCAGAC
<i>Lgr5_Enhancer</i>	Progenitor	ChIP	ATTCCAGGCAGAGCCTATGA	TGGAGAGAAGCCAATCCCTA
<i>Lgr5_Int1ATAC</i>	Progenitor	ChIP	CAGGTGCAGTGCTGGTTAAA	CCTGTCCCATACTCCTTTGC
<i>Lgr5_Int1</i>	Progenitor	ChIP	TACTGCTGCCATTGTGGGTA	GTCTCCAGTTCAACCTCCA
<i>Lgr5_Int2</i>	Progenitor	ChIP	CATTAGGAGGCTCAGGCAAG	TCTGGCACACCGTTCAGAG
<i>Lgr5_Int5</i>	Progenitor	ChIP	TCCACACCAGGATGACCATA	GCCACTGCTTTCACACTTGG
<i>Sox9</i>	Progenitor	ChIP	TGATTGGCCCGAGGTATCTA	GCTCCACAGAAAGTTCCAG
<i>Axin2</i>	Progenitor	ChIP	GGGAGGAGACATGAGCAGAG	CCGCGTTAACCCCTTCTT
<i>Tr</i>	Hepatoblast/Early differentiation	ChIP	CAGAGCCTCCAACACTGTCA	TCGCCTACGAAATGTGCAG
<i>Alb</i>	Hepatoblast/Early differentiation	ChIP	GAACCAATGAAATGCGAGGT	TGGGGTTGATAGGAAAGGTG

## 2.1.6 Fluorescence activated cell sorting (FACS)

Organoids were prepared for FACS by removing them from matrigel by washing with cold advanced DMEM. The organoids were then dissociated into single cells by incubation with 1x Tryple solution for 5 minutes at 37°C, the cell suspension is periodically further mechanically dissociated using a narrowed glass Pasteur pipette. Once a single cell suspension is achieved the Tryple solution is inhibited by washing with 1% FBS in DMEM/F12 before cell sorting or counting.

### **2.1.7 Western Blot**

Cell lysates were prepared by using RIPA buffer (10mM Tris-Hcl PH 8.0m 1mM EDTA, 1% Triton X-100, 0.1% SDS. 150mM NaCl) supplemented with proteinase inhibitor cocktail (Roche, 11836153001) and sonicated for 5 minutes using a Bioruptor sonicator (Diagenode) at 4°C. Lysates were cleared by centrifugation at 10,000g for 15 minutes at 4°C. Samples were loaded on Precast Mini Protean TGX gels (Bio-Rad, 4561083) and then transferred to a nitrocellulose membrane. Membranes were blocked in 5% milk and incubated overnight with ARID1A (1:5000), TET1 (1:5000) or ACTIN (1:2000) antibodies at 4°C. After that anti rabbit or mouse horseradish peroxidase (HRP) conjugated secondary antibodies were used and antibody-protein complexes were visualised using ECL (GE Healthcare, RPN2106).

### **2.1.8 Chromatin immunoprecipitation (ChIP)**

Organoids were harvested and removed from matrigel and dissociated into single cells as described above. At least three million cells were used to purify enough chromatin for the ChIP. The cells were fixed in 1% formaldehyde (Sigma, F8775) for 15 minutes at room temperature after which the fixation was stopped by addition of glycine to a final concentration of 125 mM. The cells were then lysed by sonication in IP buffer made up by 1:2 mix of SDS buffer and dilution buffer (Table 2.4). 10-25 ug of chromatin was incubated with the 2-5 ug of the primary antibody for 16 hours at 4°C. Next the chromatin was incubated with beads coated with the appropriate secondary antibody (50% slurry) for 2 hours at 4°C. The chromatin was then washed with low salt then high salt buffer (Table 2.4). The DNA was then eluted by incubating with 110 µl elution buffer (Table 2.4) for 16 hours at 65°C. DNA enrichment was then analysed by qPCR described above (Table 2.3).

Table 2.4 – ChIP solution recipes

	SDS buffer	Dilution buffer	Low Salt buffer	High salt buffer	Elution buffer
NaCl	100 mM	100 mM	140 mM	500 mM	-
Tris-HCl (pH 8.1)	50 mM	-	-	-	-
SDS	10%	-	-	-	1%
EDTA (pH 8)	5 mM	5 mM	-	-	-
Tris-HCl (pH 8.6)	-	100 mM	-	-	-
HEPES (pH 7.5)	-	-	50 mM	50 mM	-
Triton-X	-	5%	1%	1%	-
NaHCO <sub>3</sub>	-	-	-	-	100 mM
All solutions made up in H <sub>2</sub> O					

### 2.1.9 RNA sequencing and analysis

EpCAM<sup>+</sup> freshly isolated cells were embedded in matrigel and collected at different time points after culture (time 12h, 24h, 48h and 6 days, with this last time point named as organoids). The starting time point, 0h was collected after seeding in matrigel but prior to adding any medium. Total RNA was extracted using RNeasy micro kit according to manufacturer instructions. RNA libraries were prepared by using Smartseq2. RNA sequencing was performed using Illumina Hiseq sequencer. High quality reads were mapped to *Mus Musculus* GRCm38 genome reference with STAR aligner (v 2.5.0c). Feature counts (version 1.4.6-p5) was used together with the version GRCm38.84 to calculate gene expression values as raw read counts. RPKM was also calculated. HTSFilter was applied to remove non-expressed genes or genes showing too much variability. Heatmap of expression were performed based on scaled RPKM values. Hierarchical clusterisation was performed by calculating Pearson Correlation among genes and by applying the average clusterisation method. The Trimmed Means of M-values (TMM) normalisation strategy was used to analyse data across the different samples. Differentially expression (comparing each time point to the previous one) was calculated using edgeR with  $FDR \leq 0.05$ . Clustering was done taking in account Differentially Expressed genes at least in one comparison (comparing each time point to the previous one and organoids vs 0h) applying a cutoff of RPKM >1 based on average RPKM of duplicates. Numbers indicate normalised expression values after applying a scaling procedure on the average RPKM.

## 2.2 Animal studies

### 2.2.1 Animal breeding and maintenance

The University of Cambridge Animal Welfare and Ethical Review Body (AWERB) have regulated this research under the Animals (Scientific Procedures) Act 1986 Amendment Regulations 2012 following ethical review. Both male and female mice were used throughout this work and were of a mixed background. Mice were kept under standard handling procedures in a pathogen free environment with a 12-hr day/night cycle. Sterile food and water were given to the mice *ad libitum*. Breeding the mice with the alleles described in Table 2.5 generated experimental genotypes.

Table 2.5 – Experimental animal lines

Gene/Locus	Allele type	Abreviation	Full name	MGI ID
<i>Arid1a</i>	Floxed allele	<i>Arid1a<sup>flx</sup></i>	<i>Arid1a<sup>tm1a(KOMP)Wtsi</sup></i>	4362765
<i>Tet1</i>	Hypomorph	<i>Tet1<sup>hypo</sup></i>	<i>Tet1<sup>tm1a(KOMP)Wtsi</sup></i>	5286193
<i>Tet1</i>	Floxed allele	<i>Tet1<sup>flx</sup></i>	<i>Tet1<sup>tm1c(KOMP)Wtsi</sup></i>	In house
<i>Tet1</i>	Knock out	<i>Tet1<sup>fko</sup></i>	<i>Tet1<sup>tm1b(KOMP)Wtsi</sup></i>	In house
<i>Prom1</i>	CreERT2	<i>Prom1Cre<sup>ERT2</sup></i>	<i>Prom1<sup>tm1(cre/ERT2)Gilb</sup></i>	3830624
<i>Rosa26</i>	CreERT2	<i>RosaCre<sup>ERT2</sup></i>	<i>Gt(ROSA)26Sor<sup>tm1(cre/ERT2)Tyj</sup></i>	3699244
<i>Lgr5</i>	CreERT2	<i>Lgr5iCre<sup>ERT2</sup></i>	<i>Lgr5<sup>tm1(cre/ERT2)Cle</sup></i>	3764660
<i>Rosa26</i>	Tomato Reporter	<i>Rosa26<sup>TdTomato</sup></i>	<i>Gt(ROSA)26Sor<sup>tm14(CAG-tdTomato)Hze</sup></i>	3809524
<i>Rosa26</i>	ZsGreen Reporter	<i>Rosa26<sup>ZsGreen</sup></i>	<i>Gt(ROSA)26Sor<sup>tm6(CAG-ZsGreen1)Hze</sup></i>	3809522
<i>Rainbow</i>	Repoter	<i>Rainbow2.1</i>	<i>Gt(ROSA)26Sor<sup>tm1(CAG-Brainbow2.1)Cle</sup></i>	4835542
<i>Rosa26</i>	FLPe	<i>Rosa26<sup>FLPe</sup></i>	<i>Gt(ROSA)26Sor<sup>tm1(FLP1)Dym</sup></i>	2429412
<i>Sox2</i>	CRE	<i>Sox2<sup>CRE</sup></i>	<i>Edi3<sup>Tg(Sox2-cre)1Amc</sup></i>	2656539

### 2.2.2 Genotyping

Ear biopsies of new litters were taken and then incubated in lysis buffer (Bioquote, 102-T) overnight at 60°C. After lysis DNA solutions were diluted 10 fold and stored at 4C until analysis. Genotype was determined by PCR using allele specific primers (Table 2.6). PCR reactions were carried out using GoTaq PCR kit (Promega, M5001) following reaction mixes and protocols defined by the manufacturer and visualised by gel electrophoresis.

Table 2.6 – Genotyping primer sequences

Allele	Detection	Forward (5'-3')	Reverse (5'-3')
<i>Arid1a<sup>flx</sup></i>	Knock In/WT allele	TCAAGGGGCATGATGGGAAC	CATCCCCAAGGCCATCATCT
<i>Tet1<sup>hypo</sup>/Tet1<sup>flx</sup>/Tet1<sup>flko</sup></i>	WT allele	TGAACATGCTGCCCGTTAG	AGATGCTGTTGGTGTGGTTG
	Knock In allele	TGAACATGCTGCCCGTTAG	TCGTGGTATCGTATATGGCC
<i>Prom1Cre<sup>ERT2</sup></i>	WT allele	GAGTTTCCAGAAAGTACCTCATGCT	ACAGCAGGGCACTGAAAGAC
	Knock In allele	GAGTTTCCAGAAAGTACCTCATGCT	GCAAAATTTGGTGTACGGTCAGTAA
<i>Lgr5iCre<sup>ERT2</sup></i>	WT allele	CACCA GCTTACCCCATGACT	CTCCTGCTCTAAGGCACCAC
	Knock In allele	CACCA GCTTACCCCATGACT	CAAAGGGTGGTACAGACG
<i>Rosa26<sup>TdTomato</sup></i>	WT allele	AAGGGAGCTGCA GTGGAGTA	CCGAAAATCTGTGGGAAGTC
	Knock In allele	GGCATTAAAGCAGCGTATCC	CTGTCCTGTACGGCATGG
<i>Rosa26<sup>ZsGreen</sup></i>	WT allele	AAGGGAGCTGCA GTGGAGTA	CCGAAAATCTGTGGGAAGTC
	Knock In allele	AACCAGAA GTGGCACTGAC	GGCATTAAAGCAGCGTATCC
<i>Rainbow2.1</i>	WT allele	CAAATGTTGCTTGTCTGGTG	GTCAGTCGAGTGCACAGTTT
	Knock In allele	GGCACGCTGATCTACAAGGI	GGGAGGTGTGGGAGGTTTT
<i>Sox2<sup>CRE</sup></i>	Generic CRE	GCCTGCATTACCGGTCGATGCAACGA	GTGGCAGATGGCCGGCAACACCATT
<i>RosaCre<sup>ERT2</sup></i>	Generic CRE	GCCTGCATTACCGGTCGATGCAACGA	GTGGCAGATGGCCGGCAACACCATT

### 2.2.3 Tamoxifen injection

Mice were injected with 0.1-0.2 mg/g up to 4 times (refer to experimental scheme for specific tamoxifen regimen) via intraperitoneal injection. A working dilution of 20 mg/ml of tamoxifen was prepared by initially dissolving tamoxifen (Sigma, T5648) in ethanol at a concentration of 3 g/ml before diluting to a final concentration of 20 mg/ml in sterile sunflower oil (Sigma, S5007) with strong agitation at 37°C until fully dissolved.

### 2.2.4 CCl<sub>4</sub> treatment

Mice were given either a single dose of 1 ml/kg CCl<sub>4</sub> via intraperitoneal injection. CCl<sub>4</sub> (Sigma, 270652) was diluted 1/10 in corn oil (Sigma, C8267) to generate a working solution for injection.

### 2.2.5 DDC treatment

Mice were transferred to wheat free cages and fed chow supplemented with 0.1% 3,5-diethoxycarbonyl-1, 4-dihydrocollidine (DDC)(Custom animal diets LLC, AD5001) ad libitum for 5-7 days. Mouse weights were recorded every day throughout DDC feeding. Chronic DDC experiments were carried out by repeating a 5 day 0.1% DDC dose after mice were switched back to maintenance diet for 3-4 days for a total of eight times.

### **2.2.6 AAV8-p21 delivery**

AAV8.TBG.p21.BGH viral particles were provided as a gift from Professor Forbes (University of Edinburgh).  $7.5 \times 10^{11}$  viral particles were suspended in 100 ul of sterile PBS and delivered into mice by tail vein injection using BD ultrafine insulin needles.

### **2.2.7 Serum preparation and analysis**

Blood samples were allowed to clot at room temperature for 45 minutes. They were then spun down at 2000g for 15 minutes at room temperature to separate the blood clot from the serum. Finally, the supernatant (serum fraction) was removed and analysed for GLDH, AST, ALT and bile acid concentrations, performed by the Clinical pathology lab at the University of Cambridge Veterinary School.

## 2.3 Histology, immunohistochemistry and immunofluorescence

### 2.3.1 Tissue preparation and embedding

Mice were euthanised by lethal exposure to a high concentration of CO<sub>2</sub>. After sacrifice, blood samples were taken via cardiac puncture and kept at 4°C until further processing. Mice were then dissected and the livers, small intestine (SI) and pancreata were harvested and stored in PBS at 4°C. Small biopsies were taken of each organ harvested, snap frozen on dry ice and stored at -80°C for downstream genetic and gene expression analysis. Livers were split into the individual lobes, then further divided into ~5 mm<sup>3</sup> pieces and fixed in 10% neutral buffered formalin (NBF)(Fisher scientific, 5701) overnight at 4°C. SI samples were initially flushed with clean PBS and NBF then fixed submerged in NBF overnight at 4°C. Finally, pancreas samples were divided into two and submerged in NBF overnight at 4°C. Fixed tissues were then washed in PBS 3x for 5 minutes each and then embedded in paraffin, optimal cutting temperature (OCT) compound (VWR, 3611603E) or agarose. For paraffin embedded samples, fixed samples were dehydrated through ascending concentrations of Ethanol (70%, 96% and 100%) and xylene, each for 2 hours at room temperature. After incubation in xylene samples were transferred to molten paraffin (Thermo scientific, 6774006) and incubated overnight at 55°C. Finally, samples were transferred to moulds, submerged in molten paraffin and allowed to cool and solidify at 4°C for 10 minutes. For OCT, embedding, samples were incubated in 30% sucrose (Fisher scientific, S/8600/60) overnight at 4°C. Samples were then transferred to plastic moulds, submerged in OCT compound and frozen on dry ice, samples were then stored at -20°C until sectioning. For agarose embedding, samples were submerged in molten 4% low melt agarose (Bio-Rad, 161-3111) and allowed to cool and solidify at 4°C.

### 2.3.2 Immunohistochemistry

Paraffin embedded samples were sectioned at 5 µm with a microtome (Leica, RM2235), sections were then transferred to superfrost (Thermo Scientific, 12372098) slides and dried overnight at 60°C. Sections were then deparaffinised with 2 incubations of xylene for 5 minutes at room temperature. The sections were then hydrated via incubation in descending concentrations of ethanol (100%, 96%, 70% and 50%) and finally H<sub>2</sub>O each

for 5 minutes at RT. After rehydration, samples were then subject to antibody dependent antigen retrieval techniques (Table 2.7). Sections were then transferred to a humidified chamber and blocked in 1% Bovine serum Albumin (BSA)(Sigma, A7906), 2% Foetal Bovine serum (FBS) and 1% Triton-X (Sigma, T8787) diluted in tris-buffered saline (TBS) for 1.5 hours at room temperature. Primary antibodies were then incubated on sections at an assay dependent concentration (Table 2.2) diluted in a 1/100 dilution of the blocking buffer overnight at 4°C. After antibody incubation sections were rinsed 3x in TBS and blocked for endogenous peroxidase activity by incubation in 3% H<sub>2</sub>O<sub>2</sub> diluted in methanol for 20 minutes at room temperature. Sections were then rinsed in TBS and antibody binding was detected by using the DAB-Bright system (Immunologic, BS04-110) following manufacturer's instructions. After detection nuclei were counterstained by incubation in Haematoxylin (Sigma, MHS16) for 8 minutes at room temperature, sections were then washed of excess haematoxylin by washing under a running tap. Finally, slides were dehydrated in ascending concentrations of ethanol (50%, 70%, 96% and 100%) before clearing in xylene and mounting in DPX mounting medium (Fisher scientific, 15538321). Images were acquired using brightfield microscopy (Leica DM4000b) and analysed using Imagej.

### **2.3.3 Haematoxylin and eosin stain**

Tissue sections were prepared and rehydrated as described above. Nuclei were then stained in Haematoxylin for 1 minute at room temperature before being rinsed under a running tap for 5 minutes. The sections were partially dehydrated by incubation with 50%, 70% and 96% ethanol for 5 minutes each. Sections were then quickly incubated in eosin (Sigma, HT110316) for 10-15 seconds before being rinsed in 96% ethanol twice. Finally, sections were fully dehydrated by incubation in 100% ethanol and cleared in two washes in xylene before being mounted in DPX mounting medium and a coverslip. Images were acquired using brightfield microscopy and analysed using ImageJ.

Table 2.7 – Antibody information

Epitope	Source	Catalogue #	Dilution					Anitgen retrieval
			FACS	IHC	IF	CHIP	WB	
Arid1a	Atlas Antibodies	HPA005456	-	1/500	1/250	5 ug	1/5000	Heat meditated 10 mM citrate pH 6
Ki67 (sp6 clone)	ThermoScientific	MA5-14520	-	1/200	1/200	-	-	Heat meditated 10 mM citrate pH 6
5mC	Active Motif	39649	-	-	1/1000	5 ug	-	4N HCl and trypsin treatment
5hmC	Active Motif	39791	-	-	1/1000	5 ug	-	4N HCl and trypsin treatment
Pan-Cytokeratin	Dako	Z0622	-	1/500	-	-	-	Enzyme mediated Protinase K Treatment
p21	Abcam	EPR18021	-	1/1000	-	-	-	Heat meditated 10 mM Tris-EDTA pH 9
Brg1	Santa-Cruz	sc-17796	-	-	1/50	2 ug	-	-
Tet1	Millipore	ABE1034	-	-	-	5 ug	1/5000	-
Osteopontin	R&D systems	AF808	-	-	1/80	-	-	-
EpCAM	eBioscience	14-5791-81	1 µl	-	1/250	-	-	-
CD45	BD bioscience	BD 552848	1 µl	-	-	-	-	-
CD11b	BD bioscience	BD 552850	1 µl	-	-	-	-	-
CD31	Abcam	ab46733	1 µl	-	-	-	-	-
Actin	Abcam	Ab3280	-	-	-	-	1/2000	-

### 2.3.4 Picrosirius Red stain

Tissue sections were prepared and rehydrated as described above. Rehydrated sections were then incubated in Picrosirius red solution (Abcam, ab150681) for 1 hour at room temperature after which they were quickly rinsed in acetic acid twice. After washing, sections were incubated in absolute ethanol three times for five minutes each before being cleared with xylene and mounted with DPX mounting medium and a coverslip. Images were acquired using brightfield microscopy and analysed using ImageJ. Fibrotic area was calculated using an ImageJ macro developed in house.

### 2.3.5 Thick OCT section immunofluorescence

Thick frozen sections (100-50 µm) were cut from OCT embedded samples using a cryostat (Leica, CM3050s), transferred to a 24 multi well plate and washed in PBS twice to remove excess OCT compound. Sections were blocked in 5% DMSO (Sigma, D8418), 2% Donkey serum (Sigma, D9663), 1% Triton-X diluted in PBS overnight at 4°C. Sections were then incubated in primary antibody at specific concentrations (Table 2.7) diluted in 1% DMSO, 2% Donkey serum and 0.5% Triton-X diluted in PBS for 72

hours at 4°C. After antibody incubation sections were washed five times in 1% DMSO and 0.5% Triton-X diluted in PBS for 1 hour each at room temperature. Fluorophore conjugated secondary antibodies were incubated with sections at a 1/250 dilution in 2% Donkey serum, 1% DMSO and 0.5% Triton X in PBS for 48 hours at 4C and protected from light. After secondary antibody incubation sections were incubated with Hoechst 33342 (Thermo scientific, H3570) diluted 1/1000 in PBS for 1 hour at room temperature. Sections were then incubated in ascending concentrations of glycerol (10%, 30%, 50%, 70% and 90%) for 1 hour each at room temperature. Sections were finally transferred to slides, mounted in Vectashield (Vector laboratories, H-1000) with a cover slip and sealed with nail polish. Images were acquired using confocal microscopy (Leica SP8) and analysed using ImageJ.

### **2.3.6 Thin OCT section immunofluorescence**

Thin frozen sections (10 µm) were cut from OCT embedded samples using a cryostat and transferred to superfrost+ slides (VWR, 631-0108). After sectioning samples were washed in PBS twice to remove excess OCT compound, placed in a humidified chamber and blocked in 2% Donkey serum, 5% DMSO and 1% Triton-X for 1.5 hours at room temperature. Sections were then incubated in primary antibodies at antibody specific concentrations (Table 2.7) diluted in a 100-fold dilution of the blocking buffer, overnight at 4°C. Sections were then rinsed PBS 3x and then incubated in fluorophore conjugated secondary antibodies diluted 1/250 in 2% donkey serum, 1% DMSO and 0.5% Triton-X in PBS for 2 hour at room temperature. After which, sections were rinsed in PBS three times and incubated in Hoescht 33342 diluted 1/1000 in PBS for 5 minutes at room temperature. After a final wash in PBS sections were mounted with Vecatshield and a coverslip and sealed using nail polish. Images were acquired using confocal microscopy and analysed using ImageJ.

### **2.3.7 Organoid immunofluorescence**

Organoids were removed completely from the matrigel matrix by several washes with cold Advanced DMEM. The organoids were then fixed with 4% paraformaldehyde at 4°C for 20 minutes. The fixative was removed by washing the organoids in PBS three times. Blocking and permeabilisation was carried out by incubating the fixed organoids

in 0.3 % Triton-X, 1% BSA, 1% DMSO, 2% Donkey serum dissolved in PBS for 2 hours at room temperature. The organoids were then incubated with the primary antibody at the relevant concentration dissolved in a 1/100 dilution of blocking buffer at 4°C overnight (Table 4). After washing the organoids in 1/100 dilution of the blocking buffer three times the appropriate fluorophore conjugated secondary antibodies were added at a concentration of 1/250, dissolved in 0.05% BSA in PBS and incubated for 2 hours at room temperature. Organoids were washed in PBS then incubated with Hoechst 33342 dissolved 1/1000 in PBS for 5 minutes at room temperature. The organoids were rinsed one further time in PBS and imaged suspended in PBS using confocal microscopy (Leica SP8) and analysed using ImageJ.

## 2.4 Liver wholemount staining protocols

### 2.4.1 Tissue preparation

Liver samples were prepared as described above, however, livers were also flushed to remove excess blood from the vasculature prior to removal from the mouse. This was performed by initially making an incision in the lower aorta before injecting 10 ml of heparinised PBS (10 U/l)(Sigma, H3149) using a 10ml syringe and a 21g needle into the left ventricle of the heart. After perfusion with PBS livers were removed, fixed and embedded in agarose as described above.

### 2.4.2 Vibratome sectioning

Agarose embedded samples were placed in the vibratome (Leica, VT1000s) bath that was then flooded with PBS. Sections were then taken at several thicknesses (50, 100, 400  $\mu$ m and 1 mm), transferred to PBS and stored at 4°C until further processing.

### 2.4.3 See Deep brain optical tissue clearing

See deep brain (SeeDB) optical clearing was optimised for liver sections based from protocols published by Ke et al. (2013) and Lloyd et al. (2016) (Ke, Fujimoto and Imai, 2013; Lloyd-Lewis *et al.*, 2016). Liver sections of varying sizes were initially blocked in 10% BSA and 1% Triton-X in PBS overnight at 4°C. Sections were then incubated in primary antibodies, diluted in blocking buffer, for 4 days at 4°C. After primary antibody incubation samples were washed for 3 times for 1 hour with 0.1% Triton-X in PBS at room temp. Appropriate fluorophore conjugated secondary antibodies were incubated with sections and were incubated for 2 days at 4°C. Samples were then washed in 0.1% Triton-X in PBS three times for 1 hour at room temperature and then incubated with Hoescht 3342 diluted 1/1000 in PBS for 60 minutes at room temperature. Samples were then immersed in ascending concentrations of fructose (Fisher scientific, 10579760) with 0.5%  $\alpha$ -thioglycerol (Sigma, M1753) every 12 hours (20, 40, 60 and 80%) at room temperature whilst being agitated. Sections were then incubated in 100% fructose for 24 hours followed by incubation in SeeDB solution (115% w/v) for a final 24 hr. Sections were imaged mounted in SeeDB solution by confocal microscopy.

#### 2.4.4 CUBIC optical tissue clearing

CUBIC clearing was adapted from protocols published by Susaki et al. (2015) and Lloyd et al. (2016) (Susaki *et al.*, 2015; Lloyd-Lewis *et al.*, 2016). Tissues of varying size were submerged in reagent 1 or 1a (A less harsh variant of reagent 1, unpublished from protocol on <http://cubic.riken.jp/>) for 5 days whilst being agitated at 37°C. CUBIC reagents were refreshed daily. After incubation, sections were blocked in 10% donkey serum and 0.5% Triton-X in PBS overnight at 4°C. The next day primary antibodies were added, and samples incubated for 4 days at 4°C. After primary antibody incubation samples were washed for 3 times for 1 hour with 0.1% Triton-X in PBS at RT. Appropriate fluorophore conjugated secondary antibodies were incubated with sections and were incubated for 2 days at 4°C. Samples were then washed in 0.1% Triton-X in PBS three times for 1 hour at room temperature and then incubated with Hoescht 3342 diluted 1/1000 in PBS for 60 minutes at room temperature. Samples were then immersed in CUBIC reagent 2 and agitated for 48 hours at 37°C before being imaged by confocal microscopy. Imaging was carried out with sections mounted in CUBIC reagent 2. For all CUBIC reagent recipes see Table 2.10.

Table 2.8 – CUBIC reagent recipes

Ingredient	R1 (% w/v)	R1a (% w/v)	R2 (% w/v)
Urea	25	10	25%
Quadrol	25	5	-
Triton-X	15	10	0.10%
5M NaCl	-	0.18	-
Sucrose	-	-	50%
Triethanolamine	-	-	10%
All made up in H <sub>2</sub> O			

#### 2.5 Statistical analysis

Unless otherwise stated all appropriate statistical analysis was carried out in statistical program R and visualised using the ggplot2 package (R Core Team, 2018).

### 3. Results

The siRNA knock-down screen in section 3.1 and some *in vitro* data in sections 3.2 and 3.3 was carried out in close collaboration with Dr Luigi Aloia. His contribution is stated in External Contributions and at the end of relevant figure legends, when not stated, the results have been produced entirely by me.

#### 3.1 Identification of *Arid1a* and *Tet1* as candidates involved in ductal progenitor dynamics

We began the search to find potential candidate genes by analysing gene expression changes in response to liver damage. In order to focus on the liver's ductal regenerative response, we analysed a previously generated gene expression dataset derived from livers that had been damaged using carbon tetrachloride (CCl<sub>4</sub>). CCl<sub>4</sub> is a potent cytotoxic agent which causes massive death of central vein hepatocytes resulting in a ductal and hepatocyte proliferative response to facilitate regeneration of the lost tissue (Weber, Boll and Stampfl, 2003) In this experiment mice were subject to a single dose of CCl<sub>4</sub> (1 ml/kg) delivered via intraperitoneal injection and allowed to recover for either 2.5, 6 or 12 days (labelled T2.5, T6 or T12 respectively). At each time-point whole liver biopsies were taken for gene expression analysis performed via microarray and compared to mock injected undamaged controls (labelled T0) (Figure 3.1a).

Analysis of the raw G-median intensity (a read out of gene expression) showed a remarkable spike of gene expression in several components of the BAF complex 6 days after CCl<sub>4</sub> induced liver damage (Figure 3.1b). These included components involved in DNA binding (*Arid1a*, *Arid1b* and *Arid2*), and the crucial ATP hydrolysis activity (*Brg1* and *Brm*). Interestingly, only one of the two ATPases in the complex is up-regulated suggesting that after damage there could be a more specific set of BAF components activated. In order to confirm our results and understand further if the response is the result of a progenitor response, we validated the results by qPCR. As expected, the select components (labelled in red) were shown to have the same pattern of expression by qPCR. Furthermore, the peak of expression seen in the BAF complex after 6 days correlates with the peak of expression of progenitor and WNT signalling markers (hallmarks of the ductal progenitors) *Lgr5* and *Axin2* (Figure 3.1c). This provides some evidence that the BAF complex might be involved in the ductal progenitor response.

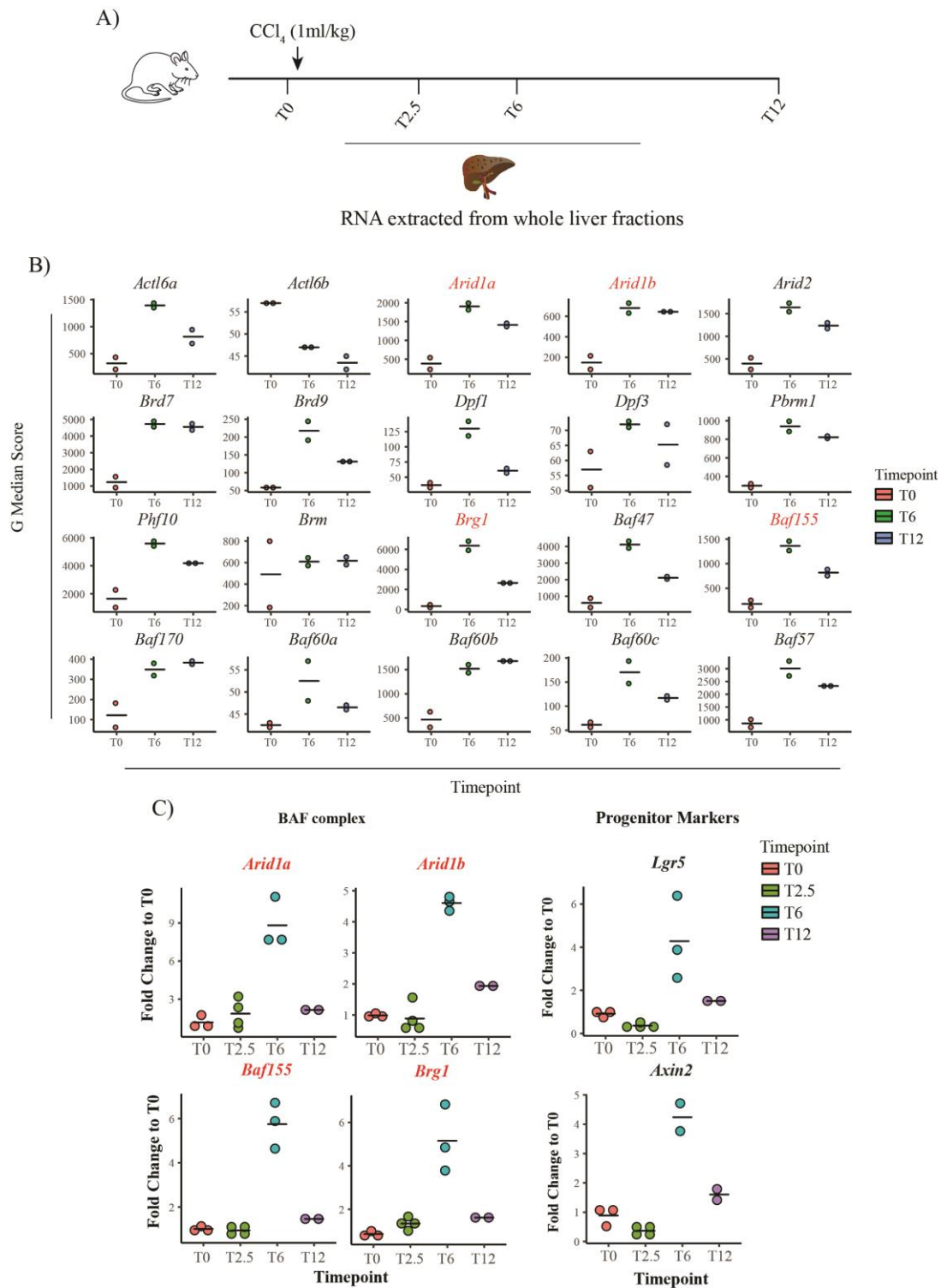


**Figure 3.1 - Multiple components of the BAF complex are upregulated during CCl<sub>4</sub> induced liver damage.** A) Schematic of the liver damage protocol. Mice were injected with CCl<sub>4</sub> at a dose of 1 ml/kg and whole liver samples were taken at 2.5 (T2.5), 6 (T6) or 12 (T12) days post-injection, as well as from non-injected controls (T0). B) Gene expression analysis was carried out by microarray and the G-median intensity score was plotted against the T0, T6 and T12 timepoint for the different components of the BAF complex. Each timepoint was analysed in duplicate from two independent biological replicates, replicates are represented as dots with a bar to represent the group mean. C) Microarray analysis was validated by qPCR and several BAF components were compared to progenitor markers *Lgr5* and *Axin2*. At least two independent biological replicates were analysed per timepoint (T0 n=3, T2.5 n=4, T6 n=3, T12 n=2) represented as dots with a bar as the group mean.

It is important to note that as the gene expression data was derived from whole liver biopsies it is likely that the gene expression changes were heavily influenced by the bulk hepatocyte population. Therefore, it is impossible to tell whether the changes in gene expression identified are due to ductal progenitors rather than another cell type. To solve this problem and remove the confounding influence of the heterogeneous cell population found in the whole tissue biopsy and ensure we are only looking at the ductal response we want to study, we took advantage of the liver organoid model. Liver organoids are generated when quiescent or otherwise non-proliferative ductal cells are put in defined 3D culture conditions during which there is activation of proliferation and the cells enter a bi-potent state that are able to differentiate into ductal and hepatocyte-like cells (Huch, Dorrell, *et al.*, 2013; Huch *et al.*, 2015). As a result, by following liver organoids during their initial formation *in vitro* we can analyse the changes in ductal cells in isolation from other cell types. Thus, allowing us to better dissect the initial steps of progenitor activation before the onset of proliferation and bi-potency.

As a result, we isolated EpCAM<sup>+</sup> ductal cells using a FACS strategy generated and optimised by Aloia and colleagues (Unpublished) and placed them in 3D culture before either immediately (0h), or after a specific time in culture isolating for gene expression analysis by RNA sequencing (Figure 3.2a). We initially looked at the changes in the ductal, proliferative and progenitor signature of the cell populations at each time point by analysing specific markers of each. Interestingly, there was a peak of expression of proliferative marker *miKi67* at 48 hours before the peak of the expression of the progenitor markers *Lgr5* and *Trop2*, which only happens after the organoids become established after 6 days. This suggests that perhaps the onset of proliferation and stem cell marker expression are uncoupled. Moreover, throughout organoid derivation we found there was a fascinating dynamic change in the expression pattern of certain ductal markers. Where in some cases there was down-regulation (*Cftr*, *Ggt1*), others were up-regulated (*Krt7*, *Krt19*) and some were transiently altered (*Hnf1b*) (Figure 3.2b). Taken together this suggests that although liver organoids remain largely ductal in nature, they do not resemble fully mature ductal cells from which they are derived. This highlights a potential problem with our model, these gene expression changes could indicate that organoid generation may represent the emergence of a non-physiological ductal cell population. Evidence against this idea has

been shown by Aloia and colleagues (in press) where the gene expression changes seen in organoid generation were observed to be similar to those in EpCAM+ cells isolated during liver damage, suggesting that the organoid generation does faithfully model ductal cells during damage.

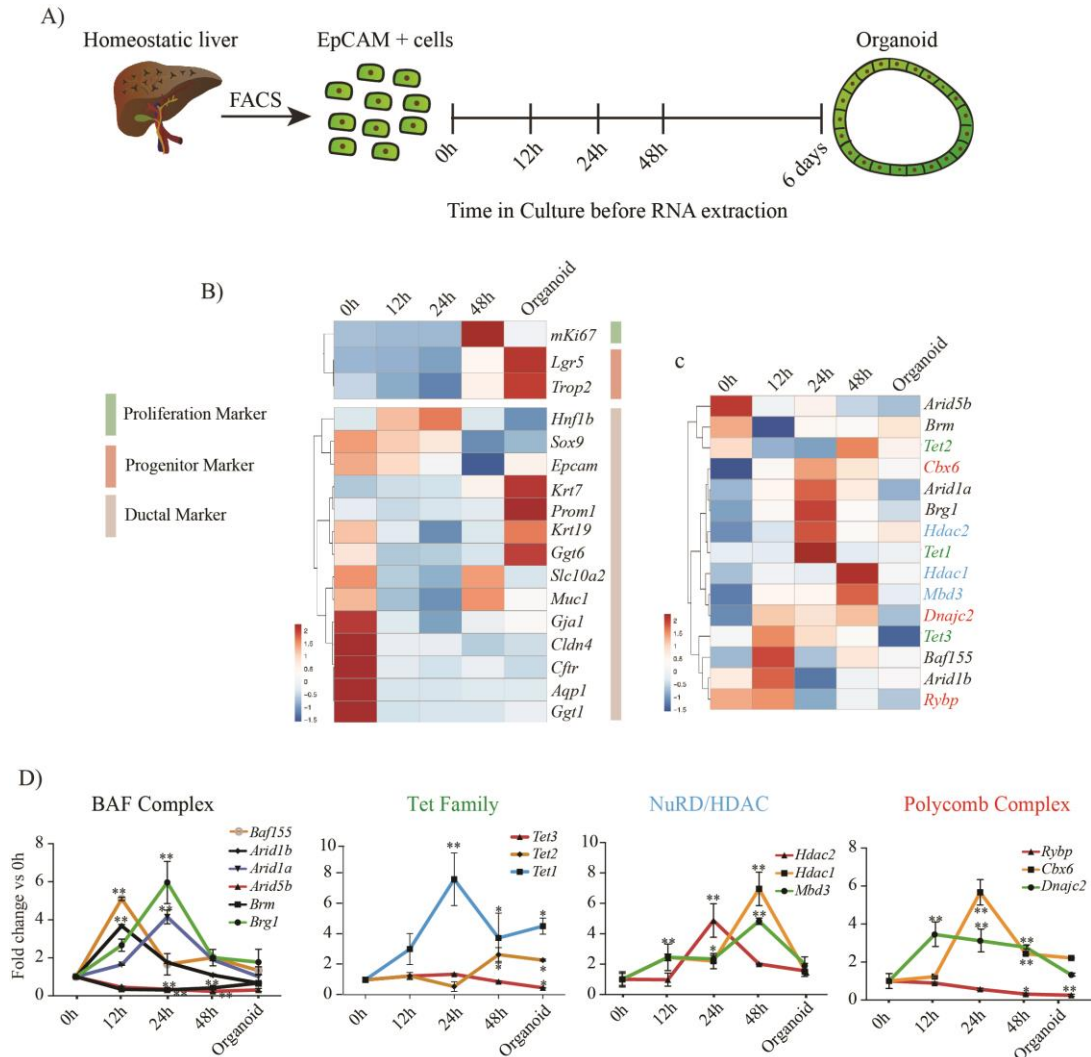


**Figure 3.2 – Several epigenetic modifiers are dynamically regulated during organoid derivation.** A) Experimental scheme, EpCam+ cells were isolated from healthy livers and placed in 3D culture before RNA isolation either just after Matrigel embedding (0h) or 12 hours (12h), 1 day (24h), 2 days (48h) and 6 days (Organoid) of 3D culture. B) Hierarchical clustering of RPKM values of selected progenitor (red), proliferation (green) or ductal (brown) markers throughout the time course. Values were derived from two independent biological replicates. C) Hierarchical clustering of RPKM of selected epigenetic families or complexes throughout the time course. D) qPCR validation of RNAseq derived values. Error bars show stand error of the mean of two independent replicates. (Aloia *et al.* unpublished).

In any case, we next wanted to assess which genes could be responsible for such a large change in genetic programming, we therefore analysed changes in expression

of candidate epigenetic regulators that have been previously implicated in fate changes, before or at the onset of the expression of proliferative markers at 48 hours. We began by analysing the expression of the BAF complex to validate previous evidence (Figure 3.1) but also widened our search to other epigenetic modifiers that have been described as instrumental either in cell fate changes during development or adulthood. Remarkably, we found that several components of the BAF, NuRD, Polycomb complexes and Tet family of genes are dynamically expressed throughout organoid derivation (Figure 3.2c). These findings were further validated by qPCR which again showed that several components were significantly up regulated over the time course. Most interestingly, components of the BAF complex such as *Arid1a* and *Brg1* and the Tet family member *Tet1* had peaks of expression at 24 hours, before the onset of proliferation at 48 hours (Figure 3.2d). As a result, these candidates could be crucial for the activation of the proliferative response.

To understand whether this was the case we carried out a small and targeted siRNA screen against each of the candidates. If the candidates were involved in the activation of proliferation during the generation of organoids knock down during isolation would result in fewer organoids being formed. Freshly sorted EpCAM+ cells were isolated and transfected with a pool of 4 siRNAs against one of the candidates as well as a non-targeting siRNA control (Figure 3.3a). After transfection cells were seeded in organoid culture conditions and then analysed for organoid formation efficiency. Interestingly, only *Tet1*, a member of the Tet family of enzymes, showed significant impairment in organoid formation, suggesting that *Tet1* is crucial for ductal progenitor activation (Figure 3.1.3b-c). It is important to note that the lack of effect from the other epigenetic regulators in the screen may be as a result of insufficient siRNA mediated knockdown rather than a true lack of effect. However, it was shown that the pooled siRNA induced >50% knockdown in all genes when compared to control siRNA (data not shown, Aloia *et al.* in press). Despite this, if only a small amount of the target gene is required for function it may be possible that any level knockdown would still be insufficient to see the effect of the gene. In this case, full knockout through a strategy such as CRISPR may yield different results and more conclusive results. Finally, as siRNA knockdown may have off-target effects, something that is made more likely when using 4 pooled siRNAs, the reduced organoid formation observed with the knockdown of *Tet1* may be as a result of knockdown of

an unknown gene. To unravel this problem specific genetic ablation of *Tet1* would be required to validate the result (see Chapter 3.3.1 for further details).

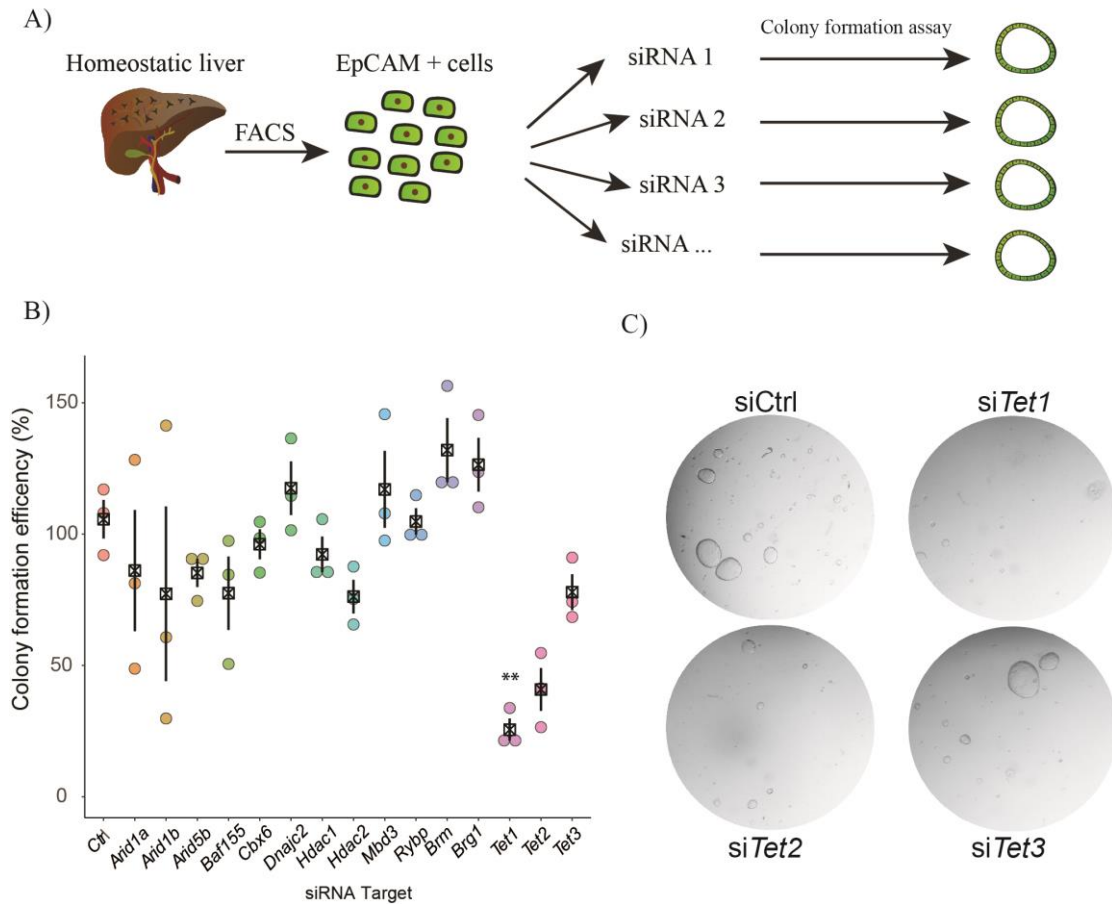


**Figure 3.3 - siRNA knockdown reveals organoid derivation is dependent on *Tet1* expression.** A) Experimental scheme: Freshly sorted EpCAM+ cells were transfected with a small library for epigenetic modifiers and put into 3D culture. B) Colony formation efficiency of transfected populations after seeding at a density of  $1 \times 10^5$ . Values were normalised against a control siRNA derived from three independent biological replicates represented as dots with a box representing the group mean. Error bars show standard error of the mean. \*\*  $p > 0.01$  determined by one way ANOVA and Tukey HSD test. C) Representative images of the resultant colonies grown from cells transfected with control siRNA or siRNA against the Tet family of genes. (Aloia *et al.* unpublished).

In our initial screen we found knock down of members of the BAF complex to have no effect on organoid establishment (Figure 3.3b-c), as explained above this may be as a result of insufficient knockdown. However, we wanted to understand whether different machinery was involved in the maintenance of proliferation after the initial generation of organoids. We therefore, repeated the screen on a smaller scale with a subtle change whereby instead of using freshly isolated EpCAM+ cells we used single cells dissociated from established organoids (Figure 3.4a). In this situation we found that knock down of certain components of the BAF complex including *Arid1a* and the APTase *Brg1* resulted in an increase in organoid formation efficiency (Figure 3.4b-c).

As a result, components of the BAF complex may be involved in the maintenance of organoid culture rather than their establishment. It is important to note that this experiment was carried out once and further repetition would be required to make robust conclusions. However, considering several specific BAF components showed a similar result we could suggest a potential involvement of the complex as a whole.

In summary, using initial gene expression and knockdown studies we have identified *Tet1* as crucial for the establishment liver organoids, and members of the BAF complex such as *Arid1a* and *Brg1* as important for correct maintenance of liver organoids. As a result, *Tet1* and *Arid1a* were taken forward for further functional analysis in order to understand their underlying mechanism of action and overall importance in liver regeneration.

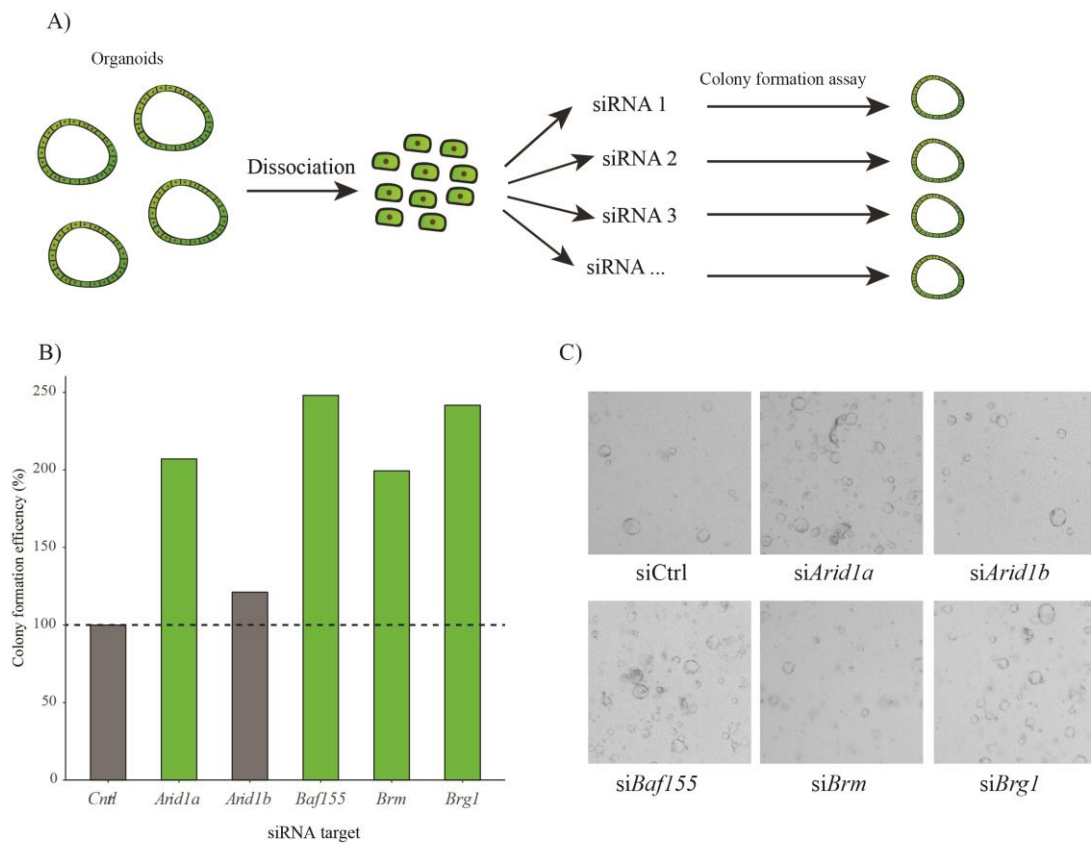


**Figure 3.4 - siRNA knockdown of components of the BAF complex enhances organoid survival.** A) Experimental scheme: Established organoids were dissociated into single cells before being transfected with siRNA against specific BAF components and seeded into 3D culture to assess colony formation efficiency. B) Quantification of colony formation efficiency of organoids after transfection, values were normalised against control siRNA derived from a single experiment. C) Representative images of cells transfected with specific siRNAs after 4 days of 3D culture. (Aloia *et al.* unpublished).

## 3.2 The role of *Arid1a* in ductal progenitor maintenance and differentiation.

### 3.2.1 Dosage of *Arid1a* modulates the proliferative and differentiation capacity of ductal progenitors in vitro.

siRNA mediated *Arid1a* knockdown showed altered progenitor dynamics only in established organoids and not during the derivation of organoids which suggests a role in progenitor state maintenance rather than acquisition. We wanted to further understand the role of *Arid1a* in this phenomenon by manipulating *Arid1a* in established organoid lines. This will allow us to remove any confounding effects of *Arid1a* in *de novo* organoid generation as well as validate the siRNA studies ruling out any off-target effects. To achieve this, we took advantage of the CRISPR genome-editing tool to mutate *Arid1a* in established organoids. Two independent clonal organoid lines with the same 11 bp deletion in the first exon of the longest isoform - isoform B of *Arid1a* (Figure 3.5a) were established (labelled *Arid1a* isoB<sup>-/-</sup>). The mutation results in a frame shifted transcript and ultimately a nonsense protein sequence. Since the mutation is identical in the two organoid lines we pooled the data from subsequent studies from the two clonal lines. However, it is crucial to note that a second isoform of *Arid1a* exists that does not include the exon in which we targeted our mutation (Figure 3.5a). As a result, at the protein level we can detect ARID1A expression both by immunofluorescence and western blot (Figure 3.5b-c). Interestingly, there was a downward shift in size of ARID1A band in the western blot providing evidence that expression is due to the unaltered smaller isoform. Therefore, any observations derived from the *Arid1a* isoB<sup>-/-</sup> lines can only be attributed to the loss of only isoform B and not the total loss of *Arid1a*.

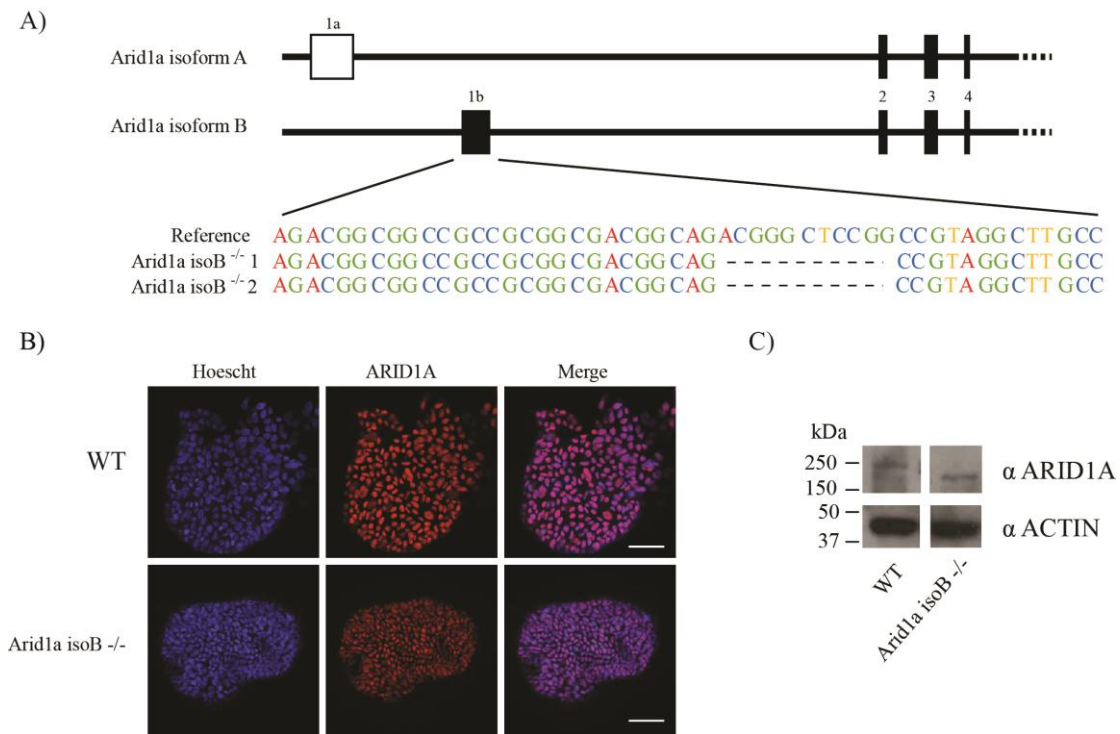


**Figure 3.5 - CRISPR mediated deletion of ARID1a isoform B.** A) Schematic of the *Arid1a* Genetic locus showing an expanded region of exon 1b highlighting the deletion of two independent mutant clones. B) Representative immunofluorescent images of WT of mutant clones stained for ARID1A (red) and nuclear marker Hoechst (blue). Scale Bar = 50  $\mu$ m. C) Western blot showing ARID1A and ACTIN protein expression, representative of two independent experiments.

The liver organoid progenitor capacity is down to two crucial properties, the ability to self-renew and differentiate towards a hepatocyte fate. Therefore, we wanted to understand how *Arid1a* may regulate these key progenitor features. As a primary read out of self-renewal either WT or *Arid1a* isoB<sup>-/-</sup> lines were dissociated into single cells and seeded in 3D culture conditions to understand how *Arid1a* mutation affects organoid formation efficiency (Figure 3.6a). In line with previously described siRNA data, mutation of *Arid1a* isoB results in significantly increased organoid formation efficiency (Figure 3.6b-c). This suggests that partial loss of *Arid1a* either through siRNA-mediated knock down or by removal of one isoform results in increased organoid formation efficiency. However, this increased organoid formation may not be as a result of increased progenitor self-renewal but by some other non-specific pro-proliferative pathway that is not involved in liver regeneration but results in an increased organoid formation in our *in vitro* system.

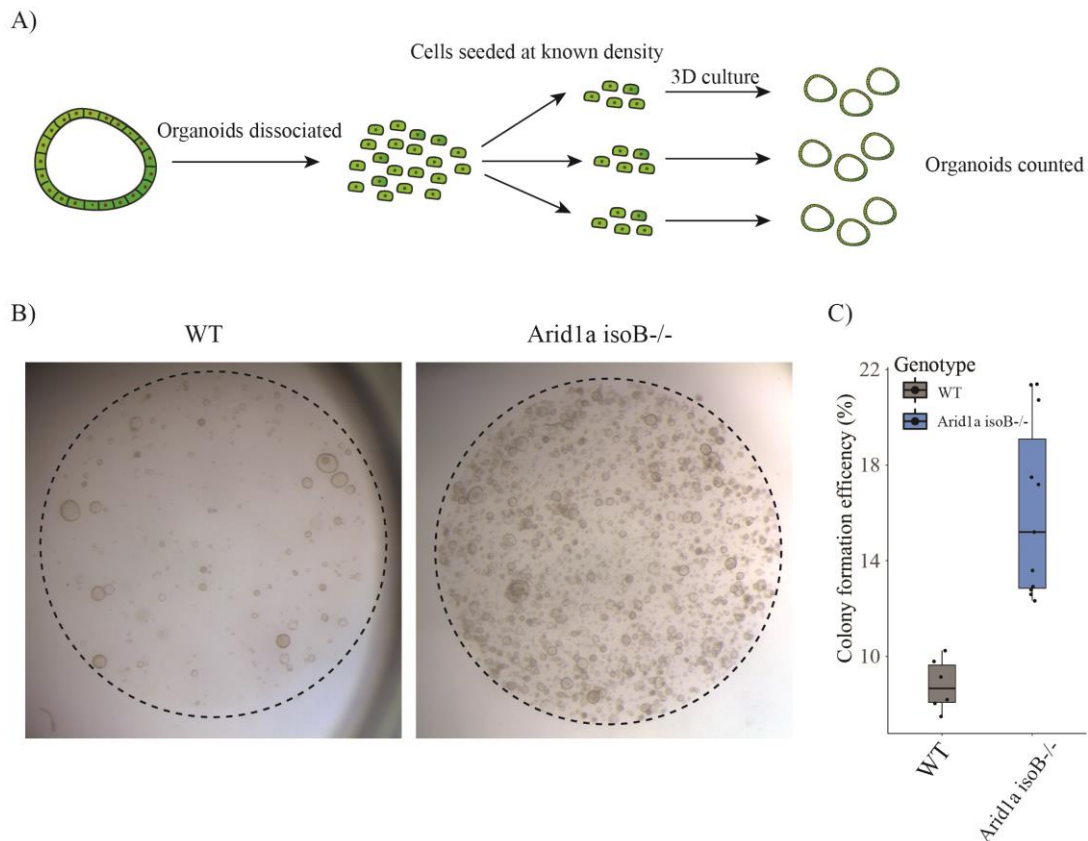


**Figure 3.6 - Arid1a isoB<sup>-/-</sup> organoids have increased organoid formation efficiency.** A) Experimental scheme: Either WT or mutant organoids were initially dissociated before being seeded at a density of 10,000 cells per well. The number of organoids was counted after 10 days. B) Representative images of single wells after 10 days of organoid growth. C) Organoid formation efficiency expressed as the number of organoids formed over the total number of cells seeded. Boxplots show group median, interquartile range as well as the overall range of data. Boxes represent every individual well quantified from two independent experiments.

Therefore, in order to further understand whether the observed increased organoid formation efficiency can be explained by an enhanced self-renewal and survival and rule out non-physiological pathways we assessed the expression markers of liver progenitor activation. Molecular characterisation of the Arid1a isoB<sup>-/-</sup> lines compared to WT organoids in normal expansion conditions showed that loss of isoform B causes a reduction in expression of *Lgr5*, *Axin2* and *Sox9* whilst showing increased expression of differentiation markers *Alb* and *Ttr* (Figure 3.7a-b). As a result, organoids lacking Arid1a IsoB are displaced from a ground liver organoid state and are seemingly pushed to a more hepatocyte fate when compared to WT organoids. This is contrary to the idea that the enhanced organoid formation efficiency is because of an enriched progenitor population. Instead, the opposite was true where increased organoid formation is linked to an increased differentiation state. This may represent a transit-amplifying (TA) population much like what is observed in other organs such as the

small intestine where during differentiation cells go through a short phase of increased proliferation (Barker, van de Wetering and Clevers, 2008). Whether this is the case and crucially whether this TA population represents a true population *in vivo* requires more study.

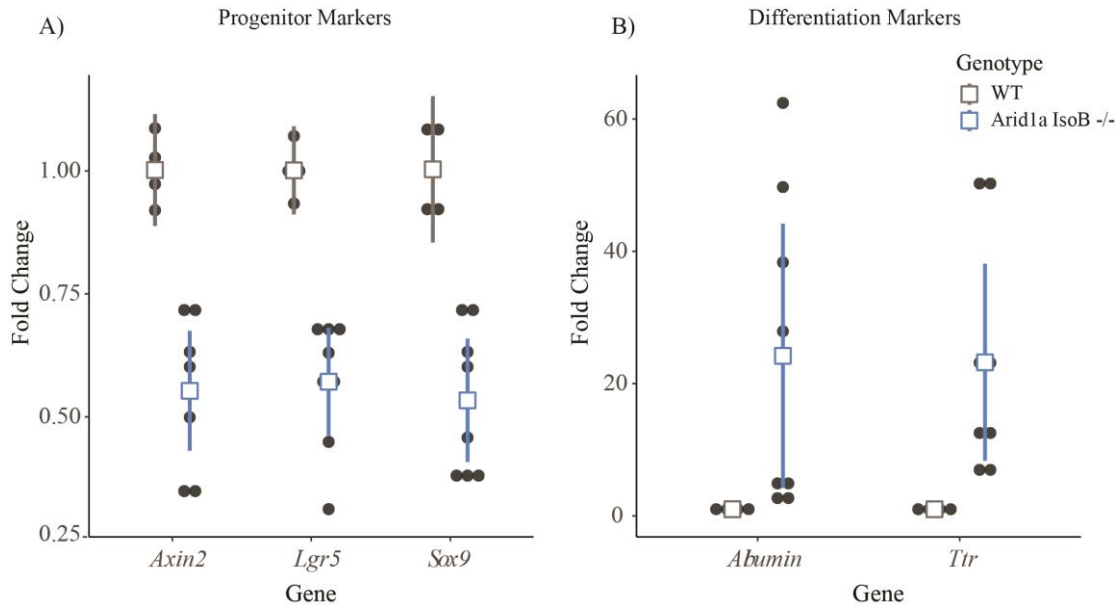


**Figure 3.7 - *Arid1a* isoB<sup>-/-</sup> organoids have decreased expression of progenitor markers whilst increasing the levels of hallmark differentiation genes.** Gene expression of progenitor markers *Axin2*, *Lgr5* and *Sox9* (A) or markers of early differentiation, *Alb* and *Ttr* (B) during normal organoid expansion. Data is expressed as fold change against WT organoids with each dot representing an individual reading, a box representing group mean (+/- 95% confidence interval). Data represents two experiments with a bulk WT population (n=1) and two independent mutant clones (n=2) carried out in duplicate. (Aloia *et al.* unpublished).

In any case, the increased expression of markers of differentiation may indicate an enhanced ability to differentiate, another key property of liver organoid culture. *In vivo*, ductal driven liver regeneration is dependent on the efficient and complete differentiation from the bi-potent ductal progenitor cell to either mature hepatocytes or ductal cells. Therefore, if manipulation of *Arid1a* either enhances or impairs complete differentiation it may ultimately lead to an altered liver regeneration capacity. Therefore, we next wanted to further understand the role of isoform B in the differentiation of ductal progenitors. To study this, we used liver organoids as a model of progenitor differentiation. Either WT or *Arid1a* isoB<sup>-/-</sup> organoids were initially seeded in normal expansion conditions before being switched to differentiation media for 14 days inducing organoids to acquire hepatocyte fate as described by Huch and colleagues (2013) (Figure 3.8a). After differentiation organoids were analysed for several markers of early and terminal differentiation.

Gene expression analysis of progenitor markers revealed that after differentiation *Axin2*, *Lgr5* and *Sox9* expression was abolished both WT and *Arid1a* isoB  $-/-$  lines. This suggests that despite the loss of isoform B altering progenitor gene expression in organoid expansion conditions it does not alter their down regulation upon differentiation (Figure 3.8b). However, when considering the marker of early differentiation *Alb*, organoid differentiation results in further up-regulation of its expression resulting in markedly increased expression in expansion and differentiation when compared to their WT counter parts. Interestingly, another early differentiation marker, *Ttr*, has similar expression after differentiation between *Arid1a* IsoB  $-/-$  and WT organoids (Figure 3.8b). Taken together these data suggest that loss of IsoB does not affect the exit from progenitor state in liver organoids during differentiation and partially enhances the acquisition of the hepatocyte fate.

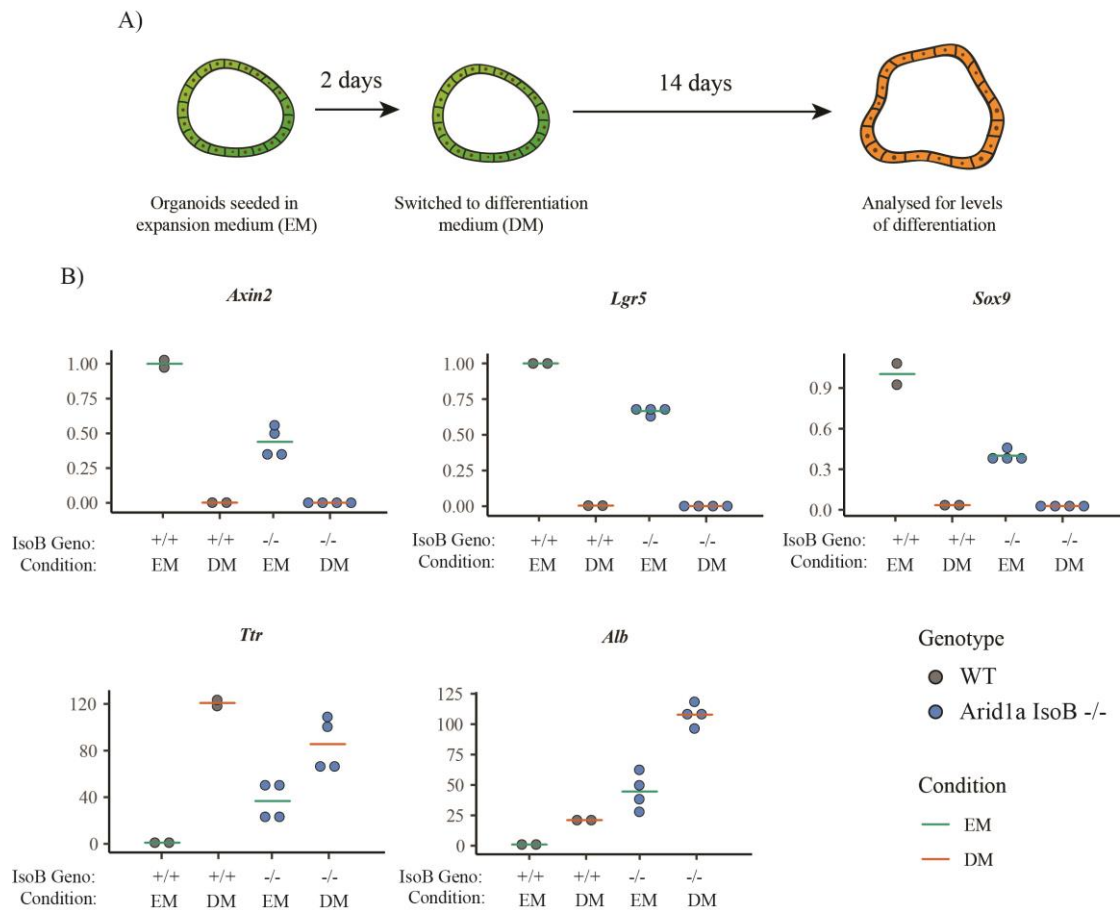


**Figure 3.8 - Loss of isoform B results in altered gene expression after differentiation towards hepatocyte fate.** A) Experimental scheme: Either WT or mutant organoids were initially seeded in expansion media and after two days switched to the differentiation protocol and analysed after fourteen days of differentiation. B) Gene expression of progenitor markers *Axin2*, *Lgr5* and *Sox9* or markers of early differentiation, *Alb* and *Tr* during normal organoid expansion or after differentiation towards hepatocyte fate. Data is expressed as fold change against WT organoids in expansion media with each dot representing an individual reading with a line representing group mean. Data represents a single experiment with a bulk WT population (n=1) and two independent mutant clones (n=2) carried out in duplicate.

It is important to note that these changes in gene expression of *Alb* and *Ttr* are the earliest read outs of hepatocyte fate, to understand if mature hepatocyte markers are also altered during organoid differentiation terminal markers of differentiation need to be assessed. The expression of mature hepatocyte markers *Glu1* and *Cyp3a11*, whose expression is crucial for proper metabolic function of hepatocytes, were upregulated in both WT and IsoB mutant organoids after differentiation (Figure 3.9b). However, WT organoids showed an increased level of induction over isoB mutants. This data suggests isoB mutants might exhibit impairment in terminal differentiation.

To further investigate the terminal differentiation capacity of *Arid1a* isoB  $-/-$  organoids, we analysed three different functional assays of hepatocyte differentiation: (1) The uptake of cholesterol by the use of a fluorescent analogue of LDL; (2) albumin production and secretion by ELISA; and (3) the activity of the cytochrome p450 family of enzymes by analysis of breakdown of a luminescent competent substrate.

Qualitative analysis of LDL uptake showed that after differentiation both WT and IsoB mutants were able to uptake the fluorescent analogue (Figure 3.9c). IsoB mutants had a seemingly increased capacity to uptake LDL, however, an accurate quantification would be required to validate that both WT and isoB mutant's uptake differing amounts of LDL. In line with the massively increased gene expression of *Alb* at the mRNA level in both expansion and differentiation conditions, IsoB mutants also showed significantly increased levels of albumin secretion in expansion and differentiation conditions compared to WT organoids (Figure 3.9d). Taken together with the LDL uptake, loss of IsoB results in the acquisition of increased functional hepatocyte features after differentiation. In contrast, loss of IsoB results in significantly lower cytochrome p450 activity after differentiation (Figure 3.9e). Therefore, as the activity of cytochrome enzymes is a crucial feature of fully mature hepatocytes, removal of isoform B limits organoid differentiation capacity making them unable to fully mature into functional hepatocyte-like cells.

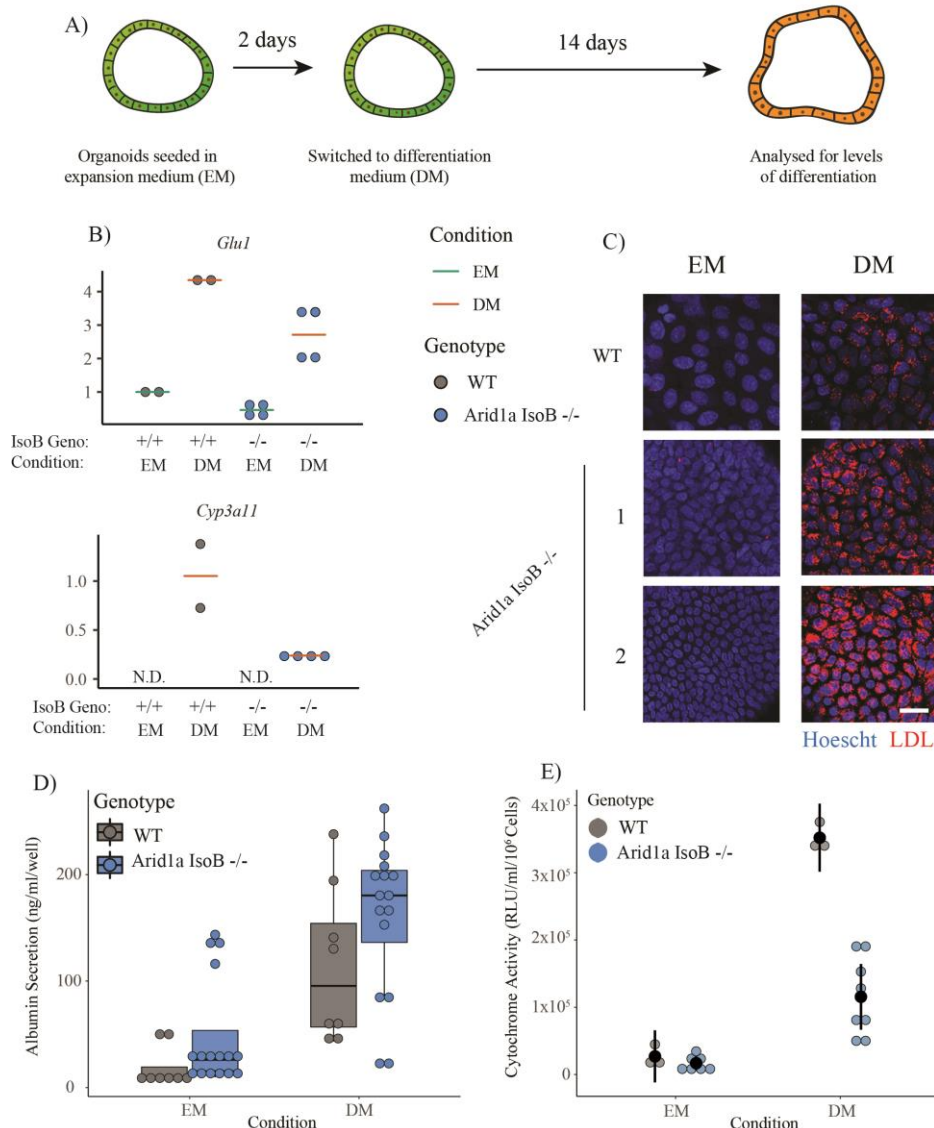


**Figure 3.9 - *Arid1a* mutation results in impaired terminal differentiation into hepatocyte fate.** A) Experimental scheme: Either WT or mutant organoids were initially seeded in expansion media and after two days switched to the differentiation protocol and analysed after fourteen days of differentiation. B) Gene expression of markers of terminal *Glu1* and *Cyp3a11* during normal organoid expansion or after differentiation towards hepatocyte fate. Data is expressed as fold change against WT organoids in expansion media (unless not expressed in expansion, in which case the differentiation state is used) with each dot representing an individual reading with a line representing group mean. Data represents a single experiment with a bulk WT population (n=1) and two independent mutant clones (n=2) carried out in duplicate. C) Representation wholemount organoid images showing uptake of LDL by fluorescent analogue (red) and nuclei with the DRAQ5 DNA marker (blue) of WT or mutant organoids. Scale bar = 10 μm. D) Quantification of the amount of Albumin secreted from WT or mutant organoids in expansion or after differentiation determined by ELISA. Data is represented as ng/ml/well, with boxplots showing group median, upper and lower quartile and overall range with dots representing each reading. Representative of four experiments with a bulk WT population (n=1) and two independent mutant clones (n=2) carried out in duplicate. E) Quantification of Cytochrome p450 activity in WT or mutant organoids in expansion or after differentiation. Shown as RLU/ml/10<sup>6</sup> Cells, with dots denoting each reading and group mean (+/- 95% confidence interval). Representative of two experiments with a bulk WT population (n=1) and two independent mutant clones (n=2) carried out in duplicate.

In summary, partial loss of *Arid1a* by removal of its longest isoform in organoids results in reduced expression of progenitor markers and an increased expression of markers of early differentiation coupled with a boost in survival in normal expansion conditions. These data suggest that correct expression of *Arid1a* is crucial for liver organoids to maintain their basal characteristics and manipulation of *Arid1a* levels results in a promotion of the hepatocyte fate. Furthermore, analysis of the differentiation capacity of mutant organoids revealed a reduced capacity to fully mature into functional hepatocyte-like cells suggesting that *Arid1a* may have more global role in controlling differentiation state and cell fate, while mis-regulation results in lost cellular identity. However, there are some limitations to this data that require consideration. First of all, the CRISPR generated mutants only remove a single isoform of *Arid1a* so it is impossible to tell whether any observation is due to partially removing *Arid1a* or improper function of the remaining full isoform. Furthermore, the CRISPR mutant creates a truncated protein which may have a spurious function that confounds our observations. Finally, the generation of CRISPR mutants relies on the specificity of your guiding RNA, if there was a similar complimentary sequence elsewhere in the genome, off target mutations could be caused. Therefore, our observations could be an artefact of non-specific mutation.

As a result, to begin to rule out some of these limitations and generated more robust data we must generate better genetic models that result in the complete loss of *Arid1a*. To carry this out we took advantage of a CRE-*loxP* system to generate complete *Arid1a* null organoid lines. To achieve this, we bred mice that express the inducible Cre<sup>ERT2</sup> recombinase from the *Rosa26* locus (*Rosa26Cre<sup>ERT2</sup>*) with a mouse line that has *loxP* sites flanking a critical exon of *Arid1a* (*Arid1a<sup>flx/flx</sup>*) generating a *Rosa26<sup>CreERT2</sup>/Arid1a<sup>flx/flx</sup>* line allowing the ubiquitous deletion of *Arid1a* in response to tamoxifen treatment. To track recombination events, we bred these mice with the Rainbow multicolour reporter system generating a *Rosa26Cre<sup>ERT2</sup>/Arid1a<sup>flx/flx</sup>/CAG<sup>Rainbow2.1</sup>* line (Figure 3.10a). Organoids were generated from *Rosa26<sup>CreERT2</sup>/Arid1a<sup>flx/flx</sup>/CAG<sup>Rainbow2.1</sup>* and *Rosa26<sup>CreERT2</sup>/Arid1a<sup>flx/+</sup>/CAG<sup>Rainbow</sup>* mice and recombination of *Arid1a* was followed by proxy of the reporter expression. Organoids that have not undergone recombination express RFP, whereas, any recombination event would lead to expression of CFP or YFP (Figure 3.10b). Taking advantage of this we treated the newly generated organoids with expansion media

supplemented with 5  $\mu$ M OH-Tam for 48hrs before switching to normal conditions for 7 days to recover and isolating recombined cells by FACS. Single CFP<sup>+</sup> or YFP<sup>+</sup> cells were grown clonally, before further downstream analysis (Figure 3.10c).

To ensure that recombination of the reporter led to *Arid1a* deletion we analysed expression of the protein by western blot and immunofluorescence. Organoids derived from *Rosa26<sup>CreERT2</sup>/Arid1a<sup>flx/flx</sup>/CAG<sup>Rainbow</sup>* recombined cells showed complete loss of ARID1A and those from *Rosa26<sup>CreERT2</sup> /Arid1a<sup>flx/+</sup> /CAG<sup>Rainbow</sup>* recombined cells showed a reduced level of ARID1A when compared to a bulk WT (*Arid1a<sup>WT</sup>*) population in line with homozygous (*Arid1a<sup>HOM</sup>*) and heterozygous (*Arid1a<sup>HET</sup>*) mutation respectively (Figure 3.10d and Figure 3.11). We also found that mutation of *Arid1a* does not affect the protein expression of the core catalytic BAF subunit BRG1, suggesting the BAF complex can still be function despite loss of ARID1A (Figure 3.11). However, it should be noted that, although BRG1 is expressed in the absence of ARID1A, we have no way of telling whether it is forming functional BAF complexes. It would therefore be interesting to pull down the protein and chromatin that is associated with BRG1 in the absence of ARID1A to assess the function of BRG1 and BAF complex. In any case, we have generated a robust model of total loss of *Arid1a* and as a result we can now begin to validate the its' effect on liver organoid function.

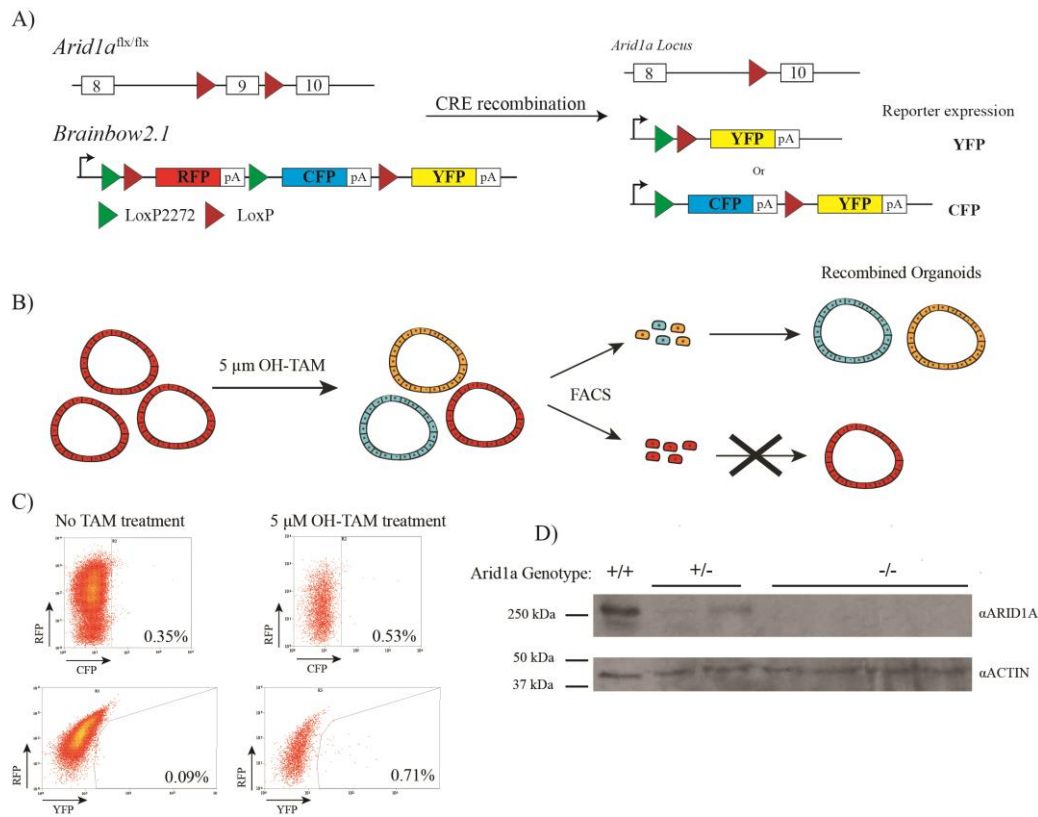


**Figure 3.10 - Generation of total heterozygous and homozygous *Arid1a* mutant organoids.** A) Schematic of transgenic alleles of *Arid1a* with loxP sites flanking exon 9 and the reporter allele *Brainbow2.1* before and after CRE induced recombination. B) Experimental scheme: Organoids were derived from *Arid1a<sup>flx/flx</sup>/Brainbow2.1/Rosa26<sup>CreERT2</sup>* or *Arid1a<sup>flx/+</sup>/Brainbow2.1/Rosa26<sup>CreERT2</sup>* mice. Organoids were then treated with 5  $\mu$ M Hydroxy-tamoxifen (OH-TAM) for 2 days. After treatment organoids were dissociated, sorted by FACS and either CFP+ or YFP+ cells were selected. Organoids were grown clonally from single cells before being tested for *Arid1a* mutation and further downstream analysis. C) Representative FACS plots generated from organoids treated with 5  $\mu$ M Hydroxy-tamoxifen (OH-TAM) or left untreated. D) Western blot showing ARID1A and ACTIN protein expression in WT (n=1), clonal heterozygous (n=2) or clonal homozygous (n=4) ARID1a mutant organoid culture.

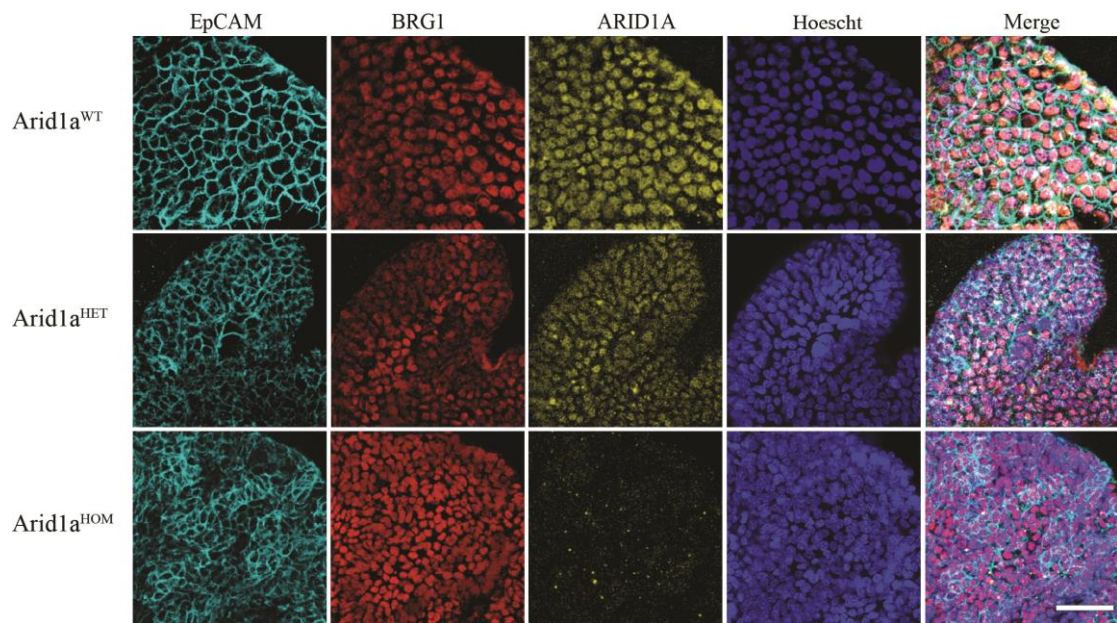


**Figure 3.11 - Immunostaining of BAF components in total *Arid1a* mutant organoids.** Maximum projection images representative of wholmount immunostaining of epithelial marker EpCAM (Cyan), BAF complex components BRG1 (Red) and ARID1A (Yellow), and nuclear marker Hoechst (Blue) in *Arid1a*<sup>WT</sup>, *Arid1a*<sup>HET</sup> or *Arid1a*<sup>HOM</sup> organoids. Scale bar = 50  $\mu$ m

We started by trying to understand whether total loss of *Arid1a* led to an increased organoid formation capacity as described from our CRISPR mutants. Remarkably, we found that only *Arid1a*<sup>HET</sup> organoid lines led to an increased organoid formation whereas homozygous mutants recovered to the WT levels (Figure 3.12b-c). This data suggests that dosage of *Arid1a* is crucial for ductal progenitor capacity and homozygous loss of *Arid1a* may lead to compensation through a pathway independent from *Arid1a*.

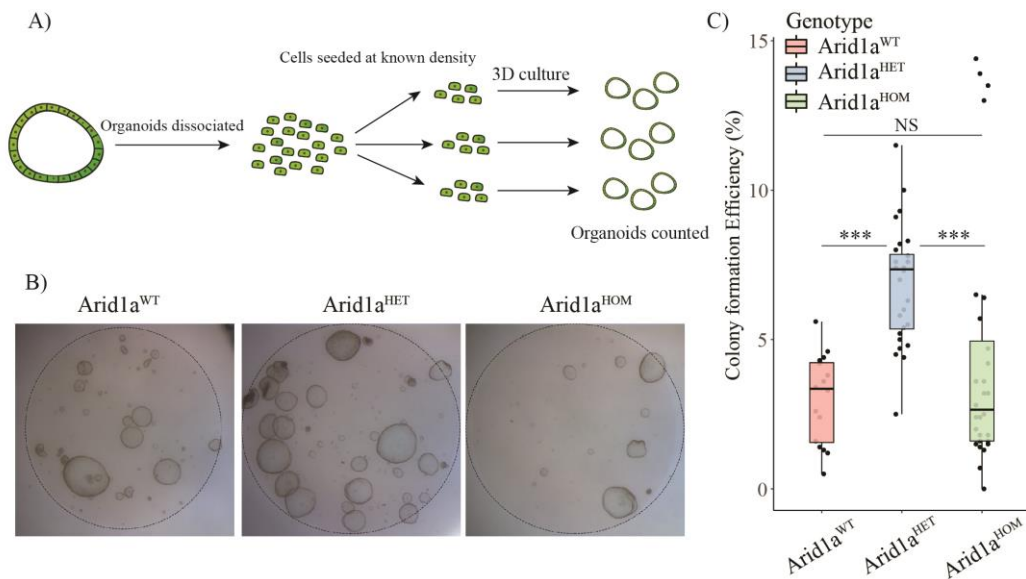


**Figure 3.12 - Dosage of *Arid1a* is crucial for organoid formation efficiency.** A) Experimental scheme: Either WT or mutant organoids were initially dissociated before being seeded at a density of 10,000 cells per well. The number of organoids was counted after 10 days. B) Representative images of single wells after 10 days of organoid growth. C) Organoid formation efficiency expressed as the percentage of organoids formed from the total number of seeded. Boxplots show group median, interquartile range as well as the overall range of data. Dots represent every individual well quantified of a bulk WT population WT (n=1), clonal heterozygous (n=2) or clonal homozygous (n=4) organoid lines from 3 independent experiments. p values were calculated using one-way ANOVA with TUKEY HSD tests, \*\*\* = p < 0.001, NS = Not significant.

To see whether the similarities extend to the molecular characteristics seen in the CRISPR mutants. *Arid1a*<sup>WT</sup>, *Arid1a*<sup>HET</sup> and *Arid1a*<sup>HOM</sup> organoid lines were grown in expansion media and analysed for expression of progenitor and early differentiation markers. To our surprise, homozygous loss of *Arid1a* had distinct effects on the expression of the two categories of genes. *Arid1a*<sup>HOM</sup> organoids showed a similar expression of *Axin2* and *Lgr5* compared to the *Arid1a*<sup>WT</sup> line. Whereas, heterozygous mutation resulted in decreased expression of the same genes, mirroring the CRISPR generated clones (Figure 3.13 Upper panels). However, when considering markers of early differentiation homozygous mutation of *Arid1a* does not rescue expression back to WT levels. Rather, the effect is additive, homozygous mutants have increased expression of *Alb* and *Ttr* over *Arid1a*<sup>HET</sup> lines and in turn, *Arid1a*<sup>HET</sup> lines had increased expression over *Arid1a*<sup>WT</sup> organoids (Figure 3.13 Lower panels). Taken together with the organoid formation capacity of the organoid lines suggests that dosage of *Arid1a* is crucial for the liver organoid progenitor state, controlling self-renewal as well as the molecular characteristics where total loss of *Arid1a* is potentially rescued through an independent pathway. However, there is a negative dose dependent response of *Arid1a* levels and hepatocyte marker expression where less expression of *Arid1a*

results in increased expression of hepatocyte markers. This data does suggest that there may be a pathway that can partially rescue the loss of *Arid1a*, however, we have no evidence to suggest what pathway that may be. Interestingly, *Arid1a* has two genetic homologues *Arid2* and *Arid1b* under conditions of complete loss of *Arid1a* one or the other may substitute *Arid1a* restoring some BAF function. It would be fascinating, to study the expression and function of these homologues in the context of *Arid1a* depletion.

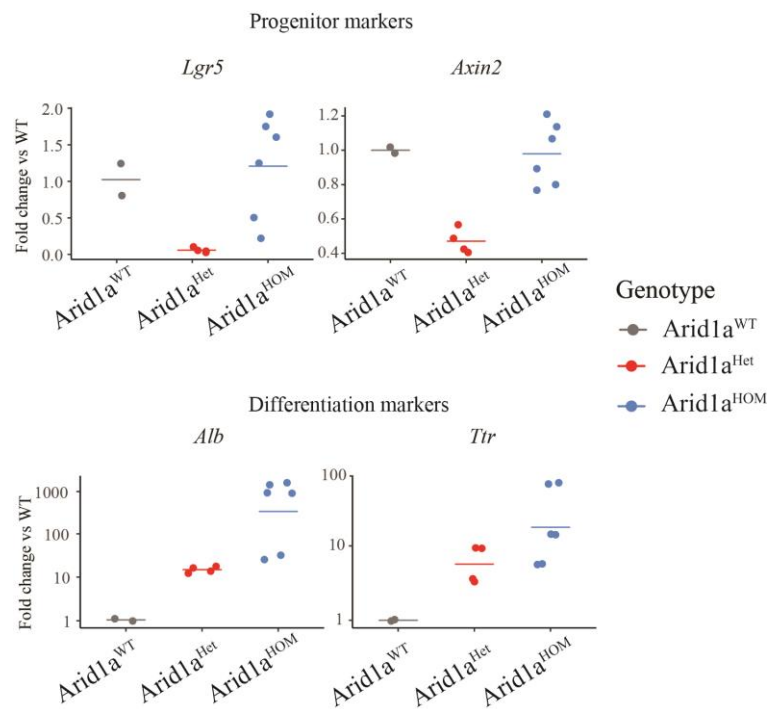


**Figure 3.13 - *Arid1a* level controls expression of progenitor and differentiation markers.** Gene expression of progenitor markers (*Lgr5* and *Axin2*) and early differentiation markers (*Alb* or *Ttr*) of WT, heterozygous or homozygous mutants of *Arid1a* in organoid expansion conditions. Data is represented as a fold change of the WT organoids, each dot represents a single reading and the bar is the group mean. Data represents a single experiment with a bulk WT population WT (n=1), two clonal heterozygous (n=2) or four clonal homozygous (n=4) organoid lines carried duplicate.

As we observed with our CRISPR mutants an increase in expression of *Alb* and *Ttr* may not translate to increased expression of more mature functional markers of hepatocyte fate. Therefore, to elucidate the effect of the complete knockout of *Arid1a* on markers of terminal differentiation we analysed albumin secretion and cytochrome p450 enzyme activity. In line with expression data both *Arid1a*<sup>HET</sup> and *Arid1a*<sup>HOM</sup> lines had increased albumin secretion in both normal expansion conditions as well as after differentiation (Figure 3.14B). Much like our CRISPR mutant organoids, homozygous loss of *Arid1a* led to completely abolished cytochrome p450 activity after

differentiation. Interestingly, heterozygous mutation of *Arid1a* resulted in no difference in cytochrome activity after differentiation when compared to *Arid1a*<sup>WT</sup> organoids (Figure 3.14c). This is interesting as it suggests that isoform B of *Arid1a* may be directly required for up-regulation of cytochrome enzymes during acquisition of the hepatocyte fate as specific mutation of isoform B by CRISPR resulted in an impairment of cytochrome up-regulation, whereas, generic down-regulation of *Arid1a* by heterozygous mutation does not.

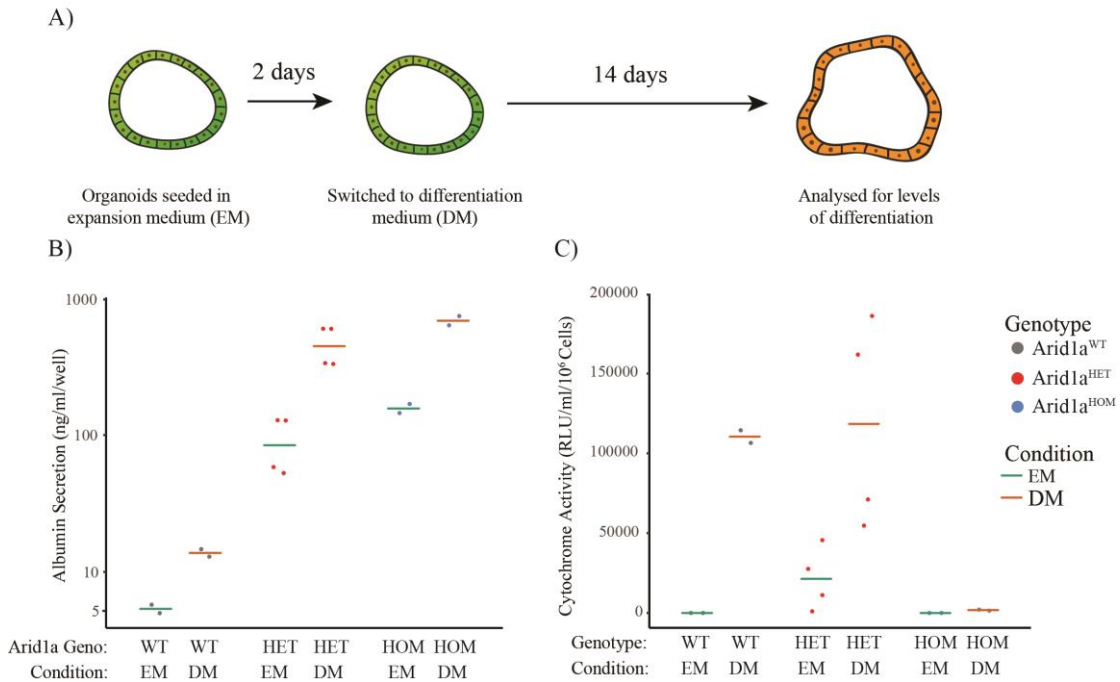


**Figure 3.14 - *Arid1a* is required for terminal differentiation.** A) Experimental scheme: Either WT or mutant organoids were initially seeded in expansion media and after two days switched to the differentiation protocol and analysed after fourteen days of differentiation. Quantification of the amount of Albumin secreted (B) or cytochrome activity (C) from WT or mutant organoids in expansion or after differentiation determined by ELISA. Data is represented as ng/ml/well, with dots showing individual readings and a bar for group mean. Representative of a single experiment with a bulk WT population (n=1), two clonal heterozygous (n=2) or one clonal homozygous (n=1) organoid lines carried duplicate.

Therefore, taken all together, manipulation of *Arid1a* by siRNA, CRISPR or CRE recombination results in a complex set of molecular characteristics surrounding liver organoid maintenance, their molecular characteristics and differentiation capacity. However, we have no evidence to implicate the BAF complex as a whole and the phenotypes we have observed may be as a result of a BAF independent function of *Arid1a*. To begin to answer this question we studied the promoter occupancy of *Arid1a* together with the catalytic ATPase of BAF complex *Brg1* in order to validate that the

presence of *Arid1a* is in the context of the BAF complex. Chromatin immunoprecipitation coupled with qPCR (ChIP-qPCR) studies on WT organoids revealed that ARID1A and BRG1 bound directly to the Transcriptional Start Sites (TSS) of progenitor markers *Axin2* and *Sox9* as well as differentiation markers *Alb* and *Ttr* during normal expansion (Figure 3.15a). This suggests that *Arid1a* directly regulates genes crucial in liver organoid maintenance.

ARID1A or BRG1 were not found bound to the TSS of the key ductal progenitor marker *Lgr5* (Figure 3.15b). However, as previous *Arid1a* depletion studies consistently found altered *Lgr5* expression, *Arid1a* may indirectly regulate *Lgr5* or binds a locus away from the TSS. To further explore the latter option, we designed several primer pairs to probe ARID1A and BRG1 binding along the *Lgr5* gene body and enhancer regions. We specifically targeted a region in intron 1 as it was identified as an open chromatin region specifically in organoids in an ATAC-seq dataset generated previously in the lab (data not shown). Remarkably, we found ARID1A and BRG1 binding to be enriched in the intronic region specified by the ATAC-seq and no other intronic regions, TSS or an upstream enhancer region (Figure 3.15b). This provides evidence of a new regulatory region of the *Lgr5* locus, in which *Arid1a* can bind and alter gene expression. Further studies would be required to validate this hypothesis. For instance, if we could artificially add the newly identified binding sequence to a reporter gene, we could directly assess its' potential as a regulatory sequence. Furthermore, it is also important to note that all these ChIP studies were carried out in organoids with normal levels of *Arid1a*. It would be interesting to repeat these experiments in our *Arid1a* knockout models to confirm that ARID1A disappears from the identified sites as well as to understand whether the other components of the BAF are also lost from the regulatory regions of the genes. These further studies would greatly enhance our understanding of the role of *Arid1a* and the BAF complex, as a whole, in liver organoid function.

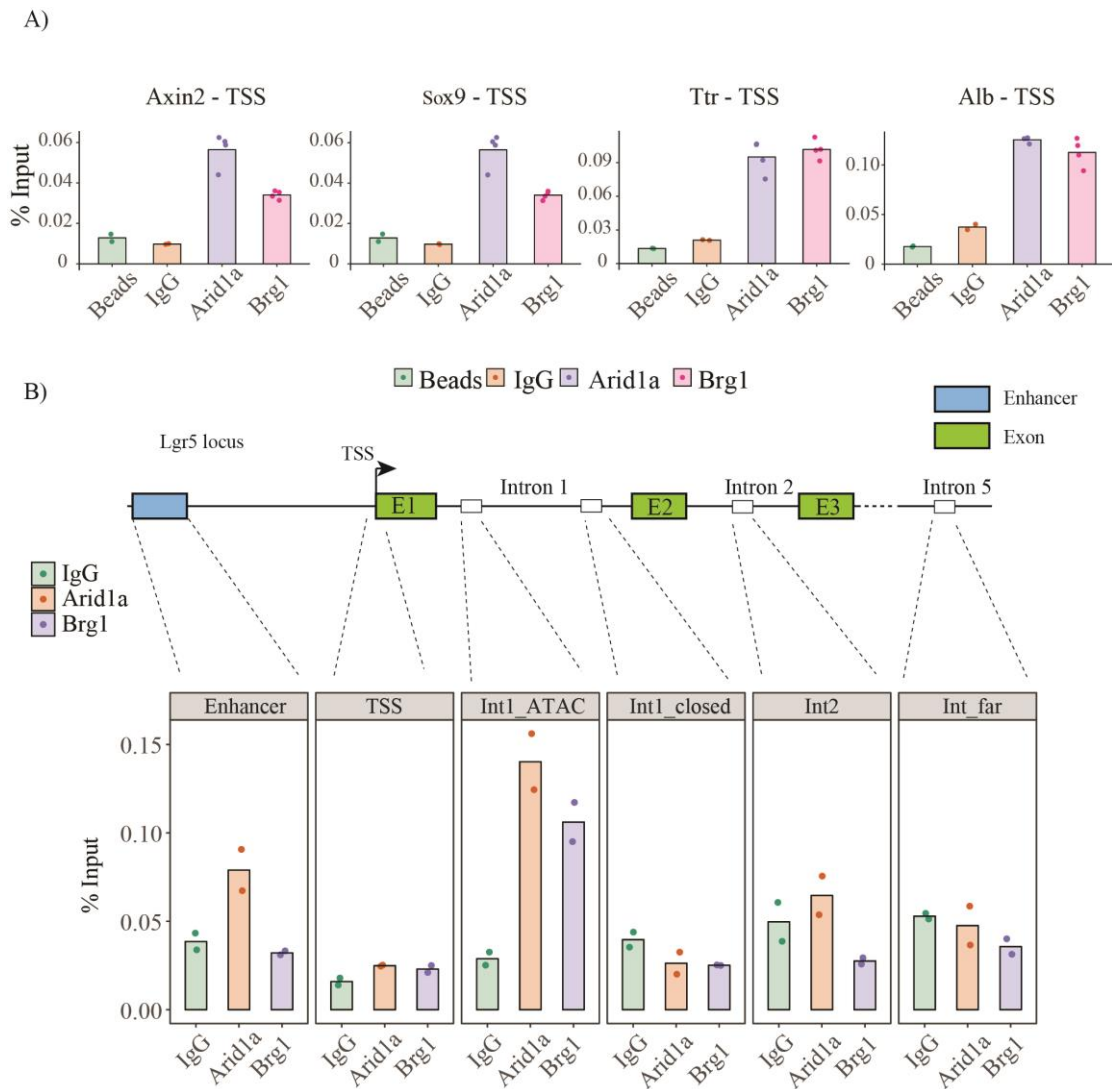


**Figure 3.15 - *Arid1a* and BAF subunit *Brg1* bind regulatory elements of crucial regulators of hepatocyte and progenitor identity.** A) Chromatin immunoprecipitation qPCR studies were used to assess the occupation of ARID1A and BRG1 on the transcriptional start sites (TSS) of progenitor (*Axin2* and *Sox9*) and hepatocyte (*Ttr* and *Alb*) markers. Data representative of two independent experiments carried out in duplicate with dots showing each individual reading and a bar for group mean. B) ARID1A and BRG1 binding was assessed across the *Lgr5* locus including an upstream enhancer, TSS and several intronic regions. Data representative of one experiment carried out in duplicate with dots showing each individual reading and a bar for group mean. (Aloia *et al.* unpublished).

### 3.2.2 Modulation of *Arid1a* specifically in ductal progenitors *in vivo*.

Taking advantage of liver organoids, we were able to identify a potential role for *Arid1a* in their maintenance and differentiation potential. More specifically, as *Arid1a* depletion in liver organoids severely diminishes expression of markers of terminal hepatocyte differentiation and results in abnormal organoid formation we hypothesised that loss of *Arid1a* in proliferating ductal progenitors *in vivo* would result in impaired liver regeneration. However, this hypothesis assumes that liver organoids correctly model the ductal progenitor response after damage. Therefore, to confirm the role *Arid1a* in liver regeneration and our model of study we must validate our findings in an *in vivo* model of ductal cell driven regeneration. We therefore bred the previously described *Arid1a*<sup>flx/flx</sup> mouse line with a mouse line expressing an inducible CRE recombinase under the endogenous promoter of the progenitor marker *Lgr5* (*Lgr5iresCre*<sup>ERT2</sup>). The resulting *Arid1a*<sup>flx/flx</sup>/*Lgr5Cre*<sup>ERT2</sup> mice were bred with the *Rosa26*<sup>Tdtomato</sup> reporter system to trace recombination events. The resultant mouse strain would allow us to mark and trace ductal progenitors as they form and facilitate liver regeneration in the presence or absence of *Arid1a*.

*Arid1a*<sup>flx/flx</sup>/*Lgr5Cre*<sup>ERT2</sup>/*Rosa26*<sup>Tdtomato</sup>, *Arid1a*<sup>flx/+</sup>/*Lgr5Cre*<sup>ERT2</sup>/*Rosa26*<sup>Tdtomato</sup> or *Arid1a*<sup>WT</sup>/*Lgr5Cre*<sup>ERT2</sup>/*Rosa26*<sup>Tdtomato</sup> counterparts were treated with food supplemented with 0.1% DDC, a potent hepatotoxic agent, for 5 days in order to activate ductal progenitors in response to damage. Deletion of *Arid1a* and reporter expression was then induced after onset of liver damage to only remove *Arid1a* after activation of the ductal progenitor fate (Figure 3.16a). Therefore, by following the reporter expression we can probe the ductal progenitor characteristics after recovery to determine their differentiation capacity.

Unfortunately, there was no apparent recombination in the ductal compartment or portal region after analysis. The only apparent recombination events were in central vein hepatocytes determined by morphology (Figure 3.16b, asterix). These recombined hepatocytes likely represent a previously described *Axin2*<sup>+</sup> population of hepatocytes (Wang *et al.*, 2015) rather than a nascent ductal derived population. This suggests that the damage protocol does not induce sufficient *Lgr5* expression in the ductal compartment to induce recombination and therefore little can be determined. Altering the damage protocol to enhance the expression of *Lgr5* in the ductal population may be a solution. However, a more pressing problem is that if we want to assess the emergence

of newly formed ductal derived hepatocytes to analyse differentiation capacity we need a way to unravel these hepatocytes from the resident *Axin2*<sup>+</sup> hepatocyte population. As a result, it is unlikely that any Wnt target gene such as *Lgr5* would **not** be appropriate to drive recombination and another Wnt independent ductal specific promoter should be used. Together this suggests, the *Arid1a*<sup>flx/flx</sup>/*Lgr5iresCre*<sup>ERT2</sup>/*Rosa26*<sup>TdTomato</sup> mouse line and DDC damage paradigm is inappropriate to understand the role of *Arid1a* in the differentiation of hepatocytes from ductal progenitors and both mouse line and mode of damage needs to be further optimised. Crucially, without an *in vivo* system we are unable fully understand to role of *Arid1a* in ductal progenitor liver regeneration despite observing interesting phenotypes in the liver organoid model. Further study is required both *in vitro* using liver organoids as well as concomitant *in vivo* validation before robust conclusions surrounding the role of *Arid1a* and the BAF complex in liver regeneration can be made.

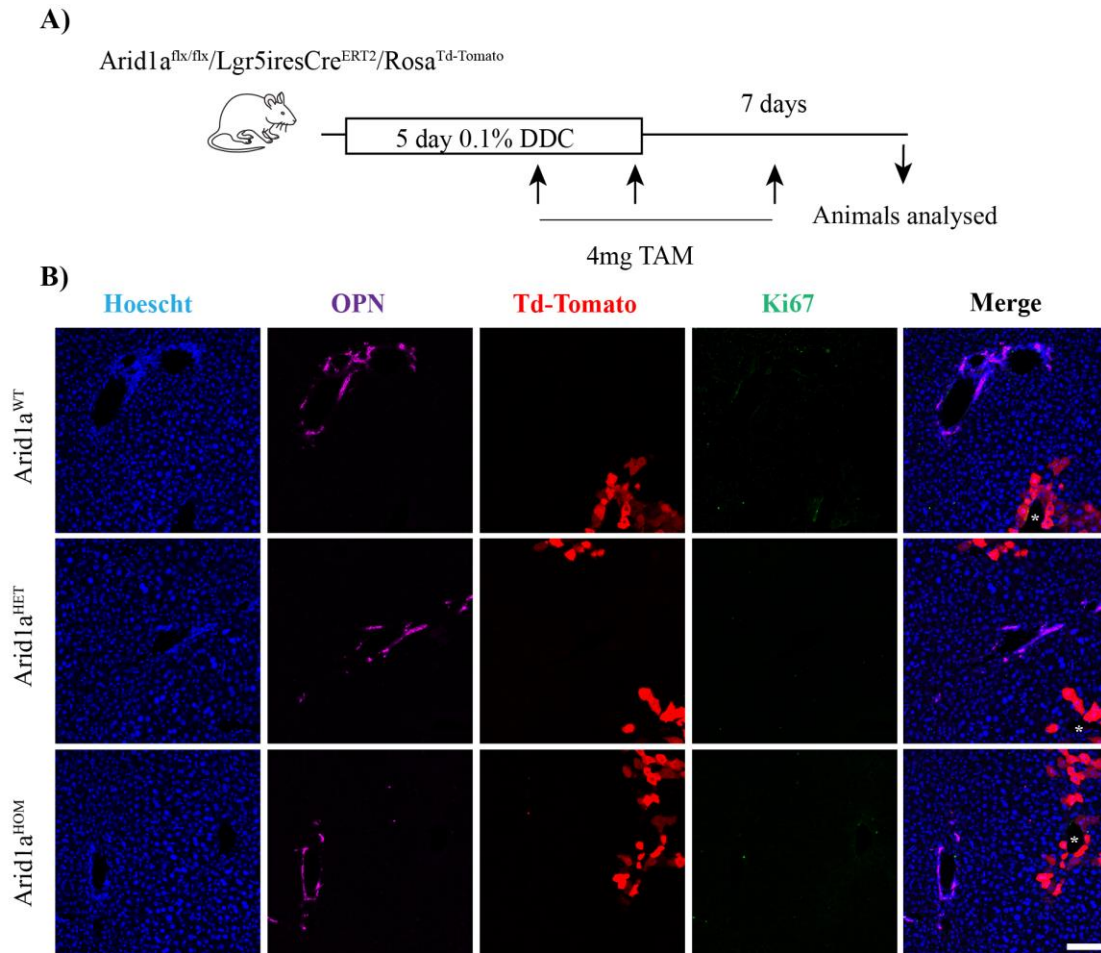


**Figure 3.16 – Recombination by *Lgr5iresCre<sup>ERT2</sup>* after DDC treatment is not sufficient to facilitate *Arid1a* deletion in emergent ductal progenitors.** A) Experimental scheme:  $Arid1a^{flx/flx}/Lgr5iresCre^{ERT2}/Rosa^{Td-Tomato}$  mice were treated with 0.1% DDC for 5 days before being injected with 3 doses of 4 mg tamoxifen to induce recombination in emergent ductal progenitors. One week after DDC treatment mice were sacrificed and analysed. B) Representative images of 100  $\mu$ m liver sections stained for ductal marker Osteopontin (OPN, magenta), Td-Tomato expression (Red), proliferation marker Ki67 (Green) and nuclear marker Hoechst (Blue). Scale bar = 50  $\mu$ m. \* = Central vein.

### 3.3 The role of *Tet1* in ductal driven liver regeneration.

#### 3.3.1 Generation of animal models to study the role of *Tet1* in the liver.

Following that siRNA knockdown of *Tet1* in mature ductal cells abrogated organoid formation we wanted to further understand the role of *Tet1* specifically in the activation of the ductal progenitor state. In order to achieve this, we took advantage of several different mouse models to further probe the role of *Tet1* in ductal driven liver regeneration.

We initially imported the “Knock out first” *Tet1<sup>tm1(KOMP)Wtsi</sup>* (labelled as *Tet1<sup>hypo</sup>*) mouse line from the Knock-Out Mouse project (KOMP) which contains a gene trap cassette that is able to trap active transcription of the *Tet1* locus and cause premature termination via the inclusion of a poly A sequence. (Figure 3.17a-b) However the allele includes the full exonic complement of *Tet1* so if the gene trap is skipped during splicing normal transcription of *Tet1* is possible. Furthermore, the *Tet1<sup>hypo</sup>* cassette includes *loxP* sites and *Frt* sites that on recombination result in permanent loss of exon 4 of *Tet1* or removal of the gene trap component leaving only *loxP* sites flanking exon 4 of *Tet1*, respectively (Figure 3.17a). To generate the *Tet1* null (*Tet1<sup>KO</sup>*) mouse line we crossed our *Tet1<sup>hypo</sup>* line with a mouse line expressing Cre recombinase under the Sox2 promoter (*Sox2<sup>Cre</sup>*). This facilitated recombination between the *Tet1<sup>hypo</sup>* *loxP* sites in the early stages of embryonic development and ultimately total removal of exon 4 of *Tet1* (Figure 3.17d). In a similar fashion to generate our *Tet1<sup>flx</sup>* line we crossed the *Tet1<sup>hypo</sup>* line with a mouse expressing the Flp recombinase under the ubiquitous Rosa26 promoter (*Rosa<sup>Flpe</sup>*). The resulting recombination between the resident *Frt* sites in the *Tet1<sup>hypo</sup>* line removed the gene trap allele leaving only *loxP* sites surrounding exon 4 of *Tet1* (Figure 3.17c). Therefore, the *Tet1<sup>flx</sup>* will have normal expression of *Tet1* until Cre mediated removal of exon 4 allowing spatiotemporal control of *Tet1* deletion based on Cre recombinase expression. *Tet1<sup>hypo</sup>*, *Tet1<sup>flx</sup>*, or *Tet1<sup>KO</sup>* allele generation was confirmed by genomic PCR (data not shown).

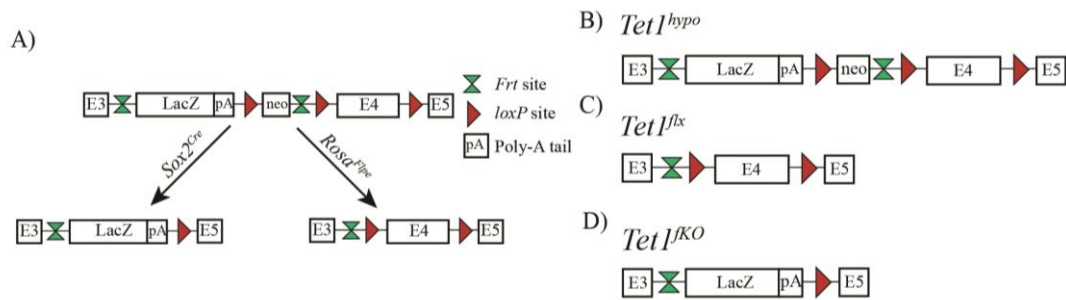


**Figure 3.17 - Generation of *Tet1* hypomorphic, conditional and null mouse models.** Schematics of the imported *Tet1<sup>tm1(KOMP)Wtsi</sup>* (known as *Tet1<sup>hypo/hypo</sup>*) mouse line (A-B) and derivative *Tet1<sup>flx/flx</sup>* (C) or *Tet1<sup>KO/fKO</sup>* (D) mouse lines. *Tet1<sup>flx/flx</sup>* and *Tet1<sup>KO/fKO</sup>* lines were generated by breeding with a Flp recombinase or CRE recombinase expressed under ubiquitous promoters, respectively.

There are several studies that show varied lethality in response to loss of *Tet1*, therefore, after generation of our models we wanted to test viability. To achieve this, we analysed the outcome of heterozygous crosses of each line against the expected 1:2:1 ratio of homozygous, heterozygous and WT genotypes. As expected, due to the hypothetical nearly normal expression of *Tet1* in the *Tet1<sup>flx</sup>* line, the observed genotype ratios did not differ significantly from the expected ratios (Figure 3.18b). However, the *Tet1<sup>KO</sup>* had a significantly altered distribution of genotypes compared to what was expected. Specifically, there was a large reduction of observed homozygous animals compensated by an increased number of WT and heterozygous pups (Figure 3.18c). This suggests that the *Tet1* line has partial embryonic lethality. Remarkably, the *Tet1<sup>hypo</sup>* line showed the expected distribution of genotypes, similar to the *Tet1<sup>flx</sup>* line, despite disrupting *Tet1* expression by design (Figure 3.18a). This provided evidence that the *Tet1<sup>hypo</sup>* line was not completely effective at knocking out *Tet1* expression thus avoiding embryonic lethality as observed in the *Tet1<sup>KO</sup>* line.

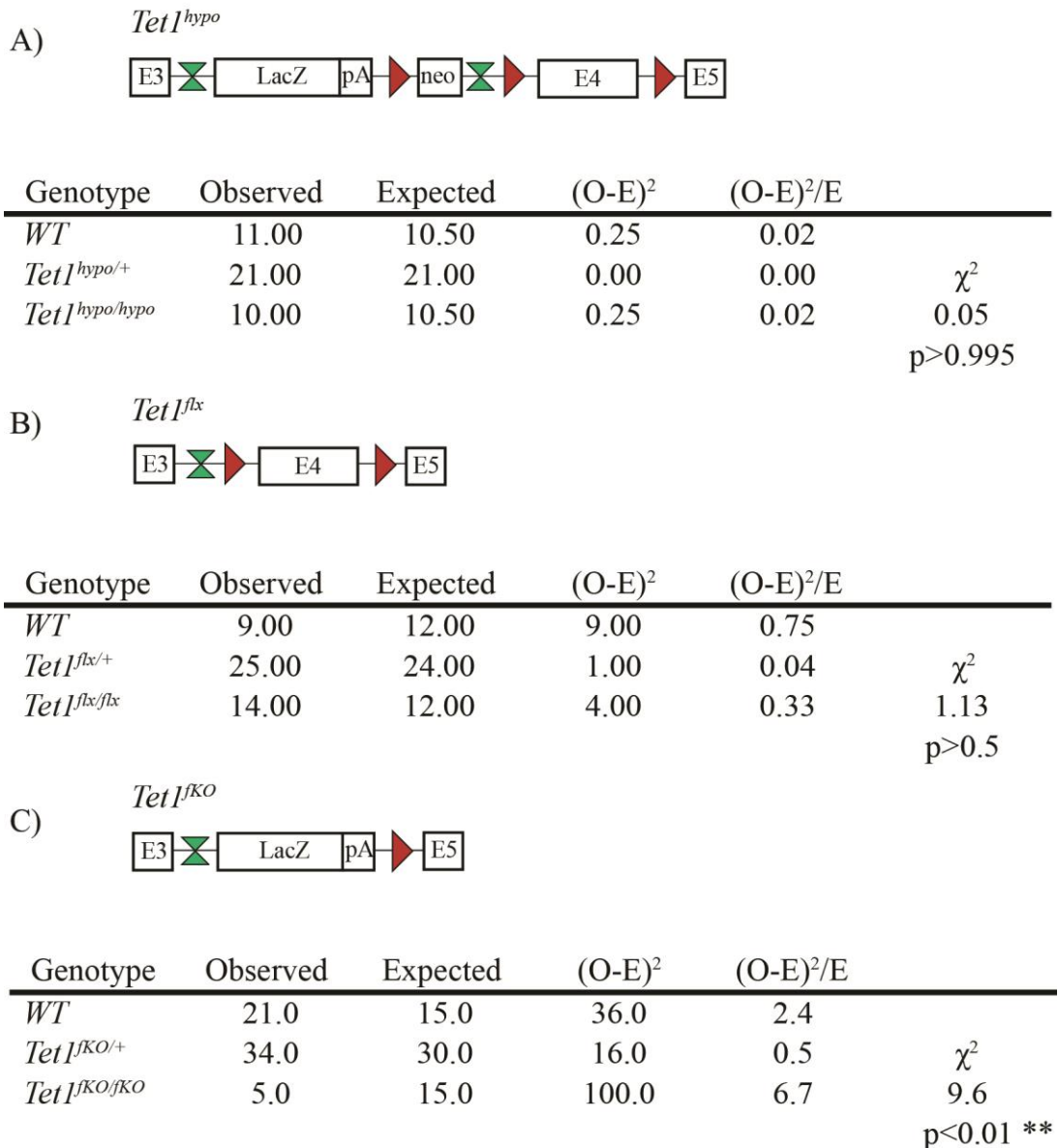


**Figure 3.18 - Viability of *Tet1* mouse models generated.** Tables showing genotype of offspring generated from heterozygous crosses of each mouse model. Values are a sum of 6 independent litters for *Tet1<sup>hypo</sup>* (A) and *Tet1<sup>fKO</sup>* (C) lines and 4 independent litters for the *Tet1<sup>flx</sup>* (B) line. *p*-values and  $\chi^2$ -values calculated by chi squared analysis.

In summary, we generated several animal models to study the function of *Tet1*. However, due to the inefficient generation of homozygous mice in the *Tet1<sup>fKO</sup>* line we decided to only further characterise the *Tet1<sup>hypo</sup>* and *Tet1<sup>flx</sup>* mouse lines.

### 3.3.2 Reduction of *Tet1* expression results in less ductal proliferation *in vitro* and *in vivo*.

The increased viability of the *Tet1<sup>hypo</sup>* line over the *Tet1<sup>fKO</sup>* line provides some evidence that there was some residual expression of *Tet1* allowing the mice to survive. This is possible through exon skipping of the gene trap of the *Tet1<sup>hypo</sup>* allele, as the full complement of *Tet1* exons is present (Figure 3.19a). To confirm the level of protein expression of TET1 in *Tet1<sup>hypo</sup>* mice we sought to detect TET1 protein expression in whole liver homogenate by western blot. We found that *Tet1<sup>hypo/hypo</sup>* mice have a lower expression of TET1 when compared to *Tet1<sup>hypo/+</sup>* and *WT* mice. Using liver organoids derived from *Tet1<sup>hypo</sup>* mice we were able to further show that *Tet1<sup>hypo/hypo</sup>* mice had 30% of the normal TET1 protein level (data not shown, Aloia *et al.* in press). Crucially, this shows that TET1 expression was not completely abolished, therefore, we have defined this line as hypomorphic for *Tet1* (Figure 3.19b).

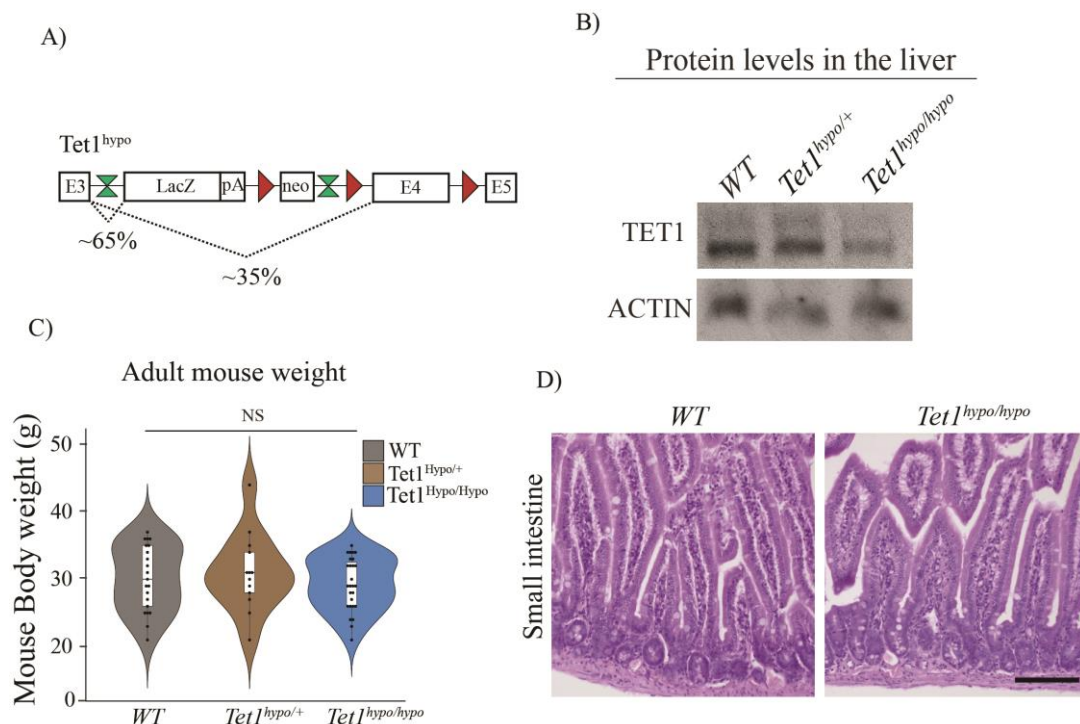


**Figure 3.19 - *Tet1<sup>hypo/hypo</sup>* mice show no major homeostatic defect compared to *WT* mice.** A) Schematic of the *Tet1<sup>hypo</sup>* allele design and possible splice variants. B) Representative western blot of TET1 and ACTIN protein expression from liver homogenate of *Tet1<sup>hypo/hypo</sup>*, *Tet1<sup>hypo/+</sup>* and *WT* mice. C) Adult mouse weights of *Tet1<sup>hypo/hypo</sup>*, *Tet1<sup>hypo/+</sup>* and *WT* mice. Data is represented as a violin plot showing population density and box-plots showing median, interquartile and range. Dots represent single mice, *Tet1<sup>hypo/hypo</sup>* n = 21, *Tet1<sup>hypo/+</sup>* n = 13 and *WT* n = 27. Statistical analysis was by pairwise Wilcoxon test with Bonferroni correction. D) Representative images of H&E staining of the small intestine from one year old *WT* or *Tet1<sup>hypo/hypo</sup>*. Scale bar = 100  $\mu$ m.

A recent study has shown that *Tet1*-null mutant mouse lines are not viable as a result of post-natal small intestinal defect (Kim *et al.*, 2016). Therefore, we next wanted

to explore whether reduction of *Tet1* expression in our *Tet1<sup>hypo</sup>* line resulted in altered small intestine architecture or mouse weight. However, unlike the previous study we found that there was no difference in average weight of adult mice (8-10 weeks old) between *Tet1<sup>hypo/hypo</sup>* *Tet1<sup>hypo/+</sup>* and *WT* genotypes (Figure 3.19c). In line with this, we found that the small intestine had no overt architectural defects between aged (1 year old) *WT* and *Tet1<sup>hypo/hypo</sup>* mice, suggesting that even in old age small intestine maintenance is maintained (Figure 3.19d). Taken together this suggests that reduced levels of *Tet1* expression does not result in fatal phenotypes described in the null mouse model by other.

Despite the lack of an overt homeostatic phenotype we wanted to examine whether the lack of normal expression of *Tet1* resulted in altered liver organoid dynamics in a similar manner to our siRNA data (Figure 3.20a). We were initially able to derive organoids from EpCAM+ ductal cells from *Tet1<sup>hypo/hypo</sup>* mice suggesting that the reduced expression does not affect organoid formation. However, upon passage organoids derived from hypomorphic mice lost their expansion potential and after roughly 5 passages had lost self-renewal ability (Figure 3.20b). These data also help to validate our siRNA data by ruling out any confounding effect of off-target knockdown as our *Tet1<sup>hypo</sup>* line is specific for *Tet1*.

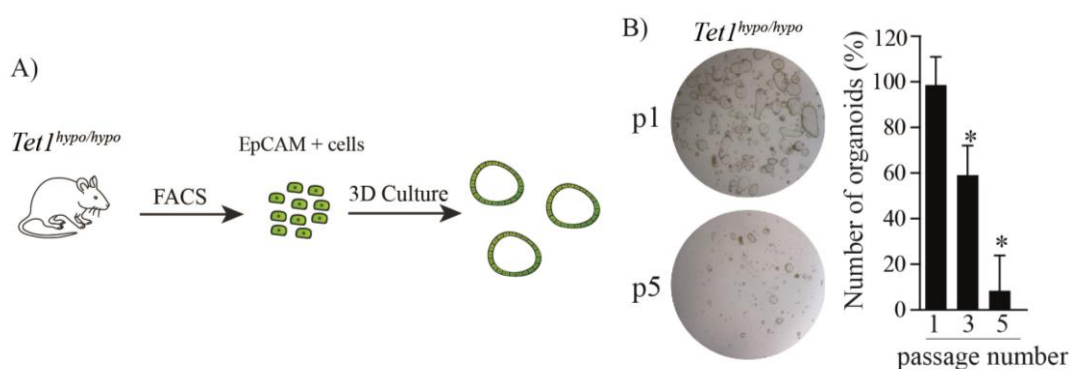


**Figure 3.20 - Reduced *Tet1* expression results in organoids with reduced self-renewal capacity.** A) Experimental design, EpCAM+ ductal cells were isolated from *Tet1<sup>hypo/hypo</sup>* mice and placed in 3D organoid expansion conditions. B) Representative images *Tet1<sup>hypo/hypo</sup>* organoids at passage 1 (p1) and passage 5 (p5). Bar chart shows organoid formation efficiency at passage 1, 3 and 5, values were normalised against p1 organoid formation. Data is represented as mean  $\pm$  S.D. of three independent experiments and p3 and p5 values were compared to p1 values by two-sided students t-test analysis.  $p < 0.05 = *$ . (Aloia *et al.* unpublished).

We next wanted to see whether the impaired liver organoid dynamics observed in *Tet1* hypomorphic organoids translated to the *bona fide* ductal progenitors present *in vivo* and was not as a result of an artefact borne out of the *in vitro* system. In order to

carry this out we took advantage of 0.1% 3,5-diethoxycarbonyl-1,4-dihydrocollidine (DDC) treatment to induce liver damage. DDC induces the activity of  $\delta$ -amino laevulinate synthetase, which controls an early and rate limiting step of haem biosynthesis, whilst simultaneously inhibiting a late stage of haem production by repressing ferrochelatase. The cumulative result is a reduced rate of haem production as well as hepatotoxic deposition of porphyrin. In addition, DDC treatment in mice has been shown to model human variegate porphyria (Gayathri and Padmanaban, 1974). Crucially, DDC has been widely shown to induce significant proliferation in the ductal compartment of the liver (Preisegger *et al.*, 1999). This acquisition of proliferation closely represents the process whereby mature EpCAM<sup>+</sup> ductal cells acquire a progenitor state when grown in 3D conditions. As a result, we postulated that DDC induced liver damage may be a good model to study the role of *Tet1* in the ductal progenitor response to damage.

Therefore, we treated *WT* and *Tet1<sup>hypo/hypo</sup>* mice with chow supplemented with 0.1% DDC for 5 days (T5) and either analysed or switched the mice to normal diet and allowed to recover for 7 days (T12) (Figure 3.21a). Throughout the time course mouse weight was monitored and *WT* and *Tet1<sup>hypo/hypo</sup>* lost a similar amount of weight as a proportion of their starting weight during damage, and in a similar fashion, there was no difference in the rate at which the mice put on weight after switching back to normal diet (Figure 3.21c). Haematoxylin and eosin staining revealed that there was porphyrin deposition, characteristic of DDC treatment, in the livers of both *WT* and *Tet1<sup>hypo/hypo</sup>* after 5 days of damage (T5) (Figure 3.21b). This validated the treatment regimen of DDC but provided very little information about the behaviour of the cell populations after DDC induced liver damage.

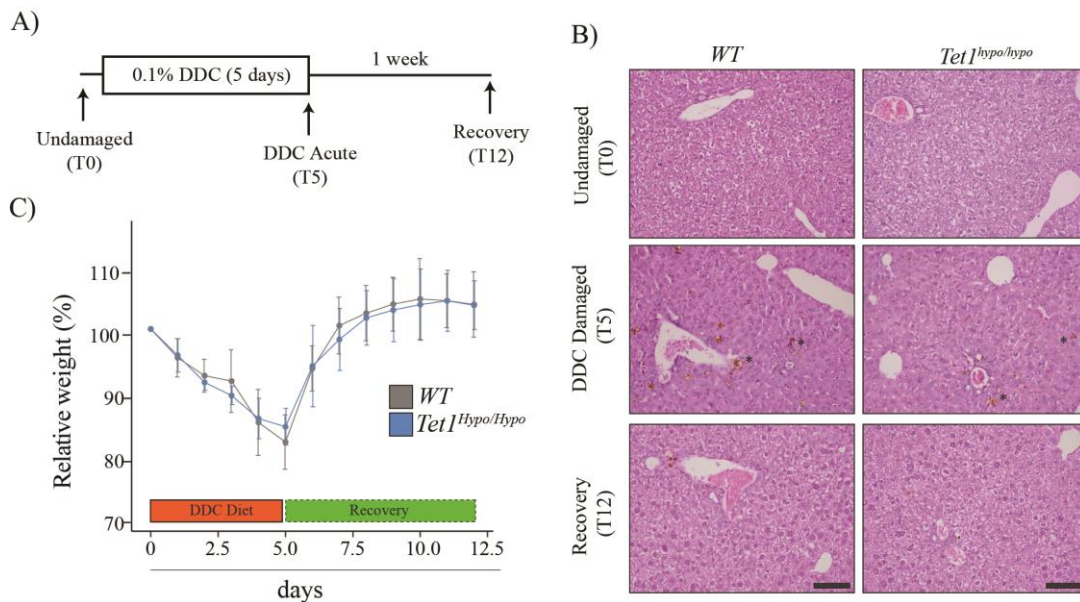


**Figure 3.21 - *Tet1* hypomorphic and WT mice lose weight and accumulate porphyrin to a similar level in response to acute DDC treatment.** A) Experimental scheme: Mice were left undamaged (T0) or treated with food supplemented with 0.1% DDC for 5 days and either analysed immediately (T5) or switched to normal chow for 7 days (T12). B) Representative H&E staining of liver sections of *Tet1<sup>hypo/hypo</sup>* and WT mice at T0, T5 and T12. Asterisks show porphyrin deposition. Scale bar = 250  $\mu$ m. C) Animal weight changes throughout the acute DDC damage protocol. Changes were expressed as a percentage of each individual mouse starting weight. Data is plotted as the group mean for every timepoint with error bars representing the 95% confidence interval (WT, n=5 and *Tet1<sup>hypo/hypo</sup>*, n=5) taken from three independent experiments.

To explore the ductal response to DDC induced liver damage we analysed the proliferative ductal fraction before (T0) and after DDC damage (T5) of WT and *Tet1<sup>hypo/hypo</sup>* mice. As previously described by others (MacDonald, 1961), undamaged WT mice (T0) had very little proliferative activity in the ductal compartment of the liver. The largely non-proliferative state of the ductal compartment is also maintained in *Tet1* hypomorphic mice. However, after 5 days of DDC treatment (T5) a significant proliferative fraction emerged. In WT mice ~20% of the ductal compartment (marked by osteopontin, OPN) was positive for proliferation marker Ki67 (OPN+/Ki67+), however, *Tet1<sup>hypo/hypo</sup>* mice showed significantly less proliferation (Figure 3.22b-d). Therefore, reduced expression of *Tet1* results in impaired activation of proliferation after damage, mirroring observations in organoid models.

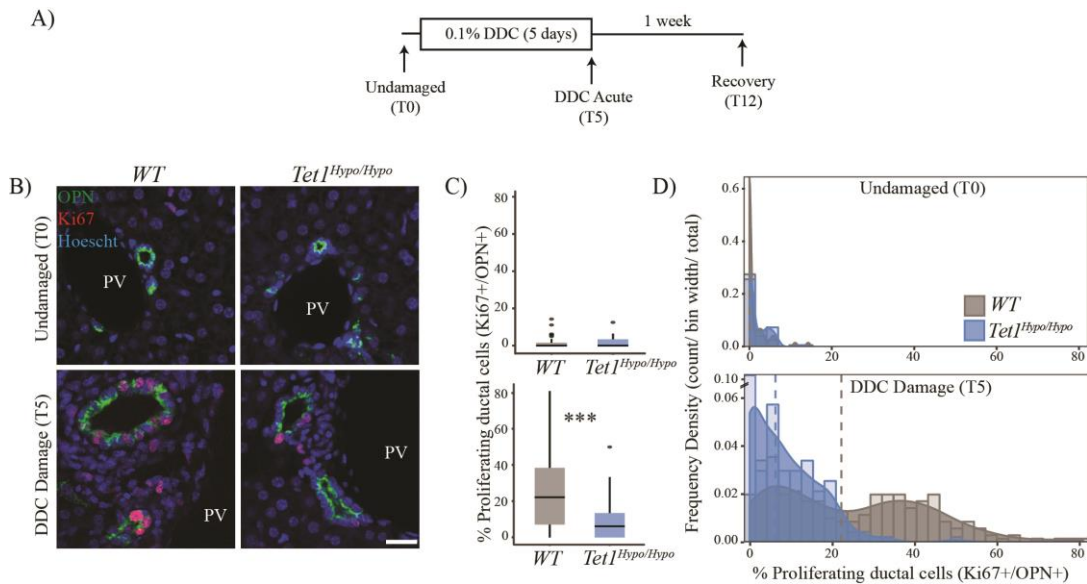


**Figure 3.22 - TET1 is crucial for initiation of ductal proliferation in response to DDC damage.** A) Experimental scheme, mice were left undamaged (T0) or treated with food supplemented with 0.1% DDC for 5 days and either analysed immediately (T5) or switched to normal chow for 7 days (T12). B) Representative images of 100um liver sections stained with the ductal marker Osteopontin (OPN) and the proliferation marker Ki67 in undamaged (T0) and DDC damaged (T5) *WT* and *Tet1<sup>hypo/hypo</sup>* mice. Scale bar = 25um. PV = portal vein. C) Box-and-whisker plot showing median and inter-quartile range and the overall range of values of proliferating ductal cells (Ki67<sup>+</sup>/OPN<sup>+</sup>). Each dot represents an outlier from a single counted field of view (FOV). D) Histogram showing the population distribution of proliferating ductal cells (OPN<sup>+</sup>/Ki67<sup>+</sup>) by plotting frequency density of counts across the sample range (bar) and the kernel density estimate (line). Dashed lines show median values. C-D) Graphs are representative of values obtained from 55 fields of view (FOV) for *WT* (n=3) and 56 FOV for *Tet1<sup>hypo/hypo</sup>* mice (n=3) at T0 (undamaged) and 253 FOV for *WT* (n=7) and 169 FOV for *Tet1<sup>hypo/hypo</sup>* (n=6) at T5 of DDC damage. p values have been obtained by using Kolmogorov-Smirnov test. \*\*\*= p<0.001.

Further analysis, of the distribution of proliferation in the portal regions we found that *WT* mice have two distinct populations. A population with a large proliferative fraction (~40%) and a second with fewer proliferative ductal cells (~10%). Interestingly, hypomorphic mice did not have the same distribution across their portal regions. Rather, there was a single population closely matching the lower proliferative fraction seen in *WT* mice (Figure 3.22d). It would be interesting to speculate that the two populations seen in the *WT* mice represent two populations of ductal cells that have different proliferative potential and reduced *Tet1* expression results in the population with highest proliferative potential not emerging upon damage. To more conclusively answer this question, we would need to understand if there are distinct spatial or molecular populations of ductal cells through single cell resolution studies in combination with advance imaging techniques, for further discussion see chapter 3.7.

We next sought to understand whether the impaired ductal proliferation of *Tet1<sup>hypo/hypo</sup>* mice at T5 was detrimental to the overall ductal population upon recovery. Therefore, we initially treated mice with 5 days of 0.1% DDC before allowing them to recover for 7 days on normal diet (T12) (Figure 3.23a). We found that the ductal population was significantly reduced in *Tet1<sup>hypo/hypo</sup>* mice compared to *WT* mice (Figure 3.23b-d). Thus, reduced *Tet1* expression results in a smaller expansion of the ductal population in response to DDC damage, likely due to impaired proliferation.

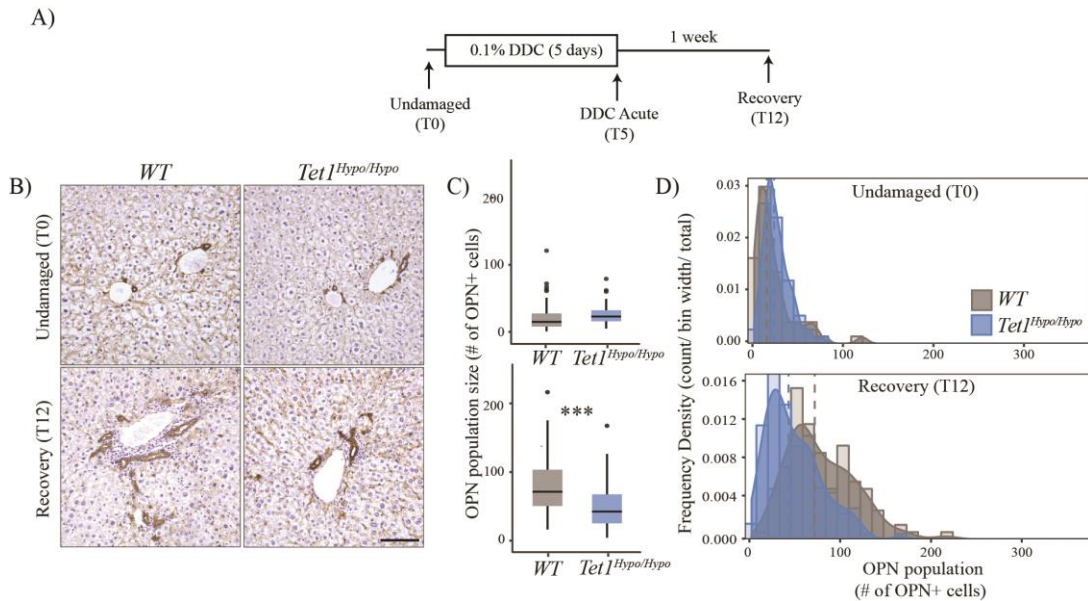


**Figure 3.23 - *Tet1* hypomorphic mice have a smaller ductal population after recovery from acute DDC damage.** A) Experimental scheme: Mice were left undamaged (T0) or treated with food supplemented with 0.1% DDC for 5 days and either analysed immediately (T5) or switched to normal chow for 7 days (T12). B) Representative immunohistochemistry images showing ductal cells marked by pan-cytokeratin in undamaged mice and upon recovery from DDC damage (T12). Nuclei are stained with Haematoxylin. Scale bar = 100µm. C) Box-and-whisker plot showing median and inter-quartile range and the overall range of values of ductal cell populations (OPN<sup>+</sup>/FOV). Each dot represents an outlier from a single counted field of view (FOV). D) Histogram showing the population distribution of the total ductal cell number (OPN<sup>+</sup>) by plotting frequency density of counts across the sample range (bars) and the kernel density estimate (line). Dashed lines show median values. C-D) Both graphs are representative of values obtained from 55 FOV (n=3) for *WT* and 56 FOV for *Tet1<sup>hypo/hypo</sup>* (n=3) mice at 0 (T0) and 110 FOV for *WT* (n=3) and 153 FOV for *Tet1<sup>hypo/hypo</sup>* mice (n=4) at day 12 (T12). p values have been obtained by using Kolmogorov-Smirnov test. \*\*\*= p<0.001.

It is important to note that this data could be explained if the *Tet1<sup>hypo/hypo</sup>* mice experience a lower level of global liver damage compared to *WT* mice and therefore, elicit a reduced regenerative response. Taken together with the fact that the hypomorph is not tissue specific and may have several indirect effects we must attempt to rule out confounding factors. At all time points analysed (T0, T5 or T12), we took blood samples and analysed the serum levels of alanine transaminase (ALT) and glutamate

dehydrogenase (GLDH) to assess liver damage. At all time points *Tet1<sup>hypo/hypo</sup>* mice had similar levels of both markers of liver damage when compared to *WT* mice (Figure 3.24b). Therefore, despite the system wide reduction of *Tet1* expression DDC treatment resulted in a similar level of global liver damage in hypomorphic mice compared to *WT* mice. As the route of DDC treatment is via food intake we also wanted to examine the effect of DDC treatment on the small intestine to rule out any defects in the *Tet1* hypomorph, which would compromise DDC uptake. We found no major defects in the architecture in the small intestine of *Tet1<sup>hypo/hypo</sup>* when compared to *WT* mice after 5 days of DDC damage (Figure 3.24c). As a result, a reduced level of *Tet1* expression does not alter the effect of DDC on the liver. However, we still cannot rule out other direct or indirect affects that the loss of *Tet1* in other cell types may have on our observations. For instance, in response to liver damage there is not only ductal and hepatocyte regeneration but also significant inflammation which aids in repair. It would be therefore, interesting and important to also rule out any involvement of *Tet1* in this inflammatory response. In any case, even if we could achieve this it is unlikely that we will be able to fully rule out all possible sources of potential confounding affects in this model. A more prudent method to validate the role of *Tet1* would be to specifically ablate *Tet1* in the ductal population. See Chapters 3.3.4 and 4.3.3 for further discussion.

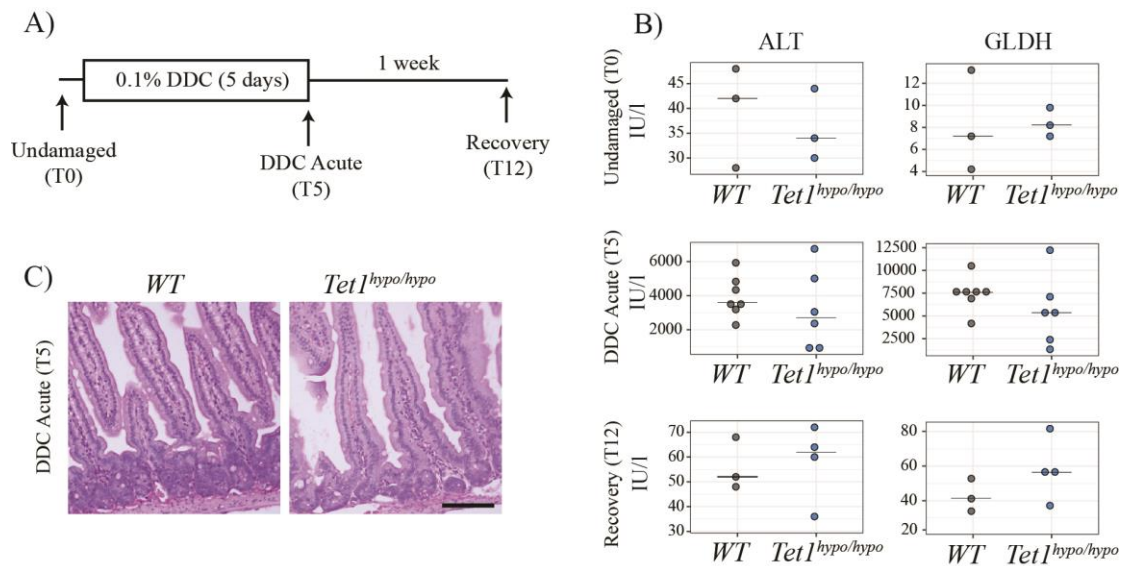


**Figure 3.24 - Impaired ductal response is not due to decreased global liver damage in *Tet1* hypomorphic mice.**

A) Experimental scheme: Mice were left undamaged (T0) or treated with food supplemented with 0.1% DDC for 5 days and either analysed immediately (T5) or switched to normal chow for 7 days (T12). B) Serum levels of alanine transaminase (ALT) and glutamate dehydrogenase (GLDH) of *Tet1*<sup>hypo/hypo</sup> or WT mice at T0, T5 and T12 timepoints. Bar represents group median and dots are individual readings from independent mice. C) Representative H&E staining of the small intestine of WT or *Tet1*<sup>hypo/hypo</sup> mice after 5 days of DDC treatment (T5).

### 3.3.3 Reduced *Tet1* expression leads to impaired liver regeneration after chronic liver damage.

The short 5-day DDC damage (acute) model is good for activating ductal proliferation but does not model some aspects of chronic liver damage such as liver fibrosis. In order to create a better model of chronic liver damage, we decided to administer eight sequential doses of 5-day DDC treatments, each with a 3-day recovery periods between each dose of DDC. After this extensive damage protocol, mice were left to recover for 3 months before analysis in order to assess how fibrosis was resolved after damage (Figure 3.25a). Throughout the damage protocol, mouse weight was monitored. Mouse weights between *Tet1<sup>hypo/hypo</sup>* mice and *WT* mouse were similar throughout the experiment (Figure 3.25b). Furthermore, after 3 months of recovery extensive porphyrin deposition was evident throughout the livers of *WT* and *Tet1<sup>hypo/hypo</sup>* mice (Figure 3.25c).

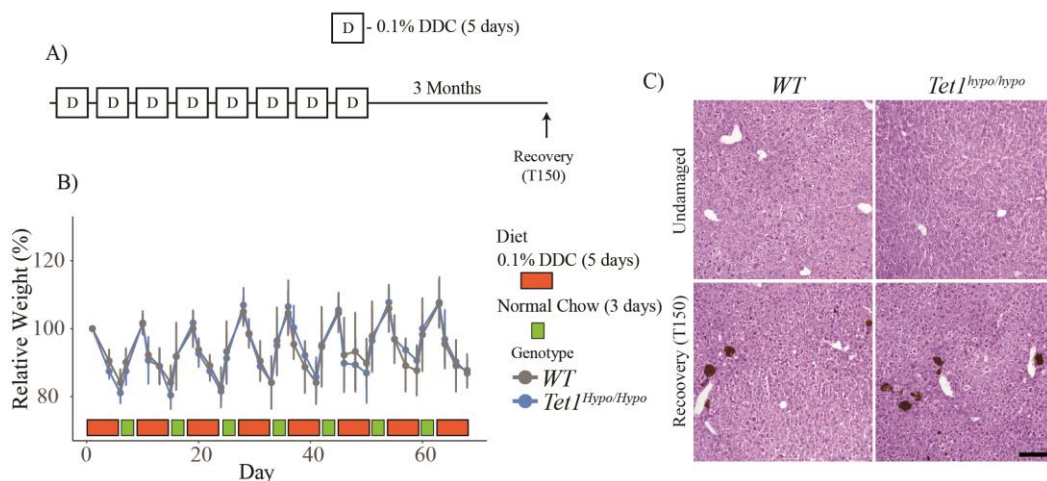


**Figure 3.25 - Chronic DDC damage results in cyclic weight loss and recovery in *Tet1* hypomorphic and *WT* mice.** A) Experimental scheme, mice were treated with eight 5 day doses of 0.1% DDC treatment each with a 3 day interval of normal diet. Mice were then allowed to recover on normal diet for 3 months before analysis (T150). B) Animal weight changes throughout the chronic DDC damage protocol. Changes were expressed as a percentage of each individual mouse starting weight. Data is plotted as the group mean for every timepoint with error bars representing the 95% confidence interval (*WT*, n=3 and *Tet1<sup>hypo/hypo</sup>*, n=3) taken from two independent experiments. C) Representative images of H&E stainings of liver sections of *Tet1<sup>hypo/hypo</sup>* and *WT* mice at T0, and T150. Asterisk show porphyrin deposition. Scale bar = 250  $\mu$ m.

After chronic DDC treatment and recovery we analysed ductal proliferation in a similar manner to the previous acute DDC model to examine whether there were similar observations. However, in this case we found that there was marginal proliferation in both *WT* and *Tet1<sup>hypo/hypo</sup>* mice and no difference in ductal population

(Figure 3.26b-c). In terms of proliferation, it is not surprising that the ductal compartment is largely non-proliferative at this stage, due to the long recovery period allowing the damage phase to resolve. However, if indeed there was a proliferative defect during the damage phase, in similar fashion to that observed in the acute DDC model, we would expect the ductal population to be smaller in the *Tet1* hypomorphic mice after recovery, but this was not the case (Figure 3.26b-c). One possible explanation for this is that due to the chronic nature of the damage protocol the residual expression of *Tet1* is able to eventually rescue the ductal regenerative response. This would suggest that the ductal proliferation impairment seen in the acute DDC model is due to a delayed response rather than an absolute defect. Another explanation could be that as it is a long-term recovery that the at one point expanded population has already returned to undamaged levels where there was no difference between *WT* or *Tet1<sup>hypo/hypo</sup>* mice (Figure 3.23). In order to understand these results further it would be interesting to analysis more time points within the damage and recovery phase to dissect the ductal response in more detail.

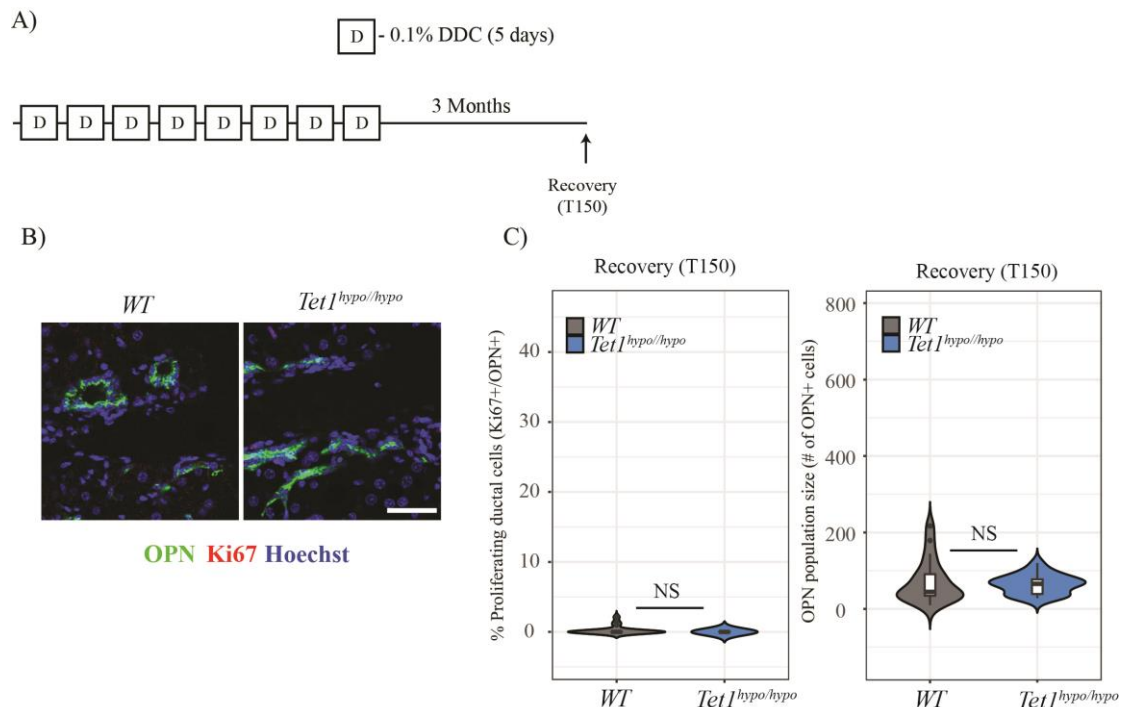


**Figure 3.26 - Reduced levels of TET1 does not alter ductal proliferation or ductal population size after recovery from chronic DDC damage.** A) Experimental scheme: Mice were treated with eight 5 day doses of 0.1% DDC treatment each with a 3 day interval of normal diet. Mice were then allowed to recover on normal diet for 3 months before analysis (T150). B) Representative images of 100um liver sections stained with the ductal marker Osteopontin (OPN) and the proliferation marker Ki67 in undamaged (T0) and DDC damaged (T150) *WT* and *Tet1<sup>hypo/hypo</sup>* mice. Scale bar = 50  $\mu$ m. C) Quantification of ductal proliferation (OPN+/Ki67+) and ductal population size (OPN+/FOV). Data is represented as violin plots showing population density with box-plots showing median, interquartile and overall range. Values are derived from *Tet1<sup>hypo/hypo</sup>* (n=1) and *WT* (n=1) mice from a single experiment. p values have been obtained by using Kolmogorov-Smirnov test, NS – Not significant.

In any case, even though we are unable to conclude whether or not there has been a ductal proliferative defect with this model we are still able to analyse other aspects of liver regeneration. Therefore, to assess whether long-term recovery from DDC damage resulted in complete liver regeneration we analysed the extent of fibrosis. We treated mice with our chronic DDC model and allowed them to recover for 3 months before assessing collagen deposition by picosirius red staining and quantified with a macro developed in Fiji. *Tet1<sup>hypo/hypo</sup>* mice had a significantly increased fibrotic area when compared to *WT* mice after recovery from chronic DDC damage (Figure 3.27b-c). Moreover, *WT* mice exposed to chronic damage and allowed to recover did not have a significantly increased level of fibrosis compared to undamaged controls. This suggests that *WT* mice were able to largely recover from chronic DDC damage after 3 months whereas prominent fibrosis was still evident in hypomorphic mice. Taken

together, reduced *Tet1* expression results in an impaired resolution of fibrosis after chronic DDC damage.

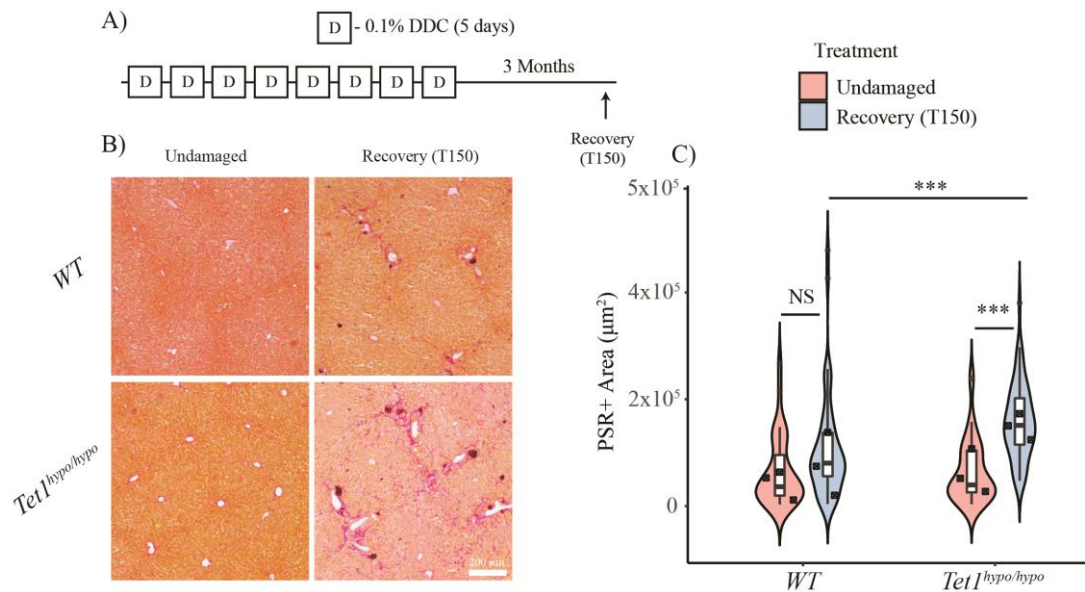


**Figure 3.27 - *Tet1* hypomorphic mice have increased fibrosis after recovery from DDC chronic damage.** A) Experimental scheme: Mice were treated with eight 5 day doses of 0.1% DDC treatment each with a 3 day interval of normal diet. Mice were then allowed to recover on normal diet for 3 months before analysis (T150). B) Representative images of thin paraffin embedded liver sections stained by picosirius red marking collagen (red) and cytoplasm (yellow) of undamaged (T0) and recovered (T150) WT and *Tet1*<sup>hypo/hypo</sup> mice. C) Collagen deposition was quantified using a plugin developed in Fiji and represented as violin plots showing population density with box-plots showing median, interquartile and overall range. Values are derived from *Tet1*<sup>hypo/hypo</sup> (n=3) and WT (n=3) mice undamaged (T0) and recovered mice (T150) from two independent experiments. Medians from each mouse are shown as boxes. p values were calculated by two-way ANOVA and Tukey HSD post hoc test. p<0.001 = \*\*\*.

In summary, we found that reduced *Tet1* expression results in impaired ductal progenitor expansion using *in vitro* organoid models. Remarkably, the defect was rescued by full-length human *Tet1* overexpression but not by a catalytic inactive variant directly implicating TET1 enzymatic activity in ductal progenitor maintenance *in vitro* (data not shown, Aloia *et al.* in press). Moreover, reduced *Tet1* expression resulted in a smaller proliferative response in the ductal compartment in the liver after DDC induced damage and ultimately after a week recovery a smaller ductal population. On the other hand, chronic, DDC treatment did not show altered ductal dynamics after recovery from damage but *Tet1* expression was crucial for the resolution of liver fibrosis.

### 3.3.4 Ductal specific genetic ablation of *Tet1* causes diminished function of *bona fide* bi-potent ductal progenitors *in vitro* and *in vivo*.

Our *Tet1<sup>hypo</sup>* mouse model combined with DDC treatment described in Chapter 3.3.2 and 3.3.3 suffers from several flaws such as the lack of spatiotemporal control of *Tet1* deletion and the inability to trace the fate of ductal progenitors. Furthermore, as DDC treatment on its own has not widely been shown to generate ductal derived hepatocytes to understand the role of *Tet1* in *bona fide* bi-potential ductal progenitors a modified model would be required.

To solve the problems associated with the lack of spatiotemporal control we took advantage of our *Tet1<sup>flx</sup>* model crossed with two inducible Cre drivers. We bred our *Tet1<sup>flx</sup>* line with a *RosaCre<sup>ERT2</sup>* line in order to facilitate the ubiquitous and complete deletion of *Tet1*. Despite lacking tissue specificity, the resultant *Tet1<sup>flx/flx</sup>/RosaCre<sup>ERT2</sup>* mice allowed us to avoid lethality seen in our *Tet1<sup>ko/ko</sup>* mice and study the effect of complete *Tet1* deletion in adult mice.

As described above, reduced expression of *Tet1* allows the successful derivation of organoids, however impairs organoid expansion potential after passage. We therefore hypothesised that complete deletion of *Tet1* would result in a more potent phenotype. To test this, mature EpCAM+ ductal cells were isolated from adult (8-12 week old) *Tet1<sup>flx/flx</sup>/RosaCre<sup>ERT2</sup>* or *Tet1<sup>flx/flx</sup>* and placed in 3D culture conditions supplemented with 5 uM OH-tamoxifen (Figure 3.28a). We found that *Tet1* deletion nearly completely abolished organoid formation (Figure 3.28b). This suggests that *Tet1* is crucial for the generation of organoids from mature ductal cells and that the residual expression of *Tet1* in *Tet1<sup>hypo/hypo</sup>* organoids is enough to sustain organoid formation but not long-term expansion.

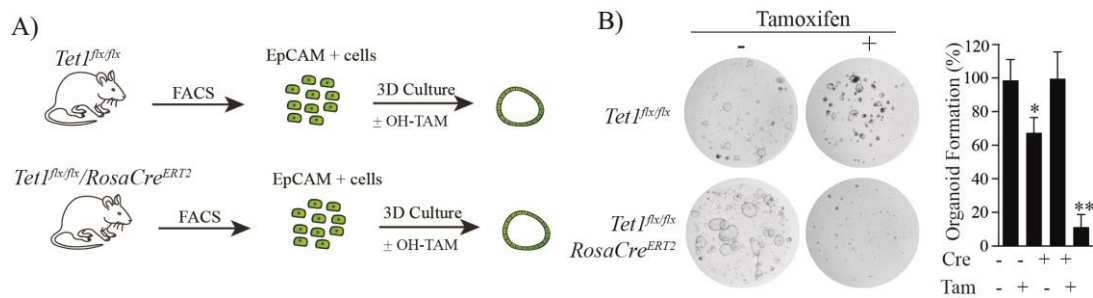


**Figure 3.28 - *Tet1* ablation abolishes organoids formation from mature EpCAM+ cells.** A) Experimental scheme: FACS-sorted EpCAM<sup>+</sup> ductal cells derived from *RosaCre<sup>ERT2</sup>* x *Tet1<sup>flx/flx</sup>* mouse livers were plated in organoid isolation medium supplemented with 5  $\mu$ M hydroxytamoxifen or left untreated *in vitro*. B) Organoid formation efficiency was evaluated after 6 days in culture. Representative bright field pictures are shown. Each dot represents the average of the count from 3 wells coming from an independent biological experiment. Graphs represent mean  $\pm$  SD of 3 independent experiments. p value was calculated by two-side students t-test statistical analysis: \* =  $p < 0.05$ ; \*\*\* =  $p < 0.001$ . (Aloia *et al.* unpublished).

We next wanted to study the effect of complete deletion of *Tet1* on ductal driven liver regeneration to see whether the proliferative defects seen in *Tet1<sup>flx/flx</sup>/RosaCre<sup>ERT2</sup>* organoid lines translate to similar effects in liver ductal progenitors. Therefore, adult *Tet1<sup>flx/flx</sup>/RosaCre<sup>ERT2</sup>* mice were treated with three doses of 4 mg tamoxifen delivered intraperitoneally to induce *Tet1* deletion before treating with liver damaging agents (Figure 3.30a). Unfortunately, we found that 7-9 days after tamoxifen induction several mice begun to show severe clinical signs and had to be culled on ethical grounds. To understand the cause of this emergent lethality we assessed the architecture of the small intestine (SI). We found that the SI of mice that had shown signs of ill health was severely compromised (Figure 3.29b). This was in line with a recent study showing that *Tet1* null animals, which have been shown to be viable in a mixed background, exhibit postnatal lethality in a pure background due to a collapse of the stem cell pool in the SI (Kim *et al.*, 2016). Interestingly, the penetrance of the lethal phenotype was not complete, 33% of treated *Tet1<sup>flx/flx</sup>/RosaCre<sup>ERT2</sup>* mice showed the SI defect. Furthermore, no lethal phenotypes were seen in controls either lacking the Cre driver or not treated with tamoxifen (Figure 3.30). Together this suggests *Tet1* expression is essential in the adult mouse to maintain SI integrity.

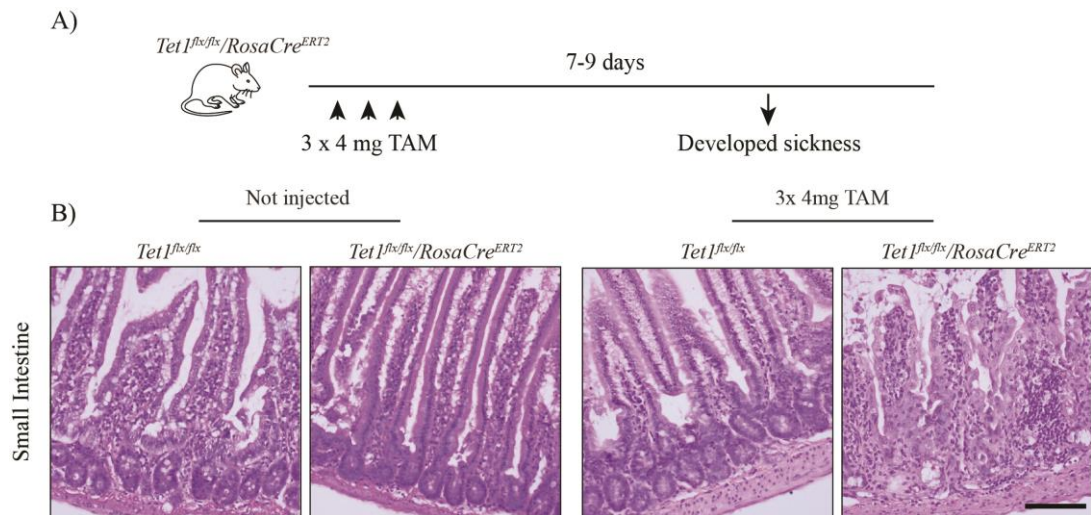


**Figure 3.29 - Ubiquitous postnatal deletion of *Tet1* is lethal and results in collapse of the small intestine.** A) Experimental scheme: Mice were treated with 3 doses of 4mg tamoxifen delivered intraperitoneally and developed sickness and were culled on welfare grounds between 7-9 days later. B) Representative pictures of Haematoxylin and eosin staining of the small intestine of conditional knock-out mice *RosaCre<sup>ERT2</sup> x Tet1<sup>flx/flx</sup>* and controls *Tet1<sup>flx/flx</sup>* treated or untreated with tamoxifen. Scale bar = 100µm.

<b><i>Tet1</i> Genotype</b>	<b>Gender</b>	<b>Tamoxifen dose</b>	<b>Died after induction</b>	<b>Intestinal epithelium</b>
<i>Tet1<sup>flx/flx</sup>/RosaCre<sup>ERT2</sup></i>	Female	3x4mg	+ (7 days)	NA
<i>Tet1<sup>flx/flx</sup>/RosaCre<sup>ERT2</sup></i>	Male	3x4mg	+ (9 days)	A
<i>Tet1<sup>flx/flx</sup>/RosaCre<sup>ERT2</sup></i>	Female	3x4mg	+ (7 days)	A
<i>Tet1<sup>flx/flx</sup>/RosaCre<sup>ERT2</sup></i>	Female	3x4mg	-	U
<i>Tet1<sup>flx/flx</sup>/RosaCre<sup>ERT2</sup></i>	Female	3x4mg	-	U
<i>Tet1<sup>flx/flx</sup>/RosaCre<sup>ERT2</sup></i>	Female	3x4mg	-	U
<i>Tet1<sup>flx/flx</sup>/RosaCre<sup>ERT2</sup></i>	Male	3x4mg	-	U
<i>Tet1<sup>flx/flx</sup>/RosaCre<sup>ERT2</sup></i>	Male	3x4mg	-	U
<i>Tet1<sup>flx/flx</sup>/RosaCre<sup>ERT2</sup></i>	Male	3x4mg	-	U
<i>Tet1<sup>flx/flx</sup></i>	Female	3x4mg	-	U
<i>Tet1<sup>flx/flx</sup></i>	Male	3x4mg	-	U
<i>Tet1<sup>flx/flx</sup>/RosaCre<sup>ERT2</sup></i>	Male	Not Injected	-	U
<i>Tet1<sup>flx/flx</sup></i>	Male	Not injected	-	U

**Figure 3.30 - Prominence of lethality after ubiquitous *Tet1* deletion.** A table showing the different genotype, gender, viability and tamoxifen dose of mice injected. N/A, not analysed. A, affected. U, unaffected.

*Tet1* expression may be crucial in other tissues such as the liver but analyses of those tissues were impaired by the lethal collapse of the SI in the *Tet1<sup>flx/flx</sup>/RosaCre<sup>ERT2</sup>* model. We therefore need a more restricted mode of deletion to target only our tissue of interest and avoid any indirect effects of *Tet1*. We took advantage of an inducible Cre under the promoter of *Prominin1* (*Prom1Cre<sup>ERT2</sup>*) whose expression has been shown to be restricted to the ductal compartment of the liver as well as many other epithelial tissues (Zhu *et al.*, 2016). We confirmed this by crossing *Prom1Cre<sup>ERT2</sup>* mice with



We then bred the *Prom1Cre<sup>ERT2</sup>/Rosa<sup>IslZsGreen</sup>* with our *Tet1<sup>flx</sup>* line to generate *Prom1Cre<sup>ERT2</sup>/Rosa<sup>IslZsGreen</sup>/Tet1<sup>flx/flx</sup>* mice. This line allowed us to specifically delete *Tet1* in the ductal compartment of the liver whilst simultaneously marking recombined cells with ZsGreen facilitating lineage tracing to follow fate of the ductal cells, solving many of the flaws of the *Tet1<sup>hyppo</sup>* line such as: the lack of control of Tet1 deletion; and the inability to trace the fate of *Tet1* mutant cells.

Furthermore, it has been argued that acute DDC damage as a liver damage model does not fully model bi-potent ductal progenitors as new hepatocytes are not formed. Therefore, we wanted to combine our new ductal specific *Tet1* deletion mouse line with a mode of liver damage that generated *bona fide* bi-potential ductal progenitors. It has been recently described that by forcing the hepatocytes into senescence abolishing their ability to contribute to liver regeneration, results in a potent ductal reaction in response to toxic liver damage whereby the ductal compartment was shown to significantly contribute to the hepatocyte pool, providing an excellent paradigm to study bi-potential progenitors (Raven *et al.*, 2017). This was achieved through either genetic ablation of  $\beta$ 1-integrin or viral induced over expression of p21, a potent repressor of proliferation. In our case the  $\beta$ 1-integrin would be inappropriate as it relies on the same *Cre-lox* knock out system as our *Tet1* condition allele therefore it would be impossible to delete either independently. As a result, we opted to use the p21 overexpression model which instead relies on expression via a viral vector allowing us to easily in conjunction with our genetic model of *Tet1* deletion.

Therefore, we initially treated either *Prom1Cre<sup>ERT2</sup>/Rosa<sup>IslZsGreen</sup>/Tet1<sup>flx/flx</sup>* or *Prom1Cre<sup>ERT2</sup>/Rosa<sup>IslZsGreen</sup>/Tet1<sup>WT</sup>* mice with three doses of 0.2mg/g tamoxifen to generate a WT (*Prom1<sup>Tet1WT</sup>*) ductal compartment or a ductal compartment depleted for *Tet1* (*Prom1<sup>ΔTet1</sup>*). In both genotypes the ductal compartment was also labelled with ZsGreen to follow the fate of the ductal cells. After induction of *Tet1* deletion, following tamoxifen treatment, we induced hepatocyte specific senescence by over expression of p21. To carry this out we treated mice with an adeno-associated viral vector with a liver specific tropism (AAV8) and p21 under the thyroxine binding globin (TBG) promoter ensuring hepatocyte specific expression of p21. *Prom1<sup>Tet1WT</sup>* and *Prom1<sup>ΔTet1</sup>* mice were treated with the AAV8-TBG-p21 virus at a dose of  $7.5 \times 10^{11}$  gc by tail vein injection. Following p21 overexpression we induced liver damage in animals by carrying out three 5 day 0.1% DDC doses in order to induce a significant ductular reaction as reported by Raven *et al.* (2017). Finally, the mice were allowed to

recover for two weeks before being culled and assessed for ductal contribution to the hepatocyte compartment (Figure 3.32a).

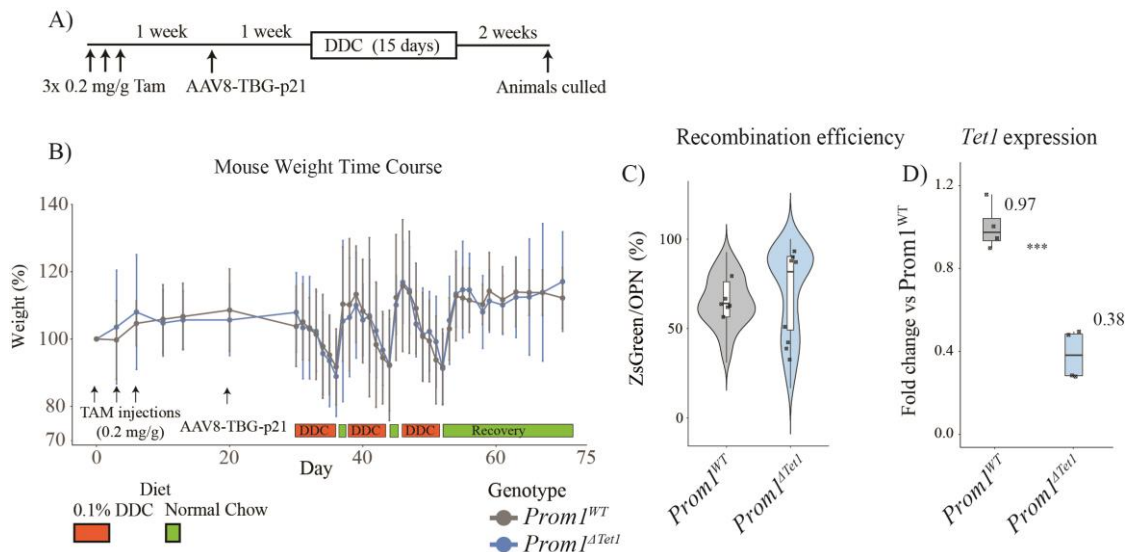


**Figure 3.32 – Efficient *Tet1* deletion in the context of hepatocyte specific p21 overexpression and DDC damage.**

A) Experimental scheme: *Tet1* depletion and ZsGreen lineage tracing were induced by three doses of 0.2 mg/g tamoxifen delivered intraperitoneally. After one week wash out, overexpression of p21 was mediated by tail vein injection of AAV8-TBG-p21 viral vector resulting in hepatocyte specific p21 overexpression. Mice were fed with 3 cycles of 5 day DDC treatments in order to monitor the regenerative response of *Prom1<sup>Tet1</sup>WT* and *Prom1<sup>ΔTet1</sup>* ductal cell when hepatocytes are compromised. B) Animal weight changes throughout p21 overexpression and DDC damage protocol. Changes are expressed as a percentage of each individual mouse starting weight. Data is plotted as the group mean for every time point with error bars representing the 95% confidence interval (*Prom1<sup>Tet1</sup>WT*, n= 4 and *Prom1<sup>ΔTet1</sup>*, n= 4). Arrows represent either tamoxifen or viral injections and orange boxes denote each dose of 0.1% DDC. C) *Tet1* expression in EpCAM<sup>+</sup> ductal cells isolated by FACS-sorting from *Prom1<sup>ΔTet1</sup>* (n=4) compared to those isolated from *Prom1<sup>Tet1</sup>WT* (n=4) mice at the end of the recovery phase after 3x DDC doses. Two-sided students t-test statistical analyses were performed: \*\*\*= p<0.001.

Throughout the p21/DDC damage protocol *Prom1<sup>Tet1</sup>WT* and *Prom1<sup>ΔTet1</sup>* had similar body weight dynamics, suggesting no overt intolerance of the protocol as a result of *Tet1* deletion (Figure 3.32b). We then validated *Tet1* deletion in the EpCAM<sup>+</sup>/ZsGreen<sup>+</sup> ductal population after the damage protocol. We found that *Prom1<sup>ΔTet1</sup>* mice showed an average reduction of ~60% in the expression of *Tet1* when compared to *Prom1<sup>Tet1</sup>WT* control mice, indicating a good recombination efficiency (Figure 3.32c-d). It is important to note that if loss of *Tet1* has a negative effect on the ductal compartment in a similar manner to what we observed in the *Tet1<sup>hypo</sup>* model, the WT ductal cells may out compete a *ΔTet1* population. Therefore, by checking deletion after the damage protocol it may not correctly reflect the original deletion efficiency as the WT ductal population may have expanded more than the deleted population. To

further investigate this, it would be prudent to induce only *Tet1* deletion before analysing recombination efficiency. We also then confirmed hepatocyte specific p21 protein overexpression by immunohistochemistry (Figure 3.33).

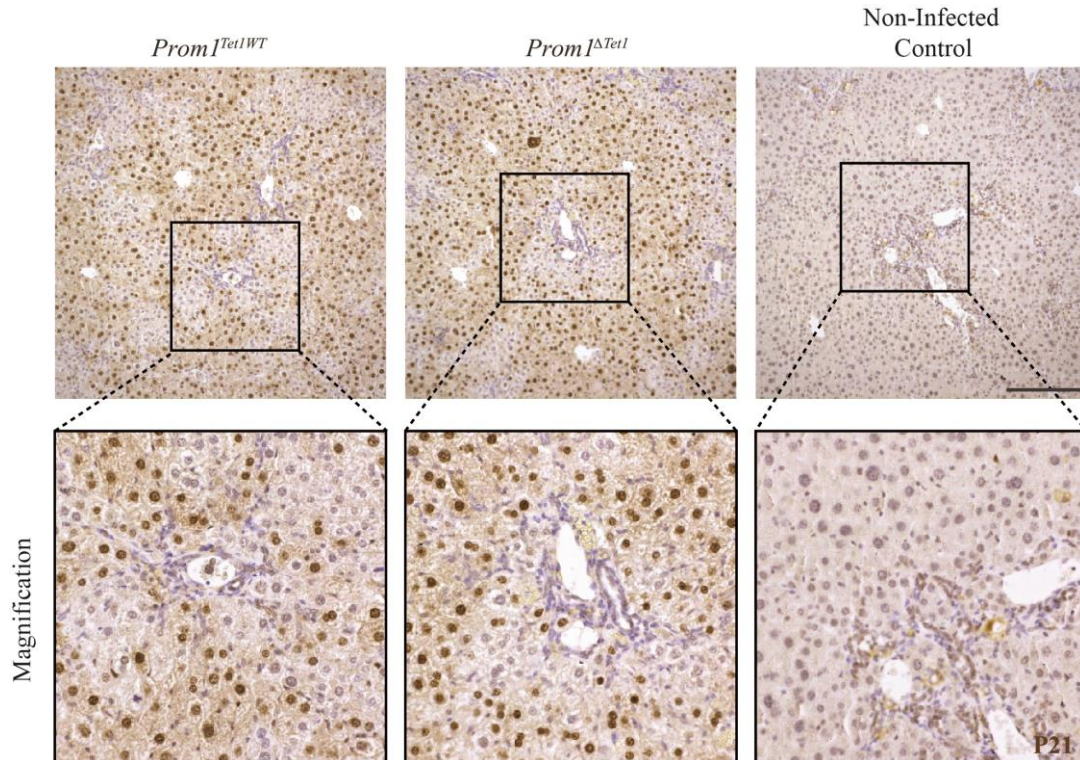


**Figure 3.33 - AAV8-TBG-p21 induced p21 overexpression is restricted to the hepatocyte compartment.** A) Representative images of 5  $\mu$ m paraffin sections of livers from either *Prom1<sup>Tet1</sup>WT* or *Prom1<sup>ΔTet1</sup>* mice after p21 over expression and DDC damage protocol compared to a mock-injected mouse. Scale bar = 200  $\mu$ m.

After confirming that the p21/DDC damage model induced the required *tet1* deletion and p21 over expression we next wanted to investigate the effect of ductal specific loss of *Tet1* on the ductal population after p21/DDC treatment. To carry this out, we quantified the number of ZsGreen+/OPN+ cells per field of view before normalising by mouse specific recombination efficiency. We found that the ZsGreen+ ductal population of *Prom1<sup>Tet1</sup>WT* mice was on average ~50% larger than the ductal population observed in *Prom1<sup>ΔTet1</sup>* mice (Figure 3.34b-c). This is very similar to observations from *Tet1<sup>hypo/hypo</sup>* mice after recovery from 5 days of DDC, suggesting that the smaller ductal population in the p21/DDC model may be down to a similar proliferative defect in the ductal compartment. Alternatively, this result could also be explained by increased cell death in *Prom1<sup>ΔTet1</sup>* mice. Analysis of further time points in the damage phase of the protocol would help to understand the underlying mechanism of the altered population sizes.

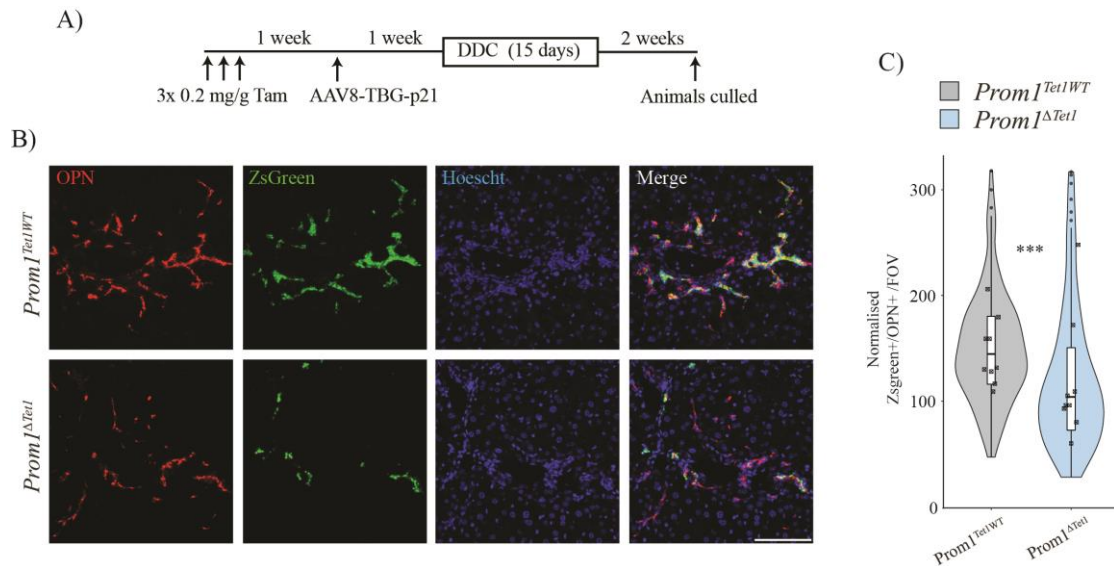


**Figure 3.34 - Ductal specific deletion of *Tet1* led to reduced ductal expansion after DDC damage in the context of hepatocyte senescence.** A) Experimental scheme: *Tet1* depletion and ZsGreen lineage tracing were induced by three doses of 0.2 mg/g tamoxifen delivered intraperitoneally. After one week wash out, overexpression of p21 was mediated by tail vein injection of AAV8-TBG-p21 viral vector resulting in hepatocyte specific p21 overexpression. Mice were fed with 3 cycles of 5 day DDC treatments. B) Representative images of 10um liver frozen sections stained for ductal marker Osteopontin (OPN-red), endogenous ZsGreen expression (Green) and Nuclei with Hoechst (Blue) of *Prom1<sup>Tet1</sup><sup>WT</sup>* or *Prom1<sup>ΔTet1</sup>* mice. Scale bar =100 μm c, Quantification of ZsGreen+ and OPN+ double positive population per field of view normalised against mouse specific recombination efficiency shows *Tet1* deletion results in a significantly reduced ductal ZsGreen population size. Data plotted as violin plots representing population density, and boxplots showing median, upper and lower quantiles and the range. Boxes represent median value for each individual mouse (*Prom1<sup>Tet1</sup><sup>WT</sup>*, n = 8 *Prom1<sup>ΔTet1</sup>*, n = 8) from three independent experiments \*\*\*= p<0.001 was determined by Mann Whitney U test.

Interestingly, we found that although p21 protein expression in was restricted in the hepatocytes in all injected animals and not in mock injected controls, we observed that there were p21-ve hepatocytes surrounding the portal regions (Figure 3.33). These negative patches of hepatocytes could be explained by either a poor infection rate by the virus or by the emergence of ductal derived hepatocytes, which would lack p21 expression. To untangle the two scenarios, we used the ZsGreen reporter to follow the cell fate of the ductal compartment to understand whether there was a significant ductal contribution to the hepatocyte pool.

*Prom1<sup>Tet1</sup><sup>WT</sup>* mice readily formed clusters of regenerative ZsGreen+ hepatocytes of between 1 to 156 cells in size after p21/DDC treatment. However, *Prom1<sup>ΔTet1</sup>* mice had a vastly different cluster size distribution with >90% of all ZsGreen+ hepatocyte clusters being either 1 or 2 cells in size. Therefore, ductal cell specific loss of *Tet1*

severely alters the dynamics of bi-potent ductal progenitors in response to liver damage (Figure 3.35b-c).

As loss of *Tet1* leads to smaller regenerative clusters it would be interesting to hypothesize that fewer emergent hepatocytes and as a result ultimately poorer liver regeneration. However, this may not be the case if the smaller clusters were compensated by a larger number of nascent hepatocyte clusters. To deconvolute these two hypotheses and count overall number of ductal derived we carried out volume analysis of thick liver sections to quantify the nascent hepatocytes across the liver. Remarkably, we observed that there was no significant difference in the overall number of traced hepatocytes between *Prom1<sup>ΔTet1</sup>* and *Prom1<sup>Tet1<sup>WT</sup></sup>*. However, *Prom1<sup>ΔTet1</sup>* did show a hugely increased number of traced clusters defined as a continuous group of cells over *Prom1<sup>Tet1<sup>WT</sup></sup>* mice. Considering the similar levels of absolute hepatocytes but the larger number of clusters in the *Prom1<sup>ΔTet1</sup>* it is not surprising that *Prom1<sup>ΔTet1</sup>* have smaller hepatocyte clusters as the same number of hepatocytes are spread amongst many more tracing events (Figure 3.36). This provides interesting insights as it shows that loss of *Tet1* seemingly does not interfere with the differentiation capacity of ductal progenitors but rather the expansion of regenerative clusters. Although, we cannot rule out that the larger *Prom1<sup>Tet1<sup>WT</sup></sup>* clusters are formed from fusion of several tracing events, which doesn't occur in mutant mice. It would be interesting to further analyse the clonal dynamics of the traced hepatocyte populations at several timepoints during damage and recovery to see how *Tet1* truly effects ductal derived hepatocyte generation. In conjunction it would be fascinating to undertake molecular characterisation of the nascent hepatocytes in mice with or without *Tet1*. This would allow us to investigate whether the loss of *Tet1* results in impaired hepatocyte function (see Chapter 4.3.3 for further discussion).

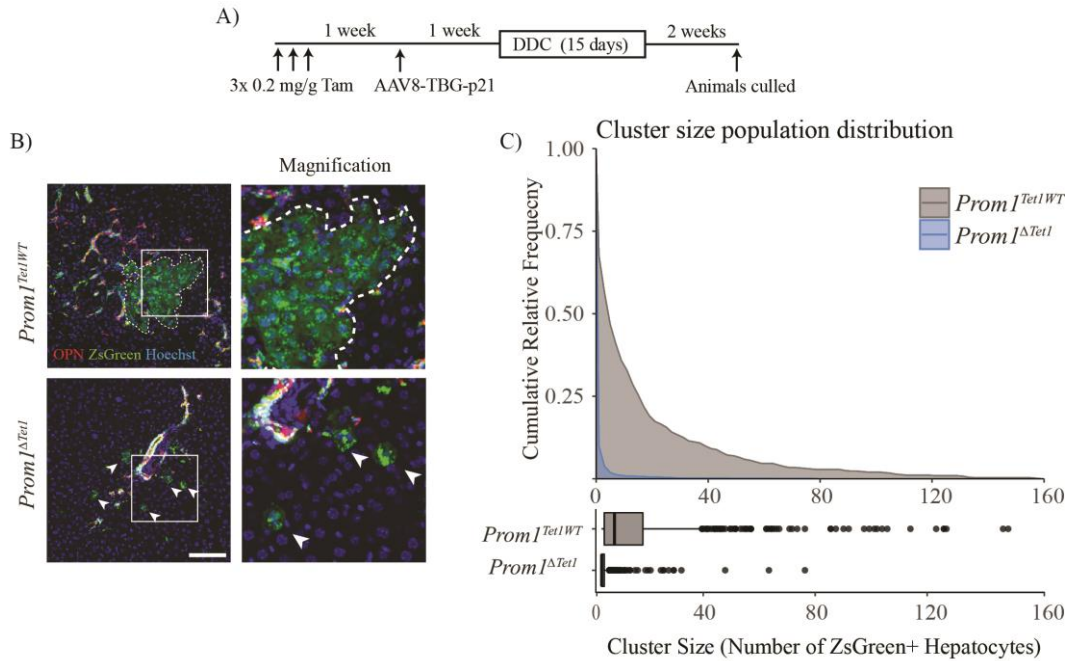


**Figure 3.35 - Loss of *Tet1* results in smaller ductal derived hepatocyte regenerative clusters.** A) Experimental scheme: *Tet1* depletion and ZsGreen lineage tracing were induced by three doses of 0.2 mg/g tamoxifen delivered intraperitoneally. After one week wash out, overexpression of p21 was mediated by tail vein injection of AAV8-TBG-p21 viral vector resulting in hepatocyte specific p21 overexpression. Mice were fed with 3 cycles of 5 day DDC treatments. B) Representative images of 50 μm frozen liver sections stained for ductal marker Osteopontin (OPN-Red), endogenous ZsGreen expression (Green) and nuclei with Hoechst (Blue) showing regenerative hepatocyte clusters in *Prom1<sup>Tet1</sup><sup>WT</sup>* and *Prom1<sup>ΔTet1</sup>* mice. Hepatocytes were identified by morphology and the lack of OPN expression. Scale bar = 100 μm. C) Cumulative relative frequency plots combined with box plots showing median, upper and lower quantiles and the range (dots represent outlier values) of ZsGreen+ hepatocyte cluster size of *Prom1<sup>Tet1</sup><sup>WT</sup>* (n=3) and *Prom1<sup>ΔTet1</sup>* (n=6) mice from three independent experiments \*\*\* = p<0.001, determined by the Kolomogorov-Smirnov test.

In summary, ubiquitous deletion of *Tet1* in EpCAM+ ductal cells inhibited the generation of organoids in 3D culture conditions *in vitro*. However, similar conditional deletion *in vivo* resulted in a collapse in the SI epithelium, before any liver specific analysis could take place. In order to avoid such lethality, we took advantage of a ductal specific *Prom1Cre<sup>ERT2</sup>* combined with a reporter to delete *Tet1* in a specific manner and follow the fate of resulting cells. Mice were then treated with a damage protocol shown to activate *bona fide* bi-potential ductal progenitors and *Tet1* was found to dramatically reduce the size of the ductal pool after damage and severely decrease the size of emergent ductal derived hepatocyte clusters. Taken together, our observations provide significant evidence that *Tet1* plays a pivotal role in the activation and dynamics of bi-potent ductal progenitors.

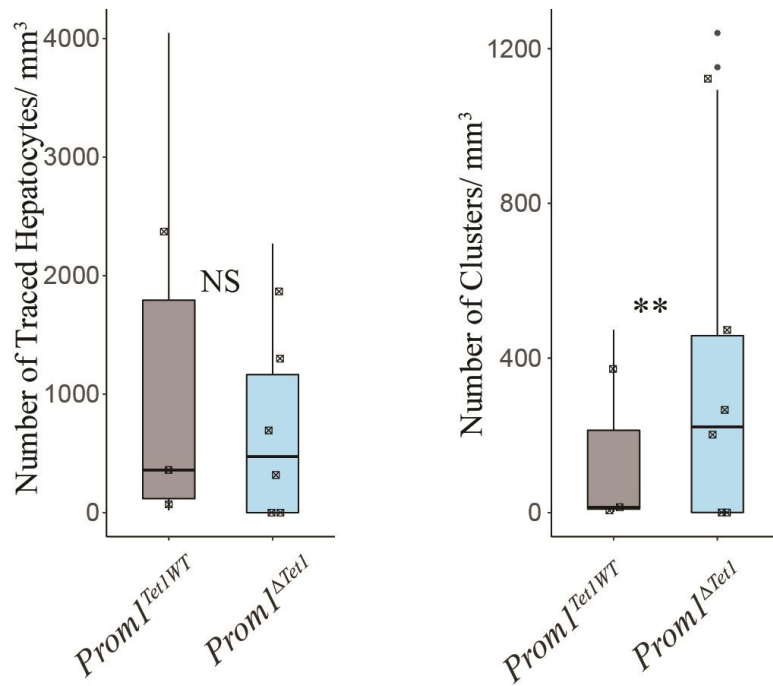


**Figure 3.36 - *Prom1<sup>ΔTet1</sup>* mice have a significantly larger number of hepatocyte clusters but similar number of overall newly derived hepatocytes.** Box plots showing median, upper and lower quantiles and the range (dots represent outlier values) of number of traced hepatocytes (Left) per mm<sup>3</sup> and the number of individual clusters per mm<sup>3</sup> of tissue (Right) of *Prom1<sup>Tet1</sup>WT* (n=3) and *Prom1<sup>ΔTet1</sup>* (n=6) mice from three independent experiments \*\* = p<0.01, determined by the Kolomogorov-Smirnov test.

### **3.3.5 Ductal cells undergo significant global changes in levels of 5mC and 5hmC DNA modification upon liver damage.**

Data presented in chapters 3.3.2 and 3.3.3 suggests that *Tet1* has a crucial role in the activation and proliferation of ductal progenitors in response to DDC induced damage. However, there is little evidence that the catalytic activity of *Tet1* is directly required for ductal progenitor activation *in vivo*. To rule out an indirect role for *Tet1* we first assessed the proliferation and global 5mC and 5hmC dynamics during DDC damage to understand when ductal proliferation is activated and whether there are significant changes to the methylome. To carry this out we treated mice with 0.1% DDC for 0, 2, 3, or 5 days and split the liver for analysis of ductal proliferation and global ductal 5mC and 5hmC levels by immunofluorescence.

We found that significant proliferation in the ductal compartment was triggered after 3 days of DDC damage (T3) that peaks after 5 days (T5) with an average of ~20% ductal proliferation (Figure 3.37a-c). Interestingly, global levels of 5hmC are increased after DDC treatment with a peak at 2 days of DDC treatment (T2) with a ~2.5 fold increase in 5hmC levels as compared to healthy mice (T0). Coupled to this increase in 5hmC levels there was a concomitant a decrease in global 5mC levels in response to DDC damage with lowest global levels of 0.25 fold after 3 days of DDC damage (T3)(Figure 3.37d-e). Crucially, the biggest changes of 5hmC and 5mC were apparent in the early stages of DDC damage and crucially before major proliferation was seen at T5. This is significant as proliferation is a key component of passive demethylation so taken together with a peak in 5hmC levels suggests that active demethylation by the Tet family (the only known family of DNA demethylases) of enzymes could play a crucial role in the activation of ductal proliferation after DDC induced liver damage.

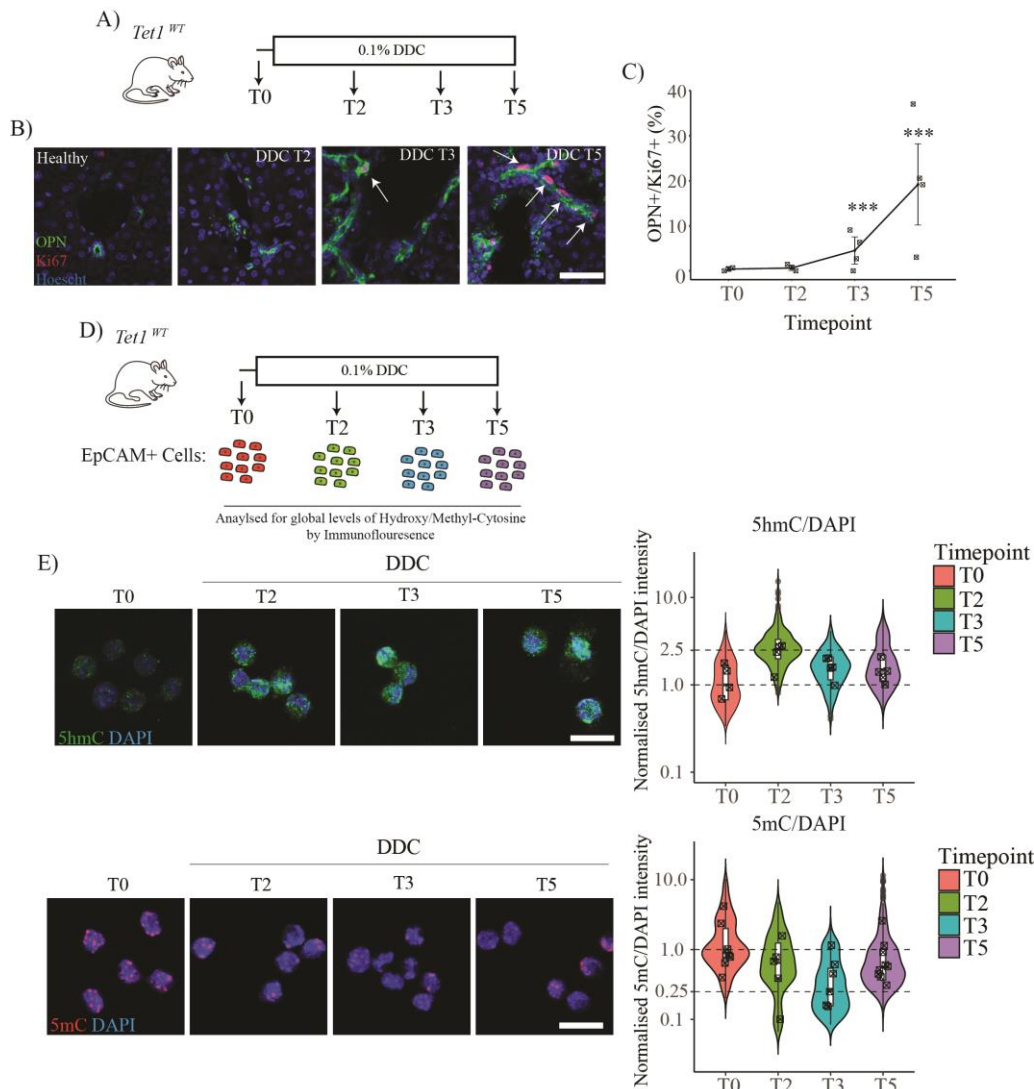


**Figure 3.37 - Global 5mC and 5hmC DNA modification levels are dynamic during DDC induced activation of ductal proliferation.** A) Experimental scheme: *Tet1*<sup>WT</sup> mice were treated with DDC diet for two (T2), three (T3), five days (T5) or left on control diet (T0). B) Representative images of 100µm thick liver sections of T0, T2, T3 and T5 mice stained with proliferation marker Ki67 (Red), ductal marker osteopontin (OPN, Green) and Hoechst (Blue). scale bar = 50 µm. C) Quantification of ductal proliferation (Ki67/OPN) throughout DDC timecourse. Quantification shows the group mean of at least 14 fields of view per liver and error bars represent the 95% confidence interval. Each box represents a different liver (T0 n=3, DDC T2 n=3, DDC T3 n=4, DDC T5 n=4). p values were calculated using ANOVA analysis and corrected by doing the Tukey HSD test: \*\*\*=p<0.001 vs T0. D) Experimental scheme, *Tet1*<sup>WT</sup> mice were treated with DDC diet for two (T2), three (T3), five days (T5) or left on control diet (T0) before EpCAM+ ductal cells were isolated and stained for global 5mC and 5hmC levels. E) Representative images of EpCAM+ cells stained for 5hmC (Green, upper panel) or 5mC (Red, lower panel) and DAPI (Blue). Scale bar = 10 µm. Violin plots shows fold change of 5mC/DAPI (upper panel) or 5hmC/DAPI (lower panel) with each box representing a different biological experiment coming from a single mouse. The fluorescence intensities of 5hmC was initially normalised with DAPI and then, each value was normalised against the median level of the T0 liver (where T0 is centred around 1). Boxplots show the group median, interquartile range and highest and lowest values. p values were calculated by comparing all time points against T0 using the Kruskal-Wallis test: \*\*\*= p<0.001. (Panel E, Aloia *et al.* unpublished).

As *Tet2*, *Tet3* as well as *Tet1* are also able to induce demethylation through oxidation of 5mC to 5hmC the global dynamics seen could be as a result of any of the Tet enzymes individually or a combination of all and not directly as a result of *Tet1* activity. To investigate the role of *Tet1* activity specifically we isolated EpCAM+ ductal cells from *Tet1*<sup>WT</sup> and *Tet1*<sup>Hypo/Hypo</sup> before and after 5 days of DDC damage (T0 and T5) and assessed the gene expression of the key progenitor marker *Lgr5* and *Tet1*, as well as the *Tet1* occupancy and 5hmC levels at the *Lgr5* transcriptional start site (TSS). We found that the expression of both *Tet1* and *Lgr5* was increased upon damage in the EpCAM+ ductal population of *Tet1*<sup>WT</sup> mice (Figure 3.38a). In line with the design of the mouse model the expression of *Tet1* at T0 and T5 was reduced compared to *Tet1*<sup>WT</sup> mice. Remarkably, *Lgr5* expression was also abolished at T5 in *Tet1*<sup>Hypo/Hypo</sup> mice when compared to *Tet1*<sup>WT</sup> mice (Figure 3.38b). Implying that the proliferation defects seen in *Tet1*<sup>Hypo/Hypo</sup> mice may be the result of a failure to activate the progenitor fate through genes such as *Lgr5*.

Furthermore, TET1 was found to bind the TSS of *Lgr5* specifically after DDC damage (T5), which correlated with an increased level of 5hmC at the TSS. Both TET1 occupancy and 5hmC deposition were then abolished in *Tet1*<sup>Hypo/Hypo</sup> mice, suggesting that the *Lgr5* specific 5hmC deposition is exclusive to *Tet1* activity (Figure 3.38b). Together with the expression data, *Tet1* is crucial for the activation of a key progenitor marker *Lgr5* during DDC induced liver damage likely due to deposition of permissive 5hmC marks.

These data do not fully rule out a mechanism of *Tet1* that is independent of the oxidative enzymatic activity. To further explore this hypothesis, it would be interesting to generate mouse models where *Tet1* is ectopically expressed either as a full transcript or as catalytically inactive construct, in a similar fashion to organoid experiments described by Aloia *et al.* (Unpublished). This would allow us to explicitly determine if *Tet1* dependent 5hmC deposition is crucial for ductal progenitor activation *in vivo* as well as *in vitro*.

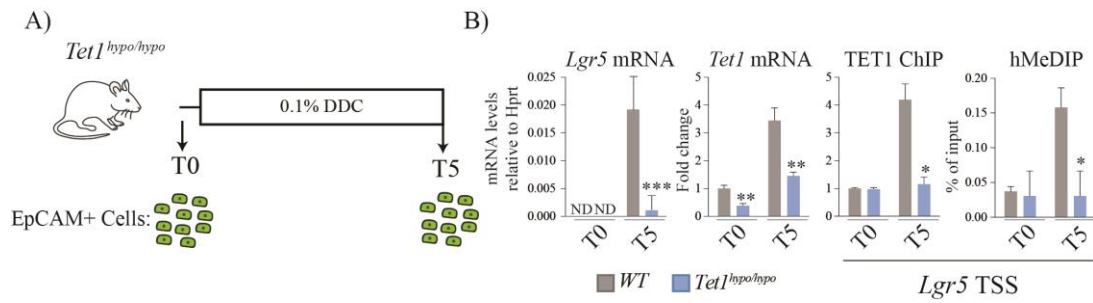


**Figure 3.38 - Reduced expression of *Tet1* abolishes the activation of stem cell marker *Lgr5* after DDC induced liver damage.** A) Experimental scheme: *Tet1<sup>WT</sup>* or *Tet1<sup>hypo/hypo</sup>* mice were treated with DDC for 5 days (T5) or left on control diet (T0) before EpCAM+ cells were isolated from the whole liver. Isolated cells were analysed for gene expression, TET1 occupancy and 5hmC localisation. B) *Lgr5* and *Tet1* mRNA levels (upper panels) and TET1 ChIP and hMeDIP (bottom panels) on *Lgr5* TSS in undamaged and DDC damaged *WT* and *Tet1<sup>hypo/hypo</sup>* mice are shown. Graphs are representative of mean  $\pm$  SD of values obtained from 3 mice. Data is presented as relative to *Hprt* (mRNA) or % of input (ChIP and hMeDIP). p values have been obtained by comparison to the corresponding WT value in undamaged or DDC by performing two-sided students t-test statistical analyses: \* =  $p < 0.05$ ; \*\* =  $p < 0.01$ ; \*\*\* =  $p < 0.001$ . (Aloia *et al.* unpublished).

### 3.4 Optical tissue clearing can provide insights into the proliferative heterogeneity of the ductal compartment.

Further analysis of the proliferative dynamics of *Tet1<sup>WT</sup>* mice after acute DDC damage (originally discussed in section 3.3.2) showed evidence of two populations of ductal cells with different proliferative potential. In response to acute DDC damage the majority of portal regions had a proliferative fraction of ~10% (blue) or ~40% (green) with an overall group median of ~20% (Figure 3.39a-b). The bimodal relationship suggests the existence of different populations within the ductal compartment, which may be spatially defined within the ductal tree.

The biliary ductal tree is a massively divergent structure with a larger central trunk and branching lumen extending to the periphery of the tissue. As result we can consider several models of regeneration that would create such a system that requires at least two populations of cells, such as tip driven branching morphogenesis (as has been described during the development of several tissues including the kidney and mammary gland (Hannezo *et al.*, 2017)), trunk driven regeneration or a combination of both (Figure 3.40).

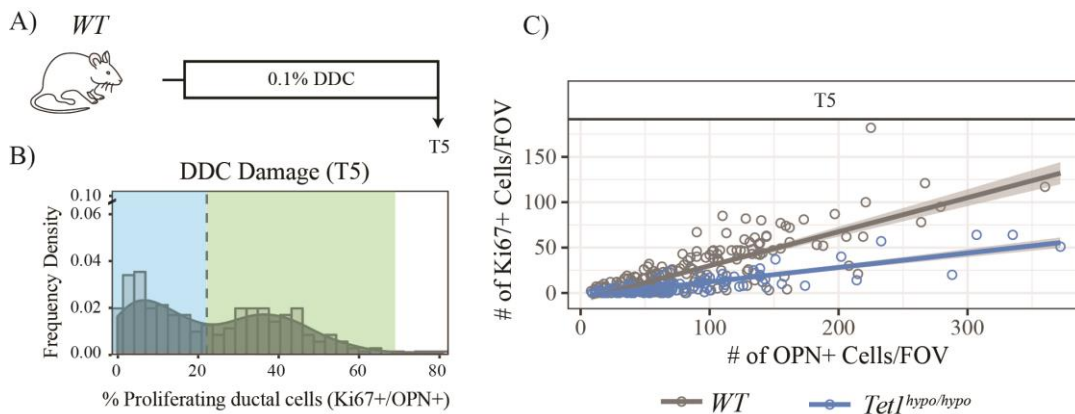


**Figure 3.39 - *Tet1<sup>WT</sup>* mice showed two proliferative responses in the ductal compartment in after acute DDC damage.** A) Experimental scheme: *Tet1<sup>WT</sup>* mice were treated with DDC for five days before ductal proliferation was assessed by immunostaining. B) Histogram showing the population distribution of proliferating ductal cells (OPN<sup>+</sup>/Ki67<sup>+</sup>) by plotting frequency density of counts across the sample range (bar) and the kernel density estimate (line). Dashed lines show median values, lower population and higher population marked in blue and green respectively. C) Scatter plot describing absolute number of Ki67<sup>+</sup> cells and OPN<sup>+</sup> cells of each FOV of *Tet1<sup>WT</sup>* and *Tet1<sup>Hypo/Hypo</sup>* mice. Line of best was calculated, and shaded region represents the 95% confidence interval. B-C) Graphs are representative of values obtained from 253 FOV for *Tet1<sup>WT</sup>* (n=7) and 169 FOV for *Tet1<sup>hypo/hypo</sup>* (n=6).

To further explore these hypotheses and understand the localisation of the bimodal distribution of the ductal compartment after damage we plotted the number of proliferative ductal cells in each portal region against the size of the ductal compartment

in that FOV from *Tet1<sup>WT</sup>* and *Tet1<sup>Hypo/Hypo</sup>*. We found that there was a positive relationship between size of proliferative fraction and size of the ductal compartment in each FOV of *Tet1<sup>WT</sup>* mice. Interestingly, *Tet1<sup>Hypo/Hypo</sup>* showed a lesser relationship of proliferation against size likely reflecting the overall lower proliferative response after damage as described in Chapter 3.4 (Figure 3.39c). As a result of the larger proliferative fractions being restricted to larger ductal populations it would be interesting to hypothesise that the highest level of proliferation is localised to the larger ductal trunk.

However, the data was derived from imaging 30-40  $\mu\text{m}$  of tissue within a 100  $\mu\text{m}$  section, resulting in the FOVs being made up of small cross sections of portal regions rather than a representation of the overall ductal structure. Therefore, the size of the ductal population in each FOV is dependent on orientation of the cross-section rather than the localisation within the ductal tree.

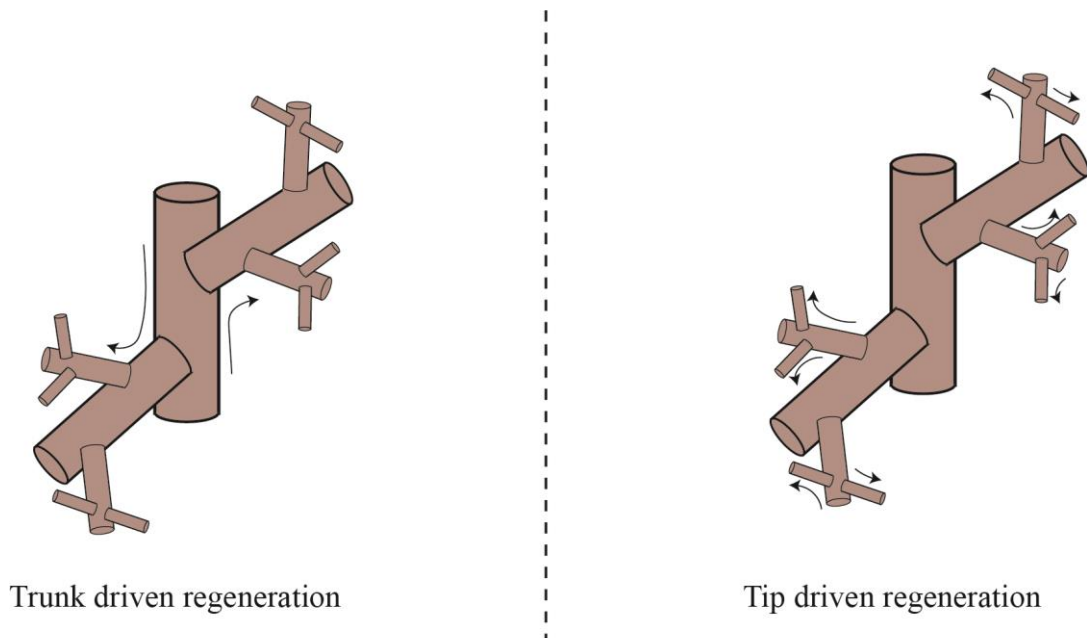


**Figure 3.40 - Models of ductal tree regeneration in response to DDC damage.** Schematics of trunk driven (left) and tip driven (right) models of ductal tree regeneration with arrows representing the direction of growth.

In order to properly understand if the proliferative dynamics are spatially localised within the ductal tree optical clarity of thick liver sections would be required to resolve the whole or a large volume of the ductal tree. We decided to investigate different tissue clearing techniques that would allow enhanced ductal imaging. Healthy mice were euthanised, and heparinised saline was pumped through the liver's vasculature prior to dissection to help remove excess blood. After perfusion, livers were

fixed overnight and sectioned at several thicknesses between 100  $\mu\text{m}$  and 800  $\mu\text{m}$  before being immunostained and cleared by SeeDB, CUBIC with either reagent 1 or 1a, or the standard glycerol gradient used in previous imaging experiments.

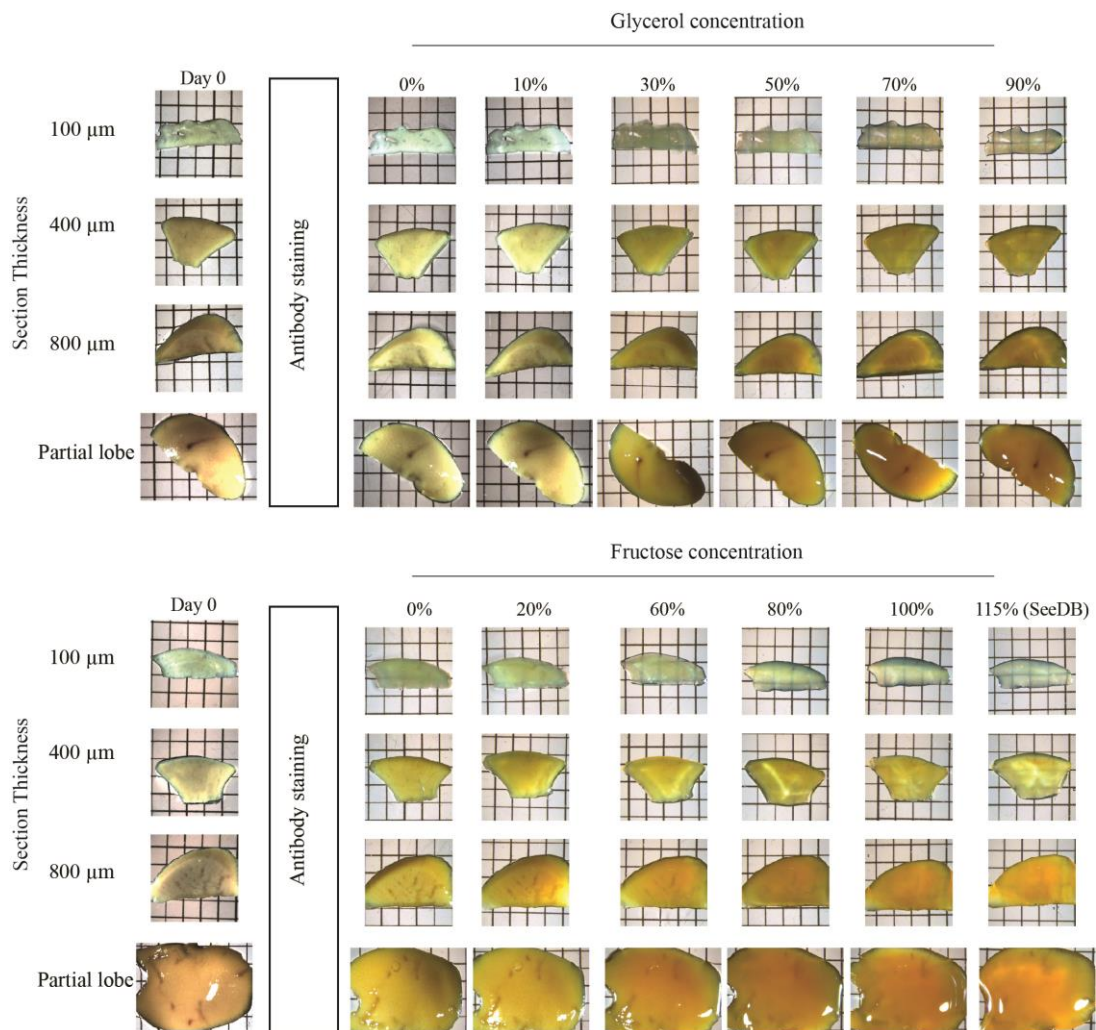


**Figure 3.41 - Tissue clearing performance of refractive index matching by Glycerol gradients or SeeDB.**

Stereoscope images of liver sections of between 100 $\mu\text{m}$  to 800 $\mu\text{m}$  in thickness as well as an unsectioned partial lobe throughout staining protocol using either a Glycerol gradient (A) or SeeDB (B). Images are representative of 2 independent experiments. Each grid square has a length of 1 mm.

SeeDB and glycerol gradients rely on refractive index matching as the primary source of optical clearing. However, in both cases only slight clarity was seen in 100  $\mu\text{m}$  thick sections. Thicker liver sections showed little affect from either technique, this is likely due to the fact that liver tissue is highly pigmented and requires more active clearing to achieve enhanced optical clearing (Figure 3.41). CUBIC tissue clearing is reliant on incubating tissue in two solutions. The first of which (reagent 1 or 1a) is made up of a high concentration of detergent and a chelating agent that remove tissue pigment. A second solution (Reagent 2, R2) is then used which is made up of urea and sucrose that facilitates refractive index matching. The combination of both reagents

showed massive optical clearing of liver sections of up 800  $\mu\text{m}$  in thickness and was even able to partially clear an unsectioned lobe of the liver. Both reagent 1a and 1 had similar clearing capacity so all further experiments were carried out with reagent 1a as the lower concentration of detergent will likely allow better epitope preservation (Figure 3.42).

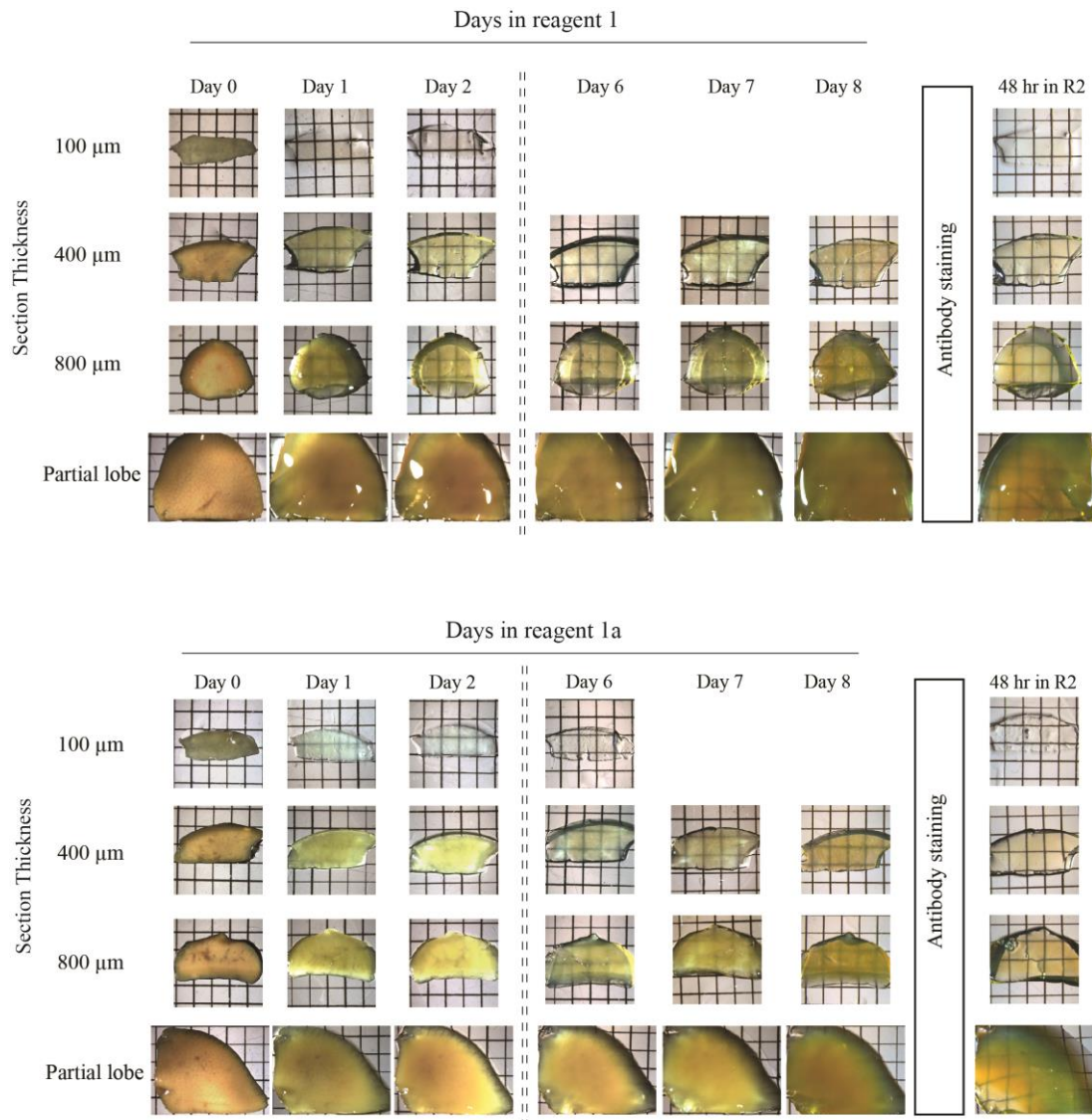


**Figure 3.42 - Tissue clearing performance of CUBIC reagents 1 or 1a on liver sections.** Stereoscope images of liver sections of between 100 $\mu\text{m}$  to 800 $\mu\text{m}$  in thickness as well as an unsectioned partial lobe throughout the CUBIC staining protocol using either reagent 1 (A) or 1a (B). Images are representative of 3 independent experiments. Each grid square has a length of 1 mm.

To confirm this, 100  $\mu\text{m}$  liver sections were cleared with CUBIC and compared to the original glycerol treatment after imaging with confocal microscopy. CUBIC cleared sections allowed for imaging throughout the whole 100 $\mu\text{m}$  section maintaining cellular resolution along the z-axis. Glycerol treated samples were limited to only  $\sim 30$   $\mu\text{m}$  resolution in the z-axis. The enhanced imaging capacity of CUBIC treated samples

allowed for a large ductal structure to be clearly resolved. Crucially, it was sufficiently resolved to identify key features such as branch points at ductal trunks (Figure 3.43A, Asterix and Arrow). Therefore, CUBIC tissue clearing represents an enhanced strategy that can enable future study into the proliferative dynamics of the ductal tree on the scale of whole organ (Figure 3.43).

In summary, we found that there was a bimodal distribution of proliferation in the ductal compartment upon acute DDC damage. We then developed a CUBIC imaging strategy that will allow us to better understand how proliferation is spatially distributed through the ductal tree in future studies. However, it is important to note that it may be the case that there is no specific spatial organisation of the ductal compartment and rather the bimodal distribution is defined by unique molecular characteristics. It would be interesting to carry out gene expression profiling of the ductal population after damage to understand if there are distinct molecular populations that may explain the proliferative dynamics.

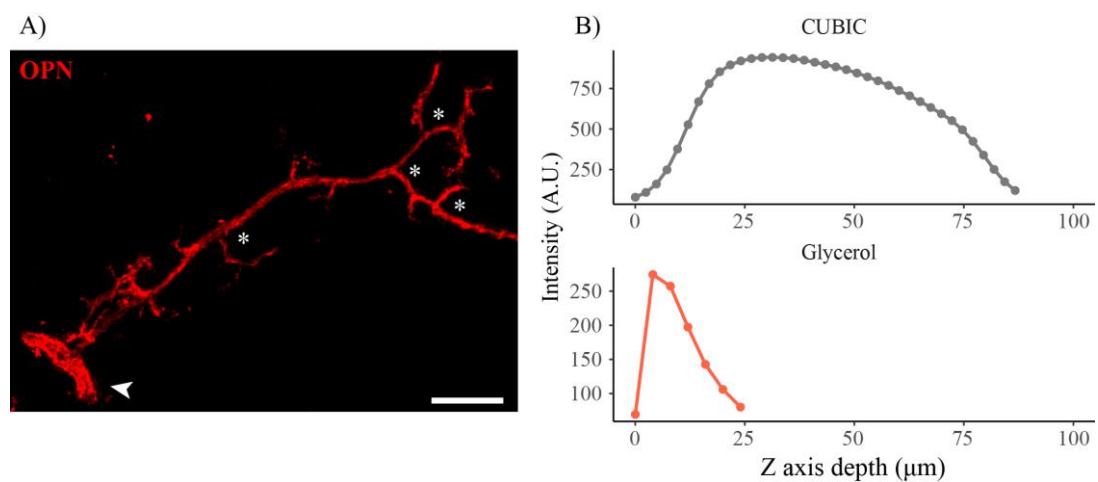


**Figure 3.43 - CUBIC clearing allows significantly increased imaging depth and reveals large ductal structures.** A) Representative max projection of a CUBIC cleared 100 μm liver section stained for osteopontin (OPN). Arrow shows ductal trunk and \* denotes branch points. Scale bar = 100 μm. B) Representative plots of fluorescent intensity throughout a 100 μm thick liver section cleared with glycerol or CUBIC.

## 4. Discussion

### 4.1 Organoids as a model of ductal cell-driven liver regeneration

In this work we have taken advantage of organoid models first characterised by Huch and colleagues (2013) to model the bi-potent ductal progenitors which have been shown to contribute to liver regeneration under certain conditions (Huch, Dorrell, *et al.*, 2013). We have identified *Arid1a* and *Tet1* as potential candidates for further analysis by performing siRNA knockdown and gene expression analysis either in established organoid lines or during organoid formation from mature ductal cells (Figures 3.2, 3.3 and 3.4). However, we make the assumption throughout these experiments that organoid formation will faithfully reproduce the molecular changes which occur *in vivo* during the transition of a ductal cell to a bi-potent ductal progenitor.

Given this assumption, it is essential to discuss the how well organoids truly model ductal progenitors. Therefore, we must benchmark the model against the true *in vivo* counterparts. In the first instance, it would be interesting to isolate RNA from the ductal compartment of damaged livers at several timepoints and compare the gene expression changes *in vivo* to those seen during organoid formation in order to further validate organoid formation as a model for the emergence of bi-potent ductal progenitors following liver damage. Such studies carried out by our group, currently in press, reveal that remarkably similar changes in gene expression occur *in vitro* during the transition from mature ductal cells to organoids to those changes seen in ductal cells *in vivo* during the first five days following DDC-induced damage (Aloia *et al.*, in press). Furthermore, the same study showed that ductal cells isolated from a liver after five days of DDC-induced damage generate significantly more organoids than ductal cells isolated from undamaged livers, and we therefore conclude that DDC-induced damage enhances the organoid-forming potential of the ductal compartment. These data support our original assumption and further validate organoid formation as an accurate model of the intrinsic molecular characteristics of bi-potent ductal progenitors.

Despite the benchmarking of liver organoids, it is important note that as models they are a simplification of the true nature of liver regeneration. Therefore, we must validate any observations derived from organoids in an *in vivo* model of liver regeneration before robust conclusions can be made, in a similar manner to those

carried out here to investigate the role of *Tet1* (Chapters 3.3.2, 3.3.3 and 3.3.4). However, the true power of organoids as hypothesis generating tools should not be overlooked. Organoids are amenable to high throughput studies that can help narrow down the field of study before candidates are taken forward and validated using *in vivo* models, which may better represent the process of liver regeneration, but are prohibitively expensive and time intensive for large scale studies. Therefore, work presented here forms a powerful framework for future studies where genes are selected for study by taking advantage of organoids before further validation.

However, there is a pressing limitation of this framework, the ductal cells are cultured in isolation from the other cell types usually found in the liver during organoid formation. As a result, we can only use liver organoids to study cell characteristics intrinsic to the ductal cell. As liver regeneration is a carefully orchestrated response of several different cell types liver organoids are insufficient to model how these processes are regulated. One possible solution to this would be to generate more complex co-culture systems that incorporate all the other cell types resident to the liver. However, creating such a system may prove technically and practically difficult. For instance, it wouldn't be surprising that the different cell populations require different culture conditions that were inherently incompatible. Furthermore, even if such a culture system was technically possible there would be no guarantee the cells would organise and interact in a similar manner to that seen *in vivo*. In any case, the hypothetical model could allow the investigation of the role of extrinsic signalling pathways during ductal-driven liver regeneration.

Despite the obvious technical difficulty of creating co-culture systems there has been success in the generation of culture systems of single cell types that reflect the heterogeneous nature of liver regeneration. Here, we have used liver organoids of ductal origin to specifically assess the role of our candidate genes in ductal-driven regeneration. However, liver organoids of hepatocyte origin have also recently been described and it would be interesting to investigate whether common molecular pathways regulate liver organoid formation independent of the cell of origin; expanding our analyses beyond the use of organoids of ductal origin may provide interesting insights into common or ductal/hepatocyte-specific molecular changes occurring upon organoid generation (Hu *et al.*, 2018; Peng *et al.*, 2018). Furthermore, organoid cultures derived from adult stem cell populations have been described in numerous other tissue

types, including, but not limited to; the colon, pancreas, stomach, lung and prostate (Sato *et al.*, 2009; Barker *et al.*, 2010; Jung *et al.*, 2011; Huch, Bonfanti, *et al.*, 2013; Karthaus *et al.*, 2014; Barkauskas *et al.*, 2017). Therefore, experiments and analyses similar to those described here could be extended to organs other than the liver to investigate the gene expression changes occurring upon organoid formation in an even broader sense. It will be important, however, to define the regenerative process being investigated for each tissue in order to integrate the data in a meaningful way and potentially reveal exciting and broad insights into the regulation of adult stem cell fate decisions.

## 4.2 The role of *Arid1a* in bi-potent ductal progenitor maintenance and differentiation.

### 4.2.1 *Arid1a* gene dosage regulates bi-potent ductal progenitor proliferation.

We found that reduction of *Arid1a* expression either by siRNA knockdown, genetic ablation of one isoform or by heterozygous knock-out of all isoforms resulted in increased efficiency of organoid formation from liver ductal cells (Figures 3.4, 3.6 and 3.12). This is perhaps not surprising, as *Arid1a* has been described as a prominent tumour suppressor in several different cancer types (Wang *et al.*, 2011; Biankin *et al.*, 2012; Muzny *et al.*, 2012; Chan-on *et al.*, 2013). Furthermore, *Arid1a* has recently been directly implicated in the positive regulation of E2F proteins, which usually act as repressors of cellular proliferation (Sun *et al.*, 2016). Therefore, it would be interesting to further probe this phenotype to see if the increased efficiency of organoid formation is indicative of the first stages of cellular transformation into a tumour-like state. Recent work by Shen and colleagues has shown that *Arid1a* co-operates with the DNA damage regulator, ATR, and is essential for the resolution of double strand breaks (Shen *et al.*, 2015). It would therefore be interesting to investigate whether the increase in efficiency of organoid formation is accompanied by an increase in chromosome instability and DNA damage. This could be performed readily by analysing the karyotype of late passage organoid lines deficient in activity of *Arid1a* to directly detect any significant aneuploidy which may have arisen as a result. Whole genome sequencing of a clonal population at multiple timepoints would provide higher resolution detection of genetic changes to further understand if deficiency in *Arid1a* results in the acquisition of further mutations, and whether these might reflect the evolution of *Arid1a*-deficient tumours. Further experiments might consider the role of DNA damage by investigating whether DNA damage is increased in *Arid1a*-deficient organoid lines through assessment of the levels of the histone variant  $\gamma$ H2AX, a prominent marker of DNA damage (Mah, El-Osta and Karagiannis, 2010). The results of such studies would provide insights into whether organoid cultures could be used to accurately model tumour evolution following the loss of *Arid1a* activity.

The increased efficiency of organoid formation could be due to increased cellular survival, increased proliferation or a combination of both. Recent evidence would suggest that deficiency in *Arid1a* would result in increased proliferation (Sun *et al.*, 2016), however, the data presented here do not allow us to determine the underlying

cause(s) of the increase in efficiency of organoid formation. Therefore, further analysis of the rate of proliferation and survival of *Arid1a*-deficient organoids is required. The rate of proliferation could be determined by quantification of the proportion of Ki67<sup>+</sup> cells during organoid formation. Cell death could be quantified during organoid formation to assess whether increased cell survival contributes to the increase in efficiency of organoid formation observed in *Arid1a*-deficient organoids. Taken together, such studies would increase our understanding of the precise role of *Arid1a* during organoid formation and maintenance.

One final, interesting observation is that total genetic ablation of *Arid1a* does not cause an increase in efficiency of organoid formation when compared to normal, wild type efficiency. This result conflicts with a previous study, where ubiquitous and total deletion of *Arid1a* results in significantly increased proliferation *in vivo* following liver damage (Sun *et al.*, 2016). We may reconcile our data with the previously published literature in several ways. For instance, we have modulated *Arid1a* in an isolated ductal organoid population only, whilst the previous study modulated *Arid1a* in total liver or in hepatocytes, so it is possible that the precise phenotype arising upon loss of *Arid1a* may be cell-type specific. It would therefore be interesting to study loss of *Arid1a* in the recently described organoids of hepatocyte origin to attempt to address this question. Furthermore, Sun and colleagues focus on the proliferation of the hepatocyte compartment and do not investigate the proliferative dynamics of the ductal compartment in their study, and thus the possibility remains that there is a ductal phenotype *in vivo* which is similar to that observed in our *Arid1a*-deficient organoid models, as their study provides no assessment of ductal phenotypes. In contrast, as organoid formation occurs in isolation from extrinsic signalling, the phenotype we observe in *Arid1a*-deficient organoids may be an artefact of the system which does not occur *in vivo*. However, our data strongly imply that gene dosage of *Arid1a* is crucial for the regulation of organoid formation and maintenance, which itself has been further validated as a model for the generation of bi-potent ductal progenitors through our unpublished analyses of gene expression changes (Aloia *et al.*, Unpublished). It has been shown that embryonic, neural and cardiac development take advantage of unique compositions of the BAF complex, of which *Arid1a* is a component, in order to facilitate cell fate transitions. Therefore, we hypothesise that differing gene dosage of

*Arid1a* may result in different BAF complex compositions that result in our observed phenotypes (Ho and Crabtree, 2010), discussed in greater detail below.

#### **4.2.2 *Arid1a* regulates could cell fate transitions through modulating hallmarks of ductal progenitor state**

Our data suggest that *Arid1a* plays a dual role in the maintenance of liver organoid culture. *Arid1a* deficiency results in reduced expression of both ductal progenitor markers as well as functional markers of mature hepatocytes (Figures 3.7, 3.8, 3.9, 3.13 and 3.14). Interestingly, similar data was presented by Sun and colleagues, where their model of liver-specific *Arid1a* deletion resulted in reduced expression of the p450 family of cytochromes both during homeostasis and following liver damage (Sun *et al.*, 2016). Taken together, the data suggest that *Arid1a* is crucial for stable lineage commitment to either a ductal progenitor like state or, upon differentiation, a mature hepatocyte fate. Furthermore, it is important to note that several models of liver damage, such as treatment with CCl<sub>4</sub>, rely on production of metabolites by the cytochrome p450 family. As a result, any assessment of the level of regeneration observed in the absence of *Arid1a* may have as a confounding factor a lesser amount of overall liver damage, as *Arid1a*-deficient hepatocytes may lack the metabolic machinery to induce full toxicity.

The presence of ARID1A, ARID1B or ARID2 in the BAF complex is mutually exclusive. Therefore, in the absence of ARID1A either ARID1B or ARID2 may take its place, a switch which may lead to differential modulation of a unique set of genes (Tang, Nogales and Ciferri, 2010). Interestingly, it has been shown that ARID1B represses Wnt pathway signalling in a BRG1-dependent manner (Vasileiou *et al.*, 2015). Taken together with data presented here, it is possible that ARID1B takes the place of ARID1A in the BAF complex of *Arid1a*-deficient organoids, leading to the reduced expression of progenitor markers and the Wnt target genes *Lgr5* and *Axin2* as observed. To further validate this hypothesis, assessing promoter occupancy by ARID1B in *Arid1a*-deficient organoids would allow a comparison with promoter occupancy by ARID1A and ARID1B in wild type organoids to determine if ARID1B can directly replace ARID1A at the promoter level (Figure 3.15). Such studies would provide insight into how *Arid1a* directs stable lineage commitment in hepatocytes or ductal cells.

As mentioned above, embryonic, neural and to some extent cardiac development is dictated by the orchestrated inclusion of mutually exclusive components of the BAF complex to create several transient, specialised and distinct complex compositions (Ho and Crabtree, 2010). *Arid1a* has here proved crucial for the stable acquisition of markers of bi-potent ductal progenitor and hepatocyte fates (Figures 3.7, 3.8, 3.9, 3.13 and 3.14) and, taken together with data from others, *Arid1a* itself may be a crucial component of the BAF complex for those fates (Sun *et al.*, 2016). However, our data do not exclude the contribution of other components being included in a regulated manner as ductal cells acquire a progenitor fate *in vitro* or during liver damage. Therefore, it would be interesting to determine the composition of the BAF complex in parallel during organoid formation *in vitro* and in the ductular reaction *in vivo* during liver damage. This could be achieved by immunoprecipitation (IP) of an invariant structural component of the BAF complex at several timepoints during liver damage and/or organoid formation, followed by determination of the composition of the complex by proteomics techniques, such as mass spectrometry, in a manner similar to that described by Ho and colleagues (Ho *et al.*, 2009b). Furthermore, using a similar experimental design, analysis of chromatin IP rather than IP of BAF-associated proteins should provide insight into how the genetic targets of the BAF complex change during liver damage and/or organoid formation. Finally, by integrating proteomics, chromatin occupancy and gene expression changes during said processes, specific gene expression changes could be associated with specific complex compositions and so provide a thorough readout on the dynamics of the complex and how these are associated with the dynamics of the acquisition and maintenance of specific cell fates.

#### **4.2.3 A model for the role of *Arid1a* in bi-potent ductal progenitor maintenance and differentiation**

To summarise, the data demonstrate that dosage of *Arid1a* is crucial for stable lineage commitment *in vitro* showing altered expression of markers of both bi-potent ductal progenitor and hepatocyte fates (Figures 3.7, 3.8, 3.9, 3.13 and 3.14). In conjunction with the reduction in stable cellular identity, there was a concomitant increase in organoid formation, which may be as a result of the prominent tumour suppressor activity of *Arid1a* (Figures 3.4, 3.6 and 3.12). Remarkably, organoid formation and progenitor identity, but not differentiation capacity, was restored in *Arid1a*-null organoids, suggesting an *Arid1a*-independent mechanism for maintaining progenitor

marker expression (Figures 3.12 and 4.1). However, it is important to note that in order to ensure that the cellular dynamics we have observed truly reflect *bona fide* bi-potent ductal progenitors we need to model *Arid1a* deletion in an *in vivo* system. We attempted to carry this out by driving *Arid1a* deletion by expression of progenitor marker *Lgr5* in the context of DDC induced liver damage. This model proved insufficient to induce *Arid1a* deletion in the ductal progenitor compartment, as a result, further study is required to generate a viable *in vivo* model and ultimately validate the data we have observed using our liver organoid model.

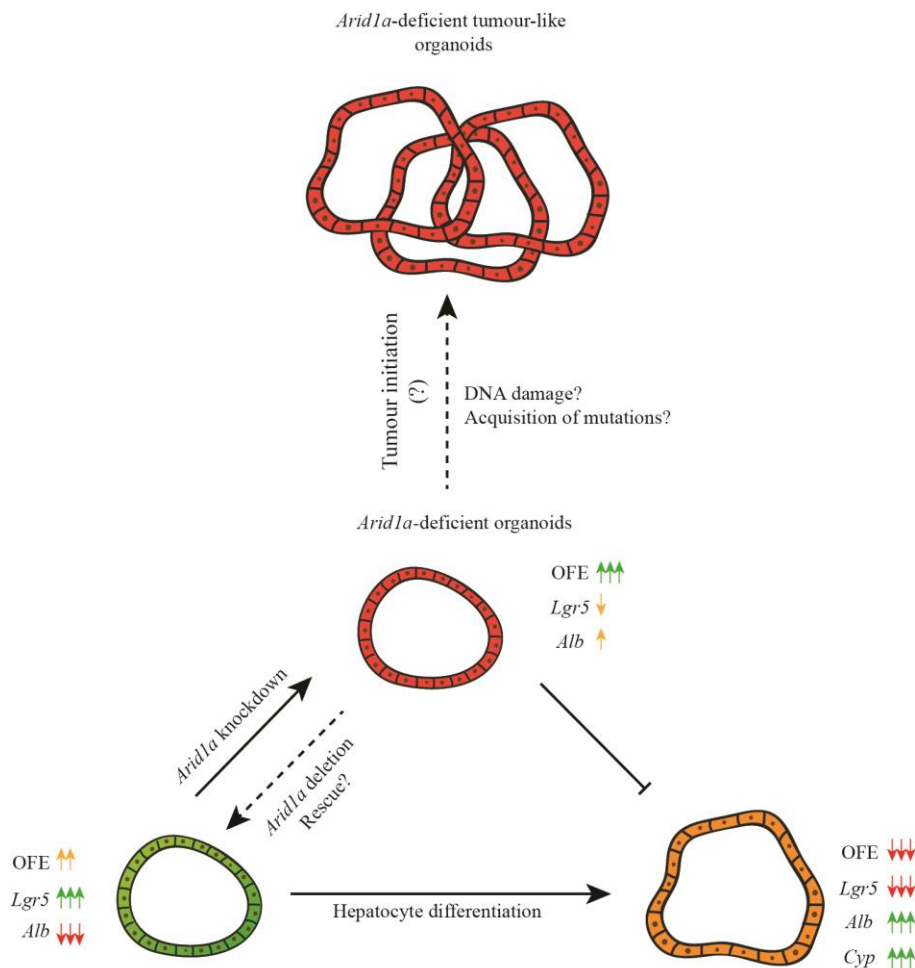


**Figure 4.1 – Working model for the regulation of bi-potent ductal progenitors by *Arid1a* in organoid culture.** *Arid1a*-deficient organoids have an increased efficiency of organoid formation (OFE) but lose cellular identity and express markers of both hepatocyte and progenitor fate, potentially being unable to commit to either fate. We hypothesise that long term passaging may result in tumour initiation through increased DNA damage and increased rate of acquisition of further mutations.

#### 4.3 The role of *Tet1* in ductal cell-driven liver regeneration.

##### **4.3.1 Global reduction of *Tet1* levels results in impaired activation of ductal cell-driven regeneration following acute damage**

In contrast to several previously described animal models of *Tet1* deletion, our hypomorphic model did not show significant post-natal lethality or a significant, overt homeostatic phenotype (Figures 3.18 and 3.19), suggesting that the reduced level of *Tet1* expression in this model is permissive for normal development and adult viability (Dawlaty *et al.*, 2011; Kim *et al.*, 2016). However, *Tet1* hypomorphic mice show impaired activation of ductal cell proliferation at the peak of the damage response following DDC-induced liver damage, resulting in a smaller ductal compartment upon recovery (Figures 3.22 and 3.23). Therefore, although levels of *Tet1* expression in this model are sufficient for normal homeostatic function, levels are insufficient to direct normal ductal cell-driven liver regeneration. In line with this, organoid formation from mature ductal cells is impaired in the presence of hypomorphic levels or following full genetic ablation of *Tet1* (Figures 3.20 and 3.28). Taken together, the data support a requirement for TET1 activity both *in vivo* and *in vitro* during the acquisition of a proliferative, bi-potent ductal progenitor fate.

TET1-driven active demethylation has been implicated in the generation of pluripotent and totipotent cell populations *in vivo* during embryonic development and *in vitro* during somatic reprogramming (Costa *et al.*, 2013; Hackett *et al.*, 2013). Therefore, a similar mechanism of epigenetic reprogramming may underlie the transition of a mature ductal cell to a bi-potent ductal progenitor. Additional data have demonstrated that a catalytically active variant of TET1 is required for rescue of the *Tet1*-deficient phenotype in organoid culture, implicating active demethylation in the acquisition of bi-potent ductal progenitor fate (Aloia *et al.* Unpublished). However, it is currently unknown as to whether TET1 catalytic activity is required *in vivo* as part of the ductal cell-driven regenerative response in the liver. It has been shown that Vitamin C is able to enhance the oxidative activity of TET1 (Minor *et al.*, 2013), providing a way of increasing TET1 activity and assessing its effect on bi-potent ductal progenitor fate. If TET1 activity is essential for ductal cell-driven regeneration, it should be sensitive to modulation by Vitamin C treatment, whereas we would expect that *Tet1* mutants would be refractory to treatment. A caveat to this methodology, however, is

that Vitamin C treatment is not specific for the modulation of TET1 activity, leaving genetic rescue of TET1 activity *in vivo* as the gold standard in terms of experimental approaches.

Although our hypomorphic model has the advantage of being permissive for normal development, in contrast to previously described null mutant models, there are still limitations of the model that should be borne in mind. For example, *Tet1* deficiency in this model is global, with no spatial or temporal control of *Tet1* deletion, resulting in constitutive *Tet1* deficiency in all tissue types. Therefore, although it is reasonable to assume that the ductal cell phenotype results from the reduction of *Tet1* within that compartment, confounding effects resulting from *Tet1* deficiency in other cellular compartments cannot be ruled out. To address this limitation, deletion of *Tet1* could be localised to the ductal compartment by using a conditional, floxed allele in combination with ductal cell-specific expression of Cre. The *Tet1<sup>flx</sup>/Prom1Cre<sup>ERT2</sup>* model generated and described herein could be used to provide such specific deletion of *Tet1* in the ductal epithelium. If impaired ductal cell proliferation and regeneration were to be observed in this model following acute DDC-induced damage also, then we could conclude with much greater certainty that this phenotype is intrinsic to the ductal compartment. The conditional allele would lend itself to further combinations with other tissue-specific Cre drivers to assess the role of *Tet1* in other cellular compartments, such as in hepatocytes, during ductal cell-driven regeneration.

#### **4.3.2 *Tet1* is crucial for the resolution of fibrosis following chronic liver damage**

When challenged with chronic liver damage induced by 8 repeated doses of DDC, it was observed that hypomorphic mice had significantly increased fibrotic collagen deposition when compared to wild type mice (Figure 3.27). Interestingly, it has been shown that fibrosis in the liver as a result of chronic damage can be attenuated by transplantation of isolated *Lgr5<sup>+</sup>* progenitor cells, and that, conversely, upon knock-down of *Lgr5* fibrosis is more extreme (Lin *et al.*, 2017), directly implicating bi-potent ductal progenitors in the resolution of fibrosis following chronic injury. Furthermore, as *Tet1* is crucial for the generation of *Lgr5<sup>+</sup>* organoids *in vitro* and *Lgr5* expression was reduced in hypomorphic mice following acute DDC-induced damage (Figures 3.20, 3.28 and 3.38), I hypothesise that the increased fibrosis observed in the

hypomorphic mice results from the impaired generation of *Lgr5*<sup>+</sup> progenitors in these animals.

Only a single recovery time point was assessed in our hypomorphic mice (Figure 3.27) and therefore, it is not possible to assess the dynamics of fibrosis. For instance, we are unable to understand whether the observed increase in fibrosis results from reduced fibrotic resolution or gradual increase in collagen deposition over time. Each possibility has subtle but distinct biological meaning; either the hypomorphic mice are unable to repair the damage, resulting in slower fibrotic resolution, or liver function remains impaired, resulting in continuing collagen deposition. To determine fibrotic dynamics and address this question, it will be necessary to analyse several time points from the onset of recovery to, and beyond, the recovery time point analysed here.

As above, it is important for us to consider the limitations imposed by the global nature of *Tet1* reduction in a similar fashion to our acute DDC-induced damage model. With chronic damage, the global nature of *Tet1* reduction is potentially more problematic when interpreting the data, as fibrosis itself is regulated by the activity of the stellate cells in the space of Disse (Mederacke *et al.*, 2013). The potential effect of reduced levels of *Tet1* in these cells upon fibrosis has not been described, and we cannot rule out that it will affect the level of fibrosis independently from the reduction of *Tet1* in the ductal compartment. Again, an elegant solution would be to use the *Tet1*<sup>flx</sup>/*Prom1**Cre*<sup>ERT2</sup> model to localise deletion of *Tet1* to the ductal compartment, and, in combination with chronic DDC treatment, to deconvolute the contribution of different cell types to the increased fibrosis observed.

### **4.3.3 Epithelial cell-specific genetic ablation of Tet1 inhibits normal ductal cell-derived hepatocyte generation.**

By taking advantage of a model of liver damage that induces significant ductal cell contribution to the hepatocyte compartment, first characterised by Raven and colleagues (Raven *et al.*, 2017), in combination with our model of ductal cell-specific *Tet1* deletion and lineage tracing, it was possible to assess the role of *Tet1* in *bona fide* bi-potent ductal progenitor-driven regeneration. Ductal cell-specific deletion of *Tet1* results in the generation of significantly smaller regenerative hepatocyte clusters (Figure 3.35). However, despite the smaller clusters, *Tet1* deletion did not result in a significantly reduced overall number of ductal cell-derived hepatocytes, with the

significantly increased number of discrete clusters in *Tet1* mutants explaining the discrepancy (Figure 3.36). Whilst these data suggest that the process of ductal cell-to-hepatocyte differentiation is not affected by *Tet1* deletion, but rather the dynamics of hepatocyte generation are altered, we cannot rule out that the nascent, ductal cell-derived hepatocytes are not fully functional in the absence of *Tet1*. To determine whether the nascent hepatocytes are indeed functional, we can take advantage of the lineage tracing induced in this model to isolate the newly derived hepatocytes and to further determine their molecular characteristics and functionality.

Around 90% of ductal cell-derived hepatocyte clusters in *Tet1* mutant mice are only a single cell in size, whereas clusters of five or more hepatocytes were readily observed in wild type mice (Figure 3.35). These data strongly imply that proliferation of nascent hepatocytes is impaired, and therefore that *Tet1* depletion doesn't directly affect hepatocyte differentiation but inhibits further proliferation of the nascent hepatocyte. One prediction resulting from this interpretation is that lineage-labelled hepatocytes would not be maintained during homeostasis and would eventually be replaced through competition by wild type hepatocytes which are competent to undergo proliferation. To explore this, it would be interesting to quantify the number of lineage-labelled hepatocytes remaining after long term recovery from damage. These data would highlight any proliferative defect present in *Tet1*-depleted hepatocytes.

The above interpretation relies on the assumption that the larger, wild type clusters are clonal in nature and have arisen as a result of expansion from single, ductal cell-derived hepatocytes rather than being generated by the parallel differentiation of several closely associated bi-potent ductal progenitors, so creating a continuous, polyclonal regenerative cluster. Our lineage tracing model relies on a single colour reporter with a high recombination efficiency, and therefore we cannot distinguish between monoclonal clusters or polyclonal cluster generation arising from the merging and splitting of several clonal populations. Several options exist for addressing this problem. Firstly, recombination efficiency can be reduced to ensure that any labelled cluster is clonal in origin. However, as recombination efficiency will be very low, any phenotype may be more difficult to discern as the loss of *Tet1* may be compensated for the large number of non-recombined cells in the ductal compartment. Therefore, a more elegant experimental design would be to take advantage of a multi-colour lineage tracing system to facilitate the analysis of clonality whilst maintaining a high overall

recombination efficiency. Furthermore, it would be interesting to assess the role of *Tet1* in hepatocyte expansion and regeneration independent of its role in the ductal compartment. This could be achieved *in vivo* by hepatocyte-specific deletion of *Tet1* in combination with models of hepatocyte-driven regeneration, such as partial hepatectomy, whilst the hepatocyte-derived organoid culture system would be an excellent tool for *in vitro* studies of the role of *Tet1* in hepatocyte proliferation and function. By combining the results of such studies with the clonal dynamics revealed by analysis of ductal compartment-specific studies, a more thorough understanding would be achieved of the role of *Tet1* in both ductal and hepatocyte compartments during liver regeneration.

It is remarkable that, despite the altered dynamics in the generation of ductal cell-derived hepatocytes, the loss of *Tet1* does not affect the overall number of new hepatocytes. Assuming that the larger cluster sizes observed in wild type animals are clonal in origin, this could point towards an impressive range of response at the level of an individual cell during regeneration. Such data suggest that, given a certain loss of tissue as a result of damage, assumed to be the same irrespective of genotype, the number of cells required to compensate for that loss can be generated either by fewer differentiation events and subsequent expansion of nascent cells or by an increased number of differentiation events but less subsequent proliferation of nascent cells. It would be interesting to investigate the signalling that monitors the generation of new tissue and the regulation of such decisions to uncover ways of modulating different mechanisms of regeneration in different cell populations, particularly for cell populations with diminished regenerative capacity.

#### **4.3.4 Is *Tet1* a regulator of proliferation or of progenitor activation?**

It is important to note that the phenotypes described in the animal models can be explained by two distinct hypotheses. *Tet1* deficiency could inhibit the transition to the bi-potent ductal progenitor state, reflected in the reduced ductal regeneration observed in the *Tet1* hypomorphic DDC-induced acute damage model and the reduced size of the ductal compartment and smaller regenerative hepatocyte clusters observed in our ductal cell-specific AAV8-p21 model (Figures 3.22, 3.23, 3.34 and 3.35). However, several studies have linked *Tet1* to the regulation of cell cycle progression and highlighted a role in promoting oncogenic transformation in haematological cancer

(Huang *et al.*, 2013; Chrysanthou *et al.*, 2018). Therefore, *Tet1* deficiency could have a more generic role in negatively regulating proliferation, the same phenotypes being explained by failure to enter the cell cycle. On the other hand, *Tet1* has also been shown to be a tumour suppressor in liver cancer (Thomson *et al.*, 2016), and as a result it is therefore likely that the effect of *Tet1* on the cell cycle is highly context-dependent and further studies would be required to understand the exact mode of action of *Tet1* in ductal cell-driven liver regeneration.

Weng and colleagues showed that *Tet1* and *Tet3* are crucial for axonal regeneration in response to central and peripheral nervous system injury, respectively. Remarkably, the study shows that the roles of *Tet1/3* are intrinsic to the mature neurons and that axonal regeneration is not dependent on proliferation (Weng *et al.*, 2017). Rather, *Tet1/3* upregulate the expression of the regenerative machinery in the injured neuron. This paradigm is partially mirrored in ductal cell-driven liver regeneration, where mature ductal cells acquire a progenitor fate upon damage. Therefore, it would be tempting to speculate that the mechanism by which *Tet1* facilitates liver regeneration is independent of proliferation.

Recent work from Kim and colleagues showed that *Tet1* expression is essential to maintain the intestinal epithelium by ensuring correct expression of *Lgr5* in the stem cell compartment (Kim *et al.*, 2016). Taken together with the data here, where *Tet1* is observed to bind the TSS of *Lgr5* and hypomorphic levels of *Tet1* result in reduced *Lgr5* expression following liver damage (Figure 3.38), this suggests that *Tet1* directly regulates the acquisition of bi-potent ductal progenitor fate at least in part by regulating expression of *Lgr5*. Furthermore, *Tet1* expression is upregulated prior to cell division according to the gene expression profiling performed during organoid generation from ductal cells, suggesting that *Tet1* may act before cell division is initiated. These data provide some evidence that *Tet1* acts to regulate progenitor activation rather than cell cycle progression during ductal cell-driven liver regeneration. Further work will be required to differentiate between cell cycle-dependent and -independent roles of *Tet1* in this setting. Cell cycle inhibitors may be helpful in uncovering phenotypes resulting upon loss of *Tet1* which are not a result of changes in cell cycle progression, but such inhibitors will frequently affect a number of cellular processes which may hinder interpretation of the data. Moreover, cell cycle progression may be essential for ductal

progenitor activation, and thus the use of cell cycle inhibitors may further confound investigation of the mechanism of action of *Tet1*.

Global levels of 5mC and 5hmC were investigated to gain insight into the overall balance of the epigenetic network underlying the acquisition of bi-potent ductal progenitor fate. Upon liver damage, there is a wave of global 5hmC observed which is linked to a concomitant but delayed decrease in global 5mC levels. Both changes are transient, suggesting that *Tet1* may induce a global redistribution of 5mC in the ductal compartment during liver regeneration (Figure 3.37). Interestingly, 5hmC levels peak after 2 days of DDC-induced damage and, crucially, prior to any proliferation, further implying that the role of *Tet1* is independent of proliferation (Figure 3.38). However, we are unable to exclude the contribution of the other *Tet* family members in this process, as they also catalyse oxidation of 5mC. It would be interesting to repeat the study using the *Tet1<sup>flx</sup>/Prom1Cre<sup>ERT2</sup>* model to directly isolate the contribution of *Tet1* to the global changes in methylation levels.

Remarkably, we observed that the TSS of *Lgr5* becomes marked with 5hmC in ductal cells in a *Tet1*-dependent manner during liver damage (Figure 3.39). Furthermore, the appearance of the 5hmC mark during liver damage correlates with *Tet1* binding and increased expression of *Lgr5*, directly linking *Tet1* activity to the increased expression of *Lgr5* during liver damage. Genome wide analysis of *Tet1* binding, 5hmC levels and gene expression could provide more detailed insight into the targets of TET1 activity and the gene regulatory network of ductal cell-derived liver regeneration.

#### **4.3.5 A model for the role of *Tet1* in ductal cell-driven liver regeneration**

Knock-down of *Tet1* by either siRNA or gene trap (hypomorph model) or its complete deletion impairs the transition of mature ductal cells to bi-potent ductal progenitors and their further growth in organoid culture (Figures 3.3, 3.20 and 3.29). Negative regulation of the progenitor state is further reflected in animal models of liver damage, where hypomorphic levels of *Tet1* lead to an impaired ductal response to DDC-induced acute damage and increased fibrosis following chronic damage (Figure 3.22, 3.23, 3.27 and 4.2a). Furthermore, genetic ablation of *Tet1* in a ductal cell-specific manner resulted in a reduced ductal compartment and altered ductal cell-derived hepatocyte generation following severe liver damage (Figures 3.34 and 3.35). The role of *Tet1* in

these processes results at least in part from the *Tet1*-dependent regulation of *Lgr5* expression (Figure 3.38). Taken together, the data highlight a crucial role of *Tet1* in the acquisition and function of bi-potent ductal progenitor fate during ductal cell-driven liver regeneration (Figure 4.2b).

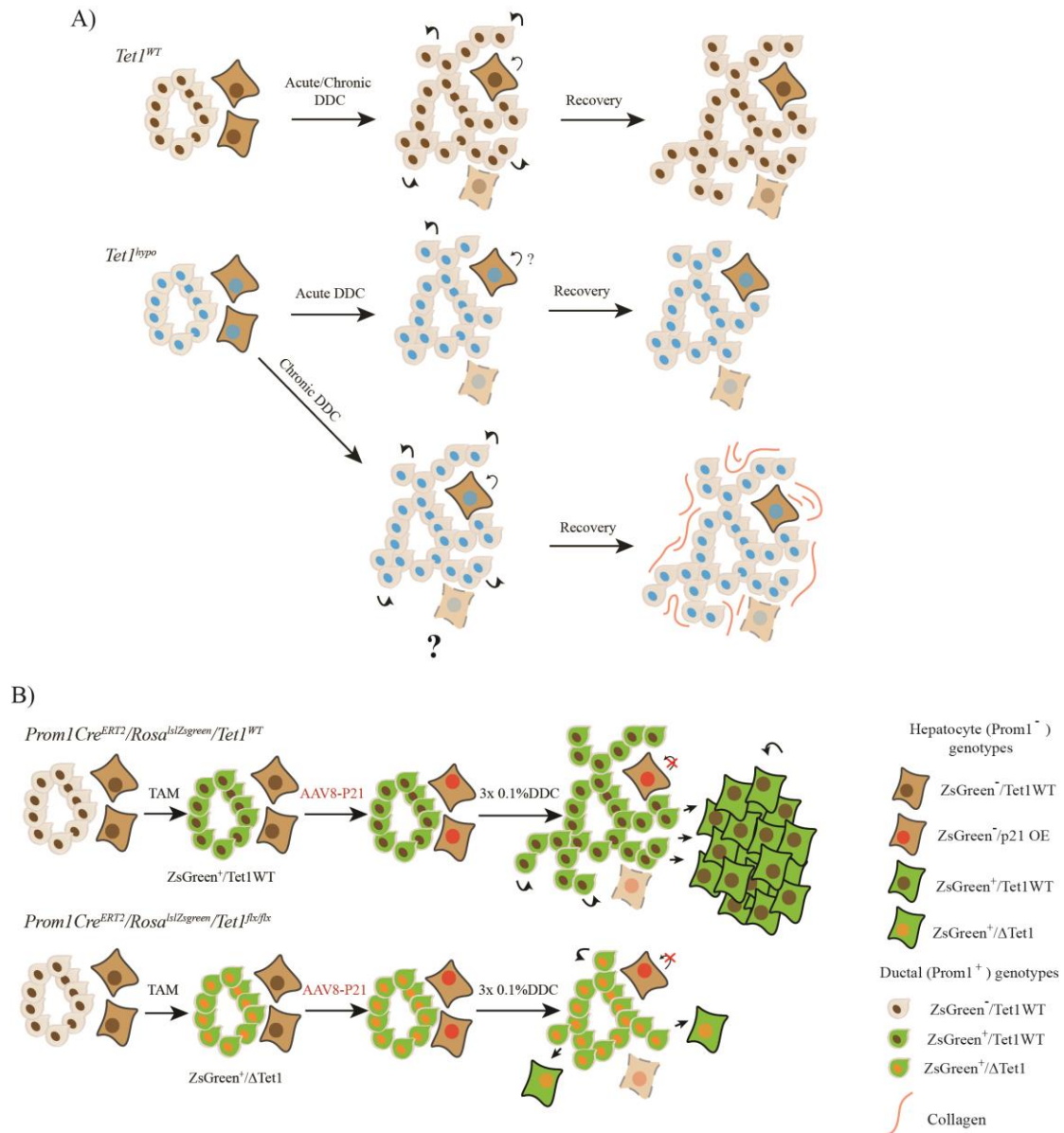


**Figure 4.2 – The role of *Tet1* in ductal cell-driven liver regeneration.** A) A schematic showing the effect of reduced *Tet1* expression in response to acute and chronic DDC treatment. Hypomorphic levels of *Tet1* result in a lower ductal proliferative response after acute DDC damage. In a chronic DDC setting reduced expression results in increased fibrotic collagen deposition. B) A schematic showing the ductal cell-specific role of *Tet1* in the generation of ductal cell-derived hepatocytes in response to extensive liver damage. In this scenario ductal specific depletion of *Tet1* results in a smaller ductal population and significantly smaller clusters of nascent hepatocytes in p21/DDC induced liver damage.

#### 4.3 Ductal proliferation dynamics suggest the existence of a heterogenous population with differing proliferative capacities.

Bimodal proliferative dynamics were observed following DDC-induced acute damage, potentially reflecting the existence of a heterogenous population of ductal cells with differing proliferative capacities (Figure 3.39). Previously described tissue clearing methods were adapted to allow the visualisation of the ductal tree on a larger scale to identify if functionality correlates with particular morphological characteristics (Ke, Fujimoto and Imai, 2013; Susaki *et al.*, 2016). CUBIC clearing allowed a sufficient depth of imaging and could be used to assess proliferative dynamics of the ductal compartment (Figures 3.42 and 3.43). It would be interesting to combine this method with the use of lineage tracing or label retention studies to visualise ductal morphogenesis during liver regeneration. In addition, similar methodologies could be used to analyse the growth of the ductal compartment during development, and by integrating the two datasets it would be possible to assess whether morphogenetic processes occur in the ducts in the embryo during development and in the adult in response to damage.

Whilst such imaging studies could provide great insight into the spatial and morphological determinants of regeneration by the ductal compartment, it is important to note that they will provide no information on the molecular characteristics of any heterogenous populations. Therefore, molecular analysis at the single cell level in conjunction with imaging studies could reveal the molecular components underlying the apparent bimodal proliferation dynamics of the ductal population during regeneration.

#### 4.4 Conclusion

In this work we have investigated the molecular machinery underlying ductal cell-driven liver regeneration using animal models *in vivo* and *in vitro* culture of ductal cell-derived organoids as a suitable model for the bi-potent ductal progenitor state. As a result, we have identified two epigenetic modifiers, *Arid1a* and *Tet1*, which are required for transition to the progenitor state and differentiation to functional hepatocytes following induction of liver damage. This work highlights the importance of orchestrated epigenetic changes in responding to and resolving liver damage and describes the development of animal models and techniques for investigating the role of these epigenetic modifiers in greater detail.

Recent work by our group and others have found evidence that *Arid1a* and *Tet1* may work in a unified system to modulate liver regeneration. Li and colleagues have shown that *Arid1a* is essential for binding of YAP to its targets stopping the expression of key progenitor markers (Li *et al.*, 2019). In a similar manner, it was shown targets of *Tet1* were enriched in the YAP/Hippo pathway. Furthermore, conditional knockout of *Tet1* also reduced the expression of components of the of the YAP pathway. Interestingly, expression was restored with overexpression of *Tet1* in a hypomorphic background (Aloia *et al.* in press). Therefore, *Tet1* expression may promote liver regeneration by activating the YAP/Hippo pathway. The YAP pathway itself has been shown to be essential for ductal liver regeneration and liver cell fate, therefore, our work here combined with others have potentially unveiled another level of regulation upstream of YAP (Yimlamai *et al.*, 2014; Pepe-Mooney *et al.*, 2019). These data suggest in order for YAP to activate the regenerative response there needs to be a permissive chromatin state laid down by regulators such as *Tet1* and *Arid1a*. Therefore, we can begin to hypothesise a novel mechanism of liver regeneration whereby some extrinsic or intrinsic signal of liver damage activates an epigenetic change, facilitated in part by *Tet1* and *Arid1a*, which allows a permissive chromatin state that promotes the YAP pathway and ultimately ductal progenitor driven liver regeneration. Such a pathway would require future validation but provides an interesting framework for future study. One particularly interesting line of study would be to begin to understand the signalling that activates this potential regenerative pathway. In any case, data presented here combined with progress in the field as a whole have shed light on novel

pathways of liver regeneration which may lead to fascinating applications in the treatment of chronic liver disease.

## Acknowledgements

There are a huge number of people I would like to thank, or blame, for pushing me forward and allowing me to achieve this work. This will be particularly hard, as the people mentioned below all know, I certainly don't have the vocabulary to adequately thank everyone. However, I will do my best.

First, I would like to thank Meri for taking the chance of hiring me as a research assistant in her lab more than 4 years ago. Without her support and guidance over the years I would not be where I am now and for that I am immensely grateful. Next, I would like to discuss my long-time collaborator and partner in crime, Luigi. From my first days in the lab he proved to be an instrumental mentor. His work and guidance provided me with many of the foundations for my own research and I have since endeavoured to return his help wherever possible. Gianmarco and Lucia as fellow old PhD students also deserve a special mention. I have always admired Gianmarco's great eye for detail without which he may not have knocked out the wrong isoform of *Arid1a* which ultimately led to intriguing insights into the nature the gene. Lucia has a tremendous work ethic that I have always aspired to, despite the inability to make coffee that isn't 'agua cha-cha', she would never shy away from a challenge (or from not paying for a takeaway). I am incredibly lucky to count myself amongst them as I am sure they will all conquer the science world.

The Huch lab as whole is a remarkable place to work that is more than the sum of its parts. It is hard to pin down exactly what makes it such an easy environment to work in, but it is ultimately the people that work there. Nicole, an excellent post-doc, colleague and close acquaintance, is unashamedly cold but fair and not afraid to tell you in no uncertain terms why you are wrong (especially when proofreading). The lesser seen Nikitas and the ever romantic Flaminia are part of the next generation of PhD students. They have the unenviable task of dealing with not one but two supervisors; but manage it with grace and are able to be patient enough to deal with my nonsense, forcing laughs at my 'hilarious' jokes. Patricia, more recently German, have injected new energy in to the lab never failing to smile and are excellent company for those infrequent sunshine breaks. Finally, Robert, our battle-hardened lab manager has never failed to find a solution to help us carry out our work. Further to those mentioned here, there are many that have come and gone that have help shaped the lab. Most

notable for me have been Chris and Berta. Chris was a beacon of wisdom and a master wordsmith that could be counted on for help at any time. Berta was a talented a master's student that helped me with the daunting collection and storage of a huge number of samples and after two years I am still grateful for this. I feel so fortunate to have worked with such a good group of people and I hope the success of the lab will continue well after I have left.

Beyond the lab I have been blessed with a great network of family and friends without which I may never have become a scientist, let alone finish a PhD. At a young age I was inspired by day trips with my Dad to carry out crucial 'PCR' experiments or work experiences with my Mum during which I had to dodge lethal radiation, both of which served to catch my imagination and set me on my journey. There have been times when I wouldn't have thanked them for that, but with the constant support of my parents I have never faltered for too long. This work is as much theirs as it is mine. Although not direct colleagues, Livvi and her 'friend-friend' John have been steadfast in their support whether related to science, business, six-nations, chicken wings or anything else. Also, my only two 'non-science' friends in Cambridge, James and Matt, have been invaluable companions over the years. Matt has always provided a big TV and a comfy sofa for movie nights, even after the 'Curry' incident. James on the other hand can be found wondering the local pubs and is always up for a pint and a chat. Finally, thank you Ayla (my 'Most of all') and more recently Gilbey (the gin and the cat), for having to put up with me coming home grumpy after countless failed experiments by always making my home my happy place, greeting me with life-saving G&Ts and a smile that made everything OK.

I'm sure I have not been able to personally thank everyone and there are many more people that have helped me over the years. Without all of you none of this would have been possible.

## Table of Figures

<i>Figure 1.1 - The structure of the hepatic lobule.</i>	11
<i>Figure 1.2 - The liver demonstrates several modes of regeneration in a damage and cellular context dependent manner.</i>	18
<i>Figure 1.3 - Epigenetic methods of gene regulation.</i>	25
<i>Figure 1.4 - The TET family oxidises 5mC in a step-wise manner facilitating the active removal of methylated cytosine.</i>	35
<i>Figure 1.5 - Specialisation of the BAF complex modulates specific gene networks driving neural development.</i>	40
<i>Figure 3.1 - Multiple components of the BAF complex are upregulated during CCl<sub>4</sub> induced liver damage.</i>	62
<i>Figure 3.2 - Several epigenetic modifiers are dynamically regulated during organoid derivation.</i>	64
<i>Figure 3.3 - siRNA knockdown reveals organoid derivation is dependent on Tet1 expression.</i>	66
<i>Figure 3.4 - siRNA knockdown of components of the BAF complex enhances organoid survival.</i>	67
<i>Figure 3.5 - CRISPR mediated deletion of ARID1a isoform B.</i>	69
<i>Figure 3.6 - Arid1a isoB<sup>-/-</sup> organoids have increased organoid formation efficiency.</i>	70
<i>Figure 3.7 - Arid1a isoB<sup>-/-</sup> organoids have decreased expression of progenitor markers whilst increasing the levels of hallmark differentiation genes.</i>	71
<i>Figure 3.8 - Loss of isoform B results in altered gene expression after differentiation towards hepatocyte fate.</i>	73
<i>Figure 3.9 - Arid1a mutation results in impaired terminal differentiation into hepatocyte fate.</i>	75
<i>Figure 3.10 - Generation of total heterozygous and homozygous Arid1a mutant organoids.</i>	78
<i>Figure 3.11 - Immunostaining of BAF components in total Arid1a mutant organoids.</i>	79
<i>Figure 3.12 - Dosage of Arid1a is crucial for organoid formation efficiency.</i>	80
<i>Figure 3.13 - Arid1a level controls expression of progenitor and differentiation markers.</i>	81
<i>Figure 3.14 - Arid1a is required for terminal differentiation.</i>	82
<i>Figure 3.15 - Arid1a and BAF subunit Brg1 bind regulatory elements of crucial regulators of hepatocyte and progenitor identity.</i>	84
<i>Figure 3.16 - Recombination by Lgr5iresCre<sup>ERT2</sup> after DDC treatment is not sufficient to facilitate Arid1a deletion in emergent ductal progenitors.</i>	87
<i>Figure 3.17 - Generation of Tet1 hypomorphic, conditional and null mouse models</i>	89
<i>Figure 3.18 - Viability of Tet1 mouse models generated.</i>	90
<i>Figure 3.19 - Tet1<sup>hypo/hypo</sup> mice show no major homeostatic defect compared to WT mice.</i>	91
<i>Figure 3.20 - Reduced Tet1 expression results in organoids with reduced self-renewal capacity.</i>	92
<i>Figure 3.21 - Tet1 hypomorphic and WT mice lose weight and accumulate porphyrin to a similar level in response to acute DDC treatment.</i>	94
<i>Figure 3.22 - TET1 is crucial for initiation of ductal proliferation in response to DDC damage.</i>	95
<i>Figure 3.23 - Tet1 hypomorphic mice have a smaller ductal population after recovery from acute DDC damage.</i>	96

<i>Figure 3.24 - Impaired ductal response is not due to decreased global liver damage in Tet1 hypomorphic mice.</i>	98
<i>Figure 3.25 - Chronic DDC damage results in cyclic weight loss and recovery in Tet1 hypomorphic and WT mice.</i>	99
<i>Figure 3.26 - Reduced levels of TET1 does not alter ductal proliferation or ductal population size after recovery from chronic DDC damage.</i>	101
<i>Figure 3.27 - Tet1 hypomorphic mice have increased fibrosis after recovery from DDC chronic damage.</i>	102
<i>Figure 3.28 - Tet1 ablation abolishes organoids formation from mature EpCAM+ cells.</i>	104
<i>Figure 3.29 - Ubiquitous postnatal deletion of Tet1 is lethal and results in collapse of the small intestine.</i>	105
<i>Figure 3.30 - Prominence of lethality after ubiquitous Tet1 deletion.</i>	105
<i>Figure 3.31 - Prom1Cre<sup>ERT2</sup> driven recombination is restricted to the ductal compartment in the liver and is not ubiquitous in the small intestine.</i>	106
<i>Figure 3.32 - Efficient Tet1 deletion in the context of hepatocyte specific p21 overexpression and DDC damage.</i>	108
<i>Figure 3.33 - AAV8-TBG-p21 induced p21 overexpression is restricted to the hepatocyte compartment.</i>	109
<i>Figure 3.34 - Ductal specific deletion of Tet1 led to reduced ductal expansion after DDC damage in the context of hepatocyte senescence.</i>	110
<i>Figure 3.35 - Loss of Tet1 results in smaller ductal derived hepatocyte regenerative clusters.</i>	112
<i>Figure 3.36 - Prom1<sup>ΔTet1</sup> mice have a significantly larger number of hepatocyte clusters but similar number of overall newly derived hepatocytes.</i>	113
<i>Figure 3.37 - Global 5mC and 5hmC DNA modification levels are dynamic during DDC induced activation of ductal proliferation.</i>	115
<i>Figure 3.38 - Reduced expression of Tet1 abolishes the activation of stem cell marker Lgr5 after DDC induced liver damage.</i>	117
<i>Figure 3.39 - Tet1<sup>WT</sup> mice showed two proliferative responses in the ductal compartment in after acute DDC damage.</i>	118
<i>Figure 3.40 - Models of ductal tree regeneration in response to DDC damage.</i>	119
<i>Figure 3.41 - Tissue clearing performance of refractive index matching by Glycerol gradients or SeeDB.</i>	120
<i>Figure 3.42 - Tissue clearing performance of CUBIC reagents 1 or 1a on liver sections.</i>	121
<i>Figure 3.43 - CUBIC clearing allows significantly increased imaging depth and reveals large ductal structures.</i>	122
<i>Figure 4.1 – Working model for the regulation of bi-potent ductal progenitors by Arid1a in organoid culture.</i>	130
<i>Figure 4.2 – The role of Tet1 in ductal cell-driven liver regeneration.</i>	138

## List of Tables

<i>Table 2.1 – 3D organoid growth media recipes</i>	44
<i>Table 2.2 – siRNA sequence library</i>	45
<i>Table 2.3 – qPCR/ChIP detection primer sequences</i>	48
<i>Table 2.4 – ChIP solution recipes</i>	50
<i>Table 2.5 – Experimental animal lines</i>	51
<i>Table 2.6 – Genotyping primer sequences</i>	52
<i>Table 2.7 – Antibody information</i>	56
<i>Table 2.8 – CUBIC reagent recipes</i>	60

## Bibliography

- Abdel-Misih, S. R. Z. and Bloomston, M. (2010) 'Liver anatomy.', *The Surgical clinics of North America*. NIH Public Access, 90(4), pp. 643–53. doi: 10.1016/j.suc.2010.04.017.
- Aloia, L., Mckie, M. A. and Huch, M. (2016) 'Cellular plasticity in the adult liver and stomach.', *The Journal of physiology*. doi: 10.1113/JP271769.
- Alpini, G. *et al.* (1996) 'Morphological, molecular, and functional heterogeneity of cholangiocytes from normal rat liver', *Gastroenterology*. Elsevier, 110(5), pp. 1636–1643. doi: 10.1053/gast.1996.v110.pm8613073.
- Asrani, S. K. *et al.* (2013) 'Underestimation of liver-related mortality in the United States.', *Gastroenterology*. Elsevier, 145(2), pp. 375–82.e1–2. doi: 10.1053/j.gastro.2013.04.005.
- Ayton, P. M., Chen, E. H. and Cleary, M. L. (2004) 'Binding to nonmethylated CpG DNA is essential for target recognition, transactivation, and myeloid transformation by an MLL oncoprotein.', *Molecular and cellular biology*. American Society for Microbiology Journals, 24(23), pp. 10470–8. doi: 10.1128/MCB.24.23.10470-10478.2004.
- Bachman, M. *et al.* (2014) '5-Hydroxymethylcytosine is a predominantly stable DNA modification', *Nature Chemistry*. Nature Publishing Group, 6(12), pp. 1049–1055. doi: 10.1038/nchem.2064.
- Bachman, M. *et al.* (2015) '5-Formylcytosine can be a stable DNA modification in mammals', *Nature Chemical Biology*. Nature Publishing Group, 11(8), pp. 555–557. doi: 10.1038/nchembio.1848.
- Bannister, A. J. *et al.* (2001) 'Selective recognition of methylated lysine 9 on histone H3 by the HP1 chromo domain', *Nature*. Nature Publishing Group, 410(6824), pp. 120–124. doi: 10.1038/35065138.
- Bannister, A. J. and Kouzarides, T. (2011) 'Regulation of chromatin by histone modifications', *Cell Research*. Nature Publishing Group, 21(3), pp. 381–395. doi: 10.1038/cr.2011.22.
- Barkauskas, C. E. *et al.* (2017) 'Lung organoids: current uses and future promise.', *Development (Cambridge, England)*. Company of Biologists, 144(6), pp. 986–997. doi: 10.1242/dev.140103.
- Barker, N. *et al.* (2010) 'Lgr5(+ve) stem cells drive self-renewal in the stomach and build long-lived gastric units in vitro.', *Cell stem cell*. Elsevier, 6(1), pp. 25–36. doi: 10.1016/j.stem.2009.11.013.
- Barker, N., van de Wetering, M. and Clevers, H. (2008) 'The intestinal stem cell.', *Genes & development*. Cold Spring Harbor Laboratory Press, 22(14), pp. 1856–64. doi: 10.1101/gad.1674008.
- Barreto, G. *et al.* (2007) 'Gadd45a promotes epigenetic gene activation by repair-mediated DNA demethylation', *Nature*. Nature Publishing Group, 445(7128), pp. 671–675. doi: 10.1038/nature05515.
- Basta, J. and Rauchman, M. (2015) 'The nucleosome remodeling and deacetylase complex in development and disease.', *Translational research : the journal of laboratory and clinical medicine*. NIH Public Access, 165(1), pp. 36–47. doi: 10.1016/j.trsl.2014.05.003.
- Batsché, E., Yaniv, M. and Muchardt, C. (2006) 'The human SWI/SNF subunit Brm is a regulator of alternative splicing', *Nature Structural & Molecular Biology*. Nature Publishing Group, 13(1), pp. 22–29. doi: 10.1038/nsmb1030.
- Battaglioli, E. *et al.* (2002) 'REST repression of neuronal genes requires components of the hSWI.SNF complex.', *The Journal of biological chemistry*. American Society for Biochemistry and Molecular Biology, 277(43), pp. 41038–45. doi: 10.1074/jbc.M205691200.
- Bestor, T. H. (1992) 'Activation of mammalian DNA methyltransferase by cleavage of a Zn binding regulatory domain.', *The EMBO journal*. European Molecular Biology Organization, 11(7), pp. 2611–7. Available at: <http://www.ncbi.nlm.nih.gov/pubmed/1628623> (Accessed: 2 February 2019).
- Bhattacharya, S. K. *et al.* (1999) 'A mammalian protein with specific demethylase activity for mCpG DNA', *Nature*. Nature Publishing Group, 397(6720), pp. 579–583. doi:

10.1038/17533.

- Biankin, A. V *et al.* (2012) 'Pancreatic cancer genomes reveal aberrations in axon guidance pathway genes.', *Nature*, 491(7424), pp. 399–405. doi: 10.1038/nature11547.
- Bilzer, M., Roggel, F. and Gerbes, A. L. (2006) 'Role of Kupffer cells in host defense and liver disease', *Liver International*. John Wiley & Sons, Ltd (10.1111), 26(10), pp. 1175–1186. doi: 10.1111/j.1478-3231.2006.01342.x.
- Bird, A. (2002) 'DNA methylation patterns and epigenetic memory.', *Genes & development*. Cold Spring Harbor Laboratory Press, 16(1), pp. 6–21. doi: 10.1101/gad.947102.
- Birke, M. *et al.* (2002) 'The MT domain of the proto-oncoprotein MLL binds to CpG-containing DNA and discriminates against methylation', *Nucleic Acids Research*. Oxford University Press, 30(4), pp. 958–965. doi: 10.1093/nar/30.4.958.
- Blouin, A., Bolender, R. P. and Weibel, E. R. (1977) 'Distribution of organelles and membranes between hepatocytes and nonhepatocytes in the rat liver parenchyma. A stereological study.', *The Journal of cell biology*. Rockefeller University Press, 72(2), pp. 441–55. doi: 10.1083/JCB.72.2.441.
- Boland, M. J., Nazor, K. L. and Loring, J. F. (2014) 'Epigenetic Regulation of Pluripotency and Differentiation', *Circulation Research*. Lippincott Williams & Wilkins/Hagerstown, MD, 115(2), pp. 311–324. doi: 10.1161/CIRCRESAHA.115.301517.
- Bondarenko, V. A. *et al.* (2006) 'Nucleosomes can form a polar barrier to transcript elongation by RNA polymerase II.', *Molecular cell*. Elsevier, 24(3), pp. 469–79. doi: 10.1016/j.molcel.2006.09.009.
- Bostick, M. *et al.* (2007) 'UHRF1 plays a role in maintaining DNA methylation in mammalian cells.', *Science (New York, N.Y.)*. American Association for the Advancement of Science, 317(5845), pp. 1760–4. doi: 10.1126/science.1147939.
- Bourhis, D. and Bestor, T. H. (2004) 'Meiotic catastrophe and retrotransposon reactivation in male germ cells lacking Dnmt3L', *Nature*. Nature Publishing Group, 431(7004), pp. 96–99. doi: 10.1038/nature02886.
- Boyer, J. L. (2013) 'Bile formation and secretion.', *Comprehensive Physiology*. NIH Public Access, 3(3), pp. 1035–78. doi: 10.1002/cphy.c120027.
- Bultman, S. *et al.* (2000) 'A Brg1 null mutation in the mouse reveals functional differences among mammalian SWI/SNF complexes.', *Molecular cell*. Elsevier, 6(6), pp. 1287–95. doi: 10.1016/S1097-2765(00)00127-1.
- Bultman, S. J. *et al.* (2006) 'Maternal BRG1 regulates zygotic genome activation in the mouse.', *Genes & development*. Cold Spring Harbor Laboratory Press, 20(13), pp. 1744–54. doi: 10.1101/gad.1435106.
- Chan-on, W. *et al.* (2013) 'Exome sequencing identifies distinct mutational patterns in liver fluke-related and non-infection-related bile duct cancers', *Nature Genetics*. Nature Publishing Group, 45(12), pp. 1474–1478. doi: 10.1038/ng.2806.
- Chargaff, E. *et al.* (1951) 'The composition of the deoxyribonucleic acid of salmon sperm.', *The Journal of biological chemistry*, 192(1), pp. 223–30. Available at: <http://www.ncbi.nlm.nih.gov/pubmed/14917668> (Accessed: 2 February 2019).
- Chen, Z. *et al.* (2017) 'Epigenetic Regulation: A New Frontier for Biomedical Engineers', *Annual Review of Biomedical Engineering*. Annual Reviews, 19(1), pp. 195–219. doi: 10.1146/annurev-bioeng-071516-044720.
- Chittock, E. C. *et al.* (2017) 'Molecular architecture of polycomb repressive complexes.', *Biochemical Society transactions*. Portland Press Ltd, 45(1), pp. 193–205. doi: 10.1042/BST20160173.
- Choi, T.-Y. *et al.* (2014) 'Extensive conversion of hepatic biliary epithelial cells to hepatocytes after near total loss of hepatocytes in zebrafish.', *Gastroenterology*, 146(3), pp. 776–88. doi: 10.1053/j.gastro.2013.10.019.
- Chrysanthou, S. *et al.* (2018) 'A Critical Role of TET1/2 Proteins in Cell-Cycle Progression of Trophoblast Stem Cells.', *Stem cell reports*. Elsevier, 10(4), pp. 1355–1368. doi: 10.1016/j.stemcr.2018.02.014.
- Clevers, H. (2016) 'Leading Edge Review Modeling Development and Disease with Organoids'. doi: 10.1016/j.cell.2016.05.082.

Cohn, J. A. *et al.* (1993) 'Localization of the cystic fibrosis transmembrane conductance regulator in human bile duct epithelial cells.', *Gastroenterology*, 105(6), pp. 1857–64. Available at: <http://www.ncbi.nlm.nih.gov/pubmed/7504645> (Accessed: 13 February 2019).

Cordero-Espinoza, L. and Huch, M. (2018) 'The balancing act of the liver: tissue regeneration versus fibrosis', *The Journal of Clinical Investigation*. American Society for Clinical Investigation, 128(1), pp. 85–96. doi: 10.1172/JCI93562.

Cortázar, D. *et al.* (2007) 'The enigmatic thymine DNA glycosylase', *DNA Repair*. Elsevier, 6(4), pp. 489–504. doi: 10.1016/J.DNAREP.2006.10.013.

Costa, Y. *et al.* (2013) 'NANOG-dependent function of TET1 and TET2 in establishment of pluripotency', *Nature*. Nature Publishing Group, 495(7441), pp. 370–374. doi: 10.1038/nature11925.

Crick, F. H. C. (1970) 'Central Dogma of Molecular Biology', *Nature*. Nature Publishing Group, 227(5258), pp. 561–563. doi: 10.1038/227561a0.

Davey, C., Pennings, S. and Allan, J. (1997) 'CpG methylation remodels chromatin structure in vitro', *Journal of Molecular Biology*. Academic Press, 267(2), pp. 276–288. doi: 10.1006/JMBI.1997.0899.

Dawlaty, M. M. *et al.* (2011) 'Tet1 is dispensable for maintaining pluripotency and its loss is compatible with embryonic and postnatal development.', *Cell stem cell*. Elsevier, 9(2), pp. 166–75. doi: 10.1016/j.stem.2011.07.010.

Dawlaty, M. M. *et al.* (2013) 'Combined deficiency of Tet1 and Tet2 causes epigenetic abnormalities but is compatible with postnatal development.', *Developmental cell*. NIH Public Access, 24(3), pp. 310–23. doi: 10.1016/j.devcel.2012.12.015.

Dawlaty, M. M. *et al.* (2014) 'Loss of Tet enzymes compromises proper differentiation of embryonic stem cells.', *Developmental cell*. NIH Public Access, 29(1), pp. 102–111. doi: 10.1016/j.devcel.2014.03.003.

Deng, X. *et al.* (2018) 'Chronic Liver Injury Induces Conversion of Biliary Epithelial Cells into Hepatocytes.', *Cell stem cell*. Elsevier, 23(1), p. 114–122.e3. doi: 10.1016/j.stem.2018.05.022.

Deutsch, G. *et al.* (2001) 'A bipotential precursor population for pancreas and liver within the embryonic endoderm.', *Development (Cambridge, England)*, 128(6), pp. 871–81. Available at: <http://www.ncbi.nlm.nih.gov/pubmed/11222142> (Accessed: 28 January 2019).

Doerge, C. A. *et al.* (2012) 'Early-stage epigenetic modification during somatic cell reprogramming by Parp1 and Tet2', *Nature*. Nature Publishing Group, 488(7413), pp. 652–655. doi: 10.1038/nature11333.

Dürr, H. *et al.* (2005) 'X-ray structures of the Sulfolobus solfataricus SWI2/SNF2 ATPase core and its complex with DNA.', *Cell*. Elsevier, 121(3), pp. 363–73. doi: 10.1016/j.cell.2005.03.026.

Ehrlich, M. *et al.* (1982) 'Amount and distribution of 5-methylcytosine in human DNA from different types of tissues of cells.', *Nucleic acids research*. Oxford University Press, 10(8), pp. 2709–21. Available at: <http://www.ncbi.nlm.nih.gov/pubmed/7079182> (Accessed: 2 February 2019).

Eisen, J. A., Sweder, K. S. and Hanawalt, P. C. (1995) 'Evolution of the SNF2 family of proteins: subfamilies with distinct sequences and functions.', *Nucleic acids research*. Oxford University Press, 23(14), pp. 2715–23. Available at: <http://www.ncbi.nlm.nih.gov/pubmed/7651832> (Accessed: 12 February 2019).

Euskirchen, G. M. *et al.* (2011) 'Diverse Roles and Interactions of the SWI/SNF Chromatin Remodeling Complex Revealed Using Global Approaches', *PLoS Genetics*. Edited by G. P. Copenhagen. Public Library of Science, 7(3), p. e1002008. doi: 10.1371/journal.pgen.1002008.

Evarts, R. P. *et al.* (1987) 'A precursor-product relationship exists between oval cells and hepatocytes in rat liver.', *Carcinogenesis*, 8(11), pp. 1737–40. Available at: <http://www.ncbi.nlm.nih.gov/pubmed/3664968> (Accessed: 17 January 2019).

Evarts, R. P. *et al.* (1989) 'In vivo differentiation of rat liver oval cells into hepatocytes.', *Cancer research*. American Association for Cancer Research, 49(6), pp. 1541–7. Available at: <http://www.ncbi.nlm.nih.gov/pubmed/2466557> (Accessed: 17 January 2019).

- Fang, J.-Z. *et al.* (2015) 'Hepatocyte-Specific Arid1a Deficiency Initiates Mouse Steatohepatitis and Hepatocellular Carcinoma.', *PloS one*, 10(11), p. e0143042. doi: 10.1371/journal.pone.0143042.
- Farber, E. (1956) 'Similarities in the Sequence of Early Histological Changes Induced in the Liver of the Rat by Ethionine, 2-Acetylaminofluorene, and 3'-Methyl-4-dimethylaminoazobenzene', *Cancer Research*, 16(2), pp. 142–148. Available at: <http://cancerres.aacrjournals.org/content/canres/16/2/142.full.pdf> (Accessed: 18 January 2019).
- Fausto, N. and Campbell, J. S. (2003) 'The role of hepatocytes and oval cells in liver regeneration and repopulation', *Mechanisms of Development*. Elsevier, 120(1), pp. 117–130. doi: 10.1016/S0925-4773(02)00338-6.
- Font-Burgada, J. *et al.* (2015) 'Hybrid Periportal Hepatocytes Regenerate the Injured Liver without Giving Rise to Cancer.', *Cell*, 162(4), pp. 766–79. doi: 10.1016/j.cell.2015.07.026.
- Francavilla, A. *et al.* (1988) 'Regulation of liver size and regeneration: importance in liver transplantation.', *Transplantation proceedings*. NIH Public Access, 20(1 Suppl 1), pp. 494–7. Available at: <http://www.ncbi.nlm.nih.gov/pubmed/3279642> (Accessed: 16 January 2019).
- Frauer, C. *et al.* (2011) 'Recognition of 5-Hydroxymethylcytosine by the Uhrf1 SRA Domain', *PLoS ONE*. Edited by S. Xu. Public Library of Science, 6(6), p. e21306. doi: 10.1371/journal.pone.0021306.
- Gao, X. *et al.* (2008) 'ES cell pluripotency and germ-layer formation require the SWI/SNF chromatin remodeling component BAF250a.', *Proceedings of the National Academy of Sciences of the United States of America*. National Academy of Sciences, 105(18), pp. 6656–61. doi: 10.1073/pnas.0801802105.
- Gavin, I., Horn, P. J. and Peterson, C. L. (2001) 'SWI/SNF Chromatin Remodeling Requires Changes in DNA Topology', *Molecular Cell*. Elsevier, 7(1), pp. 97–104. doi: 10.1016/S1097-2765(01)00158-7.
- Gayathri, A. K. and Padmanaban, G. (1974) 'Biochemical effects of 3,5-diethoxycarbonyl-1,4-dihydrocollidine in mouse liver', *Biochemical Pharmacology*. Elsevier, 23(19), pp. 2713–2725. doi: 10.1016/0006-2952(74)90042-2.
- Gebhardt, R. (1992) 'Metabolic zonation of the liver: Regulation and implications for liver function', *Pharmacology & Therapeutics*. Pergamon, 53(3), pp. 275–354. doi: 10.1016/0163-7258(92)90055-5.
- Gjerset, R. A. and Martin, D. W. (1982) 'Presence of a DNA demethylating activity in the nucleus of murine erythroleukemic cells.', *The Journal of biological chemistry*, 257(15), pp. 8581–3. Available at: <http://www.ncbi.nlm.nih.gov/pubmed/7047522> (Accessed: 8 February 2019).
- Gordillo, M., Evans, T. and Gouon-Evans, V. (2015) 'Orchestrating liver development.', *Development (Cambridge, England)*. Company of Biologists, 142(12), pp. 2094–108. doi: 10.1242/dev.114215.
- Grisham, J. W. (1962) 'A morphologic study of deoxyribonucleic acid synthesis and cell proliferation in regenerating rat liver; autoradiography with thymidine-H<sup>3</sup>.', *Cancer research*. American Association for Cancer Research, 22(7 Part 1), pp. 842–9. Available at: <http://www.ncbi.nlm.nih.gov/pubmed/13902009> (Accessed: 16 January 2019).
- Gu, T.-P. *et al.* (2011) 'The role of Tet3 DNA dioxygenase in epigenetic reprogramming by oocytes', *Nature*. Nature Publishing Group, 477(7366), pp. 606–610. doi: 10.1038/nature10443.
- Gualdi, R. *et al.* (1996) 'Hepatic specification of the gut endoderm in vitro: cell signaling and transcriptional control.', *Genes & development*. Cold Spring Harbor Laboratory Press, 10(13), pp. 1670–82. doi: 10.1101/GAD.10.13.1670.
- Hackett, J. A. *et al.* (2013) 'Germline DNA demethylation dynamics and imprint erasure through 5-hydroxymethylcytosine.', *Science (New York, N.Y.)*. American Association for the Advancement of Science, 339(6118), pp. 448–52. doi: 10.1126/science.1229277.
- Hajkova, P. *et al.* (2008) 'Chromatin dynamics during epigenetic reprogramming in the mouse germ line', *Nature*. Nature Publishing Group, 452(7189), pp. 877–881. doi: 10.1038/nature06714.

Hannezo, E. *et al.* (2017) ‘A Unifying Theory of Branching Morphogenesis.’, *Cell*. Elsevier, 171(1), p. 242–255.e27. doi: 10.1016/j.cell.2017.08.026.

Harikrishnan, K. N. *et al.* (2005) ‘Brahma links the SWI/SNF chromatin-remodeling complex with MeCP2-dependent transcriptional silencing’, *Nature Genetics*. Nature Publishing Group, 37(3), pp. 254–264. doi: 10.1038/ng1516.

Hashimoto, H. *et al.* (2012) ‘Recognition and potential mechanisms for replication and erasure of cytosine hydroxymethylation’, *Nucleic Acids Research*. Oxford University Press, 40(11), pp. 4841–4849. doi: 10.1093/nar/gks155.

Hashimoto, H. *et al.* (2014) ‘Structure of a Naegleria Tet-like dioxygenase in complex with 5-methylcytosine DNA’, *Nature*. Nature Publishing Group, 506(7488), pp. 391–395. doi: 10.1038/nature12905.

Havas, K. *et al.* (2000) ‘Generation of superhelical torsion by ATP-dependent chromatin remodeling activities.’, *Cell*, 103(7), pp. 1133–42. Available at: <http://www.ncbi.nlm.nih.gov/pubmed/11163188> (Accessed: 6 June 2016).

He, Y.-F. *et al.* (2011) ‘Tet-Mediated Formation of 5-Carboxylcytosine and Its Excision by TDG in Mammalian DNA’, *Science*. American Association for the Advancement of Science, 333(6047), pp. 1303–1307. doi: 10.1126/SCIENCE.1210944.

Hellman, A. and Chess, A. (2007) ‘Gene Body-Specific Methylation on the Active X Chromosome’, *Science*. American Association for the Advancement of Science, 315(5815), pp. 1141–1143. doi: 10.1126/SCIENCE.1136352.

Hemberger, M., Dean, W. and Reik, W. (2009) ‘Epigenetic dynamics of stem cells and cell lineage commitment: digging Waddington’s canal’, *Nature Reviews Molecular Cell Biology*. Nature Publishing Group, 10(8), pp. 526–537. doi: 10.1038/nrm2727.

Hendrich, B. *et al.* (1999) ‘Genomic structure and chromosomal mapping of the murine and human Mbd1, Mbd2, Mbd3, and Mbd4 genes’, *Mammalian Genome*. Springer-Verlag, 10(9), pp. 906–912. doi: 10.1007/s003359901112.

Hendrich, B. *et al.* (2001) ‘Closely related proteins MBD2 and MBD3 play distinctive but interacting roles in mouse development.’, *Genes & development*. Cold Spring Harbor Laboratory Press, 15(6), pp. 710–23. doi: 10.1101/gad.194101.

Hendrich, B. and Bird, A. (1998) ‘Identification and characterization of a family of mammalian methyl-CpG binding proteins.’, *Molecular and cellular biology*. American Society for Microbiology Journals, 18(11), pp. 6538–47. doi: 10.1128/MCB.18.11.6538.

Higgins, Anderson, R. . (1931) ‘Experimental pathology of the liver. I. Restoration of the liver of the white rat following partial surgical removal’, *AMA Arch Pathol*, 12, pp. 186–202. Available at: [https://www.researchgate.net/publication/304796359\\_Experimental\\_pathology\\_of\\_the\\_liver\\_I\\_Restoration\\_of\\_the\\_liver\\_of\\_the\\_white\\_rat\\_following\\_partial\\_surgical\\_removal](https://www.researchgate.net/publication/304796359_Experimental_pathology_of_the_liver_I_Restoration_of_the_liver_of_the_white_rat_following_partial_surgical_removal) (Accessed: 4 March 2019).

Hindley, C. J., Cordero-Espinoza, L. and Huch, M. (2016) ‘Organoids from adult liver and pancreas: Stem cell biology and biomedical utility’, *Developmental Biology*. Academic Press, 420(2), pp. 251–261. doi: 10.1016/J.YDBIO.2016.06.039.

Ho, L. *et al.* (2009a) ‘An embryonic stem cell chromatin remodeling complex, esBAF, is essential for embryonic stem cell self-renewal and pluripotency.’, *Proceedings of the National Academy of Sciences of the United States of America*, 106(13), pp. 5181–6. doi: 10.1073/pnas.0812889106.

Ho, L. *et al.* (2009b) ‘An embryonic stem cell chromatin remodeling complex, esBAF, is essential for embryonic stem cell self-renewal and pluripotency.’, *Proceedings of the National Academy of Sciences of the United States of America*. National Academy of Sciences, 106(13), pp. 5181–6. doi: 10.1073/pnas.0812889106.

Ho, L. and Crabtree, G. R. (2010) ‘Chromatin remodelling during development.’, *Nature*, 463(7280), pp. 474–84. doi: 10.1038/nature08911.

Hoppo, T. *et al.* (2004) ‘Thy1-positive mesenchymal cells promote the maturation of CD49f-positive hepatic progenitor cells in the mouse fetal liver’, *Hepatology*. John Wiley & Sons, Ltd, 39(5), pp. 1362–1370. doi: 10.1002/hep.20180.

Hsieh, C. L. (1999) ‘In vivo activity of murine de novo methyltransferases, Dnmt3a and

Dnmt3b.’, *Molecular and cellular biology*. American Society for Microbiology Journals, 19(12), pp. 8211–8. doi: 10.1128/MCB.19.12.8211.

Hu, H. *et al.* (2018) ‘Long-Term Expansion of Functional Mouse and Human Hepatocytes as 3D Organoids.’, *Cell*. Elsevier, 175(6), p. 1591–1606.e19. doi: 10.1016/j.cell.2018.11.013.

Hu, L. *et al.* (2013) ‘Crystal structure of TET2-DNA complex: insight into TET-mediated 5mC oxidation.’, *Cell*. Elsevier, 155(7), pp. 1545–55. doi: 10.1016/j.cell.2013.11.020.

Hu, L. *et al.* (2015) ‘Structural insight into substrate preference for TET-mediated oxidation’, *Nature*. Nature Publishing Group, 527(7576), pp. 118–122. doi: 10.1038/nature15713.

Huang, H. *et al.* (2013) ‘TET1 plays an essential oncogenic role in MLL-rearranged leukemia’, *Proceedings of the National Academy of Sciences*. National Academy of Sciences, 110(29), pp. 11994–11999. doi: 10.1073/PNAS.1310656110.

Huang, X. *et al.* (2008) ‘Coronary development is regulated by ATP-dependent SWI/SNF chromatin remodeling component BAF180’, *Developmental Biology*, 319(2), pp. 258–266. doi: 10.1016/j.ydbio.2008.04.020.

Huch, M., Dorrell, C., *et al.* (2013) ‘In vitro expansion of single Lgr5+ liver stem cells induced by Wnt-driven regeneration.’, *Nature*, 494(7436), pp. 247–50. doi: 10.1038/nature11826.

Huch, M., Bonfanti, P., *et al.* (2013) ‘Unlimited in vitro expansion of adult bi-potent pancreas progenitors through the Lgr5/R-spondin axis.’, *The EMBO journal*, 32(20), pp. 2708–21. doi: 10.1038/emboj.2013.204.

Huch, M. *et al.* (2015) ‘Long-term culture of genome-stable bipotent stem cells from adult human liver.’, *Cell*. Elsevier, 160(1–2), pp. 299–312. doi: 10.1016/j.cell.2014.11.050.

Huch, M. *et al.* (2017) ‘The hope and the hype of organoid research’, *Development*. Oxford University Press for The Company of Biologists Limited, 144(6), pp. 938–941. doi: 10.1242/DEV.150201.

Huch, M. and Koo, B.-K. (2015) ‘Modeling mouse and human development using organoid cultures.’, *Development (Cambridge, England)*. Oxford University Press for The Company of Biologists Limited, 142(18), pp. 3113–25. doi: 10.1242/dev.118570.

Ito, S. *et al.* (2011) ‘Tet proteins can convert 5-methylcytosine to 5-formylcytosine and 5-carboxylcytosine.’, *Science (New York, N.Y.)*. American Association for the Advancement of Science, 333(6047), pp. 1300–3. doi: 10.1126/science.1210597.

Iurlaro, M. *et al.* (2013) ‘A screen for hydroxymethylcytosine and formylcytosine binding proteins suggests functions in transcription and chromatin regulation.’, *Genome biology*. BioMed Central, 14(10), p. R119. doi: 10.1186/gb-2013-14-10-r119.

Iwaisako, K. *et al.* (2014) ‘Origin of myofibroblasts in the fibrotic liver in mice’, *Proceedings of the National Academy of Sciences*. National Academy of Sciences, 111(32), pp. E3297–E3305. doi: 10.1073/PNAS.1400062111.

Ji, D. *et al.* (2014) ‘Effects of Tet-induced oxidation products of 5-methylcytosine on Dnmt1- and DNMT3a-mediated cytosine methylation’, *Molecular BioSystems*. The Royal Society of Chemistry, 10(7), p. 1749. doi: 10.1039/c4mb00150h.

Jia, D. *et al.* (2007) ‘Structure of Dnmt3a bound to Dnmt3L suggests a model for de novo DNA methylation’, *Nature*. Nature Publishing Group, 449(7159), pp. 248–251. doi: 10.1038/nature06146.

Jin, S.-G., Guo, C. and Pfeifer, G. P. (2008) ‘GADD45A Does Not Promote DNA Demethylation’, *PLoS Genetics*. Edited by W. Reik. Public Library of Science, 4(3), p. e1000013. doi: 10.1371/journal.pgen.1000013.

Jin, S.-G., Kadam, S. and Pfeifer, G. P. (2010) ‘Examination of the specificity of DNA methylation profiling techniques towards 5-methylcytosine and 5-hydroxymethylcytosine’, *Nucleic Acids Research*. Oxford University Press, 38(11), pp. e125–e125. doi: 10.1093/nar/gkq223.

Jones, P. L. *et al.* (1998) ‘Methylated DNA and MeCP2 recruit histone deacetylase to repress transcription’, *Nature Genetics*. Nature Publishing Group, 19(2), pp. 187–191. doi: 10.1038/561.

Jung, P. *et al.* (2011) ‘Isolation and in vitro expansion of human colonic stem cells’, *Nature Medicine*. Nature Publishing Group, 17(10), pp. 1225–1227. doi: 10.1038/nm.2470.

- Kadoch, C. and Crabtree, G. R. (2015) 'Mammalian SWI/SNF chromatin remodeling complexes and cancer: Mechanistic insights gained from human genomics', *Science Advances*, 1(5).
- Kamiya, A. *et al.* (1999) 'Fetal liver development requires a paracrine action of oncostatin M through the gp130 signal transducer', *The EMBO Journal*. EMBO Press, 18(8), pp. 2127–2136. doi: 10.1093/emboj/18.8.2127.
- Kang, J. *et al.* (2015) 'Simultaneous deletion of the methylcytosine oxidases Tet1 and Tet3 increases transcriptome variability in early embryogenesis.', *Proceedings of the National Academy of Sciences of the United States of America*. National Academy of Sciences, 112(31), pp. E4236–45. doi: 10.1073/pnas.1510510112.
- Kanno, N. *et al.* (2000) 'Functional heterogeneity of the intrahepatic biliary epithelium', *Hepatology*. John Wiley & Sons, Ltd, 31(3), pp. 555–561. doi: 10.1002/hep.510310302.
- Karthaus, W. R. *et al.* (2014) 'Identification of multipotent luminal progenitor cells in human prostate organoid cultures.', *Cell*. Elsevier, 159(1), pp. 163–175. doi: 10.1016/j.cell.2014.08.017.
- Ke, M.-T., Fujimoto, S. and Imai, T. (2013) 'SeeDB: a simple and morphology-preserving optical clearing agent for neuronal circuit reconstruction', *Nature Neuroscience*. Nature Publishing Group, 16(8), pp. 1154–1161. doi: 10.1038/nn.3447.
- Kelso, T. W. R. *et al.* (2017) 'Chromatin accessibility underlies synthetic lethality of SWI/SNF subunits in ARID1A-mutant cancers', *eLife*, 6. doi: 10.7554/eLife.30506.
- Kiefer, C. M. *et al.* (2008) 'Epigenetics of  $\beta$ -globin gene regulation', *Mutation Research/Fundamental and Molecular Mechanisms of Mutagenesis*. Elsevier, 647(1–2), pp. 68–76. doi: 10.1016/J.MRFMMM.2008.07.014.
- Kietzmann, T. (2017) 'Metabolic zonation of the liver: The oxygen gradient revisited', *Redox Biology*. Elsevier, 11, pp. 622–630. doi: 10.1016/J.REDOX.2017.01.012.
- Kim, J. *et al.* (2006) 'Tudor, MBT and chromo domains gauge the degree of lysine methylation', *EMBO reports*. EMBO Press, 7(4), pp. 397–403. doi: 10.1038/sj.embor.7400625.
- Kim, J. K. *et al.* (2001) 'Srg3, a mouse homolog of yeast SWI3, is essential for early embryogenesis and involved in brain development.', *Molecular and cellular biology*. American Society for Microbiology (ASM), 21(22), pp. 7787–95. doi: 10.1128/MCB.21.22.7787-7795.2001.
- Kim, J. L. *et al.* (1998) 'Hepatitis C virus NS3 RNA helicase domain with a bound oligonucleotide: the crystal structure provides insights into the mode of unwinding.', *Structure (London, England : 1993)*. Elsevier, 6(1), pp. 89–100. doi: 10.1016/S0969-2126(98)00010-0.
- Kim, R. *et al.* (2016) 'Epigenetic regulation of intestinal stem cells by Tet1-mediated DNA hydroxymethylation.', *Genes & development*. Cold Spring Harbor Laboratory Press, 30(21), pp. 2433–2442. doi: 10.1101/gad.288035.116.
- Kireeva, M. L. *et al.* (2005) 'Nature of the nucleosomal barrier to RNA polymerase II.', *Molecular cell*. Elsevier, 18(1), pp. 97–108. doi: 10.1016/j.molcel.2005.02.027.
- Knezetic, J. A. and Luse, D. S. (1986) 'The presence of nucleosomes on a DNA template prevents initiation by RNA polymerase II in vitro.', *Cell*. Elsevier, 45(1), pp. 95–104. doi: 10.1016/0092-8674(86)90541-6.
- Kondo, E. *et al.* (2005) 'The thymine DNA glycosylase MBD4 represses transcription and is associated with methylated p16(INK4a) and hMLH1 genes.', *Molecular and cellular biology*. American Society for Microbiology Journals, 25(11), pp. 4388–96. doi: 10.1128/MCB.25.11.4388-4396.2005.
- Kornberg, R. D. (1974) 'Chromatin Structure: A Repeating Unit of Histones and DNA', *Science*. American Association for the Advancement of Science, 184(4139), pp. 868–871. doi: 10.1126/SCIENCE.184.4139.868.
- Kornberg, R. D. and Lorch, Y. (1999) 'Twenty-five years of the nucleosome, fundamental particle of the eukaryote chromosome.', *Cell*. Elsevier, 98(3), pp. 285–94. doi: 10.1016/S0092-8674(00)81958-3.
- Kortschak, R. D., Tucker, P. W. and Saint, R. (2000) 'ARID proteins come in from the

desert', *Trends in Biochemical Sciences*. Elsevier Current Trends, 25(6), pp. 294–299. doi: 10.1016/S0968-0004(00)01597-8.

Krokan, H. E., Standal, R. and Slupphaug, G. (1997) *DNA glycosylases in the base excision repair of DNA*, *Biochem. J.* Available at: <http://www.biochemj.org/content/325/1/1.full-text.pdf> (Accessed: 9 February 2019).

Lachner, M. *et al.* (2001) 'Methylation of histone H3 lysine 9 creates a binding site for HP1 proteins', *Nature*. Nature Publishing Group, 410(6824), pp. 116–120. doi: 10.1038/35065132.

Lajtha, L. G. (1979) 'Stem Cell Concepts', *Differentiation*. Elsevier, 14(1–3), pp. 23–33. doi: 10.1111/J.1432-0436.1979.TB01007.X.

Lange, M. *et al.* (2008) 'Regulation of muscle development by DPF3, a novel histone acetylation and methylation reader of the BAF chromatin remodeling complex.', *Genes & development*. Cold Spring Harbor Laboratory Press, 22(17), pp. 2370–84. doi: 10.1101/gad.471408.

Lee, J.-H. and Skalnik, D. G. (2005) 'CpG-binding protein (CXXC finger protein 1) is a component of the mammalian Set1 histone H3-Lys4 methyltransferase complex, the analogue of the yeast Set1/COMPASS complex.', *The Journal of biological chemistry*. American Society for Biochemistry and Molecular Biology, 280(50), pp. 41725–31. doi: 10.1074/jbc.M508312200.

Lee, J. *et al.* (2002) 'Erasing genomic imprinting memory in mouse clone embryos produced from day 11.5 primordial germ cells.', *Development (Cambridge, England)*, 129(8), pp. 1807–17. Available at: <http://www.ncbi.nlm.nih.gov/pubmed/11934847> (Accessed: 6 February 2019).

Lessard, J. *et al.* (2007) 'An Essential Switch in Subunit Composition of a Chromatin Remodeling Complex during Neural Development', *Neuron*. Elsevier, 55(2), pp. 201–215. doi: 10.1016/j.neuron.2007.06.019.

Levene, P. A. (1919) 'THE STRUCTURE OF YEAST NUCLEIC ACID', *Journal of Biological Chemistry*. American Society for Biochemistry and Molecular Biology, 40(2), pp. 415–424. Available at: <http://www.jbc.org/cgi/content/short/40/2/415> (Accessed: 2 February 2019).

Li, B., Carey, M. and Workman, J. L. (2007) 'The role of chromatin during transcription.', *Cell*. Elsevier, 128(4), pp. 707–19. doi: 10.1016/j.cell.2007.01.015.

Li, W. *et al.* (2019) 'A Homeostatic Arid1a-Dependent Permissive Chromatin State Licenses Hepatocyte Responsiveness to Liver-Injury-Associated YAP Signaling', *Cell Stem Cell*, 25(1), p. 54–68.e5. doi: 10.1016/j.stem.2019.06.008.

Lickert, H. *et al.* (2004) 'Baf60c is essential for function of BAF chromatin remodelling complexes in heart development', *Nature*. Nature Publishing Group, 432(7013), pp. 107–112. doi: 10.1038/nature03071.

Lim, Y.-S. and Kim, W. R. (2008) 'The Global Impact of Hepatic Fibrosis and End-Stage Liver Disease', *Clinics in Liver Disease*. Elsevier, 12(4), pp. 733–746. doi: 10.1016/J.CLD.2008.07.007.

Lin, S. *et al.* (2018) 'Distributed hepatocytes expressing telomerase repopulate the liver in homeostasis and injury', *Nature*. Nature Publishing Group, 556(7700), pp. 244–248. doi: 10.1038/s41586-018-0004-7.

Lin, Y. *et al.* (2017) 'HGF/R-spondin1 rescues liver dysfunction through the induction of Lgr5+ liver stem cells', *Nature Communications*. Nature Publishing Group, 8(1), p. 1175. doi: 10.1038/s41467-017-01341-6.

Lloyd-Lewis, B. *et al.* (2016) 'Imaging the mammary gland and mammary tumours in 3D: optical tissue clearing and immunofluorescence methods', *Breast Cancer Research*. BioMed Central, 18(1), p. 127. doi: 10.1186/s13058-016-0754-9.

Lorch, Y., LaPointe, J. W. and Kornberg, R. D. (1987) 'Nucleosomes inhibit the initiation of transcription but allow chain elongation with the displacement of histones.', *Cell*. Elsevier, 49(2), pp. 203–10. doi: 10.1016/0092-8674(87)90561-7.

Lu, W.-Y. *et al.* (2015) 'Hepatic progenitor cells of biliary origin with liver repopulation capacity', *Nature Cell Biology*. Nature Publishing Group, 17(8), pp. 971–983. doi: 10.1038/ncb3203.

MacDonald, R. A. (1961) ‘“Lifespan” of Liver Cells’, *Archives of Internal Medicine*. American Medical Association, 107(3), p. 335. doi: 10.1001/archinte.1961.03620030023003.

Mah, L.-J., El-Osta, A. and Karagiannis, T. C. (2010) ‘ $\gamma$ H2AX: a sensitive molecular marker of DNA damage and repair’, *Leukemia*. Nature Publishing Group, 24(4), pp. 679–686. doi: 10.1038/leu.2010.6.

Maiti, A. and Drohat, A. C. (2011) ‘Thymine DNA glycosylase can rapidly excise 5-formylcytosine and 5-carboxylcytosine: potential implications for active demethylation of CpG sites.’, *The Journal of biological chemistry*. American Society for Biochemistry and Molecular Biology, 286(41), pp. 35334–8. doi: 10.1074/jbc.C111.284620.

Marshall, A. *et al.* (2005) ‘Relation between hepatocyte G1 arrest, impaired hepatic regeneration, and fibrosis in chronic hepatitis C virus infection’, *Gastroenterology*. W.B. Saunders, 128(1), pp. 33–42. doi: 10.1053/J.GASTRO.2004.09.076.

Martin, G. R. (1981) ‘Isolation of a pluripotent cell line from early mouse embryos cultured in medium conditioned by teratocarcinoma stem cells.’, *Proceedings of the National Academy of Sciences of the United States of America*. National Academy of Sciences, 78(12), p. 7634. doi: 10.1073/PNAS.78.12.7634.

Mathur, R. *et al.* (2017) ‘ARID1A loss impairs enhancer-mediated gene regulation and drives colon cancer in mice’, *Nature Genetics*. Nature Publishing Group, 49(2), pp. 296–302. doi: 10.1038/ng.3744.

Matsui, T. *et al.* (2002) ‘K-Ras mediates cytokine-induced formation of E-cadherin-based adherens junctions during liver development’, *The EMBO Journal*. EMBO Press, 21(5), pp. 1021–1030. doi: 10.1093/EMBOJ/21.5.1021.

Matsumoto, K. *et al.* (2001) ‘Liver organogenesis promoted by endothelial cells prior to vascular function.’, *Science (New York, N.Y.)*. American Association for the Advancement of Science, 294(5542), pp. 559–63. doi: 10.1126/science.1063889.

Maurer-Stroh, S. *et al.* (2003) ‘The Tudor domain “Royal Family”: Tudor, plant Agenet, Chromo, PWWP and MBT domains.’, *Trends in biochemical sciences*. Elsevier, 28(2), pp. 69–74. doi: 10.1016/S0968-0004(03)00004-5.

Mead, B. E. and Karp, J. M. (2019) ‘All models are wrong, but some organoids may be useful’, *Genome Biology*. BioMed Central, 20(1), p. 66. doi: 10.1186/s13059-019-1677-4.

Mederacke, I. *et al.* (2013) ‘Fate tracing reveals hepatic stellate cells as dominant contributors to liver fibrosis independent of its aetiology’, *Nature Communications*. Nature Publishing Group, 4(1), p. 2823. doi: 10.1038/ncomms3823.

Michalopoulos, G. K. and DeFrances, M. C. (1997) ‘Liver regeneration.’, *Science (New York, N.Y.)*. American Association for the Advancement of Science, 276(5309), pp. 60–6. doi: 10.1126/SCIENCE.276.5309.60.

Mikkelsen, T. S. *et al.* (2008) ‘Dissecting direct reprogramming through integrative genomic analysis’, *Nature*. Nature Publishing Group, 454(7200), pp. 49–55. doi: 10.1038/nature07056.

Minor, E. A. *et al.* (2013) ‘Ascorbate induces ten-eleven translocation (Tet) methylcytosine dioxygenase-mediated generation of 5-hydroxymethylcytosine.’, *The Journal of biological chemistry*. American Society for Biochemistry and Molecular Biology, 288(19), pp. 13669–74. doi: 10.1074/jbc.C113.464800.

Miranda, T. B. and Jones, P. A. (2007) ‘DNA methylation: The nuts and bolts of repression’, *Journal of Cellular Physiology*. John Wiley & Sons, Ltd, 213(2), pp. 384–390. doi: 10.1002/jcp.21224.

Miyajima, A., Tanaka, M. and Itoh, T. (2014) ‘Stem/Progenitor Cells in Liver Development, Homeostasis, Regeneration, and Reprogramming’, *Stem Cell*, 14(5), pp. 561–574. doi: 10.1016/j.stem.2014.04.010.

Mizuguchi, G. *et al.* (2004) ‘ATP-driven exchange of histone H2AZ variant catalyzed by SWR1 chromatin remodeling complex.’, *Science (New York, N.Y.)*. American Association for the Advancement of Science, 303(5656), pp. 343–8. doi: 10.1126/science.1090701.

Mohandas, T., Sparkes, R. S. and Shapiro, L. J. (1981) ‘Reactivation of an inactive human X chromosome: evidence for X inactivation by DNA methylation.’, *Science (New York, N.Y.)*. American Association for the Advancement of Science, 211(4480), pp. 393–6. doi: 10.1126/science.6164095.

Murry, C. E. and Keller, G. (2008) 'Differentiation of Embryonic Stem Cells to Clinically Relevant Populations: Lessons from Embryonic Development', *Cell*. Cell Press, 132(4), pp. 661–680. doi: 10.1016/J.CELL.2008.02.008.

Muzny, D. M. *et al.* (2012) 'Comprehensive molecular characterization of human colon and rectal cancer', *Nature*. Nature Publishing Group, 487(7407), pp. 330–337. doi: 10.1038/nature11252.

Nan, X. *et al.* (1998) 'Transcriptional repression by the methyl-CpG-binding protein MeCP2 involves a histone deacetylase complex', *Nature*. Nature Publishing Group, 393(6683), pp. 386–389. doi: 10.1038/30764.

Neigeborn, L. and Carlson, M. (1984) 'Genes affecting the regulation of SUC2 gene expression by glucose repression in *Saccharomyces cerevisiae*.', *Genetics*, 108(4), pp. 845–58. Available at: <http://www.ncbi.nlm.nih.gov/pubmed/6392017> (Accessed: 6 June 2016).

Okano, M. *et al.* (1999) 'DNA methyltransferases Dnmt3a and Dnmt3b are essential for de novo methylation and mammalian development.', *Cell*. Elsevier, 99(3), pp. 247–57. doi: 10.1016/S0092-8674(00)81656-6.

Okano, M., Xie, S. and Li, E. (1998) 'Cloning and characterization of a family of novel mammalian DNA (cytosine-5) methyltransferases', *Nature Genetics*. Nature Publishing Group, 19(3), pp. 219–220. doi: 10.1038/890.

Onitsuka, I., Tanaka, M. and Miyajima, A. (2010) 'Characterization and Functional Analyses of Hepatic Mesothelial Cells in Mouse Liver Development', *Gastroenterology*. W.B. Saunders, 138(4), p. 1525–1535.e6. doi: 10.1053/J.GASTRO.2009.12.059.

Ooi, S. K. T. *et al.* (2007) 'DNMT3L connects unmethylated lysine 4 of histone H3 to de novo methylation of DNA', *Nature*. Nature Publishing Group, 448(7154), pp. 714–717. doi: 10.1038/nature05987.

Ooi, S. K. T., Bestor, T. H. and Pfeifer, G. P. (2008) 'The colorful history of active DNA demethylation.', *Cell*. Elsevier, 133(7), pp. 1145–8. doi: 10.1016/j.cell.2008.06.009.

Ornitz, D. M. and Itoh, N. (2015) 'The Fibroblast Growth Factor signaling pathway', *Wiley Interdisciplinary Reviews. Developmental Biology*. Wiley-Blackwell, 4(3), p. 215. doi: 10.1002/WDEV.176.

Overturf, K. *et al.* (1996) 'Hepatocytes corrected by gene therapy are selected in vivo in a murine model of hereditary tyrosinaemia type I', *Nature Genetics*. Nature Publishing Group, 12(3), pp. 266–273. doi: 10.1038/ng0396-266.

Overturf, K. *et al.* (1997) 'Serial transplantation reveals the stem-cell-like regenerative potential of adult mouse hepatocytes.', *The American journal of pathology*. American Society for Investigative Pathology, 151(5), pp. 1273–80. Available at: <http://www.ncbi.nlm.nih.gov/pubmed/9358753> (Accessed: 16 January 2019).

Paige, S. L. *et al.* (2012) 'A Temporal Chromatin Signature in Human Embryonic Stem Cells Identifies Regulators of Cardiac Development', *Cell*. Elsevier, 151(1), pp. 221–232. doi: 10.1016/J.CELL.2012.08.027.

Parikh, S. S., Mol, C. D. and Tainer, J. A. (1997) 'Base excision repair enzyme family portrait: integrating the structure and chemistry of an entire DNA repair pathway.', *Structure (London, England : 1993)*. Elsevier, 5(12), pp. 1543–50. doi: 10.1016/S0969-2126(97)00303-1.

Patel, S. A., Graunke, D. M. and Pieper, R. O. (1997) 'Aberrant silencing of the CpG island-containing human O6-methylguanine DNA methyltransferase gene is associated with the loss of nucleosome-like positioning.', *Molecular and cellular biology*. American Society for Microbiology Journals, 17(10), pp. 5813–22. doi: 10.1128/MCB.17.10.5813.

Peng, W. C. *et al.* (2018) 'Inflammatory Cytokine TNF $\alpha$  Promotes the Long-Term Expansion of Primary Hepatocytes in 3D Culture.', *Cell*. Elsevier, 175(6), p. 1607–1619.e15. doi: 10.1016/j.cell.2018.11.012.

Pepe-Mooney, B. J. *et al.* (2019) 'Single-Cell Analysis of the Liver Epithelium Reveals Dynamic Heterogeneity and an Essential Role for YAP in Homeostasis and Regeneration', *Cell Stem Cell*, 25(1), p. 23–38.e8. doi: 10.1016/j.stem.2019.04.004.

Phillips, D. M. and Johns, E. W. (1965) 'A FRACTIONATION OF THE HISTONES OF GROUP F2A FROM CALF THYMUS.', *The Biochemical journal*. Portland Press Ltd, 94(1),

pp. 127–30. Available at: <http://www.ncbi.nlm.nih.gov/pubmed/14342219> (Accessed: 1 February 2019).

Porter, E. G. and Dykhuizen, E. C. (2017) ‘Individual Bromodomains of Polybromo-1 Contribute to Chromatin Association and Tumor Suppression in Clear Cell Renal Carcinoma.’, *The Journal of biological chemistry*. American Society for Biochemistry and Molecular Biology, 292(7), pp. 2601–2610. doi: 10.1074/jbc.M116.746875.

Pradhan, S. *et al.* (1999) ‘Recombinant human DNA (cytosine-5) methyltransferase. I. Expression, purification, and comparison of de novo and maintenance methylation.’, *The Journal of biological chemistry*. American Society for Biochemistry and Molecular Biology, 274(46), pp. 33002–10. doi: 10.1074/JBC.274.46.33002.

Preisegger, K. H. *et al.* (1999) ‘Atypical ductular proliferation and its inhibition by transforming growth factor beta1 in the 3,5-diethoxycarbonyl-1,4-dihydrocollidine mouse model for chronic alcoholic liver disease.’, *Laboratory investigation; a journal of technical methods and pathology*, 79(2), pp. 103–9. Available at: <http://www.ncbi.nlm.nih.gov/pubmed/10068199> (Accessed: 4 February 2019).

Prendergast, G. C., Lawe, D. and Ziff, E. B. (1991) ‘Association of Myn, the murine homolog of max, with c-Myc stimulates methylation-sensitive DNA binding and ras cotransformation.’, *Cell*. Elsevier, 65(3), pp. 395–407. doi: 10.1016/0092-8674(91)90457-A.

Pu, W. *et al.* (2016) ‘Mfsd2a<sup>+</sup> hepatocytes repopulate the liver during injury and regeneration’, *Nature Communications*. Nature Publishing Group, 7(1), p. 13369. doi: 10.1038/ncomms13369.

Quivoron, C. *et al.* (2011) ‘TET2 inactivation results in pleiotropic hematopoietic abnormalities in mouse and is a recurrent event during human lymphomagenesis.’, *Cancer cell*. Elsevier, 20(1), pp. 25–38. doi: 10.1016/j.ccr.2011.06.003.

R Core Team (2018) ‘R: a language and environment for statistical computing’. Available at: <https://www.r-project.org/> (Accessed: 24 February 2019).

Raab, J. R., Resnick, S. and Magnuson, T. (2015) ‘Genome-Wide Transcriptional Regulation Mediated by Biochemically Distinct SWI/SNF Complexes’, *PLOS Genetics*. Edited by J. D. Lieb. Public Library of Science, 11(12), p. e1005748. doi: 10.1371/journal.pgen.1005748.

Rabes, H. M. *et al.* (1976) ‘Analysis of cell cycle compartments of hepatocytes after partial hepatectomy.’, *Cell and tissue kinetics*, 9(6), pp. 517–32. Available at: <http://www.ncbi.nlm.nih.gov/pubmed/1000566> (Accessed: 16 January 2019).

Rasmussen, K. D. and Helin, K. (2016) ‘Role of TET enzymes in DNA methylation, development, and cancer.’, *Genes & development*. Cold Spring Harbor Laboratory Press, 30(7), pp. 733–50. doi: 10.1101/gad.276568.115.

Raven, A. *et al.* (2017) ‘Cholangiocytes act as facultative liver stem cells during impaired hepatocyte regeneration’, *Nature*. Nature Publishing Group, 547(7663), pp. 350–354. doi: 10.1038/nature23015.

Reinke, H. and Hörz, W. (2003) ‘Histones are first hyperacetylated and then lose contact with the activated PHO5 promoter.’, *Molecular cell*. Elsevier, 11(6), pp. 1599–607. doi: 10.1016/S1097-2765(03)00186-2.

Reya, T. and Clevers, H. (2005) ‘Wnt signalling in stem cells and cancer’, *Nature*, 434(7035), pp. 843–850. doi: 10.1038/nature03319.

Reyes, J. C. *et al.* (1998) ‘Altered control of cellular proliferation in the absence of mammalian brahma (SNF2alpha).’, *The EMBO journal*. European Molecular Biology Organization, 17(23), pp. 6979–91. doi: 10.1093/emboj/17.23.6979.

Richardson, M. M. *et al.* (2007) ‘Progressive Fibrosis in Nonalcoholic Steatohepatitis: Association With Altered Regeneration and a Ductular Reaction’, *Gastroenterology*. W.B. Saunders, 133(1), pp. 80–90. doi: 10.1053/J.GASTRO.2007.05.012.

Richmond, T. J. and Davey, C. A. (2003) ‘The structure of DNA in the nucleosome core’, *Nature*. Nature Publishing Group, 423(6936), pp. 145–150. doi: 10.1038/nature01595.

Rodríguez-Seguel, E. *et al.* (2013) ‘Mutually exclusive signaling signatures define the hepatic and pancreatic progenitor cell lineage divergence.’, *Genes & development*. Cold Spring Harbor Laboratory Press, 27(17), pp. 1932–46. doi: 10.1101/gad.220244.113.

Rossi, J. M. *et al.* (2001) ‘Distinct mesodermal signals, including BMPs from the septum

transversum mesenchyme, are required in combination for hepatogenesis from the endoderm.’, *Genes & development*. Cold Spring Harbor Laboratory Press, 15(15), pp. 1998–2009. doi: 10.1101/gad.904601.

Rougier, N. *et al.* (1998) ‘Chromosome methylation patterns during mammalian preimplantation development.’, *Genes & development*, 12(14), pp. 2108–13. Available at: <http://www.ncbi.nlm.nih.gov/pubmed/9679055> (Accessed: 6 February 2019).

Rountree, C. B. *et al.* (2007) ‘A CD133-Expressing Murine Liver Oval Cell Population with Bilineage Potential’, *Stem Cells*. John Wiley & Sons, Ltd, 25(10), pp. 2419–2429. doi: 10.1634/stemcells.2007-0176.

Saha, A., Wittmeyer, J. and Cairns, B. R. (2005) ‘Chromatin remodeling through directional DNA translocation from an internal nucleosomal site’, *Nature Structural & Molecular Biology*. Nature Publishing Group, 12(9), pp. 747–755. doi: 10.1038/nsmb973.

Saha, A., Wittmeyer, J. and Cairns, B. R. (2006) ‘Chromatin remodelling: the industrial revolution of DNA around histones’, *Nature Reviews Molecular Cell Biology*. Nature Publishing Group, 7(6), pp. 437–447. doi: 10.1038/nrm1945.

Sampaziotis, F. *et al.* (2015) ‘Cholangiocytes derived from human induced pluripotent stem cells for disease modeling and drug validation’, *Nature Biotechnology*. Nature Publishing Group, 33(8), pp. 845–852. doi: 10.1038/nbt.3275.

Santos, F. *et al.* (2002) ‘Dynamic Reprogramming of DNA Methylation in the Early Mouse Embryo’, *Developmental Biology*, 241(1), pp. 172–182. doi: 10.1006/dbio.2001.0501.

Sato, T. *et al.* (2009) ‘Single Lgr5 stem cells build crypt-villus structures in vitro without a mesenchymal niche’, *Nature*. Nature Publishing Group, 459(7244), pp. 262–265. doi: 10.1038/nature07935.

Scaltriti, M. and Baselga, J. (2006) ‘The Epidermal Growth Factor Receptor Pathway: A Model for Targeted Therapy’, *Clinical Cancer Research*. American Association for Cancer Research, 12(18), pp. 5268–5272. doi: 10.1158/1078-0432.CCR-05-1554.

Schaub, J. R. *et al.* (2014) ‘Evidence against a Stem Cell Origin of New Hepatocytes in a Common Mouse Model of Chronic Liver Injury’, *Cell Reports*. Cell Press, 8(4), pp. 933–939. doi: 10.1016/J.CELREP.2014.07.003.

Serls, A. E. *et al.* (2005) ‘Different thresholds of fibroblast growth factors pattern the ventral foregut into liver and lung’, *Development*. The Company of Biologists Ltd, 119(3), pp. 567–578. doi: 10.1242/dev.01570.

Sharif, J. *et al.* (2007) ‘The SRA protein Np95 mediates epigenetic inheritance by recruiting Dnmt1 to methylated DNA’, *Nature*. Nature Publishing Group, 450(7171), pp. 908–912. doi: 10.1038/nature06397.

Shen, J. *et al.* (2015) ‘ARID1A Deficiency Impairs the DNA Damage Checkpoint and Sensitizes Cells to PARP Inhibitors.’, *Cancer discovery*. American Association for Cancer Research, 5(7), pp. 752–67. doi: 10.1158/2159-8290.CD-14-0849.

Shinozuka, H. *et al.* (1978) ‘Early histological and functional alterations of ethionine liver carcinogenesis in rats fed a choline-deficient diet.’, *Cancer research*. American Association for Cancer Research, 38(4), pp. 1092–8. Available at: <http://www.ncbi.nlm.nih.gov/pubmed/76508> (Accessed: 17 January 2019).

Simonsson, S. and Gurdon, J. (2004) ‘DNA demethylation is necessary for the epigenetic reprogramming of somatic cell nuclei’, *Nature Cell Biology*. Nature Publishing Group, 6(10), pp. 984–990. doi: 10.1038/ncb1176.

Singleton, M. R. and Wigley, D. B. (2002) ‘Modularity and specialization in superfamily 1 and 2 helicases.’, *Journal of bacteriology*. American Society for Microbiology Journals, 184(7), pp. 1819–26. doi: 10.1128/JB.184.7.1819-1826.2002.

Snykers, S. *et al.* (2009) ‘In Vitro Differentiation of Embryonic and Adult Stem Cells into Hepatocytes: State of the Art’, *Stem Cells*. John Wiley & Sons, Ltd, 27(3), pp. 577–605. doi: 10.1634/stemcells.2008-0963.

Solt, D. B., Medline, A. and Farber, E. (1977) ‘Rapid emergence of carcinogen-induced hyperplastic lesions in a new model for the sequential analysis of liver carcinogenesis.’, *The American journal of pathology*. American Society for Investigative Pathology, 88(3), pp. 595–618. Available at: <http://www.ncbi.nlm.nih.gov/pubmed/18937> (Accessed: 17 January

- 2019).
- Speicher, T. *et al.* (2014) ‘Knockdown and knockout of  $\beta$ 1-integrin in hepatocytes impairs liver regeneration through inhibition of growth factor signalling’, *Nature Communications*. Nature Publishing Group, 5(1), p. 3862. doi: 10.1038/ncomms4862.
- Spruijt, C. G. *et al.* (2013) ‘Dynamic readers for 5-(hydroxy)methylcytosine and its oxidized derivatives.’, *Cell*. Elsevier, 152(5), pp. 1146–59. doi: 10.1016/j.cell.2013.02.004.
- Starzl, T. E. *et al.* (1993) ‘Baboon-to-human liver transplantation’, *Lancet*, 341(8837), pp. 65–71. Available at: <https://www.ncbi.nlm.nih.gov/pmc/articles/PMC2962592/pdf/nihms238812.pdf> (Accessed: 16 January 2019).
- Stern, M., Jensen, R. and Herskowitz, I. (1984) ‘Five SWI genes are required for expression of the HO gene in yeast.’, *Journal of molecular biology*, 178(4), pp. 853–68. Available at: <http://www.ncbi.nlm.nih.gov/pubmed/6436497> (Accessed: 6 June 2016).
- Stopka, T. and Skoultschi, A. I. (2003) ‘The ISWI ATPase Snf2h is required for early mouse development.’, *Proceedings of the National Academy of Sciences of the United States of America*. National Academy of Sciences, 100(24), pp. 14097–102. doi: 10.1073/pnas.2336105100.
- Sun, X. *et al.* (2016) ‘Suppression of the SWI/SNF Component Arid1a Promotes Mammalian Regeneration.’, *Cell stem cell*, 18(4), pp. 456–66. doi: 10.1016/j.stem.2016.03.001.
- Surani, M. A., Hayashi, K. and Hajkova, P. (2007) ‘Genetic and Epigenetic Regulators of Pluripotency’, *Cell*. Elsevier, 128(4), pp. 747–762. doi: 10.1016/j.cell.2007.02.010.
- Susaki, E. A. *et al.* (2015) ‘Advanced CUBIC protocols for whole-brain and whole-body clearing and imaging’, *Nature Protocols*. Nature Publishing Group, 10(11), pp. 1709–1727. doi: 10.1038/nprot.2015.085.
- Susaki, E. A. *et al.* (2016) ‘Whole-body and Whole-Organ Clearing and Imaging Techniques with Single-Cell Resolution: Toward Organism-Level Systems Biology in Mammals’, *Cell Chemical Biology*. BioMed Central, 23(1), pp. 137–157. doi: 10.1016/j.chembiol.2015.11.009.
- Suzuki, A. *et al.* (2008) ‘Flow cytometric isolation and clonal identification of self-renewing bipotent hepatic progenitor cells in adult mouse liver’, *Hepatology*. John Wiley & Sons, Ltd, 48(6), pp. 1964–1978. doi: 10.1002/hep.22558.
- Swisher, J. F. *et al.* (1998) ‘Analysis of putative RNase sensitivity and protease insensitivity of demethylation activity in extracts from rat myoblasts.’, *Nucleic acids research*. Oxford University Press, 26(24), pp. 5573–80. Available at: <http://www.ncbi.nlm.nih.gov/pubmed/9837985> (Accessed: 8 February 2019).
- Tahiliani, M. *et al.* (2009) ‘Conversion of 5-Methylcytosine to 5-Hydroxymethylcytosine in Mammalian DNA by MLL Partner TET1’, *Science*, 324(5929), pp. 930–935. doi: 10.1126/science.1170116.
- Takayama, K. *et al.* (2013) ‘Long-term self-renewal of human ES/iPS-derived hepatoblast-like cells on human laminin 111-coated dishes.’, *Stem cell reports*. Elsevier, 1(4), pp. 322–35. doi: 10.1016/j.stemcr.2013.08.006.
- Takebe, T. *et al.* (2013) ‘Vascularized and functional human liver from an iPSC-derived organ bud transplant’, *Nature*. Nature Publishing Group, 499(7459), pp. 481–484. doi: 10.1038/nature12271.
- Tang, L., Nogales, E. and Ciferri, C. (2010) ‘Structure and function of SWI/SNF chromatin remodeling complexes and mechanistic implications for transcription.’, *Progress in biophysics and molecular biology*, 102(2–3), pp. 122–8. doi: 10.1016/j.pbiomolbio.2010.05.001.
- Tanimizu, N. *et al.* (2003) ‘Isolation of hepatoblasts based on the expression of Dlk/Pref-1’, *Journal of Cell Science*. The Company of Biologists Ltd, 115(13), pp. 2679–2688. doi: 10.1242/jcs.00388.
- Tanimizu, N. *et al.* (2004) ‘Long-term culture of hepatic progenitors derived from mouse Dlk<sup>+</sup> hepatoblasts.’, *Journal of Cell Science*. The Company of Biologists Ltd, 117(Pt 26), pp. 6425–34. doi: 10.1242/jcs.01572.
- Tarayrah, L. and Chen, X. (2013) ‘Epigenetic regulation in adult stem cells and cancers’, *Cell*

& *Bioscience*. BioMed Central, 3, p. 41. doi: 10.1186/2045-3701-3-41.

Tarlow, B. D. *et al.* (2014) ‘Bipotential adult liver progenitors are derived from chronically injured mature hepatocytes.’, *Cell stem cell*, 15(5), pp. 605–18. doi: 10.1016/j.stem.2014.09.008.

Tarlow, B. D., Finegold, M. J. and Grompe, M. (2014) ‘Clonal tracing of Sox9+ liver progenitors in mouse oval cell injury.’, *Hepatology (Baltimore, Md.)*, 60(1), pp. 278–89. doi: 10.1002/hep.27084.

Tarlow, B. D., Finegold, M. J. and Grompe, M. (2014) ‘Clonal tracing of Sox9 + liver progenitors in mouse oval cell injury’, *Hepatology*, 60(1), pp. 278–289. doi: 10.1002/hep.27084.

Taub, R. (2004) ‘Liver regeneration: from myth to mechanism’, *Nature Reviews Molecular Cell Biology*. Nature Publishing Group, 5(10), pp. 836–847. doi: 10.1038/nrm1489.

Terpstra, V. and van Berkel, T. J. C. (2000) ‘Scavenger receptors on liver Kupffer cells mediate the in vivo uptake of oxidatively damaged red blood cells in mice’, *Blood*, 95(6).

Thomson, J. P. *et al.* (2016) ‘Loss of Tet1-Associated 5-Hydroxymethylcytosine Is Concomitant with Aberrant Promoter Hypermethylation in Liver Cancer’, *Cancer Research*. American Association for Cancer Research, 76(10), pp. 3097–3108. doi: 10.1158/0008-5472.CAN-15-1910.

Thurman, R. G., Kauffman, F. C. and Jungermann, K. (1986) *Regulation of Hepatic Metabolism : Intra- and Intercellular Compartmentation*. Springer US. Available at: [https://books.google.co.uk/books?hl=en&lr=&id=6FjaBwAAQBAJ&oi=fnd&pg=PA3&dq=Liver+structure+and+innervation.+In:+Regulation+of+Hepatic+Metabolism:+Intra+and+intercellular+Compartmentation,&ots=44goCnA7Uo&sig=-LePhFceHkS6YgJJmxZfk\\_gt4r0#v=onepage&q=Liver structure and innervation. In%3A Regulation of Hepatic Metabolism%3A Intra- and intercellular Compartmentation%2C&f=false](https://books.google.co.uk/books?hl=en&lr=&id=6FjaBwAAQBAJ&oi=fnd&pg=PA3&dq=Liver+structure+and+innervation.+In:+Regulation+of+Hepatic+Metabolism:+Intra+and+intercellular+Compartmentation,&ots=44goCnA7Uo&sig=-LePhFceHkS6YgJJmxZfk_gt4r0#v=onepage&q=Liver+structure+and+innervation. In%3A+Regulation+of+Hepatic+Metabolism%3A+Intra-+and+intercellular+Compartmentation%2C&f=false) (Accessed: 25 January 2019).

Travers, A. and Muskhelishvili, G. (2015) ‘DNA structure and function’, *FEBS Journal*. John Wiley & Sons, Ltd (10.1111), 282(12), pp. 2279–2295. doi: 10.1111/febs.13307.

Tsuchida, T. and Friedman, S. L. (2017) ‘Mechanisms of hepatic stellate cell activation’, *Nature Reviews Gastroenterology & Hepatology*. Nature Publishing Group, 14(7), pp. 397–411. doi: 10.1038/nrgastro.2017.38.

Valinluck, V. and Sowers, L. C. (2007) ‘Endogenous Cytosine Damage Products Alter the Site Selectivity of Human DNA Maintenance Methyltransferase DNMT1’, *Cancer Research*. American Association for Cancer Research, 67(3), pp. 946–950. doi: 10.1158/0008-5472.CAN-06-3123.

Vasileiou, G. *et al.* (2015) ‘Chromatin-Remodeling-Factor ARID1B Represses Wnt/ $\beta$ -Catenin Signaling’, *The American Journal of Human Genetics*. Cell Press, 97(3), pp. 445–456. doi: 10.1016/J.AJHG.2015.08.002.

Velankar, S. S. *et al.* (1999) ‘Crystal structures of complexes of PcrA DNA helicase with a DNA substrate indicate an inchworm mechanism.’, *Cell*. Elsevier, 97(1), pp. 75–84. doi: 10.1016/S0092-8674(00)80716-3.

Vignali, M. *et al.* (2000) ‘ATP-Dependent Chromatin-Remodeling Complexes’, *Molecular and Cellular Biology*. American Society for Microbiology Journals, 20(6), pp. 1899–1910. doi: 10.1128/MCB.20.6.1899-1910.2000.

Wake, K. (1971) ‘“Sternzellen” in the liver: Perisinusoidal cells with special reference to storage of vitamin A’, *American Journal of Anatomy*. John Wiley & Sons, Ltd, 132(4), pp. 429–461. doi: 10.1002/aja.1001320404.

Walsh, C. P., Chaillet, J. R. and Bestor, T. H. (1998) ‘Transcription of IAP endogenous retroviruses is constrained by cytosine methylation’, *Nature Genetics*. Nature Publishing Group, 20(2), pp. 116–117. doi: 10.1038/2413.

Wang, B. *et al.* (2015) ‘Self-renewing diploid Axin2+ cells fuel homeostatic renewal of the liver’, *Nature*, 524(7564), pp. 180–185. doi: 10.1038/nature14863.

Wang, K. *et al.* (2011) ‘Exome sequencing identifies frequent mutation of ARID1A in molecular subtypes of gastric cancer.’, *Nature genetics*, 43(12), pp. 1219–23. doi: 10.1038/ng.982.

- Wang, K. *et al.* (2014) ‘Whole-genome sequencing and comprehensive molecular profiling identify new driver mutations in gastric cancer.’, *Nature genetics*, 46(6), pp. 573–82. doi: 10.1038/ng.2983.
- Wang, W., Xue, Y., *et al.* (1996) ‘Diversity and specialization of mammalian SWI/SNF complexes.’, *Genes & development*, 10(17), pp. 2117–30. Available at: <http://www.ncbi.nlm.nih.gov/pubmed/8804307> (Accessed: 6 June 2016).
- Wang, W., Côté, J., *et al.* (1996) ‘Purification and biochemical heterogeneity of the mammalian SWI-SNF complex.’, *The EMBO journal*, 15(19), pp. 5370–82. Available at: <http://www.ncbi.nlm.nih.gov/pubmed/8895581> (Accessed: 6 June 2016).
- Wang, X. *et al.* (2004) ‘Two related ARID family proteins are alternative subunits of human SWI/SNF complexes’, *Biochemical Journal*. Portland Press Limited, 383(2), pp. 319–325. doi: 10.1042/BJ20040524.
- Wang, Z. *et al.* (2004) ‘Polybromo protein BAF180 functions in mammalian cardiac chamber maturation.’, *Genes & development*. Cold Spring Harbor Laboratory Press, 18(24), pp. 3106–16. doi: 10.1101/gad.1238104.
- Watson, J. D. and Crick, F. H. C. (1953) ‘Molecular Structure of Nucleic Acids: A Structure for Deoxyribose Nucleic Acid’, *Nature*. Nature Publishing Group, 171(4356), pp. 737–738. doi: 10.1038/171737a0.
- Weber, L. W. D., Boll, M. and Stampfl, A. (2003) ‘Hepatotoxicity and Mechanism of Action of Haloalkanes: Carbon Tetrachloride as a Toxicological Model’, *Critical Reviews in Toxicology*. Taylor & Francis, 33(2), pp. 105–136. doi: 10.1080/713611034.
- Weiss, A. *et al.* (1996) ‘DNA demethylation in vitro: involvement of RNA.’, *Cell*. Elsevier, 86(5), pp. 709–18. doi: 10.1016/S0092-8674(00)80146-4.
- Weng, Y.-L. *et al.* (2017) ‘An Intrinsic Epigenetic Barrier for Functional Axon Regeneration.’, *Neuron*. NIH Public Access, 94(2), p. 337–346.e6. doi: 10.1016/j.neuron.2017.03.034.
- Whitehouse, I. *et al.* (2003) ‘Evidence for DNA translocation by the ISWI chromatin-remodeling enzyme.’, *Molecular and cellular biology*. American Society for Microbiology Journals, 23(6), pp. 1935–45. doi: 10.1128/MCB.23.6.1935-1945.2003.
- Willekens, F. L. A. *et al.* (2005) ‘Liver Kupffer cells rapidly remove red blood cell-derived vesicles from the circulation by scavenger receptors.’, *Blood*. American Society of Hematology, 105(5), pp. 2141–5. doi: 10.1182/blood-2004-04-1578.
- Wilsker, D. *et al.* (2005) ‘Nomenclature of the ARID family of DNA-binding proteins.’, *Genomics*, 86(2), pp. 242–51. doi: 10.1016/j.ygeno.2005.03.013.
- Wisse, E. *et al.* (1985) ‘The liver sieve: Considerations concerning the structure and function of endothelial fenestrae, the sinusoidal wall and the space of disse’, *Hepatology*. John Wiley & Sons, Ltd, 5(4), pp. 683–692. doi: 10.1002/hep.1840050427.
- Woodcock, D. M. *et al.* (1997) ‘Asymmetric methylation in the hypermethylated CpG promoter region of the human L1 retrotransposon.’, *The Journal of biological chemistry*. American Society for Biochemistry and Molecular Biology, 272(12), pp. 7810–6. doi: 10.1074/JBC.272.12.7810.
- Wu, J. I. *et al.* (2007) ‘Regulation of Dendritic Development by Neuron-Specific Chromatin Remodeling Complexes’, *Neuron*, 56(1), pp. 94–108. doi: 10.1016/j.neuron.2007.08.021.
- Xu, F., Flowers, S. and Moran, E. (2012) ‘Essential role of ARID2 protein-containing SWI/SNF complex in tissue-specific gene expression.’, *The Journal of biological chemistry*, 287(7), pp. 5033–41. doi: 10.1074/jbc.M111.279968.
- Xu, Y. *et al.* (2012) ‘Tet3 CXXC domain and dioxygenase activity cooperatively regulate key genes for *Xenopus* eye and neural development.’, *Cell*. Elsevier, 151(6), pp. 1200–13. doi: 10.1016/j.cell.2012.11.014.
- Yan, Z. *et al.* (2008) ‘BAF250B-Associated SWI/SNF Chromatin-Remodeling Complex Is Required to Maintain Undifferentiated Mouse Embryonic Stem Cells’, *Stem Cells*. John Wiley & Sons, Ltd, 26(5), pp. 1155–1165. doi: 10.1634/stemcells.2007-0846.
- Yanger, K. *et al.* (2014) ‘Adult Hepatocytes Are Generated by Self-Duplication Rather than Stem Cell Differentiation’, *Cell Stem Cell*. Cell Press, 15(3), pp. 340–349. doi: 10.1016/J.STEM.2014.06.003.

- Yimlamai, D. *et al.* (2014) 'Hippo Pathway Activity Influences Liver Cell Fate', *Cell*, 157(6), pp. 1324–1338. doi: 10.1016/j.cell.2014.03.060.
- Yovchev, M. I. *et al.* (2007) 'Identification of adult hepatic progenitor cells capable of repopulating injured rat liver', *Hepatology*. John Wiley & Sons, Ltd, 47(2), pp. 636–647. doi: 10.1002/hep.22047.
- Zhang, H. *et al.* (2010) 'TET1 is a DNA-binding protein that modulates DNA methylation and gene transcription via hydroxylation of 5-methylcytosine', *Cell Research*. Nature Publishing Group, 20(12), pp. 1390–1393. doi: 10.1038/cr.2010.156.
- Zhang, H. S. *et al.* (2000) 'Exit from G1 and S Phase of the Cell Cycle Is Regulated by Repressor Complexes Containing HDAC-Rb-hSWI/SNF and Rb-hSWI/SNF', *Cell*. Cell Press, 101(1), pp. 79–89. doi: 10.1016/S0092-8674(00)80625-X.
- Zhang, Y. *et al.* (1999) 'Analysis of the NuRD subunits reveals a histone deacetylase core complex and a connection with DNA methylation.', *Genes & development*. Cold Spring Harbor Laboratory Press, 13(15), pp. 1924–35. Available at: <http://www.ncbi.nlm.nih.gov/pubmed/10444591> (Accessed: 2 February 2019).
- Zhao, L. *et al.* (2019) 'Tissue repair in the mouse liver following acute carbon tetrachloride depends on injury-induced Wnt/ $\beta$ -catenin signaling', *Hepatology*. John Wiley & Sons, Ltd. doi: 10.1002/hep.30563.
- Zhou, T. *et al.* (2014) 'Structural basis for hydroxymethylcytosine recognition by the SRA domain of UHRF2.', *Molecular cell*. Elsevier, 54(5), pp. 879–86. doi: 10.1016/j.molcel.2014.04.003.
- Zhu, L. *et al.* (2016) 'Multi-organ Mapping of Cancer Risk', *Cell*. Cell Press, 166(5), p. 1132–1146.e7. doi: 10.1016/J.CELL.2016.07.045.